ATMOSPHERIC PHYSICS:

ELECTRON DENSITY VARIATIONS IN THE MESOSPHERE

A thesis presented for the degree of

Doctor of Philosophy in Physics

in the University of Canterbury,

Christchurch, New Zealand

by

D.S. Wratt

University of Canterbury

1974

ABSTRACT

The theory of the differential absorption and differential phase experiments is examined, and it is found that the differences in predicted electron densities due to different hypothetical reflection processes are in general no larger than experimental uncertainties.

Results of differential absorption and differential phase measurements are compared.

It is found that electron densities in the mesosphere above Christchurch can be affected by energetic particle precipitation. Evidence is also found for increases in electron concentration associated with a stratospheric warming, but apart from this there is no clear evidence for stratosphere-ionosphere coupling above Christchurch.

Model studies show that much of the variation over time scales of four days or more above Christchurch could be accounted for by vertical transport of nitric oxide. However, other results make it likely that other processes, such as variations in loss rate, are also important.

CONTENTS

LIST OF FIGURES

LIST OF TABLES

NOTATION

The more important symbols are listed here, together with the sections in which they are defined.

A_X	Extraordinary mode signal	(3.2)
A_O	Ordinary mode signal	(3.2)
a	radius of the earth	
B	magnetic field flux density	
B	rate coefficient for "attachment-like" loss	(9.5)
$\mathcal{C}_{OX}, \mathcal{C}_{XO}$	coupling coefficients for reflection	(2.2)
c	speed of light	
E	electric field strength	(Appendix A)
$E_{X,O}$	electric field of ordinary, extraordinary wave	(Appendix A)
E_0	initial electron energy	(8.3)
E	electron density difference for two models	(2.4,2.5)
$\mathfrak{E}$	pulsewidth-dependent term	(2.5)
F(h)	magnitude of complex correlation	(Appendix A)
f	Coriolis parameter	(7.3)
$\mathcal{F}_0$	incident electron flux	(8.3)
g	acceleration of gravity	
h	height	
H	scale height	
$\hat{i}_x, \hat{i}_y, \hat{i}_z$	unit vectors to east, north, vertical.	
$\mathfrak{I}_m$	imaginary part of	
k	(= ω/c) propagation constant in free space	(App. A)
K	magnetic index	(7.3)
K	eddy viscosity	(App. D)

L	electron loss rate	(9.1)
L	McIlwain parameter	(8.1)
M_1	signal obtained by adding east-west and north-south signals in phase	(3.2)
M_2	signal obtained by shifting east-west phase by 180^{o} and adding it to north-south signal	(3.2)
N_e	electron density	
N	electron density	
n_o, n_x	complex refractice indices	(App. A)
N	number of measurements in sample	(Chapter 4)
P	parameter calculated in D.P.E.	(3.2)
P	ion-pair production rate	(9.1)
p	pressure	
$p_\perp$	momentum normal to magnetic field	(8.1)
Q	parameter calculated in D.P.E.	(3.2)
$\mathcal{R}$	reflection coefficient	(App. A)
R	Fresnel reflection coefficient	(App. A)
R	electron range	(8.3)
r	correlation coefficient	(5.2)
s	sample standard deviation	(4.8)
T	temperature	
u	parameter in Epstein theory	(App. A)
u	velocity to east	(7.3)
V_1	signal from east-west aerial pair	(3.2)
V_2	signal from north-south aerial pair	(3.2)
W	energy to form one ion-pair	(8.3)
w	vertical velocity	(9.2)
X	ω_0^2/ω^2	
Y	ω/ω_L	(App. C)
Y_L	$Y \cos \theta$	(App. E)

Z	ν_m/ω	(App. E)
Z_{eff}	$\frac{5}{2}\ \nu_m/\omega$	(App. E)
α	phase of Fresnel reflection coefficient	(App. A)
α	pitch angle	(8.1)
α_d	electron-ion recombination coefficient	(9.5)
α_{eff}	effective recombination coefficient	(9.5)
β	angle between geomagnetic field and vertical	(8.3)
$\beta(h)$	$\mathrm{Arg}(R_X) - \mathrm{Arg}(R_O)$	(App. A)
ε_0	permittivity of free space	
$\eta(h)$	argument of complex correlation	(App. A)
θ	angle between geomagnetic field and vertical	(2.6)
κ	absorption coefficient	(App. A)
λ	negative ion to electron ratio	(9.5)
λ	normalized energy dissipation function	(8.3)
Λ	McIlwain parameter (invariant latitude)	(8.1)
μ	real part of refractive index	(2.5)
μ	population mean	(4.8)
ν, ν_m	"effective" collision frequency	(App. B)
$\rho(h)$	complex correlation	(App. A)
ρ	wave polarization	(App. A)
ρ	density	
σ	cross-section	(9.3)
σ	Epstein layer parameter	(2.6)
τ	pulsewidth	(App. A)
τ	photochemical lifetime	(9.1)
τ	optical depth	(9.3)
ϕ	initial phase of wave	(App. A)
ϕ	geographic latitude	
ϕ_m	geomagnetic latitude	

χ	solar zenith angle	(4.8)
χ	imaginary part of refractive index	(App. A)
Ω	solid angle	(8.4)
Ω	angular frequency of earth	(7.3)
ω	angular frequency of wave	
ω_L	gyrofrequency	(App. E)
ω_0	plasma frequency	
$< \quad >$	average of a number of measurements	
$\hat{\ }$	(e.g. $\hat{x}$) unit vector	
$[\quad]$	concentration	
$*$	complex conjugate	

CHAPTER 1

INTRODUCTION

In the beginning the aim of this work was to look for meteorological effects on the electron density in the D-region. The D-region is the part of the ionosphere between about 60 and 90 kilometers above the surface of the earth. The effect of meteorological changes in the stratosphere and mesosphere on the electron concentration in the D-region has been an area of research interest during the last twenty years. It was felt that automated daily measurements of the electron densities together with measurement of mesospheric winds would make a worthwhile research project, particularly now that routine temperature information for the upper stratosphere is available from remote measurements by satellite.

However, the discovery of large changes in electron density at the time of a large solar-terrestrial disturbance in August 1972 led to the broader aim of examination of fluctuations in the electron density in the D-region at middle latitudes and their causes.

The electron densities were measured using the differential absorption and differential phase methods on radio wave pulses reflected from within the D-region. There has been some debate on the effect of the assumed reflection model on the electron densities deduced by these methods. For this reason the theory of the reflection process was examined in detail.

Thus the work described in this thesis falls into the following categories:

(a) An examination of the theories of the differential phase and differential absorption experiments.

(b) A description of the practical details of the design and operation of the apparatus, the processing of the data, and a consideration of the experimental uncertainties.

(c) Tests of the agreement between the electron densities calculated from the differential absorption data and those calculated from the differential phase results.

(d) A review of the literature for evidence and theories on meteorological effects on D-region electron densities, and stratosphere-mesosphere coupling.

(e) A comparison of variations in the electron densities measured in the D-region during the winter-spring period of 1972 with variations in meteorological variables in the stratosphere and mesosphere.

(f) An investigation of the diurnal variation of electron densities in the light of photochemical models.

(g) Consideration of the effect of energetic particle precipitation on D-region electron densities at middle latitudes.

(h) The development of a computer model of the photochemistry and transport of nitric oxide, to predict changes in electron density associated with vertical motion. These predictions were compared with experimental results of electron density and radio wave absorption measurements.

CHAPTER 2

THE THEORY OF THE PARTIAL REFLECTION EXPERIMENT

The partial reflection experiment is a method of calculating electron densities in the D-region of the ionosphere. A radio wave pulse is transmitted and the amplitude at the ground of the waves reflected from various levels in the atmosphere is measured.

There have been two approaches to the theory of the experiment. The first approach historically was that used by Gardner and Pawsey (1953), Belrose and Burke (1964), and the majority of investigators since then. It assumes that the ionosphere is horizontally stratified, and the reflections observed in the partial reflection experiment arise from plane discontinuities in electron density. This approach may be termed the Fresnel model.

The second approach was proposed by Flood (1968). It has been used in the experiments of those associated with Flood (von Biel et al., 1970). This is known as the volume scattering model. It assumes that the reflections are due to fluctuations in permittivity in the scattering volume (the entire volume over which the presence of scatterers will give a reflected signal at the receiver at a given time). These fluctuations are assumed to have a time constant long with respect to the period of the radio wave, but short with respect to the period over which the experiment is run. It is also assumed that over the period of the experiment scattering occurs equally often from all points within the scattering volume.

There has been some dispute over the relative merits of the two models (Holt 1969, Flood 1969). An experiment which can differentiate between the two to everyone's satisfaction does not appear to have been designed. Von Biel (1971) has offered some good experimental evidence for the volume scattering case. However, Austin and Manson (1969) give evidence for a localized reflector model (that is, the Fresnel case).

It will be shown that, to the benefit of the experimenter, the electron densities deduced using either model agree very well within the uncertainties introduced by the experimental techniques. In the limit of short pulsewidths the expressions deduced for electron densities from both models agree exactly.

The approach taken here (see appendix A) is to consider one or several Fresnel reflectors, which over the period of the experiment spend equal times in all parts of the scattering volume. From the point of average power returned during the duration of the experiment this approach is equivalent to the volume scatter approach, and gives some insight into the agreement between the two models.

In the actual reduction of ex perimental data the formula arising from the Fresnel method is usually used (Belrose 1970) as it is much simpler to apply than the volume scatter formula.

Another possibility is that reflections do not come from sharp discontinuities in refractive index, but from regions of more gradual change. In this case a full wave solution of the differential equations governing the propagation must be considered. However, it is shown that in this case use of the Fresnel model once again gives sufficient accuracy.

There has been one further change to the theory since the time of Gardner and Pawsey. This involves the use of refractive indices obtained from the generalized magnetoionic theory (e.g. Sen & Wyller, 1960). This theory, which is more clearly explained in a paper by Budden (1965) assumes that the collision frequency between electrons and neutral molecules is proportional to the square of the velocity of the electrons (Phelps and Pack, 1959). The older Appleton-Hartree formula (Budden, 1961) assumed that the collision frequency was directly proportional to the electron velocity. A summary of the Sen and Wyller formulae is given in appendix C.

2.1 POLARIZATION OF THE CHARACTERISTIC WAVES

If the magnetic field of the earth were vertical then vertically propagating ordinary and extraordinary waves would both be circularly polarized. However, in the usual case, when the field is not vertical, the polarization of the waves is in general elliptical.

The polarizations of the vertically propagating ordinary and extraordinary waves for a typical electron density profile above Christchurch were calculated using the Sen-Wyller theory, and are given in table 2.1. Equation C4 (appendix C) was used. The calculations were for a 2.4 MHz wave. At Christchurch the angle of dip is $68^{\circ}10'$ and the magnetic field is 5.91×10^{-5} Tesla. Details of the assumed collision frequency profile are given in appendix B (January values).

Height (km)	N_e (cm^{-3})	Polarization	
		Ordinary	Extraordinary
65	100	$1.00j - 1.58\times10^{-5}$	$-1.00j-1.58\times10^{-5}$
70	100	$1.00j - 3.57\times10^{-5}$	$-1.00j-3.57\times10^{-5}$
75	200	$1.00j - 9.85\times10^{-5}$	$-1.00j-9.85\times10^{-5}$
80	400	$1.00j - 1.64\times10^{-4}$	$-1.00j-1.64\times10^{-4}$
85	700	$0.999j-1.43\times10^{-4}$	$-1.00j-1.43\times10^{-4}$
90	1000	$0.999j-8.07\times10^{-5}$	$-1.00j-8.09\times10^{-5}$

N_e is the electron density

Table 2.1 Polarization of the characteristic waves.

The polarization ρ is defined as the ratio of the y component of the electric field in the wave to the x component, where the z direction is vertically upwards and the geomagnetic field is in the x-z plane.

From table 2.1 both characteristic waves may be considered to be circularly polarized in the D-region.

2.2 MODE COUPLING ON REFLECTION

The mode coupling problem is that on a partial reflection of say the ordinary wave, a small amount of extraordinary wave might be generated. This situation can be examined for the case of a reflection from a plane discontinuity of electron density by requiring that the tangential components of electric field intensity and magnetic field intensity should be continuous across the boundary (Jackson, 1962). The equations which result are given in Appendix A (Equations A8-A11). These

were solved by computer for the same frequency, and the same electron density and collision frequency profiles as used for table 2.1. The results, shown in table 2.2, are for a ratio of electron density below to above the boundary of 0.90. However, the values were the same to within 1% for values of 0.99, 0.90 and 0.50 for this ratio.

The notation used is as follows. Suppose an ordinary mode wave, with electric field $E_0^{(I)}$ is incident on the boundary from below. Then let $E_0^{(R)}$ be the electric field of the ordinary part of the reflected wave, and $E_X^{(R)}$ be the extra-ordinary part (the coupling echo). Define the reflection coefficients, $\mathcal{R}_{OO}$, $\mathcal{R}_{OX}$ by:

$$\mathcal{R}_{OO} = \frac{E_O^{(R)}}{E_O^{(I)}} \qquad \mathcal{R}_{OX} = \frac{E_X^{(R)}}{E_O^{(I)}}$$

$\mathcal{R}_{XX}$ and $\mathcal{R}_{XO}$ are defined similarly, for the case of an incident extraordinary wave. Define the coupling coefficients C_{OX}, C_{XO} by:

$$C_{OX} = \left|\frac{\mathcal{R}_{OX}}{\mathcal{R}_{OO}}\right| \qquad C_{XO} = \left|\frac{\mathcal{R}_{XO}}{\mathcal{R}_{XX}}\right|$$

Connolly and Tanenbaum (1972b) have considered a more general case than the plane discontinuity. They calculated coupling coefficients assuming that changes in electron density take place over a significant fraction of a wavelength. The first order coupled equations of Clemmow and Heading were used. For a wave frequency of 2.5 MHz, magnetic field of 5×10^{-5} tesla, electron density 10^4 cm^{-3}, collision frequency 10^5 sec^{-1} (roughly equivalent to 90 km over Birdling's Flat) they found that:

$C_{OX} = 3 \times 10^{-3}$ $\qquad$ $C_{XO} = 1 \times 10^{-2}$

A coupling coefficient of 3×10^{-3} is equivalent to a factor of about 50 db in power, while 1×10^{-2} is equivalent to a factor of 40 db. Since the equipment used was only sensitive down to about 30 db difference between ordinary and extraordinary waves, mode coupling on reflection can be neglected.

Height	Electron density (cm^{-3})	C_{OX}	C_{XO}
65 km	100	1.11×10^{-5}	5.33×10^{-6}
70	100	3.65×10^{-5}	1.29×10^{-5}
75	200	1.84×10^{-4}	4.83×10^{-5}
80	400	5.74×10^{-4}	1.28×10^{-4}
85	700	1.27×10^{-3}	2.59×10^{-4}
90	1000	1.94×10^{-3}	3.86×10^{-4}

Table 2.2 Coupling coefficients for reflection at a sharp boundary.

2.3 COLLISION FREQUENCY IRREGULARITIES

Since the refractive index in the D-region depends on the collision frequency ν as well as the electron density N, it is possible that changes in collision frequency could contribute to the reflection coefficients. This possibility is discussed by Gregory and Manson (1969a). Suppose the changes in collision frequency and electron density are $\Delta\nu$ and ΔN

respectively across the reflecting boundary. Then Piggot and Thrane (1966) found that for $\alpha = \frac{\Delta\nu/\nu}{\Delta N/N} < 0.2$, the reflection coefficient ratio R_X/R_O is very close to that for $\alpha = 0$. Gregory and Manson argue that for realistic processes in the D-region $\alpha < 0.2$ does hold.

The assumption that the reflection coefficient ratio does not depend on $\Delta\nu/\nu$ is made in the present work.

2.4 THE DIFFERENTIAL ABSORPTION EXPERIMENT

2.4.1 The Basic Equation

It is shown in appendix A (equations A30, A31) that:

$$|E_X| = \frac{B}{4h} |\mathcal{R}_X| \exp(-2\int_0^h \kappa_X \, dz) \tag{2.1}$$

$$|E_O| = \frac{B}{4h} |\mathcal{R}_O| \exp(-2\int_0^h \kappa_O \, dz) \tag{2.2}$$

where E_X, E_O are the electric fields at the receiving aerials of ordinary and extraordinary waves reflected from a height h. Thus

$$\langle |E_X|^2 \rangle = (\frac{B}{4h})^2 \langle |\mathcal{R}_X|^2 \rangle \langle \exp(-4\int_0^h \kappa_X dz) \rangle \tag{2.3}$$

$$\langle |E_O|^2 \rangle = (\frac{B}{4h})^2 \langle |\mathcal{R}_O|^2 \rangle \langle \exp(-4\int_0^h \kappa_O dz) \rangle \tag{2.4}$$

where the brackets denote averaging over the period of the experiment. It has been assumed that the reflection coefficient is statistically independent of the integrated absorption up to the reflecting height.

Suppose there are reflections from heights h and h+Δh. Then:

$$\frac{\langle |E_X(h+\Delta h)|^2 \rangle}{\langle |E_X(h)|^2 \rangle} = \frac{\langle |\mathcal{R}_X(h+\Delta h)|^2 \rangle}{\langle |\mathcal{R}_X(h)|^2 \rangle} \frac{\langle \exp(-4\int_0^h \kappa_X dz) \exp(-4\int_h^{h+\Delta h} \kappa_X dz) \rangle}{\langle \exp(-4\int_0^h \kappa_X dz) \rangle} \tag{2.5}$$

Making the assumption that the absorption from h to h+Δh is statistically independent of the integrated absorption up to h,

$$\frac{\langle |E_X(h+\Delta h)|^2 \rangle}{\langle |E_X(h)|^2 \rangle} = \frac{\langle |\mathcal{R}_X(h+\Delta h)|^2 \rangle}{\langle |\mathcal{R}_X(h)|^2 \rangle} \langle \exp(-4\int_h^{h+\Delta h} \kappa_X dz) \rangle \tag{2.6}$$

The approximation is now made that

$$\int_h^{h+\Delta h} \kappa_X \, dz = \bar{\kappa}_X \, \Delta h \tag{2.7}$$

where $\bar{\kappa}_X$ denotes the height average of κ_X over the interval Δh. Take natural logarithms and let the operator Δ denote the difference between a value at (h+Δh) and at h. Then

$$\Delta \ell n \langle |E_X|^2 \rangle = \Delta \ell n \langle |\mathcal{R}_X|^2 \rangle + \ell n \langle \exp(-4\bar{\kappa}_X \Delta h) \rangle \tag{2.8}$$

If it is assumed that the electron density and collision frequency stay constant over the period of the experiment $\bar{\kappa}_X$ will be constant and

$$\ell n \langle \exp(-4\bar{\kappa}_X \Delta h) \rangle = -4\bar{\kappa}_X \Delta h$$

$$\Delta \ell n \langle |E_X|^2 \rangle = \Delta \ell n \langle |\mathcal{R}_X|^2 \rangle - 4\bar{\kappa}_X \Delta h$$

Similarly,

$$\Delta \ell n \langle |E_O|^2 \rangle = \Delta \ell n \langle |\mathcal{R}_O|^2 \rangle - 4\bar{\kappa}_O \Delta h$$

Thus

$$\Delta \ell n \frac{\langle |E_X|^2 \rangle}{\langle |E_O|^2 \rangle} = \Delta \ell n \frac{\langle |\mathcal{R}_X|^2 \rangle}{\langle |\mathcal{R}_O|^2 \rangle} - 4\overline{(\kappa_X - \kappa_O)}\,\Delta h \qquad (2.9)$$

To obtain electron density, $\overline{(\kappa_X - \kappa_O)}$ is replaced by $\left(\frac{\overline{\kappa_X - \kappa_O}}{N}\right)\bar{N}$. Thus

$$\bar{N} = \frac{\Delta \ell n \frac{\langle |\mathcal{R}_X|^2 \rangle}{\langle |\mathcal{R}_O|^2 \rangle} - \Delta \ell n \frac{\langle |E_X|^2 \rangle}{\langle |E_O|^2 \rangle}}{4\left(\frac{\overline{\kappa_X - \kappa_O}}{N}\right)\Delta h} \qquad (2.10)$$

2.4.2 The differences between the results obtained from the volume scattering and the simple Fresnel models*

It is shown in appendix A (equation A27) that Flood's volume scattering theory leads to the expression:

$$\frac{\sigma_X}{\sigma_O} = \frac{\langle |\mathcal{R}_X|^2 \rangle}{\langle |\mathcal{R}_O|^2 \rangle} = \left|\frac{R_X^2}{R_O^2}\right| \left(\frac{\sinh(c\tau\kappa_X)}{c\tau\kappa_X}\right) \left(\frac{c\tau\kappa_O}{\sinh(c\tau\kappa_O)}\right) \qquad (2.11)$$

Thus for this model, as the pulsewidth τ tends to zero,

$$\frac{\langle |\mathcal{R}_X|^2 \rangle}{\langle |\mathcal{R}_O|^2 \rangle} \rightarrow \left|\frac{R_X^2}{R_O^2}\right|$$

which is the value obtained for the simple Fresnel model of a single plane discontinuity.

---

* A similar approach to this was used by Austin (1969). This section is included here for completeness.

To find the difference likely in the calculated electron densities for the experiment (pulsewidth τ = 25 microseconds) between using the volume scatter reflection coefficients and the simple Fresnel ones calculations were made for a typical electron density profile (approximately the average profile found by the DAE experiment over Christchurch for winter 1973). The difference for a given set of experimental results will be

$$E = \frac{\Delta \ell n\left(\left|\frac{\sinh(c\tau\kappa_X)}{c\tau\kappa_X}\right|\left|\frac{c\tau\kappa_O}{\sinh(c\tau\kappa_O)}\right|\right)}{4\left(\frac{\overline{\kappa_X - \kappa_O}}{N}\right)\Delta h} \qquad (2.12)$$

Calculations for a 2.4 MHz wave were made for Δh = 5 km and collision frequency profiles as in appendix B. The results are given in table 3.3.

Another possibility is that the reflection for one height could be from a simple Fresnel discontinuity, while the reflection for another height is due to volume scattering. This case is considered under the "mixed" heading in table 3.3 (Δh = 5 km)

In a typical experimental run the uncertainties due just to the random scatter of data (300 samples over ten minutes) are at least 5%. The average daily fractional uncertainty in the $\overline{\text{mean}}$ electron densities, worked out from about four runs daily near noon for winter 1973 was at least 19% for all heights (table 4.5).

Considering this, along with the assumptions made (such as the replacement of the integral in equation 2.7 and the assumption that the electron density is constant

throughout the scattering volume) it appears that the differences between the volume scatter and simple Fresnel formulae are unimportant experimentally. The equation used in the experimental work will be:

$$\bar{N} = \frac{\Delta \ell n \left| \frac{R_X^2}{R_O^2} \right| - \Delta \ell n \frac{\langle |E_X|^2 \rangle}{\langle |E_O|^2 \rangle}}{4 \left(\frac{\overline{\kappa_X - \kappa_O}}{N} \right) \Delta h} \qquad (2.13)$$

It should be noted that $\left| \frac{R_X^2}{R_O^2} \right|$ is independent of the electron density change at the boundary (Gregory and Manson, 1969a). Also both $\left| \frac{R_X^2}{R_O^2} \right|$ and $\left(\frac{\overline{\kappa_X - \kappa_O}}{N} \right)$ depend mainly on collision frequency, and their weak dependence on electron concentration can easily be allowed for by iteration.

Height (km)	N_e (cm^{-3})	Difference (E)		Difference (mixed)	
		Absolute	Percent	Absolute	Percent
65.0	100				
67.5	100	+2 cm^{-3}	2%	+2 cm^{-3}	2%
70.0	100				
72.5	140	+6	4%	+8	6%
75.0	200				
77.5	280	+11	4%	+22	8%
80.0	400				
82.5	520	+11	2%	-35	-7%
85.0	700				
87.5	830	+38	5%	-49	-6%
90.0	1000				

N_e is the electron density

Table 2.3 Differences between volume scatter and simple Fresnel electron densities from DAE measurements.

2.5 THE DIFFERENTIAL PHASE EXPERIMENT

2.5.1 The Basic Equation

It is shown in appendix A (equation A40) that for a volume scattering model the complex correlation

$$\rho(h) = \frac{\langle E_X E_O^* \rangle}{(\langle |E_X|^2 \rangle \langle |E_O|^2 \rangle)^{\frac{1}{2}}} \tag{2.14}$$

has argument

$$\eta(h) = \beta(h) - 2k\int_0^h (\mu_X - \mu_O)dz + (\phi_X - \phi_O) + \mathcal{E}(h) \tag{2.15}$$

where

$\beta(h) = \text{Arg}(R_X) - \text{Arg}(R_O)$ $\quad R_{X,O}$ Fresnel coefficients

ϕ_X, ϕ_O are the initial phases of the ordinary and extra-ordinary waves, which are assumed to have the same initial amplitude.

μ_X, μ_O are the real parts of the refractive indices. $\mathcal{E}(h)$ is a term involving the pulsewidth τ.

$$\mathcal{E}(h) = \text{Arg}\left[\frac{\sin\left\{\frac{k(n_X - n_O)c\tau}{2}\right\}}{\frac{k(n_X - n_O)c\tau}{2}}\right] \tag{2.16}$$

Suppose the complex correlation is measured at two heights h_1 and h_2. Then

$$\eta(h_2) - \eta(h_1) = \beta(h_2) - \beta(h_1) - 2k\int_{h_1}^{h_2} (\mu_X - \mu_o)dz + \mathcal{E}(h_2) - \mathcal{E}(h_1) \tag{2.17}$$

As an approximation put:

$$\int_{h_1}^{h_2} (\mu_X - \mu_O)\, dz = \overline{(\mu_X - \mu_O)}\,\Delta h \qquad (2.18)$$

and put

$$\overline{(\mu_X - \mu_O)} = \overline{\left(\frac{\mu_X - \mu_O}{N}\right)}\ \bar{N}\ \Delta h \qquad (2.19)$$

Thus

$$\bar{N} = \frac{\Delta\beta - \Delta\eta + \Delta\varepsilon}{2k\ \overline{\left(\frac{\mu_X - \mu_O}{N}\right)}\ \Delta h} \qquad (2.20)$$

Some trial computations involving the Sen-Wyller refractive indices showed that $\beta = \text{Arg}\left(\frac{R_X}{R_O}\right)$ is independent of the electron density change across the boundary. Also both β and $\overline{\left(\frac{\mu_X - \mu_O}{N}\right)}$ are only weakly dependent on electron density, depending mainly on collision frequency. Figure 2.1, for 80 km, is typical.

2.5.2 The difference between the volume scatter and simple Fresnel formulae

The difference due to the effect of the finite pulsewidth will be:

$$E = \frac{\Delta\varepsilon}{2k\ \overline{\left(\frac{\mu_X - \mu_O}{N}\right)}\ \Delta h}$$

This was computed for the same profile as used in table 2.3, for Δh = 5 km, τ = 25 microseconds, frequency = 2.4 MHz.

Table 2.4 gives this as an absolute value and a percentage (under the "volume" column). The column headed "mixed" is the percentage difference from the Fresnel case if there is volume scatter from the upper height but Fresnel reflection at the lower height.

The uncertainty in differential phase electron density for an experimental run (75 independent samples over ten minutes) due to the scatter of the data is usually at least 30%. Thus the differences between the two formulae are unimportant experimentally below about 85 km.

Height (km)	N_e (cm^{-3})	Difference (E) (cm^{-3})	Percent difference	
			Volume	Mixed
65.0	100			
67.5	100	2.6	3%	3%
70.0	100			
72.5	140	8.4	6%	7%
75.0	200			
77.5	280	19	7%	9%
80.0	400			
82.5	520	33	6%	10%
85.0	700			
87.5	830	-580	-70%	-70%
90.0	1000			

N_e is electron density

Table 2.4 Difference between volume scattering and simple Fresnel electron densities for differential phase.

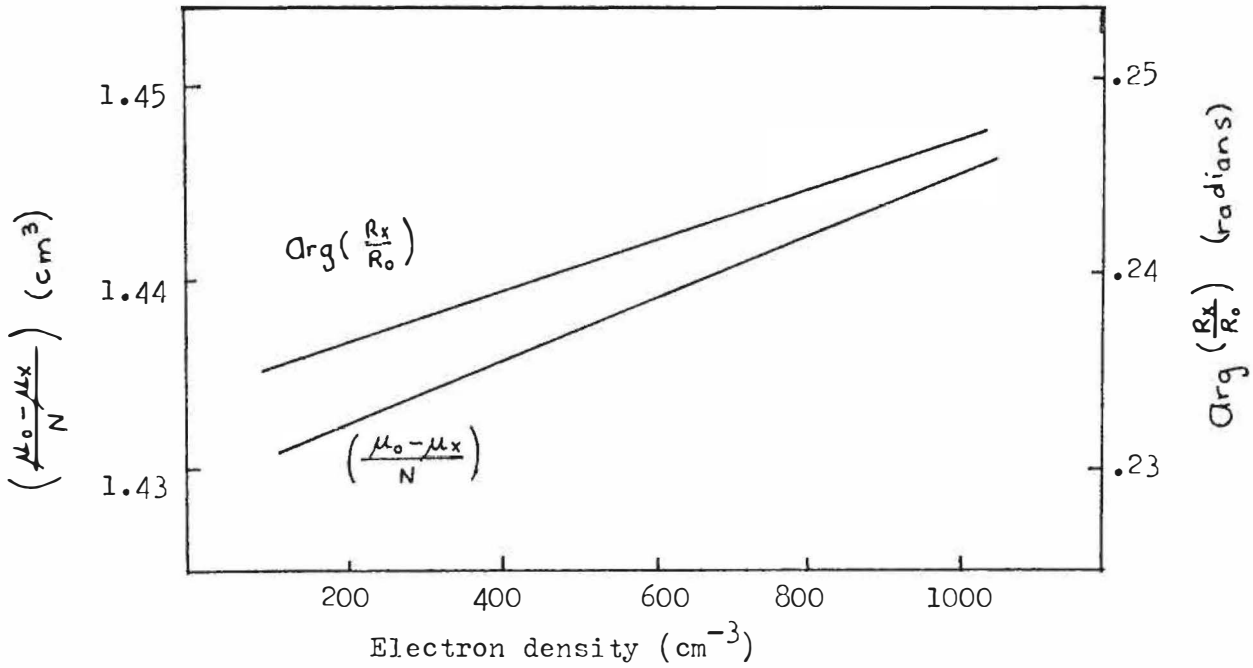

Fig 2.1 Dependence of differential phase parameters on electron density. (80 km, f=2.4 Mhz)

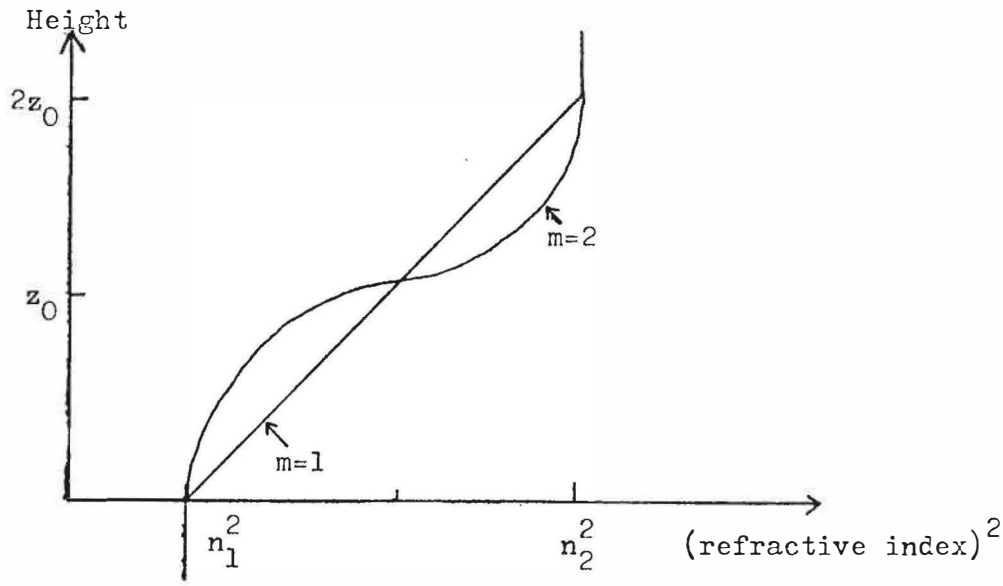

Fig 2.2 The profiles considered by Austin (1966)

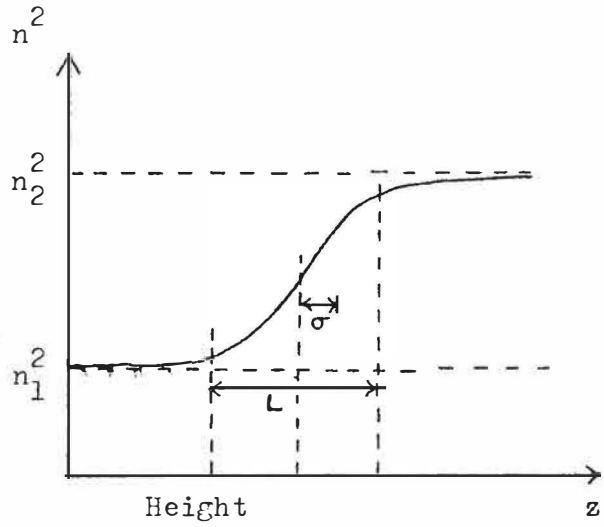

Fig 2.3 Epstein tanh profile.

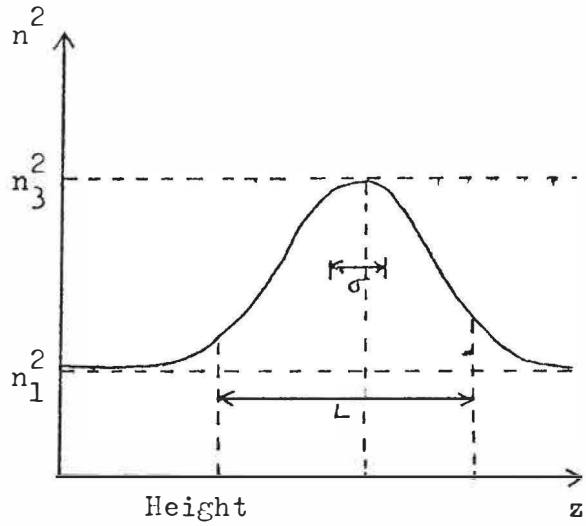

Fig 2.4 Epstein $sech^2$ profile.

tanh profile: The range L for $(n^2-n_1^2)$ to go from 10 % to 90% of its final value is $L = 4.38\sigma$

$sech^2$ profile: The range L over which $(n^2 - n_1^2)$ is more than 10% of its value at the peak is $L = 5.0\sigma$

2.6 SCATTERING FROM A GRADUAL TRANSITION IN REFRACTIVE INDEX

The scattering model discussed so far has depended on discontinuities in electron density (i.e. changes in electron density over a distance small with respect to a wavelength), so that the W.K.B. approximation could be used right up to the discontinuity from both sides, and matched across the discontinuity.

Connolly and Tanenbaum (1972a) and Austin (1966) have considered the case of a more gradual change in refractive index. In these cases a full wave solution for the differential equations governing the propagation of radio waves must be used.

Austin (1966) uses a method due to Millington (1965) to get a full wave solution to the equation

$$\frac{d^2E}{dZ^2} + k_0^2 n^2 F = 0 \qquad (2.22)$$

for profiles of the form (figure 2.2)

$$\left.\begin{aligned} n^2 &= n_1^2 && Z < 0 \\ &= n_1^2 + \frac{\delta Z^m}{2Z_0^m} && 0 < Z < Z_0 \\ &= n_2^2 - \frac{\delta(2Z-Z)}{2Z_0^m} && Z_0 < Z < 2Z_0 \\ &= n_2^2 && Z > 2Z_0 \end{aligned}\right\} \qquad (2.23)$$

where δ is a constant.

Austin draws plots of a factor F which modifies the Fresnel value of $R = \frac{n_2-n_1}{n_2+n_1}$, as a function of Λ, the thickness of the transition layer in wavelengths.

$$\mathcal{R} = FR$$

There is no discussion on whether F actually depends on n_1 and n_2. If it does depend on these F will differ for the ordinary and extraordinary modes, and the ratio $\frac{\mathcal{R}_X}{\mathcal{R}_O}$ will differ from the Fresnel value.

Austin also considers reflection from a layer of the form:

$$\left.\begin{aligned} n^2 &= 1 + \delta \sin^m \left(\frac{\pi Z}{Z_0}\right) \qquad 0 < Z < Z_0 \\ \text{and } n^2 &= 1 \qquad\qquad\qquad\qquad \text{elsewhere.} \end{aligned}\right\} \tag{2.24}$$

Here Austin finds that $|\mathcal{R}| = |R|F$ where R is the Fresnel reflection coefficient, and F is a purely geometrical factor. In this case the ratio of the reflection coefficients for O and X modes will be the same as the ratio in the simple Fresnel case. However, in his derivation Austin obtains F in the form

$$F = f_0 + \delta f_1 + \delta^2 f_2 + \cdots$$

where the f_i's are purely geometrical functions. He assumes that this series for F will converge for δ sufficiently small, and truncates it to $F = f_0$. Thus the fact that F is a purely geometrical factor is assumed in the derivation and not proven. Hence the comment of Austin and Manson (1969) that the effect of a gradual change in refractive index is "to reduce the reflection coefficient by a geometrical factor which is equivalent for ordinary and extraordinary modes" must be taken as not proven.

To investigate this effect on the electron densities calculated from experimental results the approach of Connolly and Tanenbaum (1972a) of considering partial reflections from

an Epstein profile was followed. The Epstein theory (see appendix A) gives a full wave solution for the equation

$$\frac{d^2E}{dZ^2} + k^2n^2E = 0 \qquad (2.25)$$

for profiles of refractive index n(Z) of the form:

$$n^2 = n_1^2 + \frac{e^u}{(e^u+1)^2}\{(n_2^2-n_1^2)(e^u+1)+\varepsilon_3\}; \quad u = \frac{Z}{\sigma} \qquad (2.26)$$

Several assumptions are involved in using this theory for the case of an ionosphere with a magnetic field present.

(1) It is assumed that in the region of interest there is no coupling between extraordinary and ordinary waves. That is, if an ordinary wave only is incident on the region, so that its electric field at the base of the region satisfies

$$\frac{d^2E}{dZ^2} + k^2n_0^2E = 0,$$

then the electric field will satisfy that equation throughout the region (and similarly for an extraordinary wave).

(2) It is assumed that the collision frequency is constant throughout the layer.

Two types of profile were considered:

(a) The Epstein tanh Profile (figure 2.3)

$$n^2 = n_1^2 + \frac{e^u}{e^u+1}(n_2^2-n_1^2); \quad u = \frac{Z}{\sigma} \qquad (A45)$$

It is assumed that a given electron density distribution gives rise to both ordinary and extraordinary profiles of this same type. This can be shown to be true for the Appleton-Hartree quasi-longitudinal case, since

$$n_0^2 = 1 - \frac{X}{1 - iZ + Y_L} \qquad n_X^2 = 1 - \frac{X}{1 - iZ - Y_L}$$

(Budden 1961)

where $X = \frac{N_e e^2}{\varepsilon_0 m \omega^2}$ $\quad Z = \frac{\nu}{\omega}$ $\quad Y_L = \frac{\omega}{\omega_L} \cos\theta$

N_e electron density, m electron mass, ν collision frequency, ω_L gyrofrequency, θ angle between earth's field and the vertical.

Thus

$$n_X^2 - n_{X_1}^2 - \frac{e^u}{(e^u+1)}(n_{X_2}^2 - n_{X_1}^2) = \left(\frac{1-iZ+Y_L}{1-iZ-Y_L}\right)\left[n_0^2 - n_{0_1}^2 - \frac{e^u}{(e^u+1)}(n_{0_2}^2 - n_{0_1}^2)\right] \tag{2.27}$$

So that if the collision frequency ν, and hence Z is constant throughout the layer,

$$n_0^2 = n_{0_1}^2 + \frac{e^u}{e^u+1}(n_{0_2}^2 - n_{0_1}^2)$$

implies

$$n_X^2 = n_{X_1}^2 + \frac{e^u}{e^u+1}(n_{X_2}^2 - n_{X_1}^2)$$

It was shown earlier in this section (see table 2.1) that propagation over Birdling's Flat is quasi-longitudinal. Thus the ratio of reflection coefficients is given by $\frac{R_X}{R_O}$ from equation A.46.

The maximum error due to assuming Fresnel reflection coefficients when the actual reflections are from an Epstein profile will occur when the lower reflection is from a simple Fresnel discontinuity and the upper reflection is from an Epstein profile. This error is shown in table 2.5, for

reflecting regions 5 km apart and winter collision frequencies for a 2.4 MHz wave.

Height (km)	Electron density (cm^{-3})	Difference			
		Amplitude measurements		Phase measurements	
		Absolute (cm^{-3})	Percent	Absolute (cm^{-3})	Percent
65.0	100				
67.5	100	-0.1	-0.1%	-3	-3%
70.0	100				
72.5	140	1	0.7%	-3	-2%
75.0	200				
77.5	280	3	1%	-7	-3%
80.0	400				
82.5	520	26	5%	-10	-2%
85.0	700				
87.5	830	90	11%	-10	-1%
90.0	1000				

Table 2.5 Differences in predicted electron density between the Epstein tanh profile and the Fresnel discontinuity model.

It was found that $\frac{\mathcal{R}_X}{\mathcal{R}_O}$ was identical to the Fresnel ratio $\frac{R_X}{R_O}$ for small values of σ, but there was an increasing disparity between $\frac{\mathcal{R}_X}{\mathcal{R}_O}$ and $\frac{R_X}{R_O}$ as σ increased. However, as σ increased the values of $\mathcal{R}_O$ and $\mathcal{R}_X$ decreased. In the calculations the largest value of σ which gave a value of both $\mathcal{R}_X$ and $\mathcal{R}_O$ greater than 10^{-6} (Manson et al., 1969) was used. It was found that σ had to be less than 40 m at all heights (which gives $\frac{L}{\lambda} < 1.4$). A difference of 10% between the electron density above and below the layer was used.

(b) The Epstein $sech^2$ Profile (figure 2.4)

This refractive index profile is:

$$n^2 = n_1^2 + (n_3^2 - n_1^2)\ sech^2\ (\frac{z}{2\sigma}) \qquad (A.47)$$

A similar approach to that used for the tanh profile was followed to find the possible difference from the simple Fresnel model. For a difference of 10% in electron density between the peak and the base it was found that $\sigma < 40$ m for reasonable reflection coefficients ($|\mathcal{R}| > 10^{-6}$). This corresponds to $\frac{L}{\lambda} < 1.4$.

Height (km)	Electron density (cm^{-3})	Difference			
		Amplitude measurements		Phase measurements	
		Absolute (cm^{-3})	Percent	Absolute (cm^{-3})	Percent
65.0	100				
67.5	100	0.5	0.5%	-3	-3%
70.0	100				
72.5	140	5	4%	-4	-3%
75.0	200				
77.5	280	16	6%	-6	-2%
80.0	400				
82.5	520	50	10%	-3	-1%
85.0	700				
87.5	830	155	19%	-2	-0.2%
90.0	1000				

Table 2.6 Differences in predicted electron density between the Epstein $sech^2$ profile and the Fresnel discontinuity model.

The differences shown in tables 2.5 and 2.6 are the maximum likely for this effect, and will be smaller for smaller values of characteristic length σ. Thus up to about 85 km the differences between the Fresnel and the Epstein tanh and $sech^2$ models in terms of predicted electron densities from the same experimental data could be about the same as or slightly larger than the uncertainties due to the random scatter of the data.

2.7 THE CHANGE OF REFLECTION COEFFICIENTS WITH HEIGHT

In the derivation of the volume scattering formulae (appendix A) it was assumed that the Fresnel reflection coefficients R_X, R_O were constant throughout the scattering volume. Coyne and Belrose (1973) discuss a model which allows for variations in the reflection coefficients within the scattering volume.

Their analysis of the experimental data involves deconvolving the observed reflection ratio curve to obtain a curve which would result from a very short pulse. Their analysis of one example, when there was a valley in the electron density profile showed that the simple theory (using the observed reflection ratio curve) badly overestimated the electron density in the valley region when a 50 microsecond transmitter pulse was used.

However, the error could be significantly less for 25 microsecond pulses. Part of the error in the simple theory is due to the neglect of the differential absorption within the scattering volume (the difference given by equation 2.12) which will be more significant for 50 microsecond pulses than for 25 microsecond pulses. Also the resolution afforded by a

25 microsecond pulse ($\frac{c\tau}{2}$ = 4 km) is much better than that of a 50 microsecond pulse (8 km).

The deconvolution process used by Coyne and Belrose was rather involved, and for 25 microsecond pulses would probably require height sampling at closer intervals than 2.5 km. There was insufficient time to make such an analysis of the Birdling's Flat results. It is realized that the partial reflection experiment analysis used in this thesis will not pick up details of structure finer than the resolution allowed by the pulsewidth. However, deep valleys in electron density profiles do not appear very frequently in rocket probe measurements (e.g. Mechtly et al., 1972a), so errors as large as those suggested by Coyne and Belrose are not likely to occur very often.

2.8 THE FUNDAMENTAL UNCERTAINTY IN THE FRESNEL MODEL

In the automatic data collection method which is used here for the partial reflection experiments, the receiver output is sampled at time intervals corresponding to 2.5 km intervals in height. Assume that a received signal for a given sampling channel has arisen from only one discrete plane irregularity. Then there is an uncertainty in the height of this irregularity of $\pm \frac{c\tau}{4}$ where τ is the pulsewidth of the transmitted pulse, since the reflections received at a given time may have returned from anywhere within the scattering volume. (A receiver bandwidth which is too narrow will lead to further uncertainty.)

In the calculation of electron densities by equations (2.13) and (2.21) data from channels 5 km apart was used. Thus, for τ = 25 microseconds ($\frac{c\tau}{4}$ = 1.8 km) this uncertainty could mean an error of up to 72% in Δh and thus in electron density.

The situation will not generally be quite this bad however. In the absence of any other information it must be assumed that the height from which a reflection comes is equally likely to be any height within the scattering volume. The situation is as in figure 2.5. In the experimental case d = 5 km, a = $\frac{c\tau}{4}$ = 1.8 km. The probability density function for ℓ, the distance between the two reflectors will be as in figure 2.6. From this figure it can be seen that there is a 75% probability that ℓ lies between (d-a) and (d+a). Thus a is a good measure of the error likely to arise. In the experimental case the percentage uncertainty $\frac{a}{d} \times 100$ from this source is 36%.

Note that this source of uncertainty disappears entirely if a volume scattering model is applicable, and it will be considerably reduced if reflections come from several heights within the scattering volume over the period of a given experimental run.

Also, if the simple Fresnel model is the appropriate one, scaling the experimental values from the receiver trace at the amplitude peaks rather than at fixed intervals could reduce this uncertainty, but this is difficult to do in an automatic system.

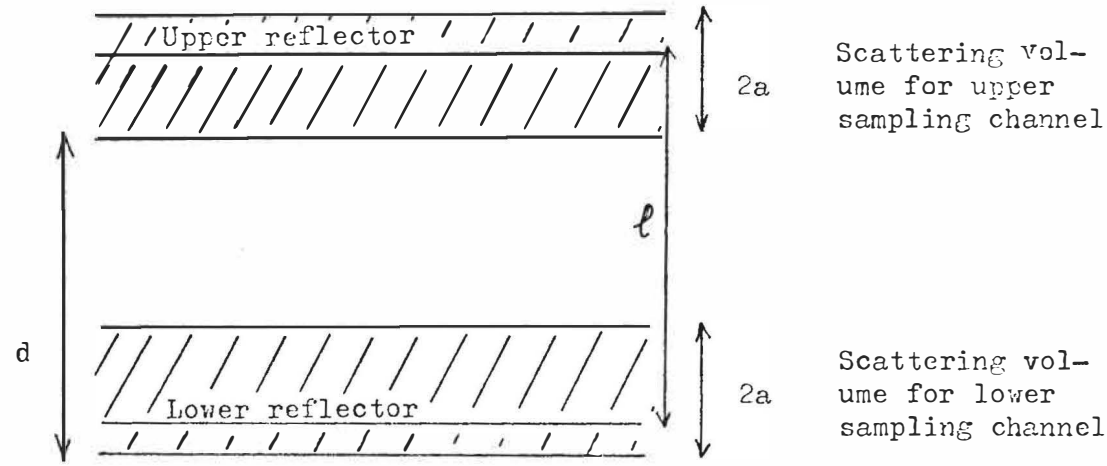

Fig 2.5: Uncertainty in reflector separation.

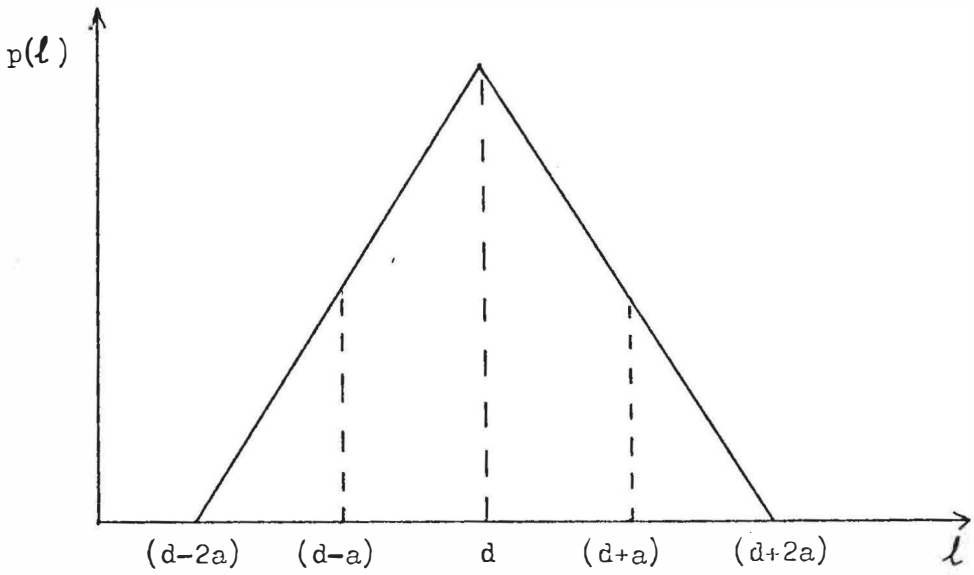

Fig 2.6: Probability density for ℓ.

2.9 SUMMARY

The main difference between the use of volume scatter and simple Fresnel models in calculating electron densities from partial reflection data is an uncertainty in the latter model because of the uncertainty in the position of the hypothetical reflecting layers. In the experiment used at Birdling's Flat this uncertainty in electron density is about 35%. Other differences in the electron density predictions of the two models are less than, or of the order of, the uncertainty due to the scatter in the experimental results below about 85 km.

If reflections arise from a gradual transition in refractive index rather than a sharp discontinuity the differential absorption electron densities based on the simple Fresnel model could be too low by a factor ranging from 0.1% to 10% for 67.5 to 82.5 km. The error in electron density predictions from differential phase measurements due to this effect is less than 3% over the same height range.

The equations used to calculate electron densities will be:

Differential Absorption:

$$\bar{N} = \frac{\Delta \ell n \left| \frac{R_X^2}{R_O^2} \right| - \Delta \ell n \frac{\langle |E_X|^2 \rangle}{\langle |E_O|^2 \rangle}}{4 \left[\frac{\kappa_X - \kappa_O}{N} \right] \Delta h} \qquad (2.13)$$

Differential Phase:

$$\bar{N} = \frac{\Delta\beta - \Delta\eta}{2k \left[\frac{\mu_X - \mu_O}{N} \right] \Delta h} \qquad (2.14)$$

$\langle|E_X|^2\rangle$, $\langle|E_O|^2\rangle$ and η are measured experimentally, at 2.5 km intervals fixed by the equipment.

The other parameters are calculated from an assumed collision frequency profile, details of which are given in appendix B.

CHAPTER 3

EXPERIMENTAL DETAILS

To determine electron densities by the differential absorption method the amplitudes of the ordinary and extra-ordinary radio wave reflections from various heights are required. For differential phase electron density calculations the difference in phase between the ordinary and extraordinary reflections is needed. This chapter describes the methods used to measure these quantities.

The phase difference between the two modes has been measured in two ways. One method is to measure the difference between the phases of the ordinary and extraordinary reflections from a given height directly (Austin 1971). A variation on this method is to measure the instantaneous phases of the ordinary and extraordinary modes to obtain the difference (Belrose et al., 1972b). The other method was first suggested and used by von Biel et al. (1970) and involves the measurement of the complex correlation $\rho(h)$ (section 2.5.1) between the ordinary and extraordinary reflections. This was the method used in the present work. (It has also been used recently by Wiersma and Sechrist (1972).)

The Birdling's Flat field station where the experiments were carried out is situated at 172.7^{o}E, 43.8^{o}S.

3.1 TRANSMITTING EQUIPMENT

The transmitter at Birdling's Flat has the following characteristics:

Frequency	2.40 MHz
Peak power	100 kW
Pulsewidth	Variable, from a minimum of about 5 microsec. For these measurements 25 microsec. was used.

The transmitter feeds a broadside array of four in-phase pairs of half-wave folded dipoles. The dipole pairs run East-West. The calculated gain of this array relative to an isotropic radiator is 14 db.

3.2 THE RECEIVED SIGNALS

The receiving array comprises four half-wave folded dipoles arranged in a square. The feeders from the two north-south dipoles are taken to the center of the square where they are connected in parallel and fed to the receiving hut. The east-west pair is treated similarly. Each aerial pair has a calculated gain of 8 db relative to an isotropic radiator.

Consider an orthogonal coordinate system (x,y,z) with $\hat{z}$ vertically upwards, $\hat{x}$ to the east (that is parallel to the transmitting array dipoles), $\hat{y}$ to the north. The electric field of a radio wave of angular frequency ω transmitted from the transmitter array can thus be expressed as:

$$\underset{\sim}{E}_T = a\,\hat{x}\,e^{j\omega t} = a\left(\frac{\hat{x}+j\hat{y}}{2}\right)e^{j\omega t} + a\left(\frac{\hat{x}-j\hat{y}}{2}\right)e^{j\omega t} \qquad (3.1)$$

where a is a constant. Thus the linearly polarized transmitted wave can be decomposed into an ordinary (polarization $\rho = +j$)

and an extraordinary ($\rho = -j$) wave, which can be considered to propagate independently in the D-region.

The field at the receiving aerials, reflected back from the ionosphere can thus be written as the sum of an ordinary and an extraordinary wave:

$$\underset{\sim}{E} = \left[\frac{E_0}{\sqrt{2}}(\hat{x}+j\hat{y}) + \frac{E_X}{\sqrt{2}}(\hat{x}-j\hat{y})\right] e^{j\omega t} \qquad (3.2)$$

where the subscripts 0 and X refer to ordinary and extraordinary respectively. E_0 and E_X are functions of time (i.e. of the height from which the transmitter pulse is being reflected), which contain both amplitude and phase parts.

The signal from the east-west aerials will be proportional to the x component of (3.2), i.e.

$$V_1 e^{j\omega t} = \frac{B}{\sqrt{2}}[E_0 + E_X] e^{j\omega t} \qquad (3.3)$$

and the signal from the north-south pair is:

$$V_2 e^{j\omega t} = \frac{Bj}{\sqrt{2}}[E_0 - E_X] e^{j\omega t} \qquad (3.4)$$

where B is a constant. From (3.3) and (3.4),

$$E_0 = \frac{1}{B\sqrt{2}}[V_1 - jV_2] = \frac{1}{\sqrt{2}B}[V_1 + V_2 e^{-j\frac{\pi}{2}}] \qquad (3.5)$$

$$E_X = \frac{1}{B\sqrt{2}}[V_1 + jV_2] = \frac{1}{\sqrt{2}B}[V_1 + V_2 e^{j\frac{\pi}{2}}] \qquad (3.6)$$

Thus the amplitude of the ordinary mode signal can be found (to within a multiplicative constant) by phase-shifting

the signal from the north-south antenna by 90^{o}, adding it to the signal from the east-west antenna, and putting the resultant signal through an amplitude detector. The extra-ordinary signal amplitude can be obtained similarly, but with a -90^{o} shift of the north-south signal. Denoting the outputs from the detector for these two signals as $|A_X|$, $|A_O|$ respectively gives:

$$\frac{\langle|E_X|^2\rangle}{\langle|E_O|^2\rangle} = \frac{\langle|A_X|^2\rangle}{\langle|A_O|^2\rangle} \tag{3.7}$$

The complex correlation coefficient is defined as:

$$\rho = \frac{\langle E_X E_O^*\rangle}{(\langle|E_X|^2\rangle\langle|E_O|^2\rangle)^{\frac{1}{2}}} \tag{2.14}$$

Let $M_1 e^{j\omega t}$ be the signal obtained by adding the signals from the east-west and north-south aerials in phase.

Thus

$$M_1 = \frac{B}{\sqrt{2}}\{(E_O+E_X) + j(E_O-E_X)\} \tag{3.8}$$

Let $M_2 e^{j\omega t}$ be the signal obtained by shifting the phase of the east-west signal by 180^{o} and adding it to the north-south signal.

$$M_2 = \frac{B}{\sqrt{2}}\{(E_O+E_X) - j(E_O-E_X)\rangle \tag{3.9}$$

$$\text{Thus } \langle|M_1|^2\rangle + \langle|M_2|^2\rangle = 2B^2(\langle|E_O|^2\rangle + \langle|E_X|^2\rangle) \tag{3.10}$$

$$\langle|M_1|^2\rangle - \langle|M_2|^2\rangle = -2jB^2(\langle E_X E_O^*\rangle - \langle E_X^* E_O\rangle) \tag{3.11}$$

$$\text{also } \langle|V_1|^2\rangle + \langle|V_2|^2\rangle = B^2(\langle|E_O|^2\rangle + \langle|E_X|^2\rangle) \tag{3.12}$$

$$\langle|V_1|^2\rangle - \langle|V_2|^2\rangle = B^2(\langle E_X E_O^*\rangle + \langle E_O^* E_X\rangle) \tag{3.13}$$

Define two new variables P and Q:

$$P \equiv \frac{\langle|V_1|^2\rangle-\langle|V_2|^2\rangle}{\langle|V_1|^2\rangle+\langle|V_2|^2\rangle}\cdot\frac{\langle|A_X|^2\rangle+\langle|A_O|^2\rangle}{(\langle|A_X|^2\rangle\langle|A_O|^2\rangle)^{\frac{1}{2}}} = \frac{\langle E_X E_O^*\rangle+\langle E_O^* E_X\rangle}{(\langle|E_X|^2\rangle\langle|E_O|^2\rangle)^{\frac{1}{2}}} \tag{3.14}$$

$$Q \equiv \frac{\langle|M_1|^2\rangle-\langle|M_2|^2\rangle}{\langle|M_1|^2\rangle+\langle|M_2|^2\rangle}\cdot\frac{\langle|A_X|^2\rangle+\langle|A_O|^2\rangle}{(\langle|A_X|^2\rangle\langle|A_O|^2\rangle)^{\frac{1}{2}}} = -j\frac{\langle E_X E_O^*\rangle-\langle E_O^* E_X\rangle}{(\langle|E_X|^2\rangle\langle|E_O|^2\rangle)^{\frac{1}{2}}} \tag{3.15}$$

Then (2.14) can be written as:

$$\rho = \frac{P}{2} + j\,\frac{Q}{2} \tag{3.16}$$

But by definition P and Q are both real. Thus if the complex correlation is written as:

$$\rho = |\rho|\, e^{i\eta} \tag{3.17}$$

then

$$|\rho| \cos\eta = \frac{P}{2} \tag{3.18}$$

$$|\rho| \sin\eta = \frac{Q}{2} \tag{3.19}$$

Hence

$$|\rho| \sin\eta = \tfrac{1}{2}\left(\frac{\langle|M_1|^2\rangle-\langle|M_2|^2\rangle}{\langle|M_1|^2\rangle+\langle|M_2|^2\rangle}\right)\left(\frac{\langle|A_O|^2\rangle+\langle|A_X|^2\rangle}{(\langle|A_O|^2\rangle\langle|A_X|^2\rangle)^{\frac{1}{2}}}\right) \tag{3.20}$$

$$|\rho| \cos\eta = \tfrac{1}{2}\left(\frac{\langle|V_1|^2\rangle-\langle|V_2|^2\rangle}{\langle|V_1|^2\rangle+\langle|V_2|^2\rangle}\right)\left(\frac{\langle|A_O|^2\rangle+\langle|A_X|^2\rangle}{(\langle|A_O|^2\rangle\langle|A_X|^2\rangle)^{\frac{1}{2}}}\right) \tag{3.21}$$

Thus measuring the mean squared values for six different signals gives the information required for calculating

electron densities from the differential absorption experiment (via 3.7) and the differential phase experiment (3.20,3.21).

3.3 RECEIVER

Two different receivers were used. The first receiver, which was used until July 1973, was valve operated apart from a silicon diode in the detector circuit. A new solid state receiver developed by J. de Voil in the electronic workshop was used in August and September of 1973. The characteristics of the two receivers were as follows:

First receiver:

Frequency:	2.40 MHz
Bandwidth:	100 KHz
Sensitivity:	Minimum discernable signal 0.1 μV
Voltage gain:	85 db
Maximum output:	1 volt

New receiver:

Frequency:	2.40 MHz
Bandwidth:	65 KHz
Sensitivity:	Minimum discernable signal 0.1 μV
Voltage gain:	90 db
Dynamic range:	60 db, linear, 75 db usable
Maximum output:	10 volts.

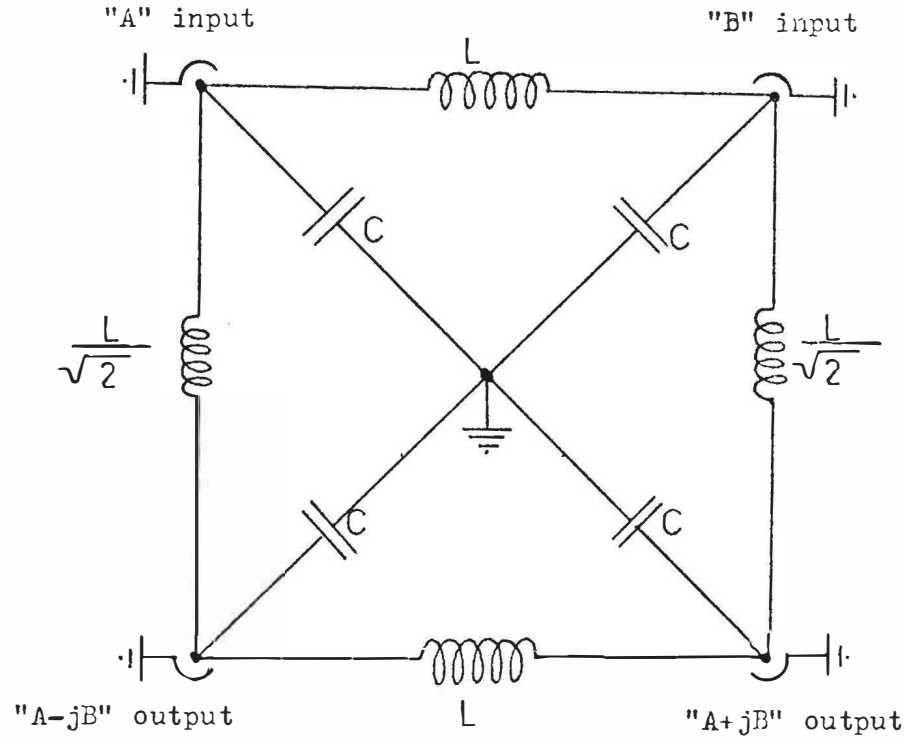

Fig 3.1: Hybrid circuit.

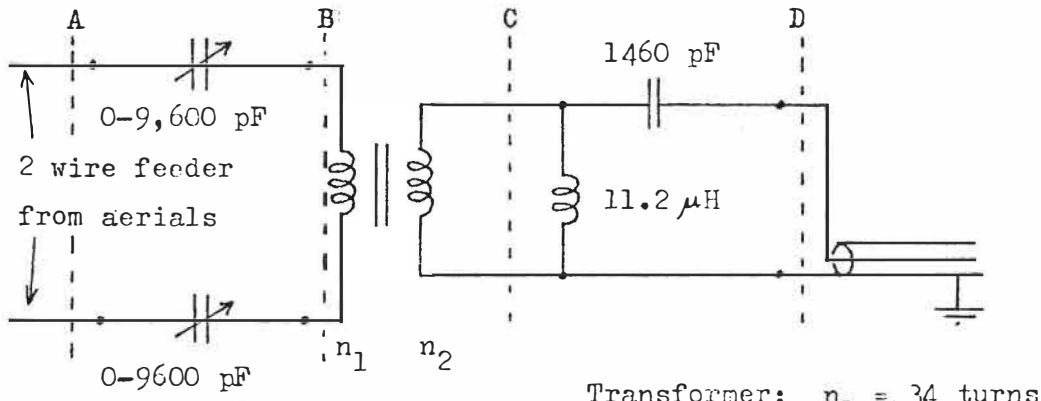

Transformer: n_1 = 34 turns
n_2 = 17 turns
Litz wire on Phillips pot-core.

Figure 3.2: Impedance matching from aerial feeders to 75 Ω coax cable.

3.4 PHASE SHIFTING, IMPEDANCE MATCHING, AND SWITCHING

3.4.1 Signal Combination and Phase Shifting

The phase shift of 90^{o} in the signal from the north-south aerial and addition to the signal from the east-west aerial required to obtain the ordinary and extraordinary mode signals was made using a hybrid circuit designed and built by Dr H.A. von Biel (figure 3.1). It is important that the input and output impedances to this circuit be close to 75Ω. In practice the A-iB output of the hybrid was permanently terminated in 75 ohms and both the ordinary and the extra-ordinary modes obtained from the A+iB output by inverting the signal to the B input on alternate cycles (Figure G7).

To obtain the signals V_1 and V_2 the hybrid was bypassed and the leads from the required pair of aerials were switched directly to the receiver.

To obtain the signal M_1 the signals V_1 and V_2 were added directly across the receiver input. The signal M_2 was obtained by adding V_1 to $-V_2$ across the receiver input.

All of the switching was done by reed relays, as described in appendix G.

3.4.2 Impedance Matching

The feeders from the receiving aerials to the receiver hut are balanced open wire transmission lines. The nominal impedance looking back down one of these feeders from the receiver hut is 600 ohms, although in practice the impedance varies from this due to incorrect spacing of the feeders and errors in the impedance matching at the aerials. However, the transmission line used between pieces of apparatus in the receiver hut is coaxial cable of 75 ohm characteristic

impedance which is unbalanced with respect to ground, and the hybrid and receiver require unbalanced inputs. Also, as was mentioned in the previous section, it is important that the input impedance to the hybrid be close to 75 ohms.

Thus it was necessary to match an approximately 600 ohm balanced line to a 75 ohm unbalanced line. The circuits used to do this are shown in figure 3.2. Identical methods were used for the feeders from the east-west and north-south aerials.

The first problem was that the impedance looking back down the transmission line from point A of figure 3.2 was partly reactive and changed to some extent from day to day. To allow for this the circuits to the right of B were temporarily replaced by an RF bridge and the capacitors C_1, C_2 altered (keeping $C_1 = C_2$) until the reactive part of the impedance was cancelled out. The impedance at point B was then typically of the order of 450-550 ohms. The following circuit is a balanced to unbalanced transformer ("balun") which also reduced the impedance to about 110 ohms. The circuit between points C and D matched this impedance to the 75 ohms required for the co-ax line.

The ultimate test of this matching system was that it regularly enabled values of 30 db or above to be obtained for the ordinary/extraordinary mode ratio for the E-region reflection. This was judged to be adequate for the differential absorption experiment (Section 4.5).

The other important point was that the output of the hybrid should be fed into 75 ohms. Since the receiver input impedance was different from this an emitter follower amplifier

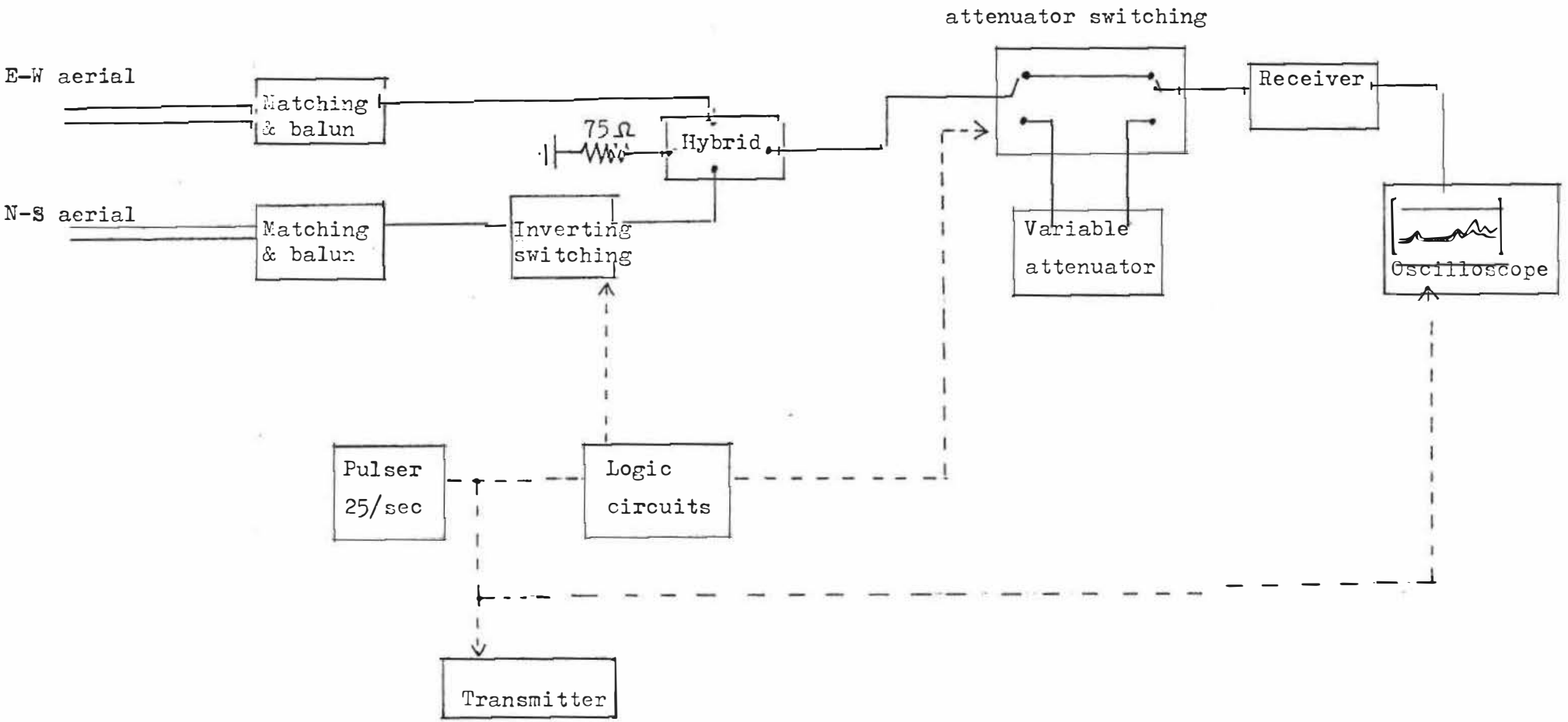

Figure 3.3: "Manual" differential absorption equipment.

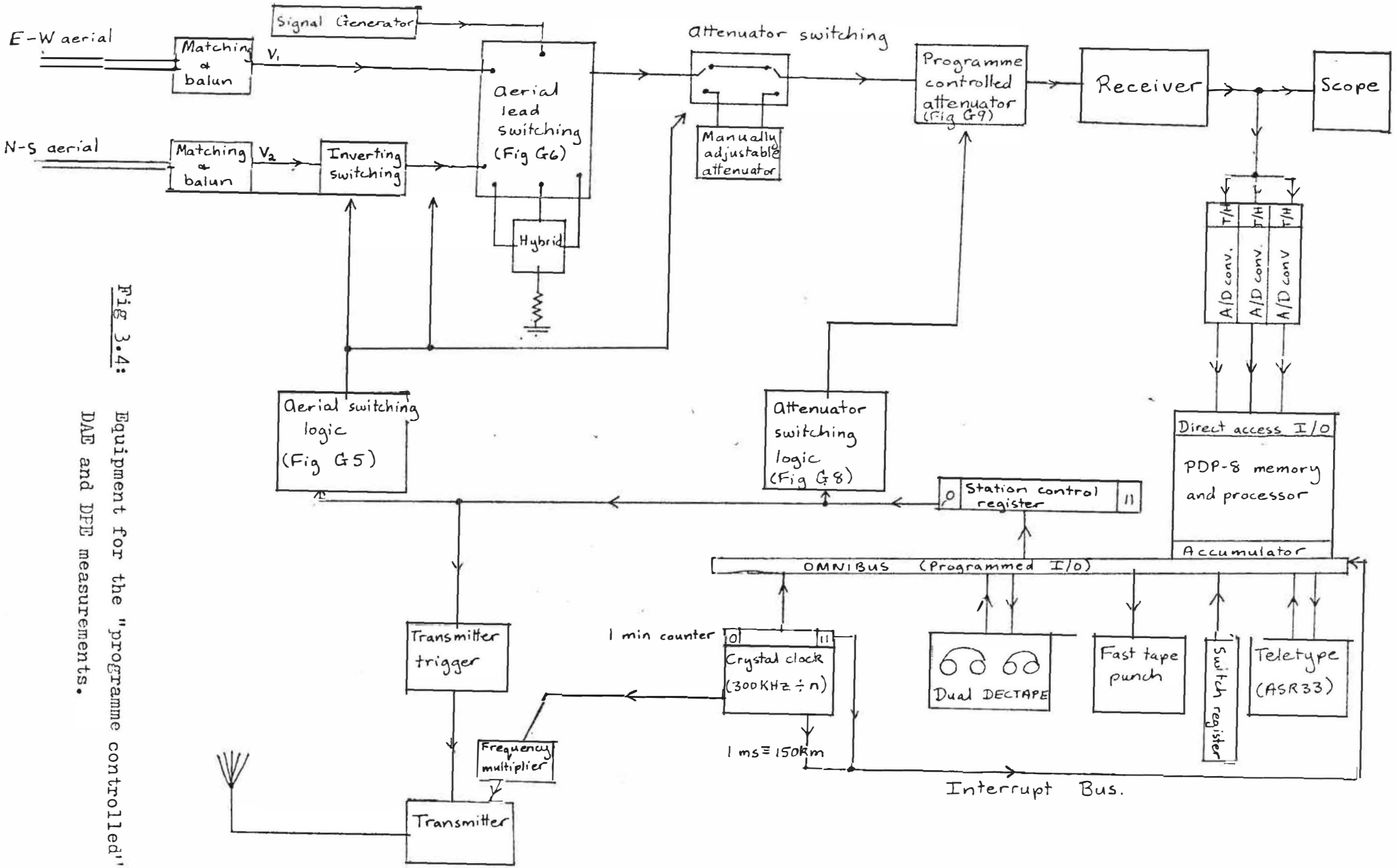

Fig 3.4: Equipment for the "programme controlled" DAE and DFE measurements.

with an input impedance of 75 ohms (again designed by Dr von Biel) was connected before the receiver.

3.5 SWITCHING AND RECORDING DETAILS

Over the period in which the experiment was run three different techniques were used. These are identified as the manual, hardware controlled, and software controlled systems.

3.5.1 The "Manual" Technique

This was the simplest system, which was built first. The ordinary and the extraordinary mode signals were switched to the receiver input for alternate transmitter pulses. The receiver output was displayed as an A-scan on an oscilloscope, also triggered by the transmitter trigger pulse. A variable attenuator could be switched in for either the ordinary or the extraordinary signal. By varying this attenuation until the two signals (displayed on an oscilloscope screen) lined up for some height, the amplitude ratio for that height was found. Figure 3.3 is a schematic diagram.

3.5.2 The "Hardware Controlled" Technique

This was the method used for routine recording from October 1971 through to January 1973. Further logic steps were built up, using TTL 7400 series integrated circuits so that the ordinary and extraordinary mode signals, and the signals V_1, V_2, M_1, M_2 were switched in turn to the receiver. Because there was insufficient dynamic range in the receiver a further attenuation (usually 10 or 15 db) was switched in ahead of the receiver for a second cycle of measurements of these signals. As well as being displayed on an oscilloscope

the receiver output was fed through an operational amplifier giving a further voltage gain of ten. This signal was fed to a system of track and hold, multiplexer and analogue to digital converter circuits which picked off the voltages corresponding to 2.5 km intervals from an adjustable starting height (usually 64 km) and stored them in a capacitor memory. From here the values were punched out on paper tape using a fast punch. The transmitter was pulsed at two cycles per second.

There were manual switches on the switching logic so that either just the ordinary and extraordinary signals could be sampled (for the DAE experiment), or all the signals could be sampled (for the combined DAE-DPE experiment). There was also the facility to run the system in the "manual" mode, so that the ordinary-extraordinary ratio for the E-region could be checked.

3.5.3 The "Software Controlled" Method

In 1973 a PDP-8 mini-computer was installed at the field station. Associated with this computer were track and hold circuits, three analogue to digital converters, a clock, a "station control register" (SCR) which could be used to turn equipment on and off, magnetic tape, and a fast paper tape punch.

The antenna switching logic used in the "hardware controlled" method was modified so that it could be controlled through the station control register. An attenuator controlled by the SCR which gave attenuation in increments of 5 db from 0 to 40 db was also built to go directly before the receiver. Thus under software control the transmitter could

be triggered and the returned signal for any antenna mode sampled. Also, the presence of the attenuator meant that the receiver, track and hold circuits, and analogue to digital converters could be calibrated under programme control, and the clock meant that the experiment could be programmed to run at predetermined times during the day. The large amount of storage available on the magnetic tape meant that in theory the apparatus could be left going unattended for several days, although this stage was not quite reached in practice because of various hardware and software bugs which had to be ironed out of the system. Figure 3.4 is a block diagram of the apparatus, the details of the logic and switching circuits are given in appendix G.

Appendix H is a listing of the programmes used.

3.6 EXPERIMENTAL PROCEDURE

3.6.1 The Manual Method

In this method the reactive component was first tuned out of the feeders as described in section 3.4.2. After checking that the ordinary to extraordinary ratio for the E-region echo was at least 30 db, the ratios for heights in the D-region where there were good echoes were measured and written down. From these measurements the differential absorption electron densities were calculated in a programme using equation (2.13) on the IBM 360/44 computer at Canterbury University.

3.6.2 The Hardware Controlled Method

A flow chart for the combined differential absorption - differential phase method is given in figure 3.5. The calibration step involved switching the output of an

accurately adjustable potentiometer (a helipot) into the recording system in place of the receiver and recording the output punched for a known series of input voltages. The resultant tape was analysed on the IBM 360 computer along with information on the receiver characteristics to give a series of cards containing calibration information for the differential absorption and phase analyses.

The only difference between the differential absorption and the combined differential absorption - phase experiment was that in the former only the ordinary and extraordinary signals were recorded while all six signals were recorded for the latter.

The raw data on the tapes was processed on the IBM 360, using the calibration information, to get mean square and mean fourth power values of background noise and total signal. These values were then processed as shown in figure 4.1 to give electron densities.

3.6.3 The "Software Controlled" Method

Figure 3.6 is a flow diagram for this method. Note that once NPR1 has been set going and the initial values for times and attenuations typed in the programme will keep running, sampling at the set times, unless certain switch register options are set to allow checks and changes to be made. The data was later dumped on to paper tape from the DECTAPE using the fast punch, and taken in to Christchurch for further analysis (figure 4.1) on the IBM 360/44.

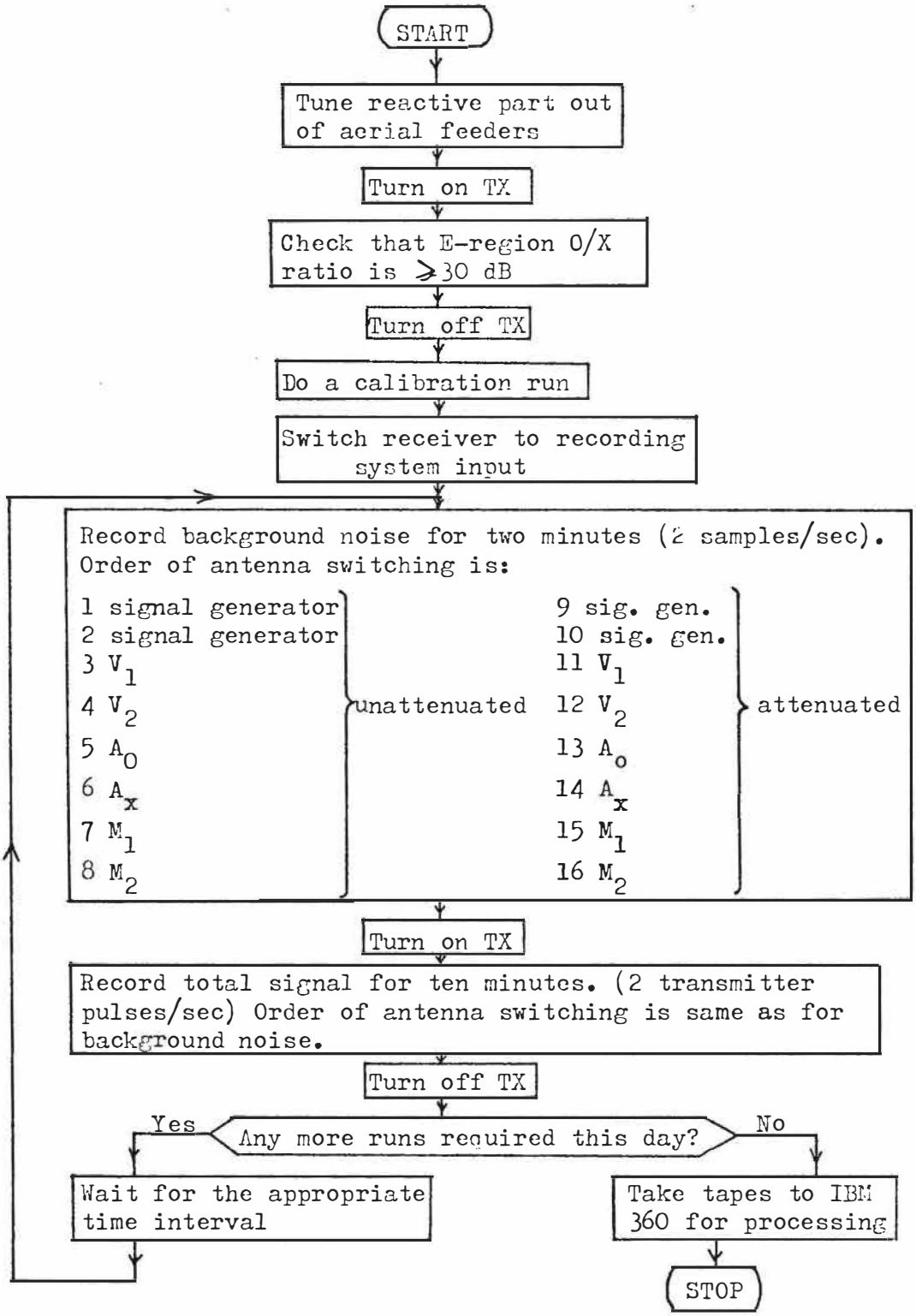

Fig 3.5: Procedure for "hardware controlled" differential absorption-phase experiment.

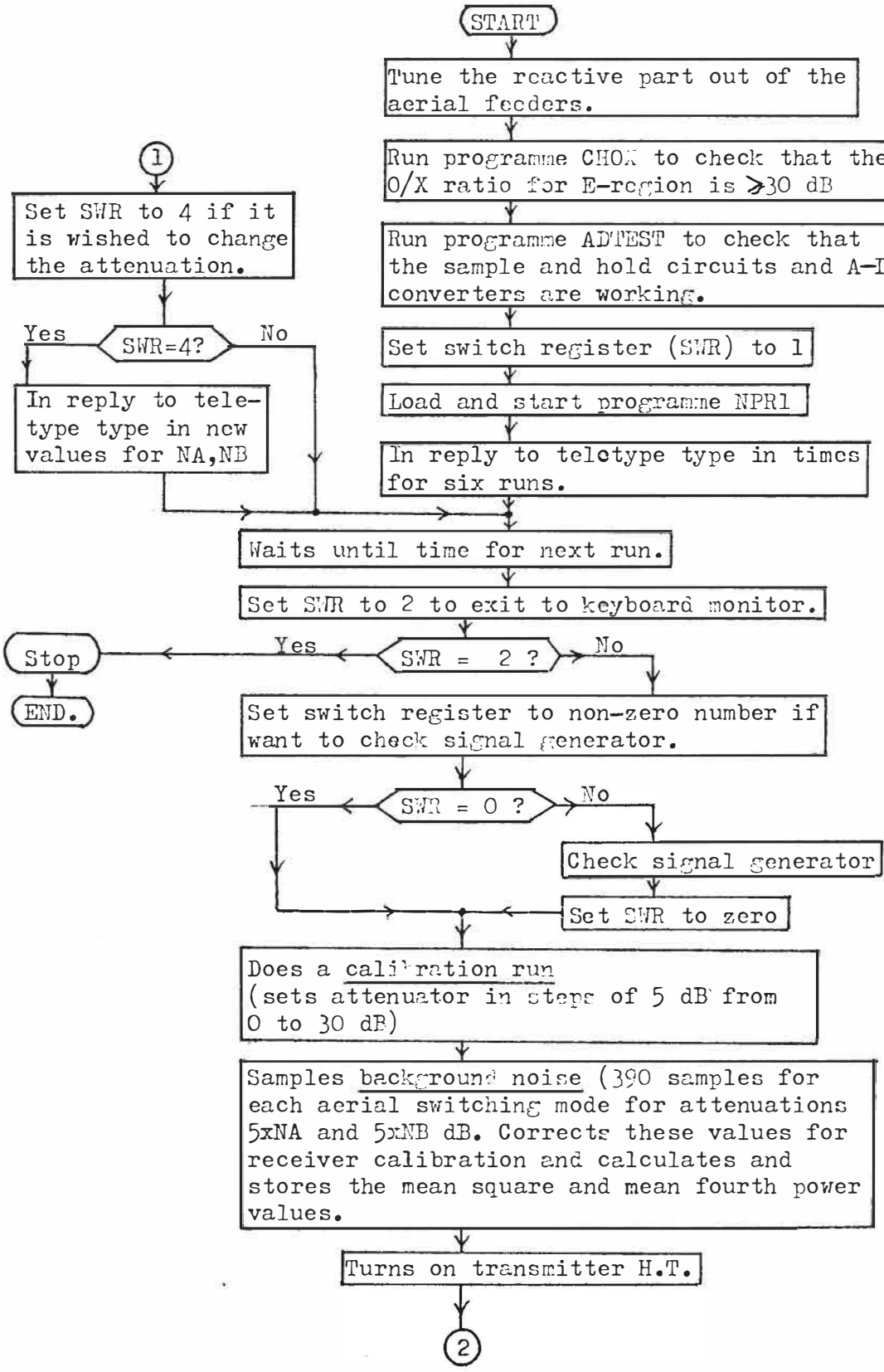
START
Tune the reactive part out of the aerial feeders.
Run programme CHOX to check that the O/X ratio for E-region is ≥30 dB
Run programme ADTEST to check that the sample and hold circuits and A-D converters are working.
Set switch register (SWR) to 1
Load and start programme NPR1
In reply to teletype type in times for six runs.
1
Set SWR to 4 if it is wished to change the attenuation.
Yes
SWR=4?
No
In reply to teletype type in new values for NA,NB
Waits until time for next run.
Set SWR to 2 to exit to keyboard monitor.
Stop
Yes
SWR = 2 ?
No
END.
Set switch register to non-zero number if want to check signal generator.
Yes
SWR = 0 ?
No
Check signal generator
Set SWR to zero
Does a calibration run (sets attenuator in steps of 5 dB from 0 to 30 dB)
Samples background noise (390 samples for each aerial switching mode for attenuations 5xNA and 5xNB dB. Corrects these values for receiver calibration and calculates and stores the mean square and mean fourth power values.
Turns on transmitter H.T.
2

Fig 3.6: (Part 1)

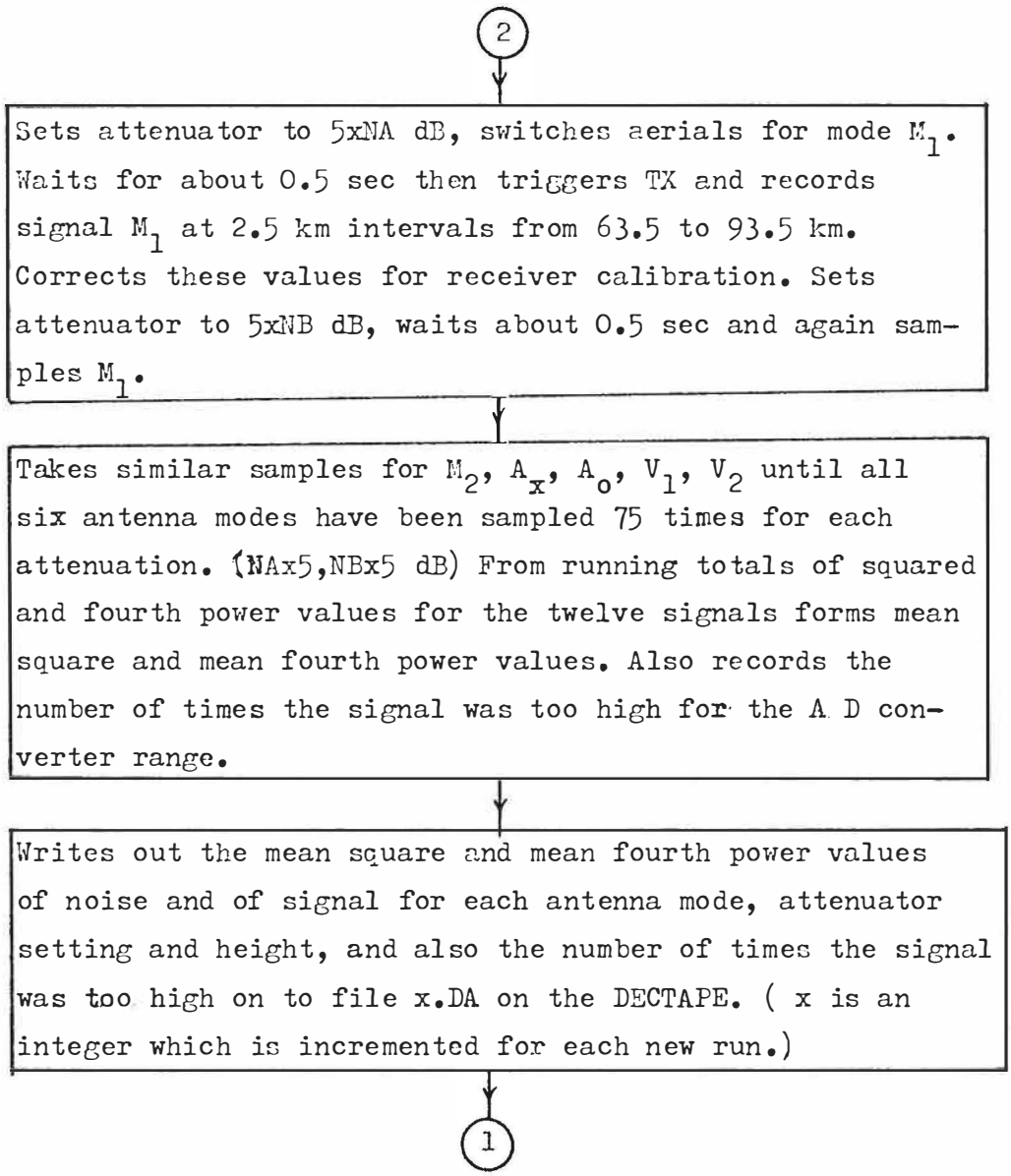

Fig 3.6: (Part 2)

Fig 3.6: Flow diagram for the "software controlled" differential phase-absorption experiment.

3.7 THE CONSTRAINTS INVOLVED IN THE VARIOUS METHODS

The simple manual method has several defects and constraints. The system of lining up two fading signals on an oscilloscope screen is very susceptible to observer bias. Also it is tedious, and it is not possible to gather the large amount of data at many height values averaged over several minutes obtained by the other two methods, or to allow for the effect of noise on weak signals. However, it is independent of the receiver characteristics.

The "hardware controlled" method had the major drawback compared to the "software controlled" method that an operator had to be present to turn the transmitter on and off at the required times, and to change the paper tapes after every few runs. Also the recording system was getting old and ingenuity was required in programming the tape reading on the IBM 360 to allow for such things as missing data frames and height channels which did not work properly. The calibration procedure was tedious and usually done only once per day. Also, as is discussed more fully in section 4.6, there were some problems with the receiver used.

The "software controlled" system had the great advantage that once it had been set going it could be left to run automatically. Also, with the same apparatus it would be possible to do different experiments, for example examining the effects of different averaging times or sampling rates, by simple changes in software. The experiment could be run amongst a series of D-region experiments such as D-region drift determinations and absorption measurements on the E-region reflection. The pre-processing to the stage of mean square and mean fourth power values saves considerable time and

trouble in the remaining analysis on the IBM 360 compared to the "hardware controlled" method. If a few simplifying assumptions were made it should be possible to process the data right through to electron densities in real time on the PDP-8.

CHAPTER 4

DATA PROCESSING AND EXPERIMENTAL UNCERTAINTIES

This chapter discusses the processing done on the records to obtain electron densities. From the mean square and mean fourth power values of signal and noise voltages the uncertainty due to statistical scatter can be estimated. Other uncertainties due to the experimental method are also described. From the variation of differential absorption results near noon on a given day the significance of the apparent day to day changes in electron densities at given heights is assessed.

4.1 CORRECTIONS FOR NOISE AND CRITERIA FOR ACCEPTING DATA

Consider a received signal of angular frequency ω made up of a wanted signal V_{sig} plus a noise signal V_{noise} where:

$$V_{sig} = V_A(t) \cos(\omega t + \phi(t))$$

$$V_{noise} = V_N(t) \cos(\omega t + \chi(t)) \qquad (4.1)$$

where $\phi(t)$, $\chi(t)$, $V_A(t)$ and $V_N(t)$ are varying only slowly compared to the time scale $\frac{1}{\omega}$.

Then the mean square signal calculated for one cycle is

$$P = \frac{\int_0^{\frac{2\pi}{\omega}} (V_{sig}+V_{noise})^2 dt}{\frac{2\pi}{\omega}} = \tfrac{1}{2}(V_A^2(t)+V_N^2(t)) + V_A V_N \cos(\phi-\chi) \qquad (4.2)$$

If ϕ and χ are independent and $(\phi-\chi)$ varies rapidly compared to the time for an experimental run (ten minutes), averaging (4.2) over a run gives

$$P = \tfrac{1}{2}\langle V_T^2 \rangle = \tfrac{1}{2}[\langle V_A^2 \rangle + \langle V_N^2 \rangle] \qquad (4.3)$$

Thus in the analysis of the results the mean square signal for a given antenna polarization with the transmitter turned off (the noise signal) was subtracted from the total mean square signal with the transmitter turned on, to eliminate the effect of background noise.

At times part of the interference was due to a harmonic of the 300 kHz reference signal fed to the transmitter. In this case ϕ and χ were not necessarily independent, and all that could be done was to reduce the harmonic as much as possible by good shielding and earthing.

When the total signal was weak the data was not used at all. The criteria were:

1972: The data at a given height was rejected if $\langle V_A^2 \rangle$ less than $\langle V_N^2 \rangle$, that is if the mean square value of the total signal was less than twice the mean square value of the noise.

1973: The data at a given height was rejected if $\langle V_A^2 \rangle$ less than $2\langle V_N^2 \rangle$, that is if the mean square value of the total signal was less than three times the mean square noise.

Data was also rejected if it was outside the range of the analogue to digital converters. For a given mode of antennae switching the signal for the lowest value of switched attenuation was checked first.

1972: If more than $\frac{1}{60}$th of the values for a given height were above the A-D range the data for that height was rejected.

1973: Data for a given height was rejected if more than $\frac{2}{75}$ of the values were above the A-D range.

If the data for a given height and antenna mode was rejected for the low attenuation value, the data from the same antenna mode but with the higher attenuation was used provided it obeyed the above criteria.

Figure 4.1 is a flow chart for the data processing.

4.2 THE UNCERTAINTY DUE TO THE SCATTER IN THE DATA

It is shown in the appendix F that the mean square values $\langle V_T^2 \rangle$ and $\langle V_N^2 \rangle$ will be approximately normally distributed with standard errors

$$\sigma_T = \left\{ \frac{\langle V_T^4 \rangle - (\langle V_T^2 \rangle)^2}{(N-1)} \right\}^{\frac{1}{2}}$$
$$\sigma_N = \left\{ \frac{\langle V_N^4 \rangle - (\langle V_N^2 \rangle)^2}{(N-1)} \right\}^{\frac{1}{2}} \qquad (4.4)$$

where N is the number of samples in a run. The parameter required for the electron density computations is $\langle V_A^2 \rangle$ where:

$$\langle V_A^2 \rangle = \langle V_T^2 \rangle - \langle V_N^2 \rangle \qquad (4.3)$$

$\langle V_A^2 \rangle$ will have standard error (Topping, 1962, p82)

$$\sigma_A = \{\sigma_T^2 + \sigma_N^2\}^{\frac{1}{2}} \qquad (4.5)$$

This assumes that each value is statistically independent, which requires that at some heights the samples for a given antenna setting be taken at intervals of ≳ 7 seconds (Noonan, 1969). In fact in 1972 the time between samples for the differential absorption experiment was only two seconds, so the uncertainty then was somewhat underestimated. For the 1973 results the sampling interval was 8 seconds.

4.3 CALCULATION OF DIFFERENTIAL ABSORPTION ELECTRON DENSITIES

The differential absorption electron densities are given by (chapter 2):

$$\bar{N} = \frac{\Delta \ell n \left| \frac{R_X^2}{R_O^2} \right| - \Delta \ell n \frac{\langle |E_X|^2 \rangle}{\langle |E_O|^2 \rangle}}{4 \left(\frac{\kappa_X - \kappa_O}{N} \right) \Delta h} \qquad (2.13)$$

This was calculated only for height differences Δh of 5 km (or 7.5 or 10 km if there was no data for a given 5 km interval), since if Δh = 2.5 km was used it was possible that the data from the two heights could be coming from the same reflection due to the finite width of the transmitter pulse.

Suppose data from heights h_1 and h_2 km was used. Then $\left(\frac{\kappa_X - \kappa_O}{N} \right)$ was calculated at $h_{av} = \frac{1}{2}(h_1+h_2)$, $\Delta \ell n \left| \frac{R_X^2}{R_O^2} \right|$ was calculated between $(h_{av} - 0.5)$ and $(h_{av} + 0.5)$ km. For $\Delta \ell n \frac{\langle |E_X|^2 \rangle}{\langle |E_O|^2 \rangle}$ the value

$$\frac{1}{(h_2-h_1)} \left\{ \ell n \frac{\langle |E_X(h_2)|^2 \rangle}{\langle |E_X(h_2)|^2 \rangle} - \ell n \frac{\langle |E_X(h_1)|^2 \rangle}{\langle |E_O(h_1)|^2 \rangle} \right. \qquad (4.6)$$

was used.

$\frac{R_X}{R_O}$ and $(\frac{\kappa_X - \kappa_O}{N})$ were calculated using the Sen-Wyller refractive indices (Appendix C) with the collision frequency profile of appendix B, and

B = geomagnetic field flux density = 5.89×10^{-5} Tesla

θ = angle between geomagnetic field and vertical

= 0.3811 radians.

Since both $\left|\frac{R_X}{R_O}\right|$ and $\left(\frac{\kappa_X - \kappa_O}{N}\right)$ are weakly dependent on electron density an iteration process was used on 2.13 with an initial electron density of 1000 cm^{-3}. $\left|\frac{R_X}{R_O}\right|$ was calculated from equation (A17) with an electron density change of 1% across the boundary.

The standard error σ in $\frac{<|E_X|^2>}{<|E_O|^2>}$ due to the scatter in the data was calculated from:

$$\sigma^2 = \frac{\sigma_0^2 (<|E_X|^2>)^2 + \sigma_X^2 (<|E_O|^2>)^2}{(<|E_O|^2>)^4} \qquad (4.7)$$

where σ_0 and σ_X are the standard errors of $<|E_O|^2>$ and $<|E_X|^2>$ calculated from (4.5).

The uncertainty in electron density was calculated by considering the largest and smallest possible values of (4.6) consistent with the standard errors $\sigma(h_1)$ and $\sigma(h_2)$ from (4.7).

Occasionally a negative value for electron density was calculated from (2.13) at one of the lower heights. This could have been due to shortcomings in the model of chapter two, incorrect allowance for interference, or poor receiver calibration. Such results were rejected.

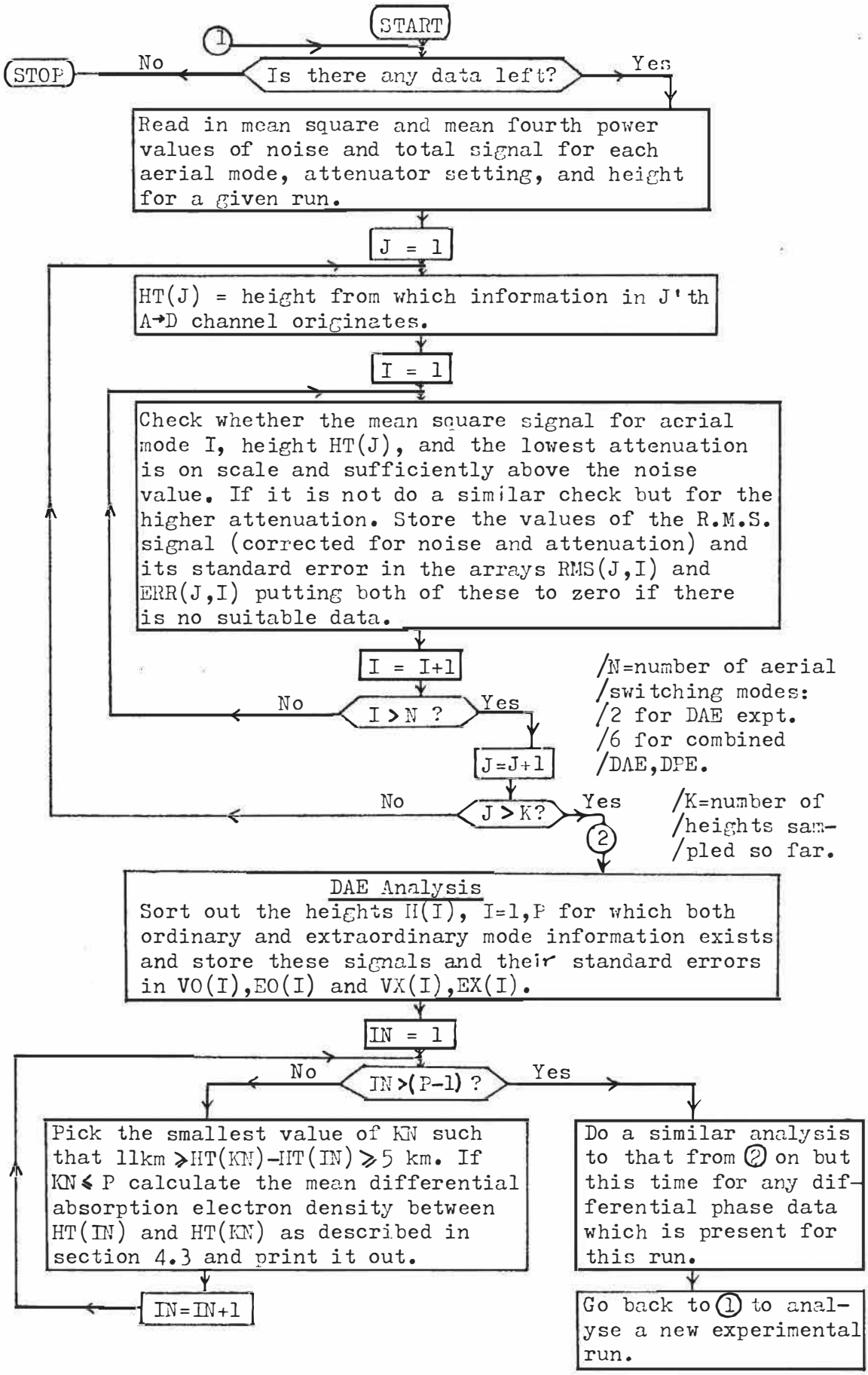

Fig 4.1: Flow chart for data processing.

4.4 CALCULATION OF DIFFERENTIAL PHASE ELECTRON DENSITIES

The differential phase electron densities are given by (chapter 2):

$$\bar{N} = \frac{\Delta\beta - \Delta\eta}{2k\left[\frac{\mu_X - \mu_O}{N}\right]\Delta h} \qquad (2.21)$$

It is shown in chapter 3 that η satisfies the relations:

$$|\rho(h)|\sin\eta = \tfrac{1}{2}\left(\frac{\langle|M_1|^2\rangle - \langle|M_2|^2\rangle}{\langle|M_1|^2\rangle + \langle|M_2|^2\rangle}\right)\left(\frac{\langle|A_O|^2\rangle + \langle|A_X|^2\rangle}{(\langle|A_O|^2\rangle\langle|A_X|^2\rangle)^{\frac{1}{2}}}\right) \qquad (3.20)$$

$$|\rho(h)|\cos\eta = \tfrac{1}{2}\left(\frac{\langle|V_1|^2\rangle - \langle|V_2|^2\rangle}{\langle|V_1|^2\rangle + \langle|V_2|^2\rangle}\right)\left(\frac{\langle|A_O|^2\rangle + \langle|A_X|^2\rangle}{(\langle|A_O|^2\rangle\langle|A_X|^2\rangle)^{\frac{1}{2}}}\right) \qquad (3.21)$$

Thus

$$\tan\eta = \left(\frac{\langle|M_1|^2\rangle - \langle|M_2|^2\rangle}{\langle|M_1|^2\rangle + \langle|M_2|^2\rangle}\right)\left(\frac{\langle|V_1|^2\rangle + \langle|V_2|^2\rangle}{\langle|V_1|^2\rangle - \langle|V_2|^2\rangle}\right) \qquad (4.8)$$

By considering the sign of $\sin\eta$ and $\tan\eta$ and the value of $\tan\eta$ a value for η in the range $[0,2\pi)$ can be found. There is some problem in getting the value of $\Delta\eta$ $(= \eta(h_2) - \eta(h_1))$ to put in (2.21) since there is an ambiguity of $2n\pi$ (n an integer). This was overcome by assuming that $|\Delta\eta| \leq 2\pi$. This was reasonable since usually $\Delta h = 5$ km, and apart perhaps from the top of the height range electron densities of the magnitude expected would lead to a phase shift obeying this rule. Generally, to give electron densities which agree reasonably with the DAE values it is necessary that $\Delta\eta$ is positive. Thus if $\{\eta(h_2)-\eta(h_1)\}$ is negative, 2π is added to $\{\eta(h_2)-\eta(h_1)\}$ before the electron density calculation is made.

The uncertainties due to the scatter in the data were again calculated using the theory of standard errors (Topping, 1961, page 82). It should be noted that the two difference factors $(\langle|M_1|^2\rangle-\langle|M_2|^2\rangle)$ and $(\langle|V_1|^2\rangle-\langle|V_2|^2\rangle)$ in (4.8) can lead to large uncertainties.

4.5 ERRORS IN THE DIFFERENTIAL ABSORPTION EXPERIMENT DUE TO POOR IMPEDANCE MATCHING

A further possible error in the experiment is that the North-South aerial system and feeders may introduce a different attenuation and phase change into the north-south signal to that introduced into the east-west signal by the east-west system. This will lead to errors in the ordinary/extraordinary ratio. These can be estimated by considering the signal returned from the E-region total reflection.

By running a programme using the Sen-Wyller refractive indices and an electron density profile due to Mechtly et al. (1972a) it was found that if both extraordinary and ordinary modes are transmitted with equal power, then effectively only the ordinary mode will be received from the E-region total reflection since the extraordinary mode will be attenuated by a further factor of about 86 db (Appendix E).

Suppose the east-west signal E_x suffers an attenuation and phase shift $\eta = Ae^{i\phi}$ relative to the north-south signal E_y. (If the equipment is set up exactly right $A = 1$, $\phi = \pm\frac{\pi}{2}$.) The polarizations of the ordinary and extraordinary modes are almost exactly (section 2.1)

$$\rho_0 = j \qquad\qquad \rho_x = -j$$

Consider the signal received from the E-region total reflection, which is ordinary mode only. The electric field at the receiving aerials will be:

$$\underset{\sim}{E} = E_0(\hat{x}+j\hat{y})e^{j\omega t} \tag{4.9}$$

(where $\hat{x}$ and $\hat{y}$ are unit vectors to the east and north)).

Thus

$$E_x = E_0\, e^{j\omega t} \qquad E_y = E_0\, e^{j(\omega t+\frac{\pi}{2})} \tag{4.10}$$

The receiver input will be:

For 'X-mode' switching: $$V_1 = V_x + \eta V_y \tag{4.11}$$

For 'O-mode' switching: $$V_2 = V_x - \eta V_y \tag{4.12}$$

(since the only difference between X and O-mode switching is a π phase difference in V_y. Here V_x, V_y are voltages proportional to E_x, E_y). Suppose

$$\frac{|V_1^2|}{|V_2^2|} = x \tag{4.13}$$

where x is typically 30 dB, i.e. 0.001. But by (4,11), (4.12)

$$\frac{|V_1^2|}{|V_2^2|} = \frac{1 + A^2 - 2A \sin\phi}{1 + A^2 + 2A \sin\phi} \tag{4.14}$$

Thus

$$A = \frac{\sin\phi(1+x) \pm \sqrt{-(1+x)^2\cos^2\phi+4x}}{(1 - x)} \tag{4.15}$$

Since by definition A is real, $\cos^2\phi < \frac{4x}{(1+x)^2}$ (4.16)

Thus for $x = 0.001$, $\cos\phi < 0.063$

i.e. $(90^{o}-\phi) < 3.6^{o} = 0.063$ radians.

The maximum and minimum values for A will be when $\cos\phi = 0$, which gives $A = 1.06, 0.94$.

Thus

$$\eta = (1.00 \pm 0.06) \exp j(\tfrac{\pi}{2} \pm 0.06) \qquad (4.17)$$

The error which this could lead to in an actual D-region experiment is now considered. In this case there will be both ordinary and extraordinary wave fields at the receiving aerials.

$$\underset{\sim}{E} = E_{O}(\hat{x}+j\hat{y}) + E_{X}(\hat{x}-j\hat{y}) \qquad (4.18)$$

Once again put: $V_1 = V_x + \eta V_y$ (X-mode switching)

$V_2 = V_x - \eta V_y$ (O-mode switching)

Thus

$$\frac{|V_1|^2}{|V_2|^2} = \frac{(\frac{E_X}{E_O})^2\{1+A^2+2A\sin\phi\}+\{1+A^2-2A\sin\phi\}+2(\frac{E_X}{E_O})(1-A^2)}{\{1+A^2+2A\sin\phi\}+(\frac{E_X}{E_O})^2\{1+A^2-2A\sin\phi\}+2(\frac{E_X}{E_O})(1-A^2)} \qquad (4.19)$$

The difference between $\frac{|V_1^2|}{|V_2^2|}$ and $(\frac{E_X}{E_O})^2$ due to a change of $\pm 3.6^{o}$ about 90^{o} for ϕ is small compared to the difference due to a change of ± 0.06 in A about 1.0. The values of $(\frac{E_X}{E_O})^2$ for given $\frac{|V_1^2|}{|V_2^2|}$ and $A = 0.94$, $\sin\phi = 1$; $A = 1.06$, $\sin\phi = 1$ are given in table 4.1. From table 4.1 it can be seen that there is little point in using data for heights where the voltage ratio is greater than 20 db. A number of the winter 1972 results were examined in the light of this uncertainty.

$\frlvert V_1^2 \frrvert / \frlvert V_2^2 \frrvert$ (dB)		-23	-20	-15	-10	-5	0	5	10	15	20	23
E_X^2 / E_O^2 (dB)	A=0.96	-28	-23	-16.5	-10.8	-5.3	0	4.7	9.2	13.5	18.0	20.0
	A=1.04	-20.0	-18.0	-13.5	- 9.2	-4.7	0	5.3	10.8	16.5	23.0	28

Table 4.1 True values of extraordinary to ordinary ratios for given measured values.

It was found that the resulting uncertainty in electron density was greatest at the top of the height range - typically about 10% at 82 km and ≤6 % below 80 km. However, at times the error may have been as large as 16% at 82 km and up to 6% at 78 km.

4.6 RECEIVER CALIBRATION

A problem with the receiver used in 1972 was that the receiver characteristics appeared to change from day to day. This was unfortunately not discovered until October 1972. By considering measurements of the receiver characteristics on different days the possible error in $\Delta \ell n \frac{\langle |E_X|^2 \rangle}{\langle |E_O|^2 \rangle}$ in (2.13) due to this was estimated at about 0.5 db. For the 'typical winter profile' of chapter 2 this would lead to the possible errors in electron density shown in table 4.2.

Height (km)	Electron density (cm^{-3})	Error (cm^{-3})	Percent error
65	100	26	26%
70	100	16	16%
75	200	14	7%
80	400	19	5%
85	700	40	6%

Table 4.2 Possible errors in the DAE experiment (1972) due to changes in receiver characteristics.

4.7 SUMMARY OF UNCERTAINTIES

Table 4.3 shows the magnitude of the uncertainties discussed in this chapter, together with the fundamental uncertainties related to the lack of knowledge of the reflecting processes discussed in chapter 2.

Height (km)	Poor matching (4.5)	Volume or Fresnel scatter? (2.4.2)	Epstein layer or Fresnel discontinuity? (2.6)	Uncert. in height of layer (2.7)	Scatter		RX calibration	
					1972	1973	1972	1973
65	6%	2%	0.5%	35%	No data	250%	26%	-
70	6%	5%	4%	35%	44%	300%	16%	-
75	6%	7%	5%	35%	14%	66%	7%	-
80	6%	7%	8%	35%	12%	36%	5%	-
85	10%	6%	15%	35%	12%	98%	6%	-

Table 4.3 Uncertainties in differential absorption electron densities for one run
(1972 ~ 300 samples/run
1973 ~ 75 samples/run).

The column headed "scatter" gives the mean uncertainty at each height due to the spread of the data in a given run as discussed in section 4.3.

For the differential phase experiment the errors due to poor impedance matching and changes in the receiver characteristics are not readily estimated, although they will probably be at least as large as in the differential absorption case. Some of the uncertainties for the differential phase experiment are shown in table 4.4.

Height (km)	Volume or 'Fresnel scatter? (2.5.2)	Epstein layer or Fresnel discontinuity? (2.6)	Uncert. in height of layer (2.7)	Scatter	
				1972	1973
65	3%	3%	35%	No data	4460%
70	6%	3%	35%	1130%	631%
75	8%	3%	35%	55%	132%
80	9%	2%	35%	1130%	136%
85	60%	1%	35%	4120%	341%

Table 4.4 Uncertainties in differential phase electron densities for one run (1972,1973 75 samples/run).

The large values for statistical spread do not immediately rule out the differential phase method as a means of measuring electron densities. This column shows the mean value for a year, but there are individual runs with uncertainties down around 50%.

4.8 DAY TO DAY VARIATIONS

From the uncertainties in table 4.3 it can be seen that care must be taken in the interpretation of apparent variations in electron density from one day to the next, as much of the variation could be due simply to the experimental uncertainty in each run.

It was planned to do three or four runs in the three hours surrounding noon each day. In looking for day to day changes at a given height the mean electron density of these several runs was used. It was assumed that the variation between runs on a given day was due mainly to scatter in the data from which the mean square signals were calculated, with perhaps also a contribution from motion on the gravity wave scale and from changes in the positions of reflecting layers between runs. The variation between runs on a given day was used as a guide to whether the apparent day to day variation was real.

Suppose N independent samples of a random variable $\mathbf{x}$ are taken to calculate the sample mean $\bar{x}$ and the sample standard deviation $s = \{\frac{1}{N-1} \sum_{i=1}^{n} (x_i - \bar{x})^2\}^{\frac{1}{2}}$. Then the true mean value $\mu_{\mathbf{x}}$ falls within the interval $\bar{x} \pm \frac{st_{n;\alpha/2}}{\sqrt{N}}$ $(n = N-1)$ with a confidence of $100(1-\alpha)$ percent (Bendat and Piersol, 1971, section 4.4).

($t_{n;\alpha}$ is the α percentage point for the student t distribution for n degrees of freedom, that is Probability $[t_n > t_{n;\alpha}] = \alpha$.)

Thus if $\mathbf{x}$ represents the calculated electron density at some height for a given differential absorption run, the true mean electron density for all the runs on that day will lie

within $\pm e$ of the sample mean $\bar{x}$ with a confidence of 70%, where $e = \frac{st_{n;0.15}}{\sqrt{N}}$. In table 4.5 the column "mean daily fractional error" is the average value of $\frac{e}{x}$ for all of the days on which there were two or more runs.

Also in table 4.5 the standard deviation of the daily electron density series has been calculated, and divided by the average of the daily electron densities. This is given as the "coefficient of variation of the mean daily electron densities" for

(i) the mean daily electron densities

(ii) the mean daily electron densities corrected to overhead sun by multiplying by a factor of $e^{x(1-\sec\chi)}$ where χ is the solar zenith angle. (This assumes a relationship of the form $N_e = Ae^{x \sec \chi}$ (chapter 10), where N_e is the electron density. A and x were found by least squares regression analysis of $\ell n\ N_e = x \sec \chi + A$).

If the mean daily electron densities were normally distributed, the value for a given day would be within one standard deviation of the average 68% of the time. Thus if the value in column (b) is higher than the value in column (a) of table 4.5 for a given height, part of the apparent variation in mean daily electron density from one day to the next is a real variation, and is not due to the fluctuations in electron density during each day. A similar argument holds for columns (d) and (c).

Thus in 1972 the change from one day to the next appears only to be significant at 69 and 74 km. Smoothing the data over several days (chapter 7) is necessary to get meaningful time series to compare with other atmospheric parameters.

Height (km)	July-Sept 1972			August-Sept 1973		
	Mean daily fractional error (a)	Coeff. of varn of mean daily electron density		Mean daily fractional error (c)	Coeff. of varn of mean daily electron density	
		Raw	(b) Overhead sun		Raw	(d) Overhead sun
61.5-64						
64-66.5						
66.5-69	1.02	0.63	0.61			
69-71.5	0.56	0.71	0.76	0.38	0.52	0.53
71.5-74	0.44	0.45	0.46	0.33	0.47	0.46
74-76.5	0.30	0.36	0.35	0.22	0.51	0.51
76.5-79	0.34	0.33	0.31	0.19	0.33	0.31
79-81.5	0.39	0.36	0.33	0.29	0.32	0.33
81.5-84	0.48	0.36	0.37	0.29	0.30	0.30
84-86.5	0.53	0.40	0.40	0.42	0.34	0.33
86.5-89				0.71	0.62	0.55

Table 4.5 Daily and seasonal variation of electron density.

The situation in 1973 was better, with significant day to day changes up to 79 km, mainly because there were usually more runs on each day. From the mean daily fractional error for 1973 (table 4.5) it appears that the uncertainties for a given run in 1973 (table 4.3) were overestimated, since one would expect the mean daily uncertainty to be approximately the uncertainty in a given run divided by the square root of the number of runs. A possible explanation for this anomaly is given in appendix F. The 1972 uncertainties appear more consistent.

4.9 CONCLUSIONS

(i) There was a real change in mean daily electron density from one day to the next in August and September of 1973, below 79 km. This was also the case at 69 and 74 km in July to September of 1972, but there were too few experimental runs each day during that period to distinguish any day to day fluctuations from fluctuations due to random scatter in the experimental data on a given day at other heights.

(ii) The uncertainties in the electron densities calculated from differential phase data are in general much larger than for electron densities calculated from differential absorption data.

(iii) The uncertainties in electron density calculations due to theoretical uncertainties about the reflecting process, apart from the uncertainty in the reflecting height if the Fresnel process is valid, are smaller than the uncertainties due to scatter in the data for runs of manageable length.

CHAPTER 5

THE DIFFERENTIAL PHASE EXPERIMENT

This chapter discusses the results obtained from the differential phase experiment, and compares them with the results of the differential absorption experiment. The theory and the experimental methods have already been outlined (Chapters 2, 3, 4).

5.1 SOME TYPICAL RESULTS

Table 5.1 gives the results of a typical combined differential absorption - differential phase run.

Height (km)	$\lvert\rho(h)\rvert$	$\eta(h)$ (radians)	N_{DPE} (cm^{-3})	$\frac{\langle\lvert E_X\rvert^2\rangle}{\langle\lvert E_O\rvert^2\rangle}$ (dB)	N_{DAE} (cm^{-3})
69	0.69±0.3	3.64±0.5		+5.91±0.6	
71.5	0.70±0.3	3.75±0.3	89±230	+6.00±0.6	85±40
74	0.73±0.3	3.80±0.3	167±80	+5.47±0.7	142±30
76.5	0.71±0.3	4.37±0.02	247±50	+3.10±0.7	195±30
79	0.50±0.2	5.11±0.03	196±50	+0.59±0.5	257±30
81.5	0.30±0.2	5.57±0.3	483±60	-2.98±0.6	525±50
84	0.30±0.2	8.63±0.4	$470\pm4\times10^3$	-9.80±0.6	781±70
86.5	0.23±0.2	9.26±35		-14.30±0.6	

Table 5.1 DAE and DPE data for 1420 hours, 13/9/72.

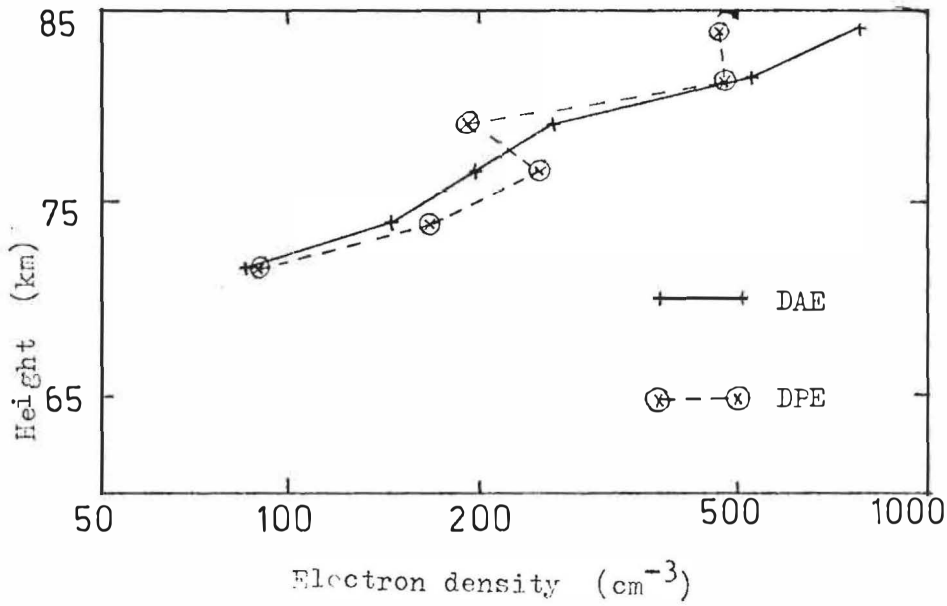

Fig 5.1 DAE and DPE electron densities.
(1416 hours, 13/9/72)

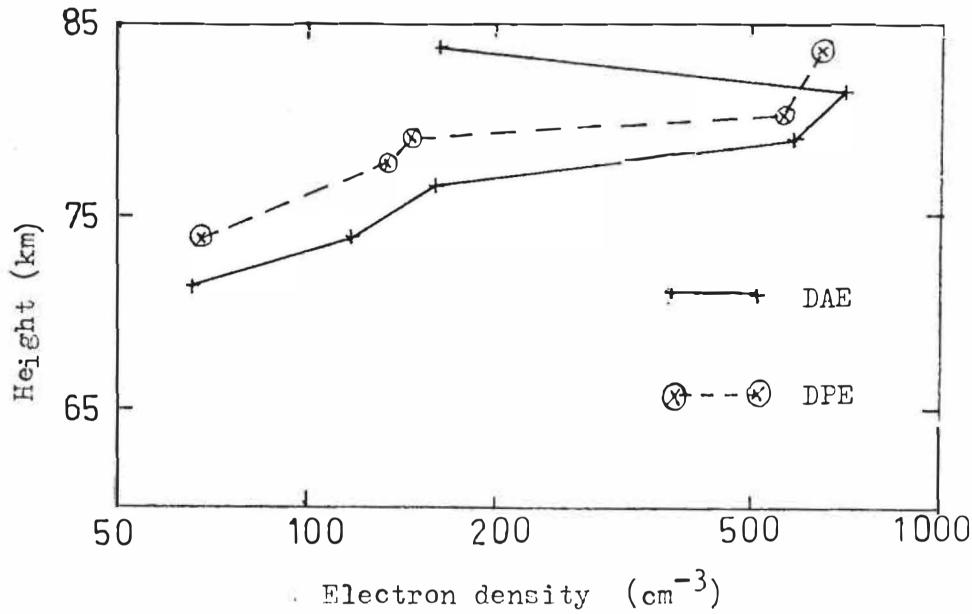

Fig 5.2 DAE and DPE electron densities.
(1435 hours, I/8/72)

$|\rho(h)|$ is the magnitude of the complex correlation coefficient between the ordinary and extraordinary signals (eqns 3.20, 3.21). $\eta(h)$ is the argument of this coefficient (eqn 4.8). The differential phase electron density (N_{DPE}), differential absorption electron density (N_{DAE}), and the extraordinary to ordinary power ratio ($\frac{\langle|E_X|^2\rangle}{\langle|E_O|^2\rangle}$) are also shown. The uncertainties are those due to the statistical spread of the data, calculated as discussed in sections 4.3 and 4.4.

The electron densities by the two methods are shown in figure 5.1. For this run the electron densities calculated from the differential absorption results agreed with the densities calculated from the differential phase results at each height to within the experimental uncertainties.

Figure 5.2 is a similar plot for 1/8/72. For several heights on this day the disagreement between the two methods was greater than the experimental uncertainty.

Ten runs between 1/8/72 and 25/1/73 were considered in detail. The results for 1/8/72 showed the poorest agreement between the absorption and phase results. Several of the other runs showed agreement similar to that of 13/9/72.

5.2 A QUANTITATIVE COMPARISON BETWEEN THE RESULTS OF THE DIFFERENTIAL PHASE AND DIFFERENTIAL ABSORPTION EXPERIMENTS

Unfortunately there are no rocket probe measurements over Birdling's Flat to compare the differential phase electron densities with. All that is available are the densities calculated by the differential absorption method for the same run.

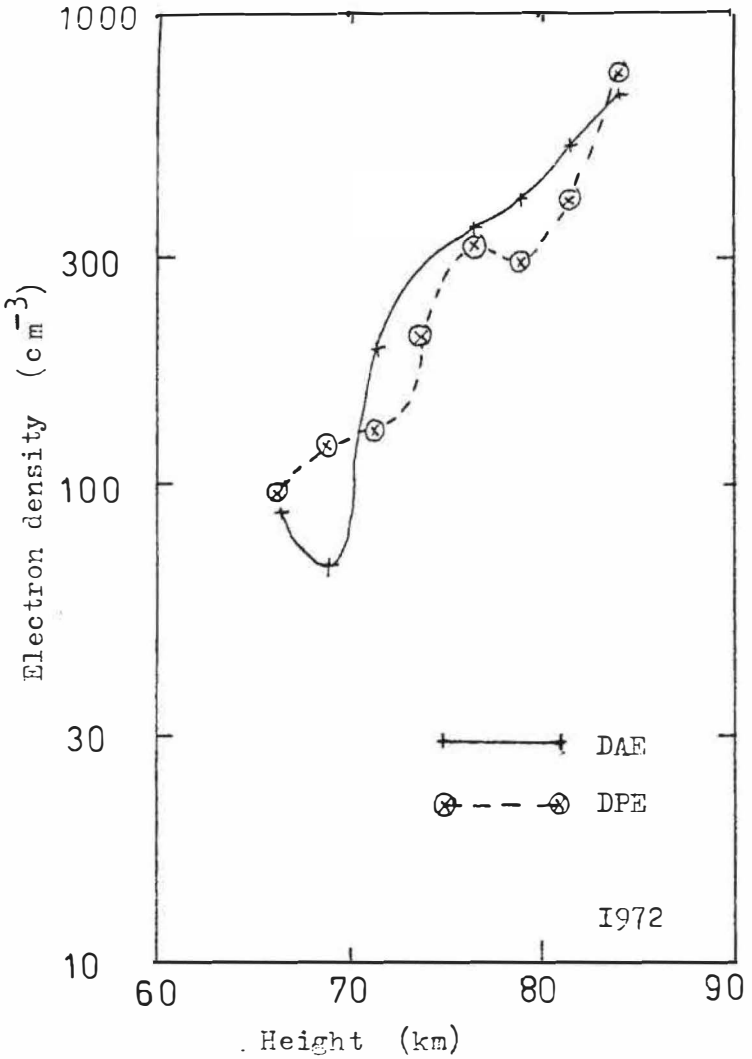

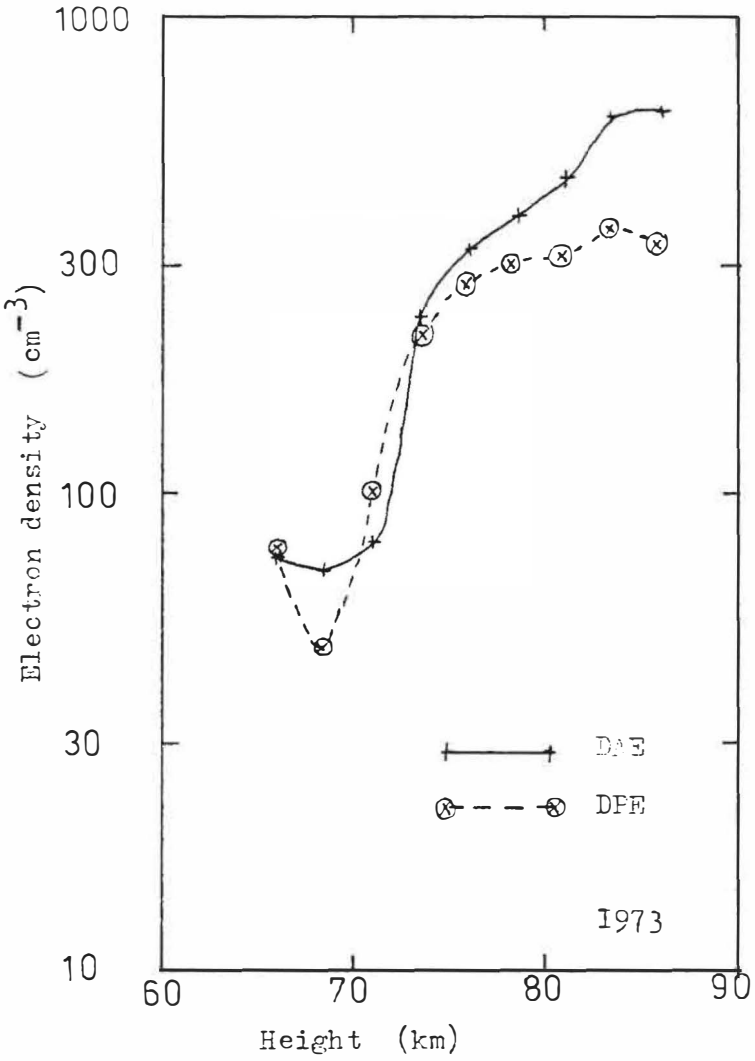

Fig 5.3 Mean values for DAE and DPE electron densities.

1/8/72 - 25/1/73

Height (km)	n	r	sig.	α	$\beta \pm$ std error	$\bar{N}_{DAE}$ (cm^{-3})	σ_{DAE}	$\frac{\sigma_{DAE}}{\sqrt{n}}$	$\bar{N}_{DPE}$ (cm^{-3})	σ_{DPE}	$\frac{\sigma_{DPE}}{\sqrt{n}}$	$\frac{\bar{N}_{DPE}}{\bar{N}_{DAE}}$
66.5	4	0.73	36%	-1	1.6±0.8	86	17	8	98	28	14	1.14
69.0	4	0.70	38%	50	1.1±0.8	66	50	25	124	80	40	1.88
71.5	9	0.05	90%	122	0.03±0.2	192	102	35	128	59	20	0.67
74.0	10	0.89	0.02%	-19	0.8±0.1	292	144	45	207	126	40	0.71
76.5	8	0.78	2%	-101	1.2±0.4	347	176	62	319	273	97	0.92
79.0	10	0.44	22%	-56	0.9±0.6	390	120	38	291	242	77	0.75
81.5	7	-0.24	62%	600	-0.4±0.8	510	153	58	378	280	110	0.74
84.0	7	0.03	-	700	0.02±0.2	657	334	126	718	170	64	1.09

1/8/73 - 30/9/73

Height (km)	n	r	sig.	α	$\beta \pm$ std error	$\bar{N}_{DAE}$ (cm^{-3})	σ_{DAE}	$\frac{\sigma_{DAE}}{\sqrt{n}}$	$\bar{N}_{DPE}$ (cm^{-3})	σ_{DPE}	$\frac{\sigma_{DPE}}{\sqrt{n}}$	$\frac{\bar{N}_{DPE}}{\bar{N}_{DAE}}$
66.0	2	-	-	-	-	74	-	-	76	-	-	1.03
68.5	2	-	-	-	-	69	-	-	47	-	-	0.68
71	6	-0.65	18%	144	-0.6±0.3	79	82	33	100	71	29	1.26
73.5	18	0.88	<0.02%	7	0.9±0.1	234	141	33	212	140	33	0.91
76	39	0.25	13%	184	0.2±0.2	324	157	25	264	156	25	0.81
78.5	54	0.28	4%	122	0.4±0.2	383	140	26	291	225	30	0.76
81	68	-0.12	35%	370	-0.1±0.1	460	186	22	302	236	29	0.65
83.5	59	0.17	20%	222	0.2±0.2	620	238	43	348	287	37	0.56
86	41	-0.06	72%	353	-0.5±0.1	633	295	46	320	260	40	0.50

Table 5.2 Comparison analysis of DAE and DPE results.

Table 5.2 (contd)

n = number of simultaneous DAE and DPE values used in analysis

r = correlation coefficient

sig = significance level of r (Bendat and Piersol, 1971, section 4.8.1)

α,β regression coefficients for $N_{DPE} = \alpha + \beta N_{DAE}$

$\bar{N}_{DPE}$, σ_{DPE}: mean and standard deviation of DPE electron densities

$\bar{N}_{DAE}$, σ_{DAE}: mean and standard deviation of DAE electron densities

$\frac{\sigma}{\sqrt{n}}$ = standard error of mean value.

First the mean values from a large number of runs were compared for both methods. Then a correlation and regression analysis was made between the electron densities deduced by the two methods. Table 5.2 shows the results of these comparisons. Separate analyses were made for 1/8/72 to 25/1/73 when the old receiver and recording system were in use, and August-September 1973 when both DAE and DPE data were collected routinely using the new receiver and the PDP-8 recording system.

5.2.1 Mean Values from the Differential Phase and Differential Absorption Experiments

The mean electron density profiles from the differential absorption and differential phase methods are shown in table 5.2 and in figure 5.3. For the 1972 values there is only one height (71.5 km) at which the DAE and DPE results do not agree to within their standard errors ($\frac{\sigma}{\sqrt{n}}$), although the DPE densities are slightly lower than the DAE results between 71 and 81 km. However, during 1973 the differential phase electron densities are significantly lower than the differential absorption densities above 76 km.

Several possible causes can be advanced for this disagreement:

(1) The collision frequency profiles may be wrong, due either to an incorrect multiplicative factor in the relation

$$\nu = 6.4 \times 10^{7} p \qquad \text{(appendix C)}$$

or to incorrect pressure-height profiles.

By considering equation (2.21) with a winter collision frequency profile (appendix C) it was found that an increase in collision frequency by a factor of 1.56 (equivalent to lowering the pressure profile by 2.5 km) would lead to an increase in the electron densities deduced from DPE data by a factor ranging from about 1.26 at 76 km down to about 1.03 at 86 km. The increases below 76 km would be even greater than 1.26 times.

The same collision frequency increase would lead to an increase below 74 km and a decrease above 76 km in the DAE densities. The decrease at 84 km would be by a factor of about 30%.

Thus an increase of about 60% in collision frequency would lead to a better agreement between the DAE and DPE densities above 76 km for 1973.

(2) There is an ambiguity of $2p\pi$ (p an integer) in the phase measurements. This was discussed in chapter 4 where it was stated that, provided the resultant electron density was positive, it was assumed that $\Delta\eta < 2\pi$. This means that at 85 km the maximum electron density measurable by the DPE experiment is about 1200 cm^{-3} (corresponding to a phase difference of 2π between 82.5 and 87.5 km). If the true

electron density is greater than 1200 cm^{-3} at this height, then the calculated density will be the true density minus 1150 cm^{-3}, so that the mean value of many measurements at 85 km could be too low. However, at 80 km the limiting value of electron density corresponding to a 2π phase shift is 1800 cm^{-3}, considerably larger than the densities usually found by the DAE method, so it is unlikely that this is the explanation for the discrepancy between the DAE and DPE mean values.

(3) The difference could be caused by an error in the reflection model. This is unlikely as none of the possible models discussed in chapter 2 could account for a 40% difference between DAE and DPE results.

(4) The cause may lie in the experimental procedure. As the height increases the difference between the experimental values $\langle|V_1|^2\rangle$ and $\langle|V_2|^2\rangle$ of equation (4.8) becomes small, as does also the difference between $\langle|M_1|^2\rangle$ and $\langle|M_2|^2\rangle$. As an example of this consider the data from 86 km for a particular run. (This run was actually at 1300 hours on 19/8/73.)

R.M.S. value of V_1 = 2.65 ± 0.14

R.M.S. value of V_2 = 2.53 ± 0.14

R.M.S. value of M_1 = 2.53 ± 0.15

R.M.S. value of M_2 = 2.44 ± 0.14

(on some arbitrary voltage scale).

Thus at this height the value of differential phase calculated from

$$\tan\eta = \left\{\frac{\langle|M_1|^2\rangle-\langle|M_2|^2\rangle}{\langle|M_1|^2\rangle+\langle|M_2|^2\rangle}\right\}\left\{\frac{\langle|V_1|^2\rangle+\langle|V_2|^2\rangle}{\langle|V_1|^2\rangle-\langle|V_2|^2\rangle}\right\} \qquad (4.8)$$

becomes rather meaningless. Also any differential attenuation

of say V_1 and V_2 due to the antennae, feeder systems, and impedance matching through to the receiver will become important. About all that can be said is that $\Delta\eta$ between 81 and 86 km will be some value less than 2π. Thus the mean of a large number of DPE electron density determinations for 83.5 km will depend on the apparatus and the laws of probability rather than the actual electron density in the mesosphere. A similar effect could occur for lower heights on days when the electron density is higher than normal, leading to a downward bias on the mean DPE electron density. The fact that there is better agreement between the DAE and DPE means in 1972 than in 1973 could perhaps be due to better impedance matching in 1972 (although it might also be due to chance and the much smaller statistical sample).

5.2.2 The Correlation Between DAE and DPE Electron Density Determinations

The results of the correlation and regression analysis between the differential absorption and differential phase electron densities are shown in table 5.2. A high correlation coefficient at a given height would suggest that both the DAE and the DPE results for a given run are following real changes in electron density which are significantly larger than the uncertainties due to statistical scatter.

The correlation is only really high near 74 km. (74 km in 1972, 73.5 km in 1973). For these heights the correlation is very significant (significance level $\leq$ 0.02%). The correlation coefficient is about 0.9, which means about 80% of the variance in the DPE densities is in phase with variance in the DAE densities (for times when there was data for both methods).

There also appears to be a significant correlation between the DAE and DPE densities at 76.5 km in 1972, when the correlation coefficient is 0.78 (60% of the DPE variance "explained" by the DAE variance). In 1973 the correlation appears significant at 78.5 km and perhaps 76 km, but in these cases only about 6% of the DPE variance is accounted for by the variance predicted by the regression equation and the DAE variance.

The strong correlation between DAE and DPE electron densities at 74 km is surprising considering the large uncertainties (about 55% in 1972, more than 100% in 1973) expected on the basis of the scatter in the data for a given run (table 4.4). This point is discussed in more detail in appendix F, the conclusion of which is that some of the assumptions implicitly used in estimating the uncertainties in table 4.4 were wrong.

5.3 CONCLUSIONS

The differential phase method for calculating electron densities using experimental determinations of the complex correlation coefficient between the ordinary and extraordinary waves gives results which are consistent with those of the differential absorption method between about 66 and 77 km. (This is for a frequency of 2.4 MHz at Birdling's Flat.) The agreement is particularly good at 74 km, where individual fluctuations in differential phase densities are in phase with fluctuations in differential absorption densities.

The combination of the two experiments does not appear to give a very accurate means of obtaining collision frequencies from a given run, since there is a considerable

amount of independent variation in calculated electron density between the two methods at most heights, probably related to the scatter in the data.

Above about 80 km the differential phase method (via the complex correlation coefficient) is not very useful, because at these heights it depends on small differences between large signals.

CHAPTER 6

METEOROLOGICAL EFFECTS IN THE MESOSPHERE

Over the past fifteen years or so there has been a considerable amount of discussion and conjecture on the meteorology of the mesosphere and its effect on the concentration of neutral gases, ions, and electrons in the region. The purpose of this chapter is to review the evidence for meteorological effects in the mesosphere and for dynamic coupling between lower parts of the atmosphere and the mesosphere, and to see how this evidence fits in with theories that have been put forward.

6.1 VARIATIONS FROM SOLAR CONTROL OF THE MESOSPHERE

One of the ground-based techniques which has been most fruitful in examining the mesosphere and lower thermosphere involves measuring the absorption suffered by a medium or high frequency radio wave in traversing the region. (Two methods are used: The vertical incidence pulse method (A1) (Piggot et al., 1957), and the A3 method (Mitra 1970) which monitors the strength of a CW radio signal over some path.) Typical frequencies used are 2.0-3.0 MHz. The absorption at a given height depends on the electron density and the collision frequency of electrons with neutral molecules (Piggot et al., op. cit.). It has been shown by Mitra and Jain (1963) that in a generalized Chapman layer the absorption should be proportional to $(\cos \chi)^n$, where χ is the solar zenith angle and n is between 0.5 and 1.5. The D-region is not a Chapman layer (since if Lyman-α is the predominant ionizing radiation the

radiation absorber (O_2) and the ionized molecule (NO) are different (ch. 9)). However, for a given nitric oxide concentration and recombination coefficient one would still expect the radio wave absorption to depend in some way on the solar zenith angle.

Sir Edward Appleton (1937) found that there was an anomaly from solar zenith angle control if winter absorption was compared to that in summer. This "winter anomaly" has been amply demonstrated since then (e.g. Appleton and Piggot 1954; Beynon and Jones 1965a; Schwentek 1963,1971; Thomas 1962). It is a mid-latitude effect; the following description is due to Schwentek (1971). If the absorption for each day is adjusted to a solar zenith angle given by cos χ = 0.1 (this can be done by using the absorption variation through a day) figure 6.1 results. The behaviour can be summarized thus:

(i) On a few days the absorption is as small as in summer.

(ii) There are days when the absorption follows a regular trend, increasing from the end of September to the winter solstice, and then decreasing until the end of March. Schwentek terms this the "normal" winter anomaly.

(iii) There are groups of days when the absorption is very high. Schwentek terms this the "anomalous" winter anomaly. Studies on "anomalous" winter days of the frequency dependence of the absorption (Thomas 1968), and rocket probe measurements of electron densities (Sechrist et al. 1969) have shown that most of the excessive absorption is due to electron density increase in the 80 to 90 km height range, although there may be some slight absorption increases from 70 to 80 km.

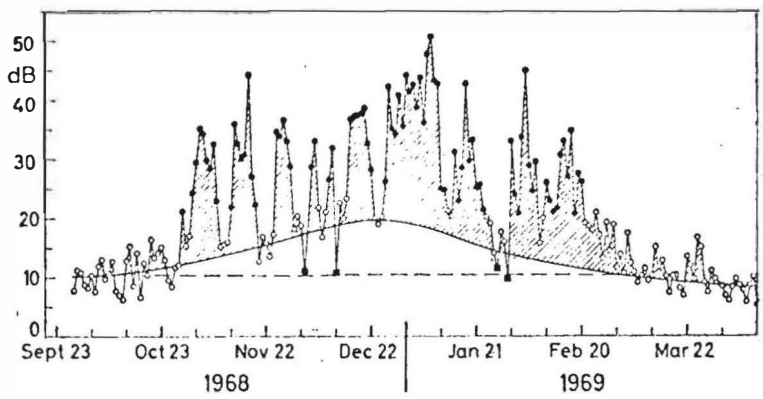

Fig 6.1: Absorption at constant solar zenith angle ($\cos\chi = 0.1$) for the 1968- 1969 winter (Schwentek 1971)

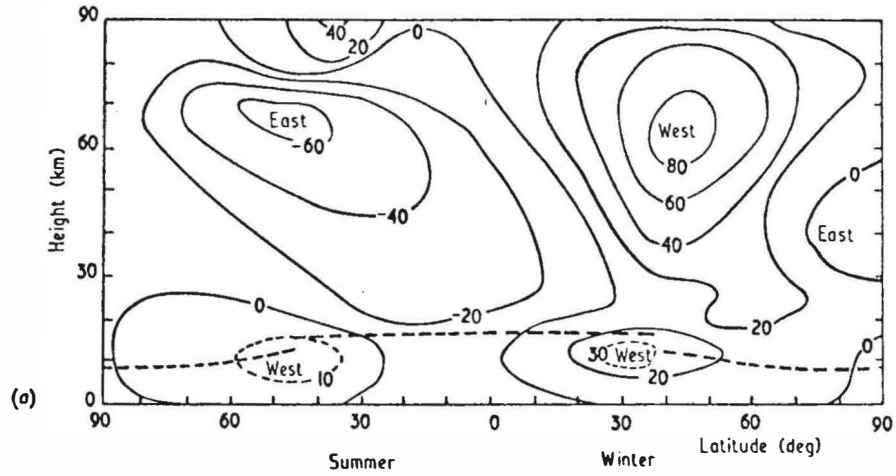

Fig 6.2: Latitudinal cross-section of zonal wind speed ($m.sec^{-1}$). From Murgatroyd (1970)

Note that "East" means from the east, ie. westward.

Thomas (1962) argued that solar flares or variations in solar radiation could not account for the anomaly, since high absorption over Europe tends to occur at times of low absorption over North America, and vice versa. Appleton and Piggot (1954) showed that the higher winter absorption is not to be ascribed to enhanced sunspot activity. Manson and Merry (1970) discussed the possible effects of energetic electron precipitation and found that this could only account for a small part of the "normal" winter anomaly, (and this part was due to seasonal meteorological changes in the atmosphere). Electron precipitation after-effects of magnetic storms can also affect electron densities and absorption in the D-region (chapter 8) but this is an unlikely explanation for the "anomalous" winter anomaly because of the anti-correlation between Europe and North America described above. Shirke and Rao (1967) found the variation of absorption with solar zenith angle on a day of high absorption to be quite similar to that on a "normal" winter day. This is further evidence against particle precipitation as a cause of the "anomalous" winter anomaly.

Thus it would seem likely, as was first suggested by Dieminger (1952), that changes in the absorbing region arise through meteorological processes. Both atmospheric motion and changes in temperature could give rise to variations in electron density (chapter 9), and thus of radio wave absorption.

Another way in which the deviation from solar control is evident was pointed out by Beynon and Jones (1965b). They found that a plot of the monthly mean absorption values through

a year against the cosine of the solar zenith angle had a figure of eight shape. It is interesting to note that the neutral density and pressure at 70 km and 60°N show a similar figure of eight behaviour, as does also the 20 mb temperature. Beynon and Jones base their suggestion for a meteorological cause of the winter anomaly on the similarity of these curves.

At this stage it is worth considering the seasonal changes in the upper atmospheric circulation, and the possible sources of shorter term fluctuations.

6.2 THE MEAN CIRCULATION OF THE STRATOSPHERE AND MESOSPHERE, WAVES AND WARMINGS

6.2.1 The Mean Circulation

Representative cross-sections of the zonal wind are given in figure 6.2 (Murgatroyd, 1970). The important features are the eastward flow throughout the stratosphere and mesosphere in winter, and the westward flow in most of the region in summer. The changeover in autumn from the summer westward flow to the winter eastward flow is usually rather steady, but the change back to westward flow during the early spring is usually a more disturbed period, and is often associated with the 'final warmings' to be discussed later. In the winter stratosphere in the northern hemisphere there is a strong stationary wave number one configuration associated with the "Aleutian High" over the North Pacific. In the southern hemisphere the winter polar vortex is much more symmetrical, and also more intense than that of the northern hemisphere.

The mean seasonal meridional and vertical motion in the upper atmosphere is much less certain. It is possible that in the winter mesosphere there is ascent at low latitudes, with polewards flow towards middle latitudes where there is a region of descent. There would also be ascent at high latitudes with equatorwards motion towards middle latitudes (Murgatroyd, op. cit.).

Any differences in the mean meridional flow or the mean vertical motion between summer and winter could contribute to the "normal" winter anomaly, either through transport of ionizable constituents or through associated temperature changes with their effect on reaction rates (Chapter 9). However, if the meteorology is to contribute to the "anomalous" winter anomaly a source of variability in winter is required. The types of variability which have been postulated for the mesosphere will now be discussed.

6.2.2 Planetary Waves

Planetary waves are waves in the motion, pressure, and temperature fields of the atmosphere which have global space scales, and time scales usually of at least several days. The original treatment of these waves was by Rossby (1939), who showed that the conservation of absolute vorticity would lead to planetary-scale oscillations if a small meridional disturbance was made in a steady uniform zonal wind. Charney and Drazin (1961) showed that planetary waves could propagate upwards from the lower atmosphere under certain conditions. The theory was put on a more realistic basis by Dickinson (1969), who showed that vertical propagation is not possible through strong eastward winds or through westward winds.

However, he found that large transmission coefficients were possible at times in the winter when the zonal wind in the stratosphere is eastward but below the critical value which reduces the Döppler shifted wave frequency to zero. A simpler treatment is given by Lindzen (1967).

There is good experimental evidence for planetary wave activity in the stratosphere. Deland and Johnson (1968) for example, made a harmonic analysis of geopotential data from 1000 mb to 10 mb. They found westward travelling waves which extended considerably further up in to the stratosphere in winter than in summer. They found a tilt in phase with height which they say implies some forcing from below.

Because there is no hemispheric network of stations measuring winds or pressures in the mesosphere at sufficiently regular intervals, or even any suitable long time series records from a given station there is no definite proof for the existence or otherwise of planetary waves in the mesosphere. The limited evidence from meteor winds is described in chapter 9.

If it is assumed that there are planetary waves propagating up through the stratosphere to the mesosphere it is not obvious how or whether these would show up in attempts to correlate stratospheric and mesospheric parameters. Firstly suppose the effect was as if some source was turned on in the lower atmosphere (such an effect could be due to a change in zonal wind at some height so that the planetary wave was no longer trapped in the lower atmosphere). Such a disturbance could be expected to travel upwards with some vertical group trace speed, but this would depend on the background state of

the atmosphere and the horizontal scale of the waves involved (Clark, 1972). The vertical speed of the front of one disturbance in a very idealized stratosphere was found to be about 7.6 km/day by Clark (op. cit), and Matsuno (1971) quotes a value of "less than 5 km day^{-1}". Thus one would expect a delay of several days between the effects of the front of such a disturbance on the 10 mb level (30 km) and the mesosphere (70 km).

Suppose instead that a planetary wave of given latitudinal and longitudinal wavenumber and given period is present in the upper stratosphere and mesosphere. Then correlations between stratospheric and mesospheric parameters above a given point on the earth will depend on the difference in the phase of the wave between stratospheric and mesospheric heights. The vertical wavelength depends on the horizontal dimensions and the period of the wave (Lindzen, 1967) and probably also on the background zonal wind. From the article by Lindzen (op. cit) it appears that planetary waves with vertical wavelengths of less than 30 km are possible. This could lead to differences of several days between the occurrence of a given phase at stratospheric and at mesospheric heights.

6.2.3 Stratospheric Warmings

During the winter of 1951-52 Scherhag (1952) discovered a sudden increase in stratospheric temperature over Berlin, and since then other sudden warming events have been observed (Scherhag, 1969). At 60^{o}N they may show up as temperature increases of about 50^{o}C in less than five days (Webb 1966, page 171). At times these temperature changes are accompanied

by changes in the zonal stratospheric circulation from eastward to westward (Murgatroyd, 1970). If the circulation does not revert to the normal winter eastward flow the event is called a final warming. Final warmings are also observed in the southern hemisphere (Phillpot, 1969). Apparent mid-winter warmings at 30 mb in the southern hemisphere stratosphere may actually be due to the passage of migratory warm ridges associated with an n = 2 planetary scale wave (Phillpot, op. cit).

Rocket measurements of temperature in the northern hemisphere have shown that the disturbance associated with a stratospheric warming extends at least into the upper mesosphere, but above a given location on the earth the temperature change has different signs at different heights (Labitzke 1972a, 1972b) (see figure 6.3). Also there may be warmings in the upper stratosphere and mesosphere which have little effect below 25 km. It should be noted that a given warming does not show up over the entire mid-latitude stratosphere at the same time; there may be several days between the onset of a warming over Europe and its appearance above North America (Scherhag, 1969).

It is possible that the warmings are due to interactions between planetary waves and the zonal flow (Matsuno, 1971). However, it is important to realize that a large temperature increase at a given height at the time of a large stratospheric warming is not simply the temperature perturbation of a planetary wave.

6.2.4 Internal Gravity Waves

Internal gravity waves in the atmosphere have periods between about five minutes and several hours (Hines 1972). If they are not dissipated or reflected their amplitudes increase exponentially with height (planetary waves also behave in this fashion). Their vertical scale size is from 5 to 50 km, and the corresponding horizontal scale size 10 to 300 km. It is thought that the main sources of the waves are in the troposphere, such as mountain lee waves, weather systems and jet streams. Typical vertical trace speeds associated with individual waves are 1-20 m/sec, and horizontal trace speeds are typically 20 to 100 m/sec. The patterns of irregular wind fields due to the interference of superposed waves move with similar speeds. Not all of the waves from the troposphere will reach the mesosphere since waves of some frequencies are reflected due to the background temperature and wind. At 'critical levels' where the frequency of the wave relative to the background wind is Doppler shifted to zero the waves are absorbed giving rise to heating and a change in the mean flow (Hines and Reddy, 1967). Gravity waves may also give rise to turbulence, by energy deposition at critical levels and also due to superadiabatic temperature gradients and wind shears associated with the waves. Turbulence gives rise to mixing of ionizable constituents (it contributes to the eddy diffusion coefficient discussed in chapter 9).

Because planetary waves give rise to changes in the background flow and temperature as seen by gravity waves, fluctuations in the stratosphere due to planetary waves might give rise to variations in the transmission of gravity waves into the mesosphere (Hines 1972). Stratospheric warmings might also affect the gravity wave flux.

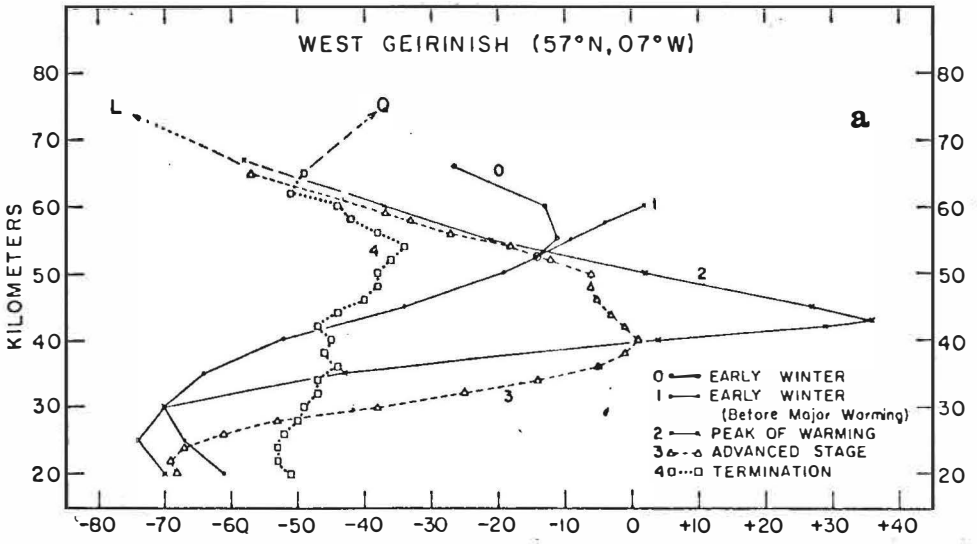

Fig 6.3: Typical mean temperature profiles for West Geirinish (Labitzke, 1972b)

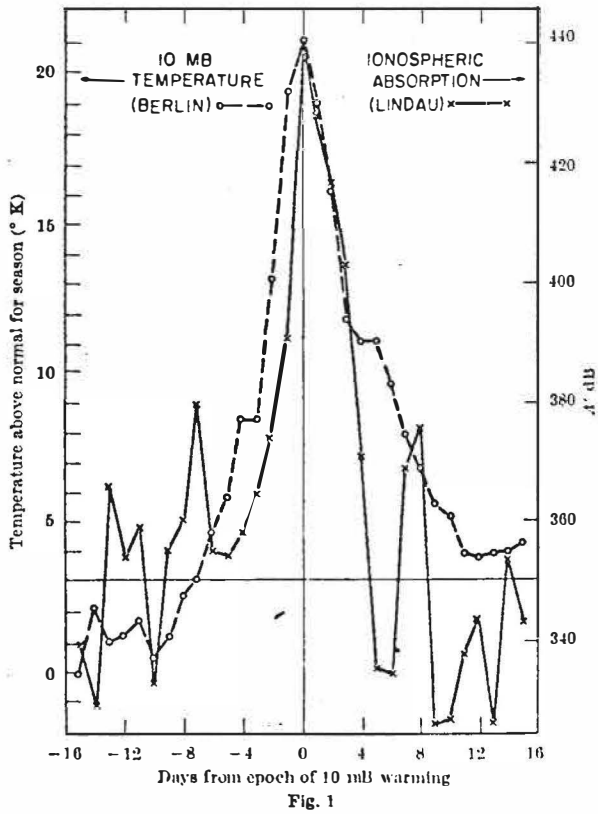

Fig 6.4: Superposed epoch comparison of daily ionospheric absorption index and stratospheric temperature. (Shapley & Beynon, 1965)

6.3 MESOSPHERIC OBSERVATIONS AT THE TIME OF STRATOSPHERIC WARMINGS

The term "stratospheric warming" tends to be applied rather loosely in ionospheric physics. In some mid-winter warmings there is breakdown of the stratospheric polar vortex (these are called major warmings) and temperature variations may be observed well down in the lower stratosphere, below 20 km (Labitzke 1972b). As has been discussed there are some warmings when there is little discernable temperature change at 20 km (50 mb) but still a large warming in the upper stratosphere, or there may be temperature increases at 30 mb due to planetary wave passage. For these reasons there are problems in using, say, the 30 mb temperature above a given station as an indication that a warming has occurred as it is not clear to which of the above classes the "warming" may belong, and a warming which occurred only in the upper stratosphere might not be detected.

There are several cases on record of anomalies in the lower ionosphere at the time of stratospheric warmings. Belrose (1967) found that during the major warming of February 1952 there was an increase in the vertical incidence absorption for MF radio waves over Slough and a decrease in the phase height (from 74 to 64 km) for the VLF path Rugby-Cambridge. The peaks of both of these effects were four days after the maximum 10 mb temperature was measured over Berlin. There was another major mid-winter warming in the winter of 1967-68 (Labitzke 1972b). At this time Rowe et al. (1969) using the radio-wave interaction technique found an increase in the electron density from 75 to 90 km above Pennsylvania State

University (48°N, 78°W) at about the same time as the 10 mb temperature peaked above Thule (77°N, 69°W). In the southern hemisphere Gregory (1965) using the differential absorption technique detected an increase in the electron density in the 65 to 80 km region above Christchurch at the same time as an increase of about 8°C in the 20 mb temperature. (This was in June 1963). During the major warming over Europe in 1963 Belrose and Thomas (1968) found that the 10 mb temperature over Berlin and the HF absorption over De Bilt and Lindau showed a clear correlation.

One problem with some of these events is that particle precipitation can also cause an increase in absorption (Ch. 8). There were increases in the planetary magnetic index A_p three days before the peak in ionospheric absorption during the 1952 Berlin warming (Belrose 1967), and there was a magnetic storm during the period of increased electron density observed by Rowe et al. (1969). The ΣK index at Amberley (near Christchurch) was above normal for four days immediately preceding the increased electron densities observed by Gregory (op. cit.) and a magnetic storm was reported at several northern hemisphere stations (Lincoln, JGR 68, 5879) two days before this increase. Another problem is that because absorption tends to be high over periods of several days in winter, and stratospheric warmings also tend to affect the atmosphere above a given point for several days there is a danger that the simultaneous occurrence of the stratospheric and mesospheric events described above could be due to chance, since it is less likely that events when there was no excess absorption at the time of a stratospheric warming would be published. In fact Belrose and Thomas (1968) found there was a lack of

correlation between 10 mb temperatures and f_{min} during the January 1963 warming, and Larsen (1971) found no significant increase in f_{min} above Trömso (Norway) during a period when the 10 mb temperature increased by 40°C (as will be discussed later f_{min} is a rather poor measure of ionospheric absorption, however). Patel and Kotadia (1972) state that the correlation between warmings at 20 mb and the 3.86 MHz absorption above Juliusruh (East Germany) was poor for the 1963-64 and 1964-65 winters. (However, there were no major warmings during these winters, and 3.86 MHz is less sensitive to D-region absorption than frequencies down around 2.0 MHz.)

A better check is possible with the superposed epoch technique, using days of maximum warming in the stratosphere as zero days. Shapley and Beynon (1965) used this technique for the years 1959-64. Figure 6.4 shows the result from fourteen distinct periods when the 10 mb temperature above Berlin exceeded the seasonal mean by 10-30°K. The absorption is for vertical incidence at 1 MHz above Lindau. There is a clear correlation with both phenomena peaking at the same time. Gregory and Manson (1970) found a correlation between 30 mb temperatures and f_{min} above Christchurch by doing a superposed epoch analysis for five events in winter 1963 and four events in May-July 1964. However, they found no correlation for August and September 1964, and Thorpe (1970) found no association in a superposed epoch analysis of Campbell Island f_{min} with Christchurch 30 mb temperatures using 26 zero days from 1964-67 when the temperature was more than 6°C above the seasonal average. Manson (1968) did a superposed epoch analysis using 14 days of high 30 mb temperature

above Maniwaki (46°N, 75°W), and found a significant correlation with f_{min} above Ottawa (45°N, 75°W). Thus the f_{min} observations appear inconclusive, particularly bearing in mind the shortcomings of f_{min} as a measure of D-region absorption and the question of whether the "warmings" considered in these analyses are true stratospheric warmings with large temperature increases higher in the stratosphere.

There have been correlations reported between other upper atmospheric parameters and stratospheric warmings. Sodium D-line emission rates measured in the twilight glow by ground based photometers are known to be sensitive to sodium in a layer about 15 km thick centred near 85 km (Chamberlain 1961). Hunten and Godson (1967) found by a superposed epoch analysis that there was a correlation between sodium abundance over Saskatoon and the occurrence of warmings in the Canadian Arctic Stratosphere at 100 mb. Rundle and Sullivan (1972) found evidence consistent with a similar association between 30 mb temperatures and sodium abundance.

Also Sprenger and Lysenko (1972) report a shift in the phase of the tidal component of drifts at 95 km over East Germany measured by L.F. reflections, at times of midwinter stratospheric warmings. (They considered five between 1958 and 1966). These shifts were similar to those observed during final warmings, and in one case the 95 km effect began about four days before the warming was detected at 30 mb.

6.4 OBSERVATIONS OF PLANETARY-SCALE EFFECTS IN THE LOWER IONOSPHERE AND STRATOSPHERE-IONOSPHERE COUPLING

Two approaches have been taken in looking for planetary wave activity and stratospheric-ionospheric coupling. One is to look for fluctuations of at least several days quasi-period over a given location on the theory that they are caused by travelling planetary waves. The other has been to look for spatial fluctuations on a given day.

In 1963 Bossalasco and Elena published figures showing the seven day running mean of vertical incidence absorption over Fribourg (Germany) and the corresponding value of the mean temperature over Central Europe (5-20^{o}E, 45-55^{o}N) for the 1958-59 and 1960-61 winters. In each winter there were two broad peaks in 10 mb temperatures. There were also two broad peaks in the absorption, and these peaked within about five days of the temperature maxima. However, if large stratospheric warmings and increases in absorption tend to be coincident (6.3) these results might be interpreted as the effects of two stratospheric warmings during each winter.

Another interesting result, although it is for the lower E-region, is a comparison between the 4.5 x 10^{4} cm^{-3} electron density isopleth (~110 km) and the 10 mb height over Aberystwyth (Brown and Williams, 1971). There is a good correlation from January to March 1965, and also a correlation for February and March 1966, with fluctuations in both parameters of quasi-period about 15 days. Deland and Cavalieri (1973) claim a correlation between f_{min} and the 10 mb temperatures at the time of the 1965 results, but this does not appear to be very clear. It should be pointed out that

there are other simultaneous time series of the temperature of pressure levels in the stratosphere and f_{min} which fail to show clear correlations (e.g. Belrose and Thomas (1968), Gregory and Manson (1970), Thorpe (1970)).

Thomas (1962) examined the spatial variation of absorption during the 1957-58 winter. He found that anomalously high absorption on a particular day extended over an area of Europe of at least 10^6 square kilometers. He also discovered an inverse relationship between the incidence of anomalously high absorption over America and over Europe, and also over America and over Western Russia.

Another analysis was made by Deland and Friedman (1972). For each day between November 1964 and April 1965 they calculated the amplitude and phase of the first zonal Fourier component of f_{min}, using stations in the latitude range 40-60^{o}N. They also calculated the amplitude and phase for this component of the 10 mb height and the 50-10 mb thickness at middle latitudes (50 or 60^{o}N). The average correlations and phase shifts between the meteorological and f_{min} components for each month were then calculated and plotted on a polar diagram. For delays of -1, 0, 1 days between the meteorological and the f_{min} data most of the points fall within the quadrant centred on zero degrees. The authors suggest that this indicates a connection between very large scale fluctuations in the upper and lower atmosphere, due to vertical disturbances in the temperature field with no significant time delay with height. They do point out that only about 10% of the f_{min} variance at a given station can be explained by the regression on the geopotential harmonic of wavenumber one.

A possible objection to this conclusion is based on the nature of f_{min}. Although f_{min} is dependent to some extent on absorption (Thomas, 1962) it also depends on the sensitivity of the ionosonde and on local radio interference (King, 1967). For example there are a lot of local radio stations in Europe and an operator might therefore keep the sensitivity of his ionosonde low, with correspondingly high values of f_{min}. If there is less radio interference over the more sparsely populated areas north of Japan and in the Aleutians, where three of the ionosondes are, it is possible that the ionosondes are run on higher sensitivity with correspondingly lower f_{min}. Thus a stationary wavenumber one component in f_{min} with its minimum roughly over the Aleutians might result merely from the effect of local radio stations. Also, in the winter stratosphere there is a stationary $n = 1$ wave with high pressure over the Aleutians (Hare and Boville, 1965). This would give a minimum in the 10 mb height over the Aleutians, and the overall result would be an apparent correlation between the first Fourier harmonics of f_{min} and the 10 mb height, with very little phase difference. It must be admitted that Deland and Friedman find slightly smaller correlation coefficients and more scatter in the phase difference when they consider lags of four or five days between the stratospheric and ionospheric parameters, which does not fit in with this argument. However, I feel that their results should be interpreted with caution.

Wu and Newell (1972) investigated the correlation at different seasons between vertical incidence absorption and 10 mb winds and temperatures from March 1964 up to Feburary

1966 for nine mid-latitude stations. They found that the absorption correlated negatively with the zonal wind but positively with the temperature in a majority of cases, and that the absorption is correlated with the meridional wind in winter. They admit that trends within seasons may give rise to some of the correlations, but feel this is not likely for the winter meridional winds and temperatures.

The passage of a stratospheric planetary-scale wave over North America was observed by Williams et al. (1972). This wave was evident in synoptic analyses at 40 and 50 km, and these authors discovered increases in f_{min} at Boulder, White Sands and Washington D.C. coincident with the passage of the wave in the stratosphere. However, there was also an increase in the planetary magnetic index A_p about two days before the increase in f_{min}.

Gregory and Manson (1970) have suggested a relationship between electron density in the D-region and the passage of cyclonic waves at 200 mb. Firstly they considered the days when the first obvious increase of winter absorption occurred or the largest increase of absorption occurred during the winter from 1956 up to about 1965. On 80% of these days there was a pressure ridge at upper balloon levels approaching New Zealand across the Tasman Sea. However, the scale of the disturbances at 200 mb is such that there is about one chance in two of there being a pressure ridge over the Tasman Sea. Second, they give three cases when a peak in D-region electron density corresponded to within a day of a pressure ridge crossing Christchurch at 200 mb. A quick analysis of N.Z. Meteorological Service data reveals that pressure ridges at

this level cross Christchurch on average about once per week. Hence, if a day is picked at random there is about a 40% chance that a pressure ridge crossed Christchurch on that day, the previous day, or the following day. Thus although Gregory and Manson's results may be suggestive, they are not statistically convincing.

6.5 METEOROLOGICAL MEASUREMENTS IN THE D-REGION

There have been very few comparisons of winds and temperatures in the D-region between times of normal and anomalous absorption.

Sechrist et al. (1969) made rocket measurements of temperature and wind speed in the D-region on 31 January 1967 (a day of anomalously high absorption) and 3 February 1967 (a normal winter day). On the anomalous day they found a temperature inversion at 70 km, with a warm layer from the inversion to 80 km. Zimmerman and Narcissi (1970) calculated the Richardson number throughout the D-region using this data. They found that on the anomalous day the mesosphere was likely to be stable from 60 to 78 km ($Ri > 1$) but turbulent ($Ri < 1$) from 78 to 90 km. On the normal day the condition for turbulence ($Ri < 1$) extended through all of the D-region above 68 km.

Rose et al. (1972) launched 26 rockets at Arenosillo ($37^{o}N$) during the 1969-70 winter-spring period. From measurements of wind and the chaff fall rate they calculated the air mass flow at intervals of 1 km between 75 and 95 km. At the same time (local noon) they measured the A3 absorption on 2.83 MHz on a 424 km path from Arenosillo. They found that absorption increased in winter with increasing air mass flow

from northern directions between 90 and 93 km and from southern directions at 85 km. Unfortunately most of the rocket firings were on days of anomalously high absorption.

6.6 CONCLUSIONS

From the preceding discussion it can be seen that the influence of meteorological processes on electron density in the D-region is not very clear-cut. However, the following characteristics appear:

(1) The D-region electron density is not under strict solar control. It is likely that part of the deviation from solar control at medium latitudes is due in some way to meteorological processes.

(2) The balance of the evidence is that changes in the D-region electron density do occur at the time of large stratospheric warming events. The electron density increase occurs at about the same time as the temperature at about 25 km increases. This is not surprising since the temperature changes associated with these events appear to spread both ways in height from about 40 km, reaching the lower stratosphere and the mesosphere at about the same time. There is also evidence for wind changes in the upper atmosphere at these times.

(3) The occurrence of anomalously high absorption over some longitude sectors (e.g. Europe) appears to be negatively correlated with the occurrence over others (e.g. North America). Suggestions that meteorological influences could be on a planetary wave scale are strengthened by theoretical predictions that planetary waves could propagate from the

lower atmosphere up into the mesosphere in winter. An apparent correlation has been found between the strength and phase of the first Fourier component of the 10 mb geopotential height and the first component of f_{min} in winter, but this is open to some doubts. While correlations between stratospheric winds or temperatures and D-region absorption in winter appear to be significant at some mid-latitude stations, studies at other mid-latitude locations have failed to reveal any correlations.

While it is likely that planetary waves propagate up into the mesosphere it is also possible that upward propagating gravity waves are important. These waves could give rise to turbulence with associated transport of minor constituents, and also to temperature changes in the D-region. The propagation time from the troposphere to the mesosphere is of the order of hours. Also the gravity wave spectrum reaching the mesosphere could have been filtered by the stratospheric planetary wave field. Such correlations as have been found between stratospheric and mesospheric parameters are for time lags of zero or one day between the two regions. One possible source of gravity waves is from weather systems in the troposphere, which could tie in with the suggestions of Gregory and Manson (op. cit.) on the influences of pressure ridges in the troposphere (although as was pointed out there is no definite proof of such an influence).

From these conclusions several ideas emerge. First, if planetary waves in the stratosphere are important the southern hemisphere may be the best place to look. This is because there are no large stationary waves in the southern hemisphere,

and travelling planetary waves may be important (Phillpot, op. cit.). Travelling waves could be observed at one station. To my knowledge the only day-by-day analysis so far in the southern hemisphere not using f_{min} was by Thorpe (1970) who used the A1 absorption method. One of the aims of the present thesis work was to extend such measurements to the differential absorption technique. Also, it appears important from the work of Labitzke (op. cit.) to measure meteorological parameters as high as possible in the stratosphere, and data from channel A of the selective chopper radiometer on NIMBUS IV (Harwood 1971) which is sensitive to temperatures at about 2 mb was available for 1972.

The objections to the analysis of Deland and Friedman relate mainly to the use of f_{min} as a measure of absorption. Daily A1, A3 or differential absorption measurements from stations well spread over a latitude circle would be useful, but this is probably only feasible in the Northern hemisphere. It would be interesting to compare results between Adelaide and Christchurch however.

More details of the temperature and wind in the mesosphere on days of normal and anomalous absorption would be useful. With this in mind an attempt was made to run the partial reflection drifts experiment at Birdling's Flat at the same time as the differential absorption experiment.

Finally, a full understanding of the winter anomaly will depend on a better knowledge of the chemical processes in the mesosphere than is presently held (Chapter 9).

CHAPTER 7

D-REGION ELECTRON DENSITIES OVER BIRDLING'S FLAT

In this chapter the results of the differential absorption electron density measurements at Birdling's Flat are discussed. Firstly, the seasonal means and variances are examined, to look for evidence of a winter anomaly and as a comparison with the earlier results of Gregory and Manson (1969b). Secondly, some measurements which were made of diurnal electron density variations are discussed.

Finally, the time series of electron densities at various heights are examined for the winter-spring periods of 1972 and 1973. Possible meteorological influences are searched for through the use of D-region drift measurements for 1972. Evidence for stratosphere-ionosphere coupling is searched for using data from New Zealand Meteorological Service radiosonde balloons, and from the selective chopper radiometer experiment on the satellite NIMBUS-IV.

In this chapter when an electron density for a given day (the "daily mean electron density") is quoted it is a weighted mean of all the electron densities for that height from all runs between 11 a.m. and 2 p.m. local time.

i.e.
$$N_e = \frac{\Sigma(\sqrt{n_i}\, N_i)}{\Sigma(\sqrt{n_i})} \qquad (7.1)$$

where n_i is the number of data samples and N_i the calculated electron density for the i^{th} run.

This was done because it was considered that the data from longer runs was more reliable. For most days in 1972, n_i = 300, but for technical reasons there were quite a few runs of different length. In 1973 n_i = 75.

7.1 THE SEASONAL BEHAVIOUR OF ELECTRON DENSITY

Table 7.1 gives the mean seasonal values of electron density ($\bar{x}$) with their standard error (e), the number of days on which values were obtained (n), the coefficient of variation (V), and its standard error (e_r).

The standard deviation σ is calculated from the estimator s, where

$$s^2 = \frac{1}{(n-1)} \sum_{i=1}^{n} (x_i - \bar{x})^2$$ (Bendat & Piersol 1971, section 4.1)

The standard error of the mean value is

$$e = \frac{s}{\sqrt{n}}$$ (Topping 1962, p62)

The standard error of the coefficient of variation is

$$e_V = \frac{V}{\sqrt{2n}}$$ (Moroney 1953, p137)

The seasons are defined as:

Spring: September, October, November

Summer: December, January, February

Autumn: March, April, May

Winter: June, July, August.

This is the assignment of months to seasons used by Gregory and Manson (1969b).

$\bar{x}$ and e are in cm^{-3}.

SPRING	1972					1973					
Height (km)	n	$\bar{x}$	e	V	e_V	Height (km)	n	$\bar{x}$	e	V	e_V
66.5	23	78	10	0.63	0.09	66	1	72			
69	26	123	13	0.55	0.08	68.5	1	58			
71.5	27	174	13	0.38	0.05	71	5	104	33	0.72	0.23
74	26	229	9	0.21	0.02	73.5	9	258	37	0.43	0.10
76.5	26	298	13	0.22	0.02	76	17	310	43	0.57	0.10
79	26	377	23	0.31	0.04	78.5	11	324	49	0.51	0.11
81.5	26	515	30	0.34	0.04	81	7	443	81	0.48	0.13
84	26	713	46	0.31	0.04	83.5	6	596	65	0.27	0.08
86.5						86	4	828	114	0.28	0.10

SUMMER	(1971-72 and 1972-73)				
Height (km)	n	$\bar{x}$	e	V	e_V
69	3	149	30	0.36	0.16
71.5	5	184	45	0.55	0.22
74	7	241	30	0.36	0.11
76.5	9	305	30	0.32	0.08
79	7	361	40	0.35	0.10
81.5	5	470	80	0.39	0.14
84	3	618	160	0.57	0.24

AUTUMN	(1972)				
Height (km)	n	$\bar{x}$	e	V	e_V
71.5	4	99	40	0.86	0.43
74	3	170	62	0.63	0.34
76.5	8	265	36	0.38	0.11
79	9	303	32	0.30	0.08
81.5	6	367	51	0.37	0.11
84	5	532	100	0.51	0.17

WINTER	1972						1973				
Height (km)	n	$\bar{x}$	e	V	e_V	Height (km)	n	$\bar{x}$	e	V	e_V
						63.5	1	112			
66.5	29	71	7	0.57	0.10	66	3	96	25	0.45	0.18
69	35	123	17	0.83	0.15	68.5	4	70	5	0.14	0.05
71.5	41	164	13	0.51	0.07	71	8	91	10	0.32	0.08
74	48	252	15	0.40	0.05	73.5	12	175	23	0.45	0.09
76.5	48	342	18	0.35	0.04	76	18	271	28	0.44	0.07
79	50	413	24	0.40	0.05	78.5	18	373	21	0.24	0.04
81.5	46	435	33	0.48	0.06	81	18	473	32	0.28	0.05
84	40	561	46	0.49	0.07	83.5	16	630	49	0.31	0.05
						86	14	631	63	0.37	0.07
						88.5	10	883	170	0.61	0.14

Table 7.1 Seasonal statistics for electron densities

In figure 7. 1 the seasonal mean profiles of electron density from table 7.1 are plotted, along with error bars for some heights and the profiles of Gregory and Manson (1969b). In interpreting these results it must be borne in mind that the mean densities, particularly at the lowest and highest heights, are probably calculated from a biased sample. For example if the electron density is high there will be strong absorption, so that the extraordinary signal from above 80 km could be too weak to observe, leading to a lack in data from that height. It is also possible that strong returns from around 65 km might only be present on days when the electron dnesity is higher than normal.

There is agreement between the spring results from 1972 and those for 1973 to within the standard errors. The winter 1972 and winter 1973 results differ between 69 and 79 km, with

the 1973 densities up to 30% lower than those for 1972. (However, there were no measurements in July 1973 while the 1972 results include about 20 days in July.) There is generally a good agreement with the profiles of Gregory and Manson, except in winter when Gregory and Manson found lower densities from 70 to 80 km, and below 71 km in summer when both curves are from small numbers of measurements. The last sunspot minimum year was 1964, and the next is expected to be 1975, so both the results of Gregory and Manson (taken between 1963 and 1967) and the present results (1972-73) are for years of relatively low sunspot activity.

From figure 7.2 (which shows the mean density from the 1971-72 and 1972-73 summers, and the 1972 mean winter profile) the winter electron density is higher than the summer density between 76 and 82 km, and very little lower than the summer densities for the other heights between 69 and 84 km. This is evidence of a "winter anomaly", with the winter electron densities higher compared to the summer densities than would be the case for strict solar control.

Figure 7.3 shows the coefficients of variation (standard deviation/mean) of the series of mean daily electron densities for each season in 1972. If several experimental runs are done near mid-day on one day, there is considerable variation in the resulting calculated electron densities (chapter 4). Thus there is some uncertainty in the calculated "daily mean" electron density as a measure of the true mean electron density on a given day. The "mean daily error" of table 7.2 is an estimate of the fractional uncertainty in the calculated "mean daily" electron density. It has been estimated as described in section 4.8.

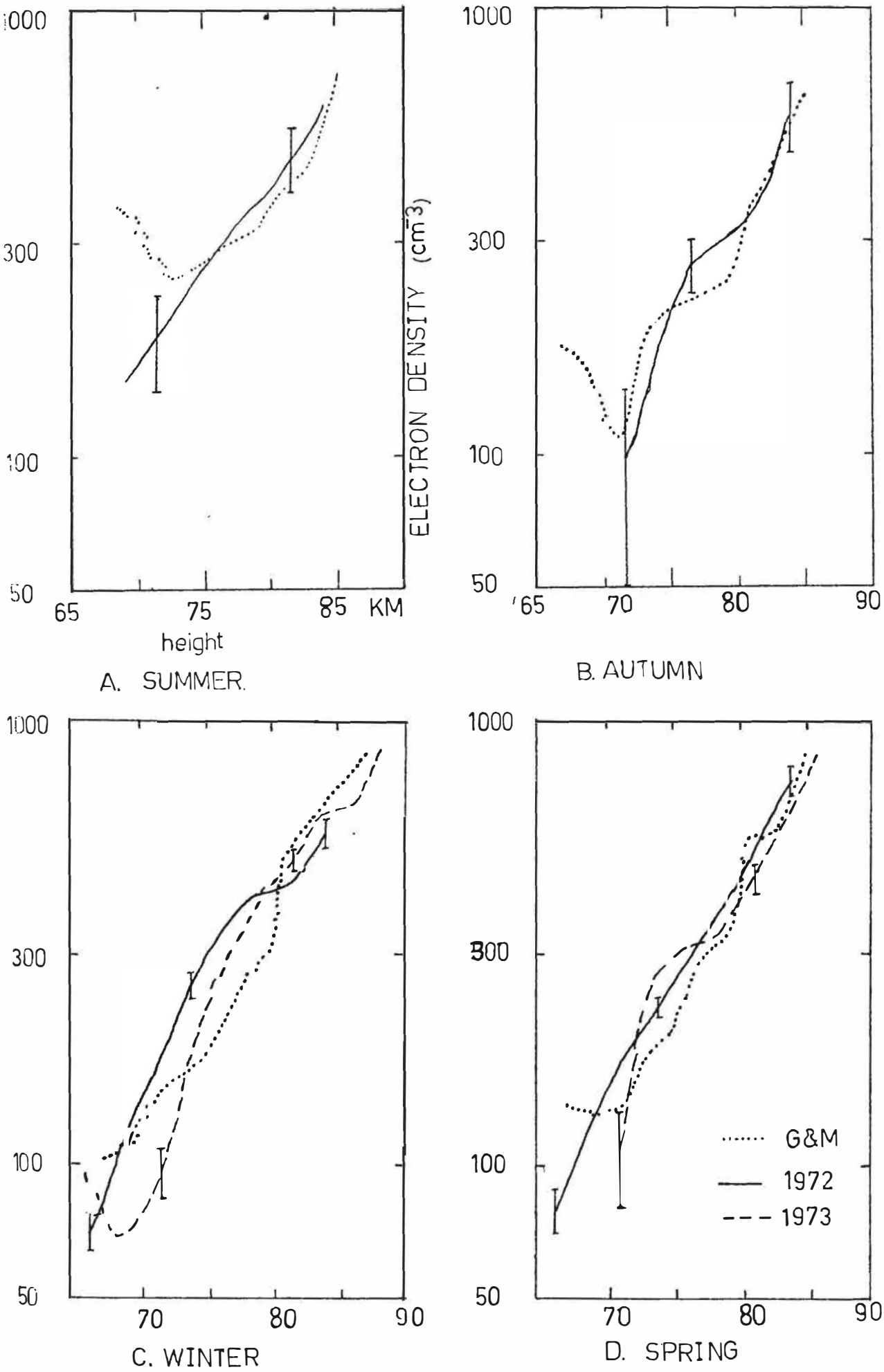

Fig 7.1 MEAN SEASONAL PROFILES.

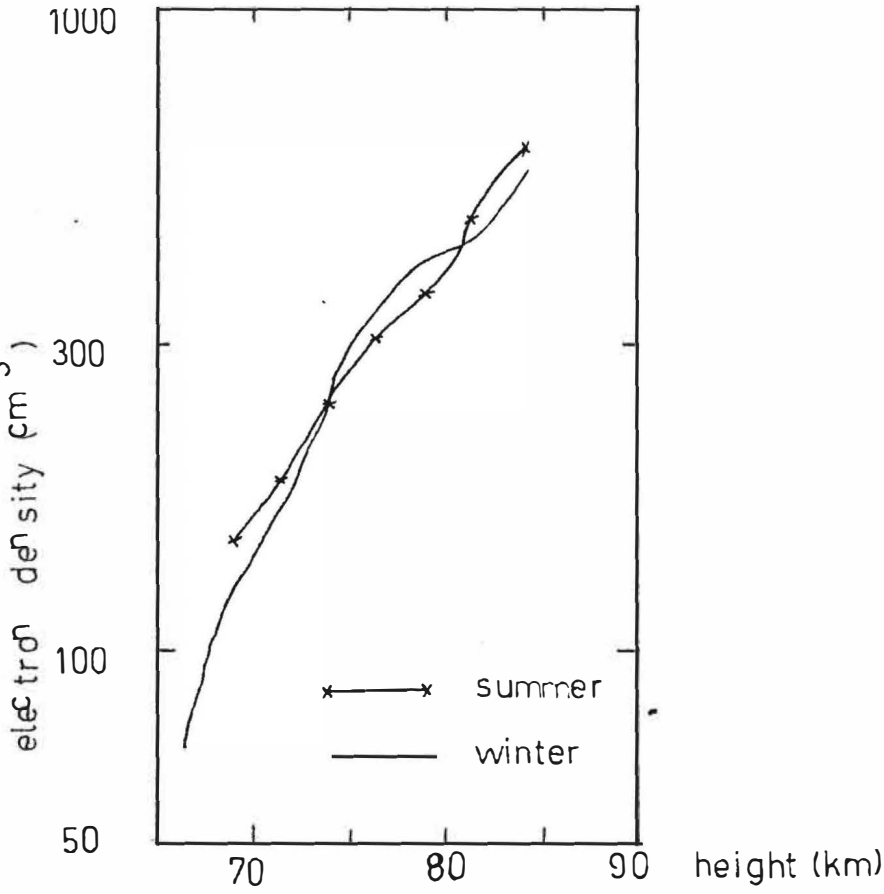

fig 7.2 SUMMER & WINTER PROFILES

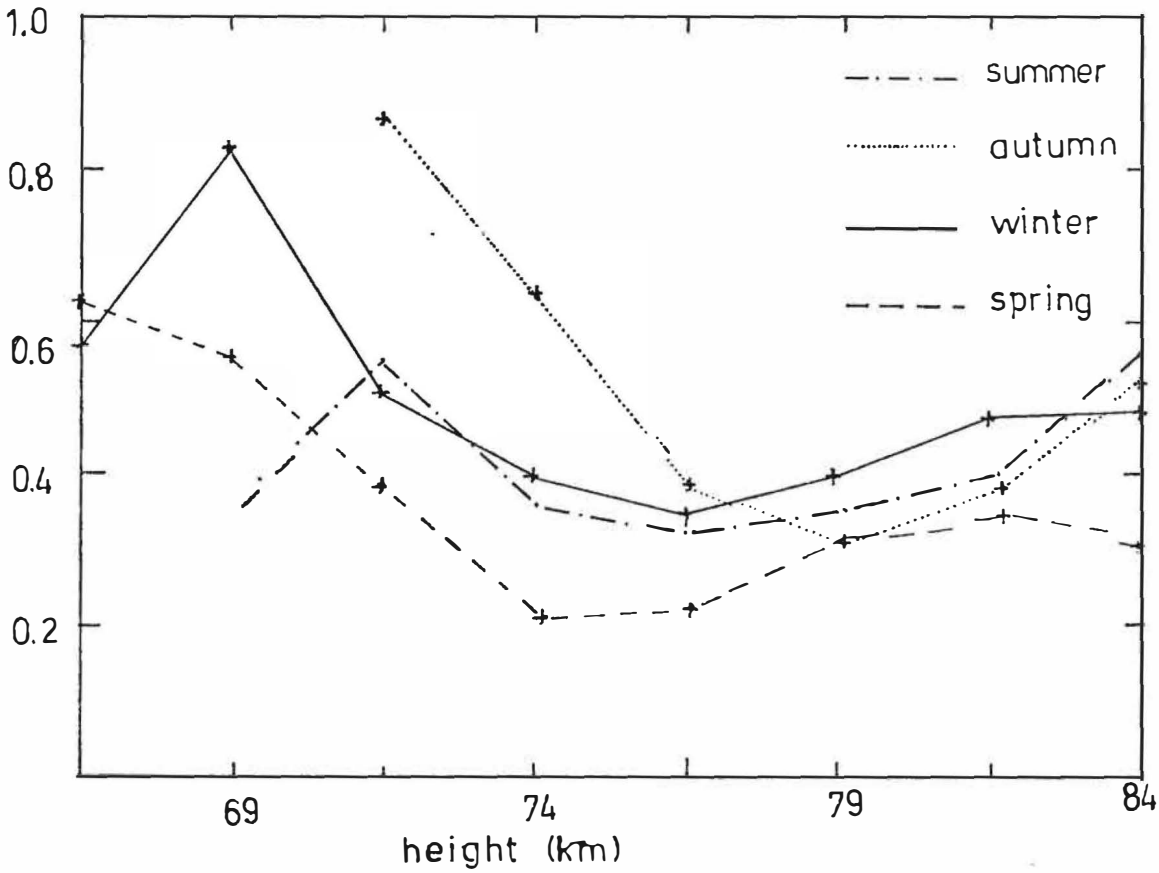

fig 7.3 Coefficient of variation. (1972)

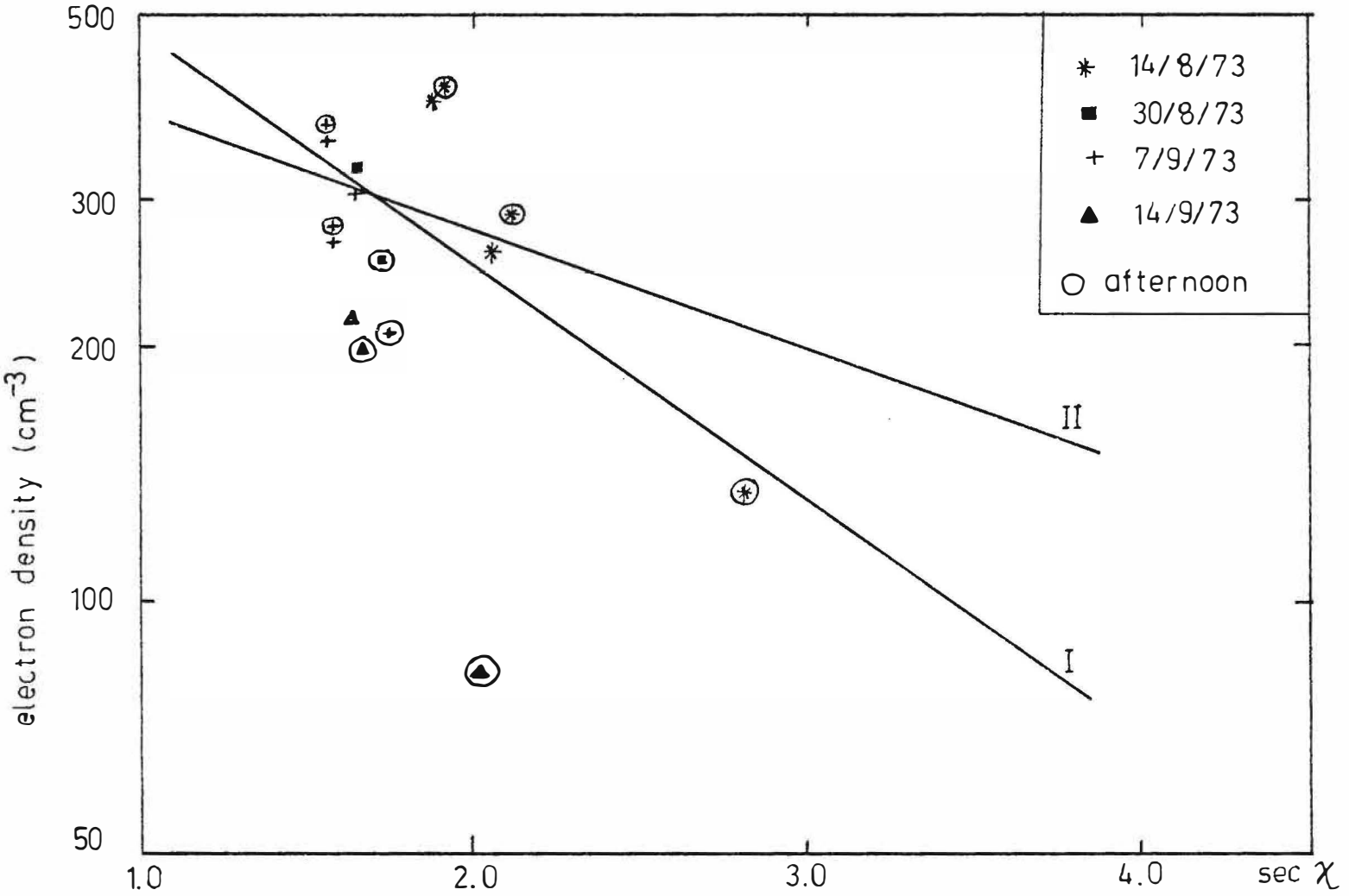

fig 7.4 Diurnal variation at 76km.

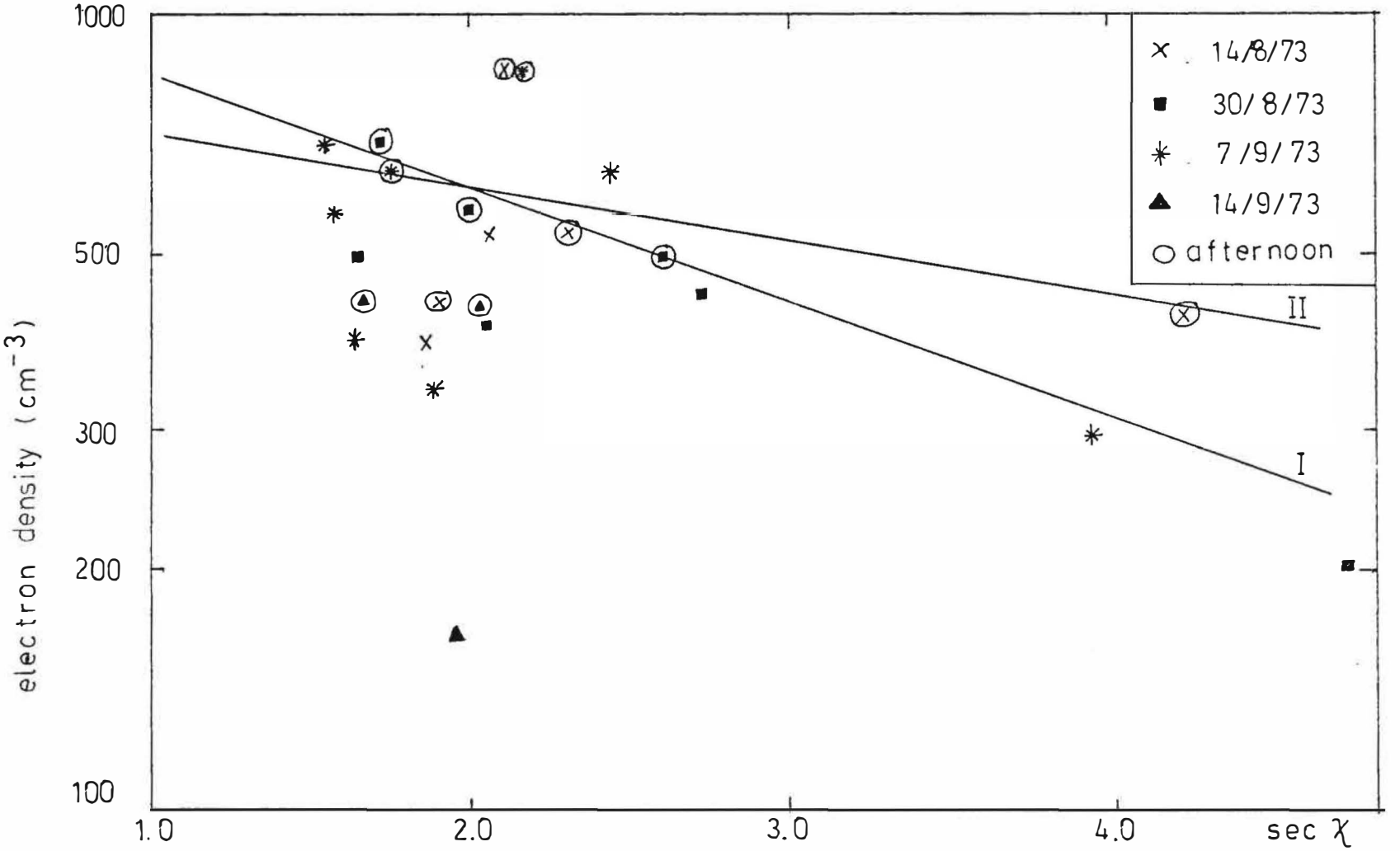

fig 7.5 Diurnal variation at 81km.

Thus from table 7.2, the uncertainty in the daily results is too large for the coefficients of variation for each season to give an indication of the relative day to day fluctuation in electron density.

Height (km)	Summer		Autumn		Winter		Spring	
	Mean daily error	Coeff of varn	Mean daily error	Coeff of varn	Mean daily error	Coeff of varn	Mean daily error	Coeff of varn
66.5	-	-	-	-	0.87	0.58	1.2	0.63
69	-	0.36	-	-	0.55	0.83	0.64	0.55
71.5	0.88	0.55	-	0.86	0.56	0.51	0.32	0.38
74	0.83	0.36	-	0.63	0.32	0.40	0.26	0.21
76.5	0.26	0.32	0.14	0.38	0.34	0.35	0.32	0.22
79	0.29	0.35	0.22	0.30	0.37	0.40	0.42	0.31
81.5	0.39	0.39	0.56	0.37	0.52	0.48	0.41	0.34
84	0.76	0.57	0.87	0.51	0.61	0.49	0.37	0.32

Table 7.2 Variation in electron density by season

7.2 DIURNAL CHANGES IN ELECTRON DENSITY

From section 9.3 the rate of production of electrons from the photoionization of nitric oxide by Lyman-α radiation at a height of h km is

$$P = \sigma_i(NO)[NO]Q_\infty \exp(-\tau) \qquad (7.2)$$

where $$\tau = \sigma_a(O_2)\int_h^\infty [O_2]\sec\chi \, dh \qquad (7.3)$$

(the symbols are defined in 9.3).

The loss rate could be given by either (section 9.5)

$$L = (1+\lambda)\alpha_d N_e^2 \qquad (9.18)$$

or

$$L = (1+\lambda) \beta N_e \qquad (9.20)$$

Thus for steady state conditions (P = L) and recombination like loss (9.18)

$$N_e = A_1 \exp(-\tfrac{1}{2}A_2 \sec \chi) \qquad (7.4)$$

where

$$A_1 = \left(\frac{\sigma_i(NO) Q_\infty}{\alpha_d} \frac{[NO]}{(1+\lambda)} \right)^{\frac{1}{2}} \qquad (7.5)$$

$$A_2 = \sigma_a(O_2) \int_h^\infty [O_2] dh \qquad (7.6)$$

For attachment-like loss (9.20)

$$N_e = A_3 \exp(-A_2 \sec \chi) \qquad (7.7)$$

where

$$A_3 = \frac{\sigma_i(NO) Q_\infty}{\beta} \frac{[NO]}{(1+\lambda)} \qquad (7.8)$$

Thus if (9.18) or (9.20) holds the gradient of a graph of ln N_e versus sec χ for a given day should be $-\frac{1}{2}A_2$ or $-A_2$ respectively. This assumes that λ, [NO], and α_d or β stay constant through a day.

Figure 7.4 is a plot of electron density (on a logarithmic scale) against sec χ for 76 km. It can be seen that although there is a difference between days it is conceivable that the values for a given day lie on a line. To test this hypothesis

a correlation and regression analysis was made of the dependence of ln N_e on sec χ, assuming a curve of the form

$$\ln N_e = \alpha + \beta \sec \chi \qquad (7.9)$$

The results are shown in table 7.3. r is the correlation coefficient between ln N_e and sec χ.

Date	r	Significance level	α	β ± standard error
14/8/73	-0.97	0.3%	8.03	-1.1 ± 0.2
7/9/73 & 30/8/73	-0.68	4%	7.52	-1.1 ± 0.5
14/9/73	-1.0	only 3 points	9.35	-2.5

Table 7.3 Correlation analysis for 76 km

The pressure (dynes/cm^2) at a height of h metres is

$$P \simeq \frac{g}{A} \int_h^\infty \{m(O_2)n(O_2) + m(N_2)n(N_2)\}dz \qquad (7.10)$$

A is Avagadro's number

$m(O_2)$, $m(N_2)$ are the gram molecular weights of O_2 and N_2

$n(O_2)$, $n(N_2)$ are the number densities (cm^{-3}) of O_2 and N_2

g = 980 cm sec^{-2}.

$$\text{Assume } \frac{n(N_2)}{n(O_2)} = 3.73 \qquad (7.11)$$

(Since the atmosphere is mixed up to about 105 km, and the scale height in the mesosphere is about 6 km this should be a valid approximation in (7.10) up to about 85 km.)

Then

$$\int_h^\infty n(O_2)dz = 4.5 \times 10^{18} P \qquad (7.12)$$

Now

$$\sigma_a(O_2) = 8.54 \times 10^{-21} \text{ cm}^2 \quad \text{(Manson \& Merry, 1971)}$$

$$p(76 \text{ km}) = 17 \text{ dyne cm}^{-2} \quad \text{(mean winter, Kantor \& Cole, 1965)}$$

Thus

$$A_2 = 0.65$$

which is smaller than the value of β in table 7.3. The electron density at 76 km appears to follow a relation

$$N_e \simeq A \exp(-1.7\, A_2 \sec \chi) \qquad (7.13)$$

which agrees with neither (7.4) nor (7.7).

Ganguly (1974) discussed the variation of electron density with solar zenith angle at a low latitude station in years of medium sunspot activity. He found that the best agreement with theory at 80 km was when lower values of nitric oxide concentration than those of Meira (1971) were used and a substantial production of electrons by X-ray ionization of O_2 was allowed for. This had the effect of increasing A_2 for $\sec\chi < 1.5$. Also, if production of electrons by $O_2(^1\Delta_g)$ ionization was important, this could also increase A_2 for lower values of solar zenith angle.

On figure 7.4 lines of gradient $-A_2$ (I) and $-\frac{1}{2}A_2$ (II) are shown. Although table 7.3 indicates a small standard error for the regression coefficient β, when the possibility of a 30% uncertainty in each measurement (sections 4.7, 4.8) is allowed for, the disagreement of the points for a given day with curve I is less convincing. Variations in the intercept value (α) from day to day could be due to changes in the

nitric oxide concentration, the reaction rates α_d or B, or the negative ion to electron ratio λ. More diurnal runs would be required to come to a definite conclusion.

Figure 7.5 is a similar plot for 81 km. There is more scatter in the data for a given day than at 76 km, and a correlation and regression analysis did not appear worthwhile. Again curves of gradient $-A_2$ (I) and $-\frac{1}{2}A_2$ (II) are shown, but it is impossible to choose between them.

Results were also obtained for 78.5, 83.5 and 86 km but these were similar to the 81 km results and inconclusive because of the large scatter.

7.3 THE WINTER-SPRING PERIODS OF 1972 AND 1973

In this section the time series of electron densities obtained by the differential absorption experiment during the winter and spring of 1972 and 1973 are examined. Meteorological influences on the electron density in the D-region, and possible coupling between the stratosphere and mesosphere are searched for using the data from D-region drifts, satellite remote temperature measurements, and balloon-borne radiosondes for the winter and spring of 1972. There is no D-region drifts data for 1973, and the satellite and radiosonde data for July to September 1973 were not available at the time of writing.

7.3.1 The Sources and Treatment of the Data: Electron Densities

To get time series of electron densities to compare with other atmospheric parameters the daily mean electron densities, calculated as in chapter 4 from the data between 1100 and 1400

hours, were smoothed using normal (i.e. Gaussian) smoothing over five days (Holloway, 1958). The smoothing was carried out because of the uncertainty of the calculated "daily mean" electron density as a measure of the true density on a given day (chapter 4). Normal smoothing was used rather than equally weighted running means as the latter may lead to misleading high frequency ripples in the smoothed curve (Holloway, op. cit.). The weights used were 0.03, 0.23, 0.48, 0.23, 0.03. The smoothed plot for a given height was discontinued and a new line started if there were more than two consecutive days with no data at that height. If data for one day only was missing the mean of the values for the two adjacent days was used. If data was missing for two consecutive days the data of the previous day was used for the first missing day, and that of the following day for the second missing day.

The resultant smoothed curves, along with the actual data points, are given in appendix I.

Magnetic Indices

In appendix I the time series of ΣK is given for Amberley geomagnetic observatory (43^{o}S, 173^{o}E). ΣK is the sum for a day of the three-hourly K indices (Davies 1966, Page 30) which indicate the extent of the variation in the magnetic field.

D-Region Drifts

The drifts were measured using the spaced receiver method on partial reflections from the D-region of 2.4 MHz pulses (Fraser, 1968). Most of the measurements were taken in the three hours centred on noon. However, tidal components of the winds can be important as well as the prevailing wind at these

heights (Fraser, op. cit.), and three hours is equivalent to a 90^{o} shift in the phase of the diurnal tide. To reduce this variation, and the variation introduced by other factors such as gravity wave motion and experimental uncertainties, the meridional and zonal components were averaged over ten day periods. Thus the time resolution in the drifts data is poor.

Upper Stratospheric Temperatures

The selective chopper radiometer (SCR) on the Nimbus IV satellite measures the emission from atmospheric carbon dioxide in the 15 micron band.

By selecting six spectral channels at slightly different wavelengths emissions from six different atmospheric layers are monitored. The intensity of a particular channel depends on the temperature of the appropriate layer. The theory, and the "weighting functions" for each channel (which are actually a function of pressure) are given by Houghton and Smith (1970), and some results are given by Barnett et al. (1972). For the winter-spring period of 1972 some of the channels were not operating properly, and the only data available for the stratosphere was from channel A, for which the weighting function peaks at about 2 mb. Quiroz and Gelman (1972) using a series of 75 temperature profiles found that there was a strong correlation between channel A radiance and the 10 mb - 0.5 mb thickness (correlation coefficient = 0.984). Thus the channel A data should be a good indicator of upper stratospheric temperatures.

The data was provided by the Department of Atmospheric Physics, Clarendon Laboratory, University of Oxford, in the form of a southern hemisphere map for every second day showing

lines of constant radiance. Thus some idea of the synoptic situation can be obtained. The time series of channel A temperatures above Christchurch is given in appendix I. There are several groups of days with no data above Christchurch however.

Radiosonde Data

The New Zealand Meteorological Service supplied magnetic tapes containing records of radiosonde temperatures, heights of pressure levels, and upper wind records for Christchurch at 0000 and 1200 hours GMT up to the end of 1972. These records were converted to a form suitable for analysis on the University of Canterbury's Burroughs B6700, and a programme was written to plot out time series of temperatures and heights of selected pressure levels, and the zonal wind at selected heights. These plots are given in appendix I. There were gaps in the radiosonde data above 20 mb, and in the winds above 25 km, so the highest plots given are for 20 mb and 25 km respectively.

7.3.2 The Electron Densities

The only outstanding events shown by the smoothed electron density time series are an increase centred at about 76.5 km on July 19th 1972, a large increase from 69 to 74.5 km around 6th August 1972, and a similar increase from about 71 to 78 km near 3rd September 1973. In general the changes in electron density at a given height over times of about four days appear to be less than or of the order of 150%, apart from the periods just mentioned. Because of the uncertainty in the daily values it is not possible to make a very good estimate

of the electron density variation over time scales shorter than this.

The 1972 data can be examined for the height range over which changes in electron density are correlated. Similar fluctuations occur in the electron densities for heights separated by 2.5 and 5 km, and occasionally for 7.5 km separation, with time scales of about four to eight days. There is no evidence for correlation over larger height ranges, apart from a rather similar bump in all the data from 69 to 84 km, around August 22nd 1972, which occurred three days earlier at 84 km than at 69 km. However, the magnitude of this increase is not large compared to the other changes during the winter, and the similarity may well be due to chance.

There were more gaps in the 1973 data, and little can be deduced about the relationship between electron density changes at different heights for that winter and spring.

7.3.3 Electron Density Time Series in the 1972 Winter-Spring Period and Other Geophysical and Atmospheric Changes

ΣK index

The most noticeable feature of the ΣK time series for the 1972 winter-spring period is the high value on the 4th, 5th and 6th of August. This increase was associated with a large solar-terrestrial disturbance (chapter 8), and the large increase in electron density from 69 to 75 km near this time was caused by ionization of the atmosphere by precipitating high energy electrons. However, there is no clear evidence for other electron density increases following ΣK increases during the 1972 period.

An interesting period in 1973 was August 30th to September 3rd. There was a large increase in electron density from 71 to 78.5 km, peaking on September 3rd. The ΣK indices for Amberley show that the days August 25-26 and 28-29 were magnetically disturbed, while September 1,2,3 were magnetically very quiet at Amberley. A magnetic storm commenced on 24 August (U.S. Dept of Commerce Solar-Geophysical reports). However, the peak in the electron density associated with the August 1972 storm occurred only three days after the storm's sudden commencement, so it is likely that the peak on September 3rd 1973 was not associated with a magnetic storm.

Mesospheric Winds

The ten day means of the D-region drifts for the winter and spring of 1972 are given in table 7.4. The zonal wind from 65 to 90 km was generally eastward, which is similar to the behaviour found for other winters (Fraser 1968).

For the period August 7th-16th the zonal flow from 80 to 90 km appeared weaker than normal, or even reversed, while at 75 km and below it was at least as high as for the rest of the winter. The thermal wind equation relating the height rate of change of the zonal wind u (positive eastward) to the meridional temperature gradient (positive northward) is (Hess 1959, page 191)

$$\frac{\partial u}{\partial z} \approx - \frac{g}{fT} \frac{\partial T}{\partial y} \qquad (7.1)$$

where $f = 2\Omega \sin \phi$ (ϕ latitude) is the Coriolis parameter, and is negative in the southern hemisphere. Thus the weaker zonal winds above 80 km of this period suggest that there was more heating than normal going on above 75 km to the south of

Height (km) / Date	65	70	75	80	85	90
30/6 - 7/7	11	64	-	8	-12	3
8/7 - 17/7	22	42	13	-	156	-
18/7 - 27/7	2	29	-	-	-	14
28/7 - 6/8	18	20	5	28	37	18
7/8 - 16/8	63	35	10	11	2	-12
17/8 - 26/8	28	42	6	52	47	47
27/8 - 5/9	11	32	4	48	64	25
6/9 - 15/9	18	37	12	57	30	46
16/9 - 25/9	16	25	12	21	18	20

Zonal Wind (m/sec). Positive values are eastward.

Height (km) / Date	65	70	75	80	85	90
30/6 - 7/7	-10	11	-	10	-5	-6
8/7 - 17/7	-72	10	45	-	19	-
18/7 - 27/7	-23	10	-	-	-	33
28/7 - 6/8	-34	7	-6	2	5	9
7/8 - 16/8	-55	8	7	16	44	-17
17/8 - 26/8	-1	-8	2	-5	55	-20
27/8 - 5/9	-3	-1	-2	-	7	16
6/9 - 15/9	2	-1	-11	4	17	21
16/9 - 25/9	2	-	4	5	-2	-4

Meridional Wind (m/sec). Positive values are northward.

Table 7.4 Ionospheric Drifts for July-September 1972.

New Zealand. ($\frac{\partial T}{\partial y}$ smaller, that is more negative, than usual). This period coincides with the period of enhanced electron densities observed from 69 to 75 km in early August, which was due to particle precipitation. It is suggested that the zonal wind decrease could have been caused by heating of the atmosphere south of Christchurch by energetic particles.

The meridional wind appeared to be predominantly southward at 65 km and northward from 70 to 90 km, although there were some exceptions. A northward meridional wind could be important in the transport of nitric oxide from regions of increased production at auroral latitudes (chapter 9), but there is insufficient time resolution in the drifts data to test for a correlation with D-region electron densities.

Temperatures in the lower mesosphere

The upper height limit for which the N.Z. Meteorological Service zonal wind records have few gaps is 25 km. As already discussed, the Nimbus IV S.C.R. channel A radiance data correlates well with the 10 mb (about 30 km) to 0.5 mb (about 52 km) thickness, and thus with the temperature of this layer. If it is assumed that the meridional temperature gradient of the layer between 52 and 65 km is similar to that of the 10 to 0.5 mb layer, the thermal wind equation (7.1) should predict the zonal wind at 65 km given the 25 km wind and the meridional temperature gradient of the 10 to 0.5 mb layer (calculated from the Nimbus IV data).

The 65 km zonal wind predicted in this way was averaged over the same ten day periods as the drifts data, and is given along with the 65 km zonal component of the drifts in table 7.5.

Date	Predicted wind	Drifts data
30/6-7/7	142 m/sec	11 m/sec
8/7-17/7	98	22
18/7-27/7	24	2
28/7-6/8	17	18
7/8-16/8	63	63
17/8-26/8	70	28
27/8-5/9	76	11
6/9-15/9	115	18
16/9-25/9	56	16

Table 7.5 Zonal wind above Christchurch as predicted by the thermal wind equation and measured by ionospheric drifts.

The results are in reasonable agreement between July 18th and August 16th, but for the rest of the period the predicted winds are significantly higher than those measured.

The meridional temperature gradient from channel A of the S.C.R. is generally positive over Christchurch (warmer further north). However, further south the meridional temperature gradient is generally negative (e.g. figure 7.7, day 197). If the meridional temperature gradient in the lower mesosphere (say 52 to 65 km) above Christchurch was also negative for the period when the predicted values in table 7.5 were too high, then the thermal wind equation would lead to better agreement with the drifts results.

Thus it is suggested that for some of the winter the meridional temperature gradient over Christchurch has opposite senses in the upper stratosphere and lower mesosphere.

Stratospheric Warmings

According to Quiroz (1974) no major midwinter warmings (warmings resulting in an Antarctic circulation reversal at 10 mb or lower) were observed in the southern hemisphere stratosphere during the period 1969-73. However, Quiroz says that there was clear evidence for minor warmings which significantly influenced the structure of the Antarctic stratosphere.

The strongest warming above Christchurch in the 1972 winter shown by the Nimbus IV S.C.R. data began on the 15th July, with the temperature peak on July 19th. (Appendix I, also figure 7.6). If the electron density time series (appendix I) are now examined it can be seen that at 76.5 km the highest measured electron density of the winter-spring period occurred on 19th July. The second highest measured density at 74 km also occurred on this day, and there were peaks in the electron density at 71.5 and 79 km. There were no solar flares reported near the times of the electron density measurements (U.S. Dept of Commerce - Solar-Geophysical Data), and the ΣK index at Amberley was relatively low from the beginning of July until after the 19th, so it is not likely that the electron density increase was due to flare or magnetic storm effects. Thus it is suggested that the electron density increase was associated with the stratospheric warming.

The zonal wind at 25 km (appendix I) showed a steady decrease from July 16th, with the direction reversing to westward flow on July 24th. At 65 km the ten day average of the zonal wind (table 7.4) showed the weakest eastward flow of the entire winter-spring period in the interval 18th-27th July. Thus it appears that there was a disturbance through much of the upper stratosphere and lower mesosphere. The 30 mb temperature over Christchurch also increased during the first part of July reaching a peak on the 17th, while the 20 mb temperature showed a broad peak from 15th-18th July. The heights of both the 30 mb and 100 mb surfaces increased through July to reach a peak on the 25th. Some of these results are shown in figure 7.6.

From the Nimbus IV SCR channel A synoptic maps (fig. 7.7) it can be seen that on July 15th (day 197) there was a strong wavenumber two pattern in the thermal field, with a cold area over Christchurch. This pattern rotated in an eastward direction while a warm area originally over the Indian Ocean intensified and moved polewards (days 199, 201). The temperature maximum on July 19th (day 201) occurred when the edge of this warm area was over Christchurch.

As has already been mentioned there was also a large electron density increase from 71 to 79 km at the beginning of September 1973, which did not appear to be related to magnetic activity. It will be interesting to examine meteorological data for this period when it becomes available.

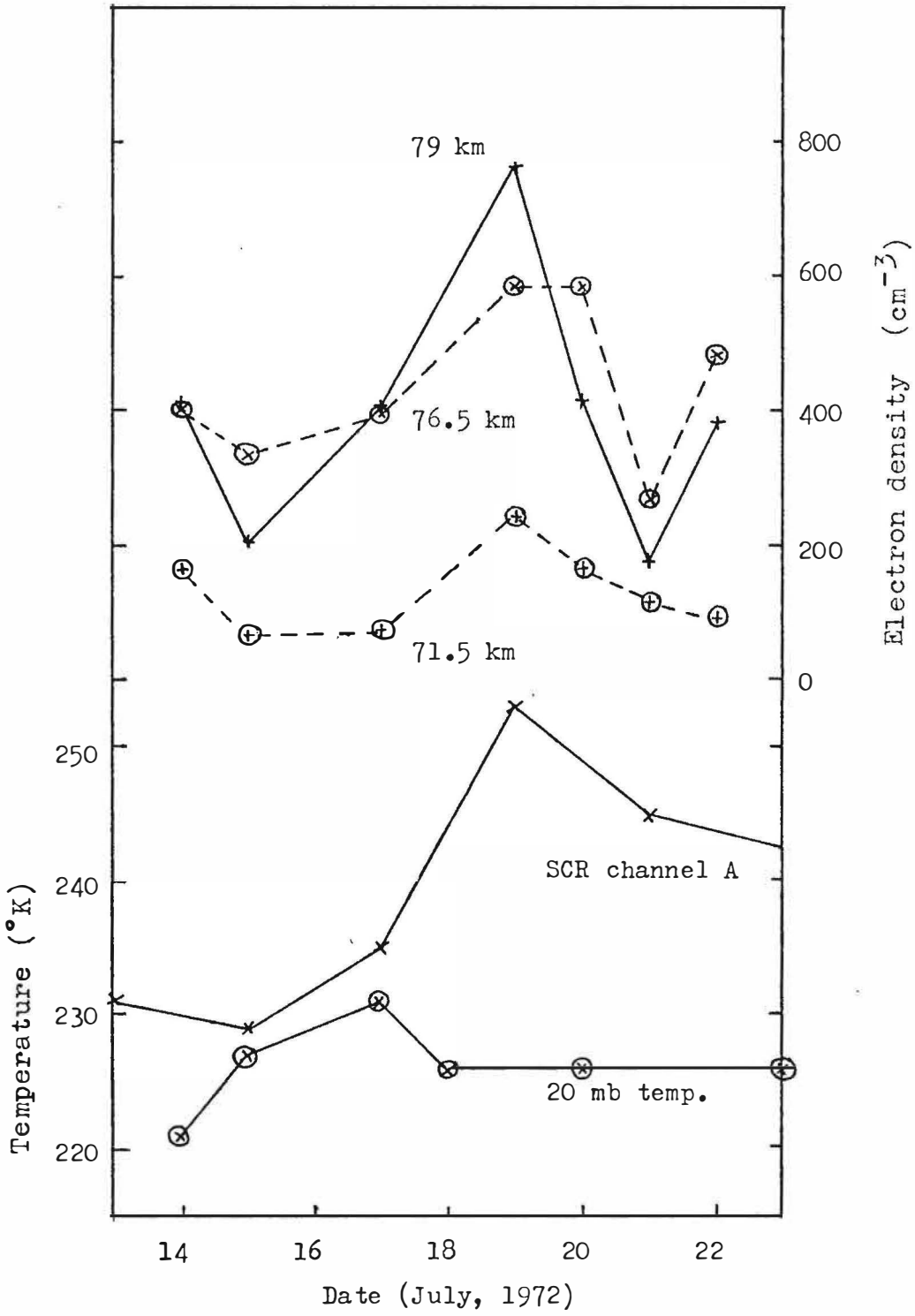

Fig 7.6: Electron densities and stratospheric temperatures.
(13 - 23rd July, 1972)

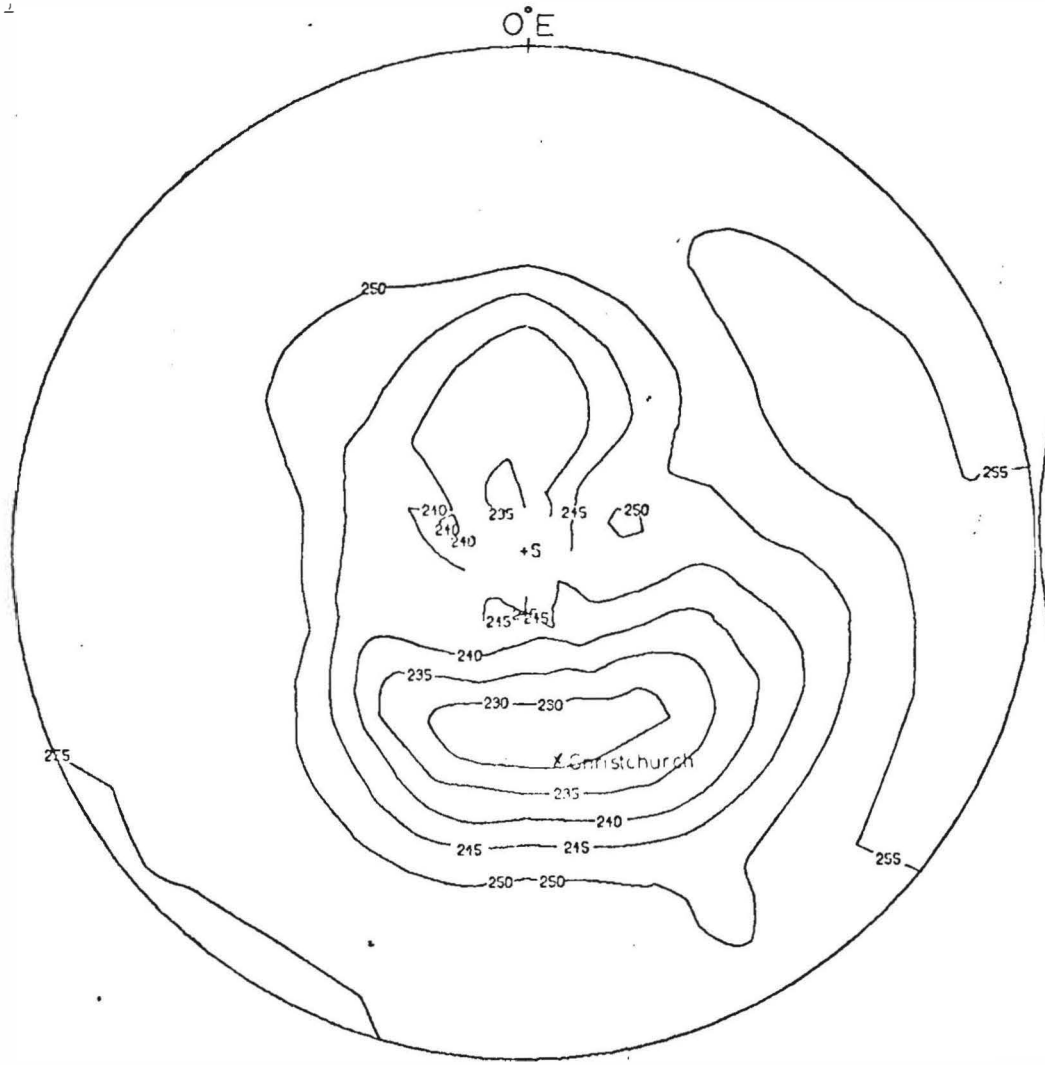

TEMPERATURE CHAN 1 DN DAY 197 1972

PLOT 2 198 1971
NIMBUS 4 05 2

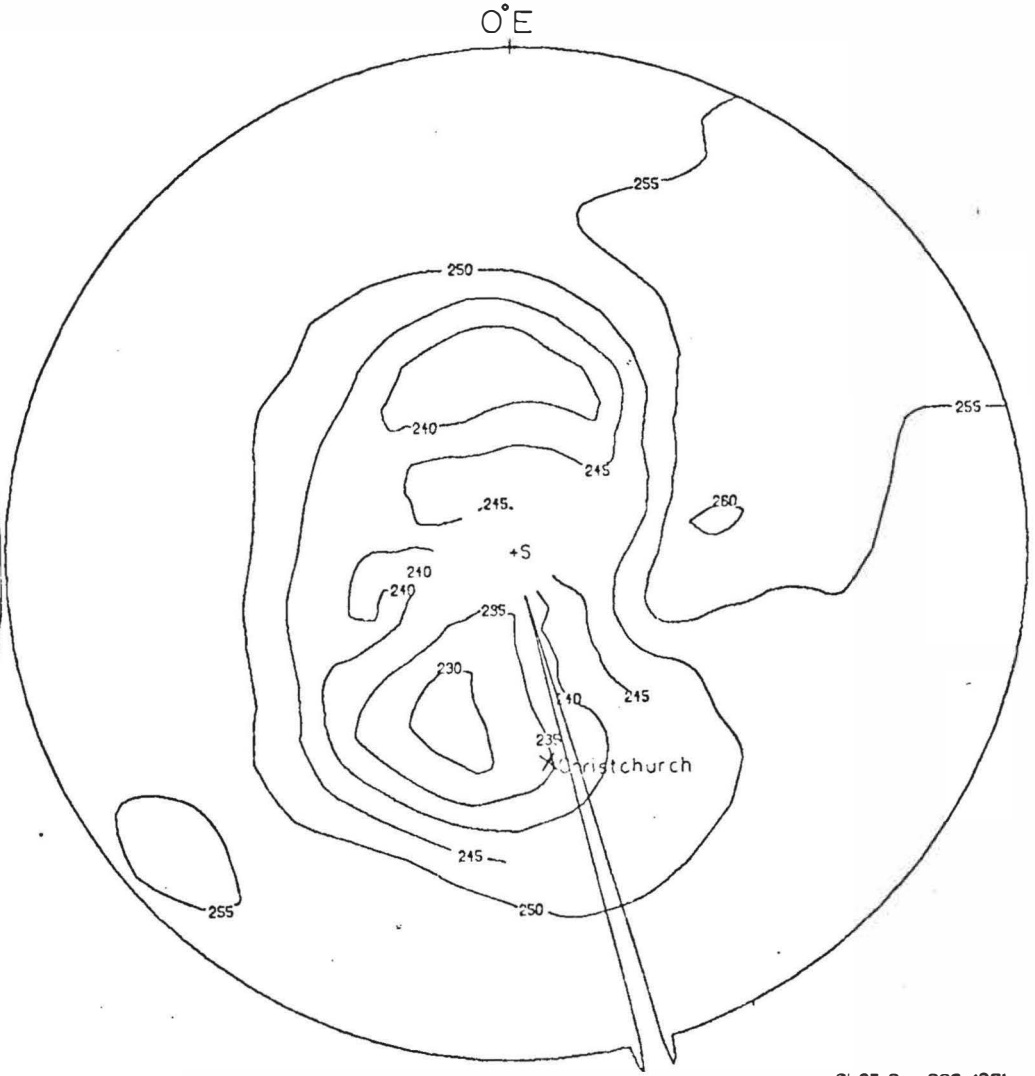

TEMPERATURE CHAN 1 DN DAY 193 1972

PLOT 2 200 1971
NIMBUS 4 05 2

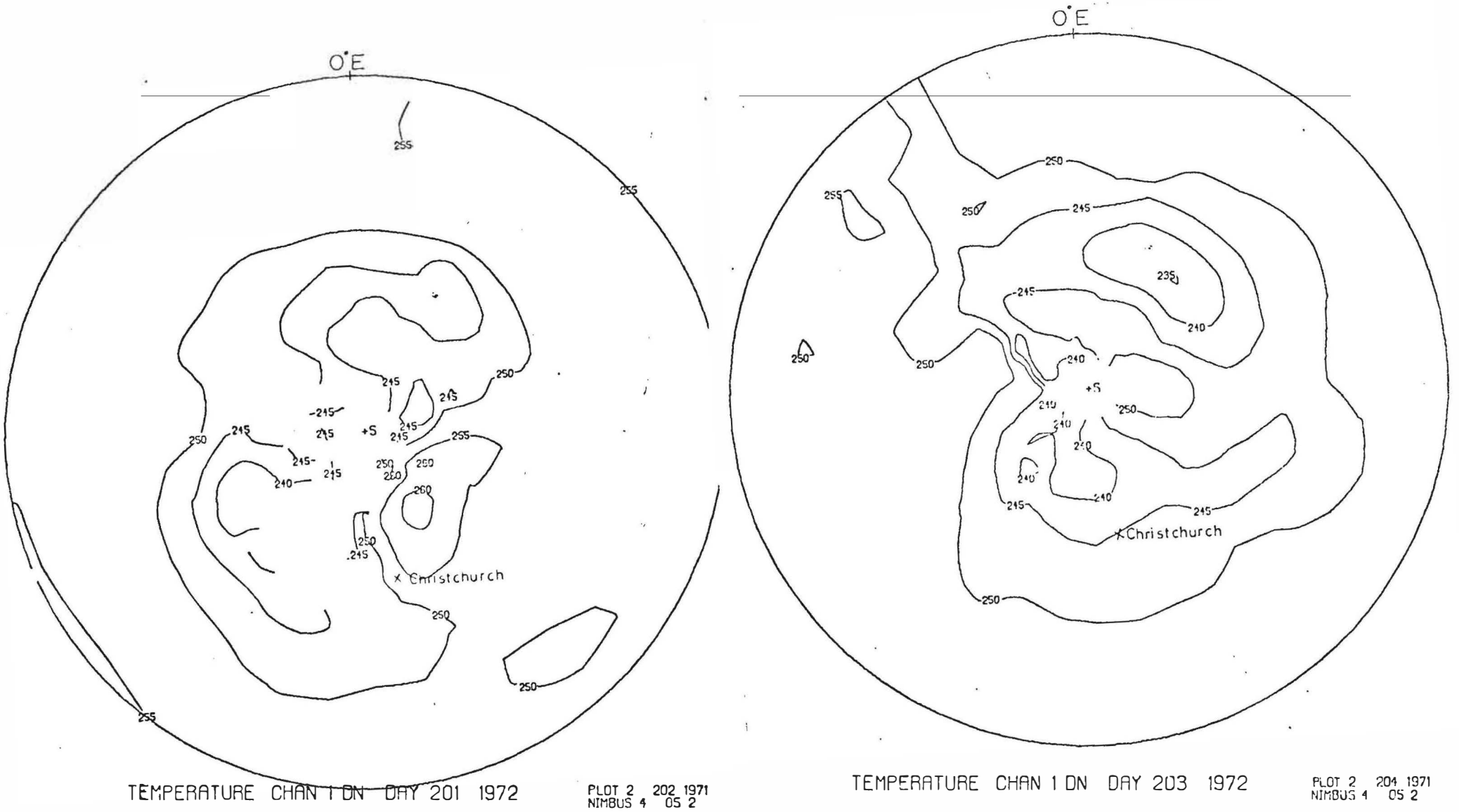

Fig 7.7: SCR Channel A radiances, July 15-July 21 1972.

Stratospheric Time Series

When the electron density time series in appendix I for July-September 1972 are compared with the stratospheric time series (100 mb and 30 mb height, 30 mb and 20 mb temperature, 25 km zonal wind, SCR channel A radiance), there are no clear indications of simultaneous variations in stratospheric parameters and mesospheric electron densities apart from the period of the warming described above. Such an analysis is complicated by the uncertainty in the electron density measurements, but it is felt that any "direct" (that is with delay less than two days) stratospheric-mesospheric coupling, in the sense of simultaneous variations of time series, cannot account for all of the real variation in electron density between 70 and 84 km in winter. This is not to say that stratospheric conditions do not lead to changes in electron density in the lower D-region (for example through some of the processes described in chapter 6). Such processes would not necessarily lead to simple correlations between stratospheric and mesospheric parameters.

7.4 CONCLUSIONS

The seasonal mean height profiles from the differential absorption measurements of 1972-73 showed general agreement with those of Gregory and Manson for 1963-67. There was a "winter anomaly" in electron density between 69 and 84 km, with the winter electron densities higher with respect to the summer densities than would be expected for strict solar control.

The diurnal change in electron density at 76 km was more consistent with attachment-like loss than recombination-like loss if Lyman-α ionization of nitric oxide was the main production process. The change did not agree very well with either model, but there was too much uncertainty in the data to come to a definite conclusion.

For most of the winter and spring the electron density change over four days was by less than a factor of 2.5. Changes over shorter time intervals could not be reliably deduced. Changes in electron density do not appear to be correlated over height ranges greater than 7.5 km.

There was an increase in electron density from 69 to 75 km associated with the solar-terrestrial disturbances of early August 1972. There may have been heating in the mesosphere south of Christchurch at the same time.

An electron density increase from 71.5 km to 79 km which peaked on July 19th, 1972 was probably associated with a warming in the stratosphere over Christchurch.

The zonal flow in the mesosphere above Christchurch during July to September 1972 was similar to that found in other winter-spring periods. Apart from the warming in July there was no clear evidence for simultaneous fluctuations of mesospheric electron densities (69-84 km) with meteorological parameters in the stratosphere.

CHAPTER 8

ELECTRON DENSITY VARIATIONS ASSOCIATED WITH GEOMAGNETIC STORMS

It has been known for some time that there are pronounced effects in the mid-latitude D-region associated with some magnetic storms (Lauter and Knuth 1967, Belrose and Thomas 1968, Bourne and Hewitt 1968, Manson and Merry 1970, Thomas 1971). These effects are evident as changes in very low frequency, low frequency and medium frequency radio-wave paths, and vertical medium and high frequency absorption measurements. These measurements are consistent with an increase in the electron density of the D-region which often reaches a maximum two to four days after the onset of the storm, and may last for as long as ten days.

There have been two theories put forward to account for this increase. Belrose (1963) has suggested that there could be a change in atmospheric composition at auroral latitudes at the time of the storm, with the delay between the onset of the storm and the electron density peak at mid-latitudes arising from the time taken for the composition change to be transported from auroral to medium latitudes. It is interesting to note that Zipf et al. (1970) measured an anomalously high nitric oxide concentration at 110 to 130 km in an auroral form over Fort Churchill which they suggested was produced via dissociative excitation of molecular oxygen and nitrogen by electron impact.

The second theory, put forward by Lauter and Knuth (1967) is that the outer radiation belt can be overfilled with electrons during a magnetic storm. A steady leakage of high

energy electrons following this could lead to ionization in the lower atmosphere, with the time taken for the decay back to normal conditions accounting for the duration of the effect. This is the theory to be examined here.

8.1 ENERGETIC ELECTRONS, AND THE RADIATION BELTS OF THE EARTH

If a charged particle moves through a region where the magnetic field $\underset{\sim}{B}$ varies only slowly in space or time, and if the component of the particle's momentum normal to the field is $p_\perp$, then $\frac{p_\perp}{B}$ is an adiabatic invariant (Jackson 1962, section 12.10). If a static magnetic field is considered, with no other forces acting on the particle, the speed of the particle will be constant, and it will move along a given field line in a helix with pitch angle α. Because of the invariance of $\frac{p_\perp}{B}$, $\frac{\sin^2\alpha}{B}$ will be a constant along a field line.

The magnetic field of the earth is approximately a dipole field. This means that along a given field line the magnetic field is higher at lower altitudes. Thus for a particle at $\phi_m = 0$ (ϕ_m geomagnetic latitude) with sufficiently large pitch angle there will be two points on the field line (mirroring points) where $\alpha = 90^o$. The particle will then be "trapped" on a field line, and will travel along a helical path being reflected at the mirroring points. (At the same time there will be a slow azimuthal drift due to the curvature of the field lines and gradient of the field). If the mirroring points are low down in the atmosphere the energetic electrons may collide with neutral atmospheric particles causing ionization and losing their own energy.

The magnetic field of the earth is not a true dipole field, and the motions of trapped particles are usually discussed in terms of the McIlwain parameters (L,Λ), (McIlwain, 1961). L is the "shell parameter" and is constant (to within 1%) along a given field line. A trapped particle will thus remain on a given surface L = constant. The invariant latitude Λ is defined by $L \cos^2\Lambda = 1$. For a dipole field the L parameter of a given field line is the distance from the earth's centre to the field line in the plane of the dipole equator, in units of earth radii, and Λ is equal to the geomagnetic latitude at the point where the field line cuts the earth's surface. A world map of L-contours for the actual field of the earth is given by Campbell and Matsushita (1967). The L parameter at Christchurch is 2.6 (Manson & Merry, 1970).

For the earth, energetic electrons (>100 KeV) are observed trapped in two zones at geomagnetically quiet times (Lyons et al., 1972). Inner zone fluxes peak between L = 1.2 and L = 1.8 and then decrease, falling below the level of detectability near L = 2 to L = 3.5. The fluxes increase again near the plasmapause to form the outer zone. The region between these two zones is called the electron slot and contains very few electrons in magnetically quiet times.

During storms the slot can be filled with electrons of all energies. Following the storm the fluxes decay and the quiet time slot is reformed (figure 8.1).

Lyons et al. (1972) show that the slot could be caused by a mechanism for preferential electron losses in the region. Resonant interactions can take place between the electrons and a turbulent band of whistler mode waves. Due to these

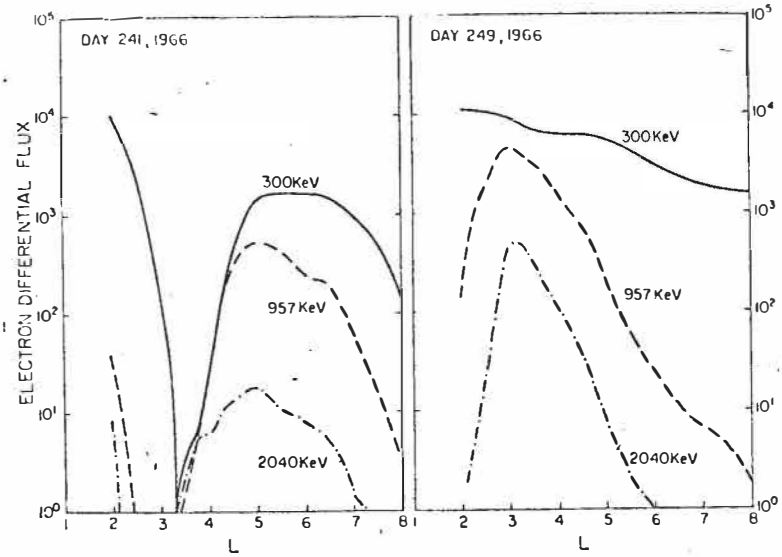

Fig. 1. Plots of $J_\perp$ (electron flux with a local pitch angle $\alpha = 90° \pm 8°$) versus L for three energy channels at times prior to and immediately following the magnetic storm of September 4 (day 247), 1966. Day 241 shows a well pronounced electron slot for all energy channels, whereas day 249 shows the slot-region filling that occurred as a result of the magnetic storm. Following day 249, the slot-region fluxes decayed and the quiet-time slot was reformed. The figure is from *Vampola* [1971].

Fig 8.1: Radiation belt morphology. (From Lyons et al, 1972)

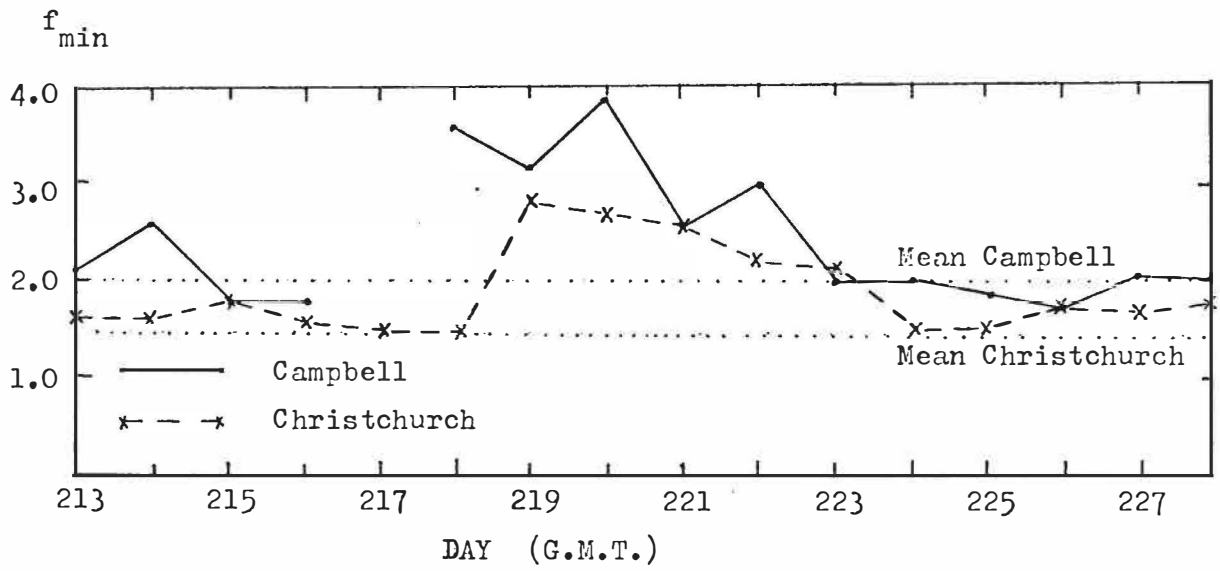

Fig 8.4: f_{min} for Christchurch and Campbell Island, August 1972. (The values are the means of the 1200 and 1300 hrs NZST measurements.)

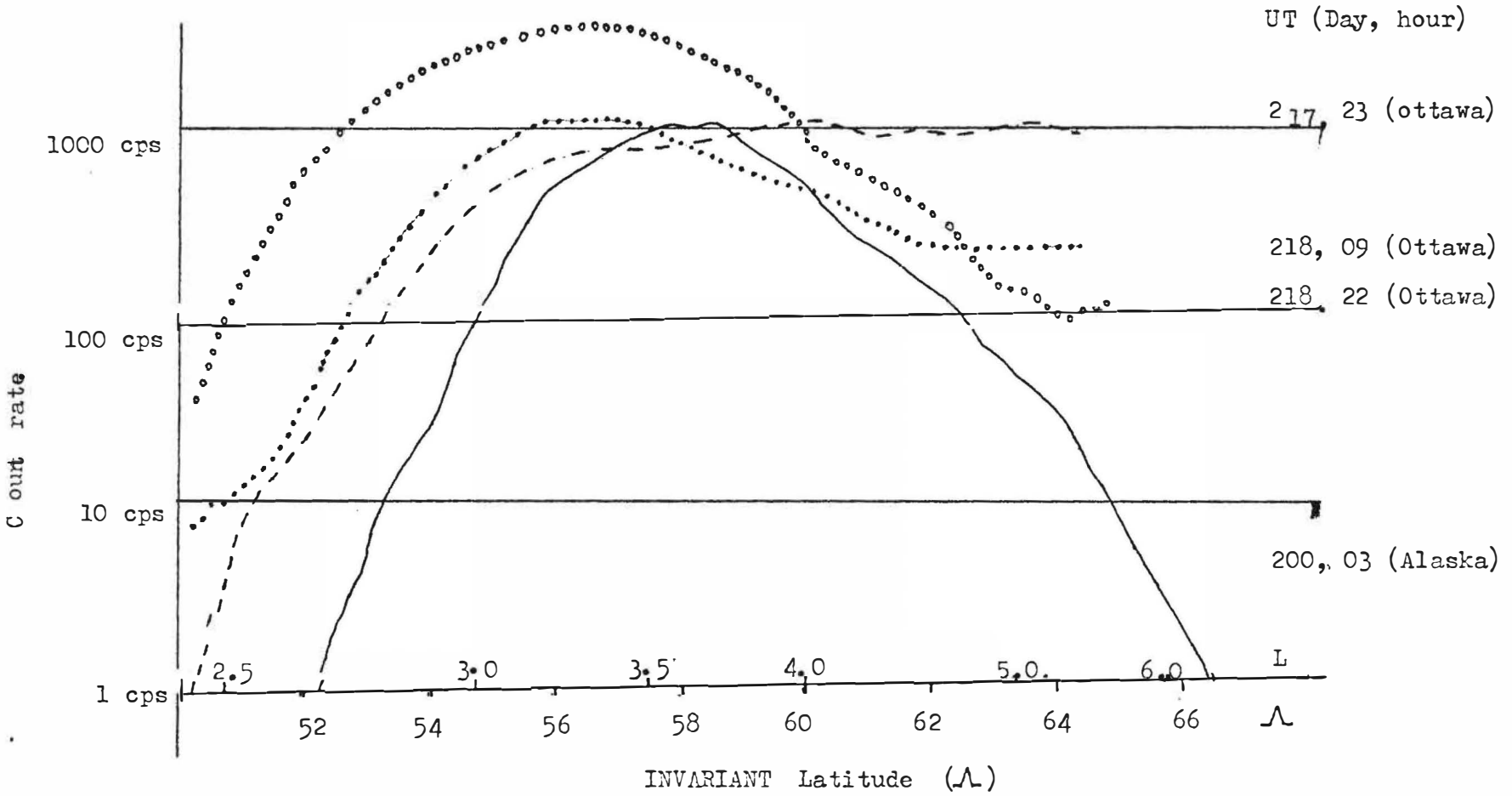

Fig 8.2: D3E latitude profiles. (Burrows, private communication)

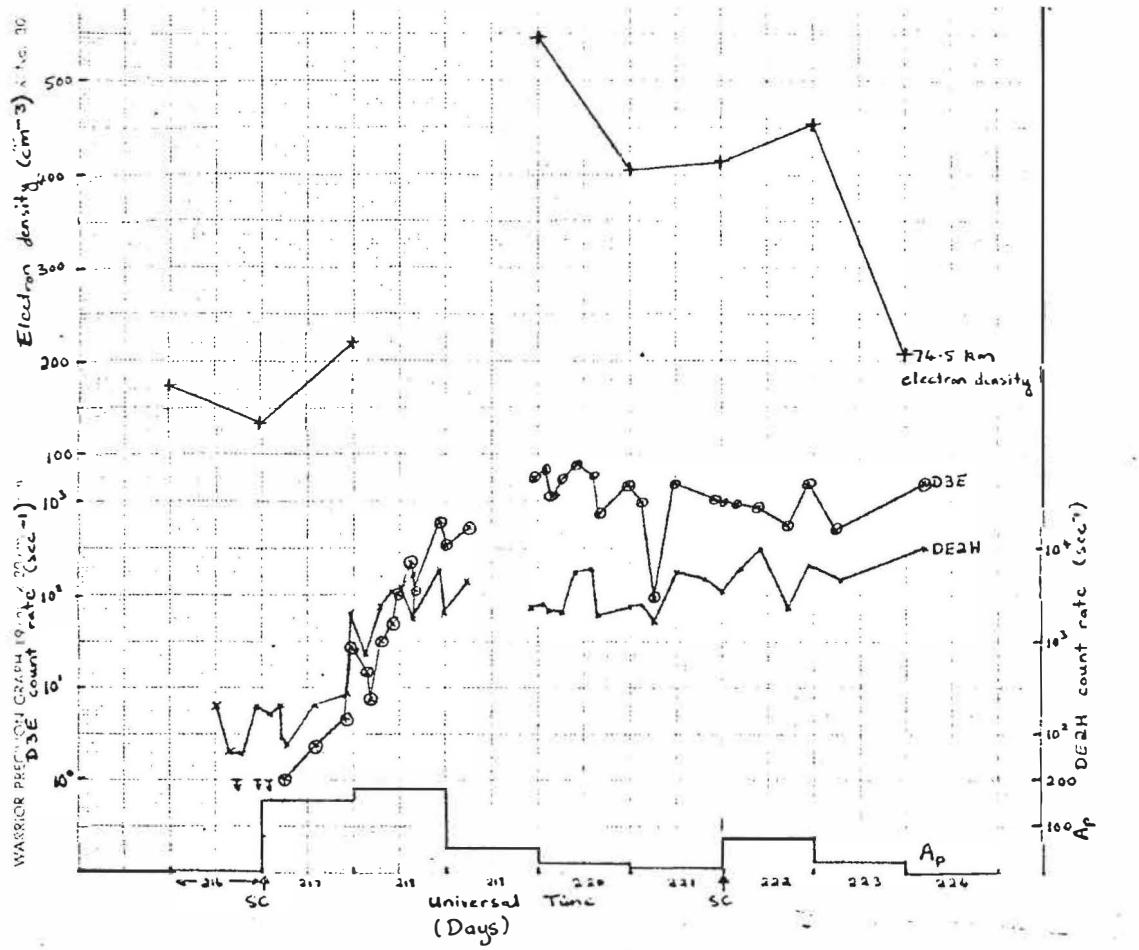

Electron densities: Above Birdling's Flat ($\Lambda = 52^{\circ}$) by DAE.

D3E: Isis-2 count rate for electrons with energy between 1.0 MeV and 2.0 MeV. Pitch angle= 90° +/- 45°
$\Lambda = 52^{\circ}$, Height= 1400 km.

DE2H: Isis-2 count rate for electrons with energy greater than 210 KeV. Pitch angle= 90° +/-7°
$\Lambda = 52^{\circ}$. Height= 1400 km.

A_p : World daily magnetic index.

SC : Magnetic storm commencement.

Fig 8.3: Electron densities, particle fluxes, and magnetic indices for August 1972.

interactions the pitch angles of the electrons change, a process which these authors call 'pitch angle diffusion'. Through pitch angle diffusion the electrons eventually get pitch angles so small that they penetrate down to a depth where collisions with neutral amtopsheric molecules occur and they are lost. It is shown that the pitch angle diffusion mechanism would occur for L-shell values near the slot but not at L values for the two quiet time bands. The theoretical precipitation lifetimes at L = 2.6 vary from about forty days for 200 KeV particles down to about ten days for 0.5 to 2.0 MeV particles.

Thus the filling of the slot region with electrons at the time of a magnetic storm, and the slow decay of these fluxes due to pitch angle diffusion could possibly account for the storm after-effects seen in the D-region, as the pitch angles diffuse into the loss cone giving rise to ionization in the atmosphere.

8.2 THE SOLAR-TERRESTRIAL EVENTS OF AUGUST 1972

The solar activity in the first half of August 1972 was exceptionally large for the declining stage of the solar cycle. Two flares reached level 3B (outstanding level of importance) and there were several other important flares. There were two main geomagnetic storms commencing on August 4th and 9th respectively. The storm of August 4-6 was a great one, and that of August 9 was the third larges of the year. The solar-terrestrial events led to the most severe disruptions to telecommunications for ten years (Roederer and Shapley, 1973). Thus it would seem that if the magnetic storm

after-effects discussed in the previous section lead to ionization of the D-region over Christchurch, this should have been observable over that period.

Fortunately both D-region electron densities over Birdling's Flat, measured by the differential absorption method, and energetic electron fluxes at 1400 km, measured by the experiment of Dr J.R. Burrows on board the Isis-2 satellite are available for the period August 3rd to 10th. Unfortunately there are no electron densities for several days after August 10th as the transmitter caravan blew over.

8.2.1 The Energetic Electron Fluxes, and D-Region Electron Densities of August 1972.

Figure 8.2 shows the D3E ($1 < E \leq 2.0$ MeV) count rate for electrons with pitch angles of $90^{o} \pm 45^{o}$ at the satellite (1400 km). The trace for day 200, 0300 UT is typical of magnetically quiet times. There is a peak at about L = 3.6, and a slot for L less than about 2.9. However, during days 217 and 218 the slot is filling, in fact the count rate over the whole region has increased.

The DE2H counter (electrons with energies greater than 210 KeV) also shows the filling of an electron slot at the time of the storm. On day 214 there is a well-developed slot at L = 2.9-3.6, with a count rate of 40 sec^{-1} at L = 3.0. However, on day 218 there is actually a peak at L = 3.0 with count rates of the order of 10^{4} sec^{-1}.

Thus the storm beginning on August 4 (day 217) appears to fit the pattern discussed earlier, the slot region filling with electrons at the time of the storm.

Looking now at the fixed invariant latitude of 52° (L ~ 2.6), the dominant feature is the increase of the D3E and DE2H fluxes at the satellite around about day 217 (figure 8.3). The D3E flux increased by a factor of about 25 during days 217 and 218. From day 219 until at least day 223 the fluxes remained at a high level.

The electron densities in the D-region between about 70 and 75 km over Birdling's Flat (L = 2.6) also showed a large increase at this time. In fact it was during this period that the 72 and 75 km densities reached their highest measured values of the whole winter-spring period. At 70 km there was about a threefold increase in electron density on days 220 and 221. At 72 km there was a threefold increase on days 220 and 221, with normal values on days 222 and following. At 75 km there was a threefold increase on days 220 and 221, while the density remained high for the following three days.

At 76.5 km and 79 km there was no clear difference between the period of the storm and the rest of the winter. (The uncertainty in these measurements was about ±30%.) The experiment yielded no results above 79 km between days 218 and 222.

The effect of these electron density increases on radio wave absorption was also calculated. For 2.4 MHz the increases would give an enhancement of about 1.2 db (Sen-Wyller refractive index with the winter collision frequency profile of appendix B). Bourne and Hewitt (1968) in a superposed epoch analysis of 2.6 MHz absorption and planetary magnetic index found that the average increase in absorption following the onset of a magnetic storm was about 1 db. (This was for the

Lindau-Norddeich circuit where the McIlwain L parameter is 2.5 and the geomagnetic field 4.7×10^{-5} Tesla (0.47 gauss). The L-parameter is thus similar to Christchurch (L = 2.6, B = 5.8×10^{-5} Tesla). Lauter and Knuth (1967) found that the increased absorption at 0.24 MHz at Kühlunbsborn (L = 2.5, B = 4.7×10^{-5} Tesla) was about 12 to 18 db. The non-deviative absorption of a wave of frequency f is approximately proportional to $(f+f_L)^{-2}$ (Davies 1966, page 84) where f_L is the gyrofrequency. Thus if the 0.24 MHz absorption increase was non-deviative the equivalent absorption increase on 2.4 MHz at Birdling's Flat would be 1.8 to 2.7 db. In fact the additional 0.24 MHz absorption may be partly deviative. Also the ionization rate at Kühlungsborn could be higher at a given time than at Christchurch because the geomagnetic field at Kühlungsborn is weaker and thus more particles will mirror below 75 km.

The absorption on 2.6 MHz measured by the A3 method is available for Lindau (52^{o}N, L = 2.5) for the August 1972 period (Schwentek, 1973). This peaked on day 218 with an increase of 23 db over the mean August absorption. (The values are for a solar zenith angle of 78.5^{o}.) The absorption stayed above normal until day 226. Absorption of this magnitude cannot be explained by increases in electron density from 70 to 75 km of the size measured at Birdling's Flat. Although the L-parameter at Lindau is similar to that at Christchurch, the ionization rate from energetic particles could be higher at Lindau since the geomagnetic field is weaker. However, the absorption at Christchurch as measured by the parameter f_{min} was also above normal between days 219

and 223 (data from Geophysical Observatory, D.S.I.R., shown in figure 8.4). This indicates that there probably was extra absorption above 80 km during this period.

To sum up this discussion, many of the magnetic storm after effects in absorption than have been reported in the literature may have been due to electron density increases in the height range (70-75 km) and of the magntiude (times 3) observed at Birdling's Flat. However, in the particular case of the August 1972 disturbances there appear also to have been electron density increases above 80 km, somewhere in the D- or lower E-region.

8.3 THE IONOZATION OF THE ATMOSPHERE BY ENERGETIC ELECTRONS

The problem of ionization of matter by beta rays is complicated by effects such as multiple scattering, reflections and straggling (Bethe and Ashkin, 1953). A fully satisfactory theoretical treatment is very difficult, and calculations are normally based on empirical, or a mixture of empirical and theoretical relationships.

The first approach taken in this work was based on the method outlined by Whitten and Poppoff (1971, page 351) except that the empirical range-energy relations of Katz and Penfold (1952) were used in the place of the theoretical rate of energy loss used by Whitten and Poppoff.

The range R of an energetic electron is essentially the distance it would travel on the average from the source to the point where it stops. Katz and Penfold give an experimentally determined relation between range and energy:

$$R = 412\, E_0^{1.265-0.0954\, \ell n\, E_0} \qquad E_0 < 2 \text{ MeV} \tag{8.1}$$

R is the range (mg/cm^2) for an electron of initial energy E_0 MeV (R is measured in a direction parallel to the incident direction of the electron).

This relation was used, together with a mean winter atmosphere for $45^{o}N$ based on Kantor and Cole (1965) and Champion (1967) to calculate the minimum altitude which an electron travelling down a field line at 22^{o} to the vertical (corresponding to Christchurch) would reach. The results are shown in figure 8.5. It can be seen that D-region electron densities at 75 km will only be affected by β-particles with energies greater than 130 KeV, while to have any effect at 70 km the beta particle energy must be greater than 200 KeV.

The ionozation production rate was originally calculated as follows. Suppose two electrons of energies E_0, and $E_0 + dE_0$ respectively are incident on an absorber. Then they will travel distances R and R+dR (mg/cm^2).

Thus the energy lost in distance dR is

$$dE_0 = \frac{dE_0}{dR}\, dR \tag{8.2}$$

and the production rate of electrons will be

$$P = \frac{1}{W}\frac{dE_0}{ds}\mathcal{F}_0 = \frac{\rho}{W}\frac{dE_0}{dR}\mathcal{F}_0 \tag{8.3}$$

Here $\mathcal{F}_0$ is the incident flux, dx is the path increment in cm, W is the energy required to form one ion pair, (35 eV, Whitten and Poppoff 1971, page 59). ρ is the atmospheric density.

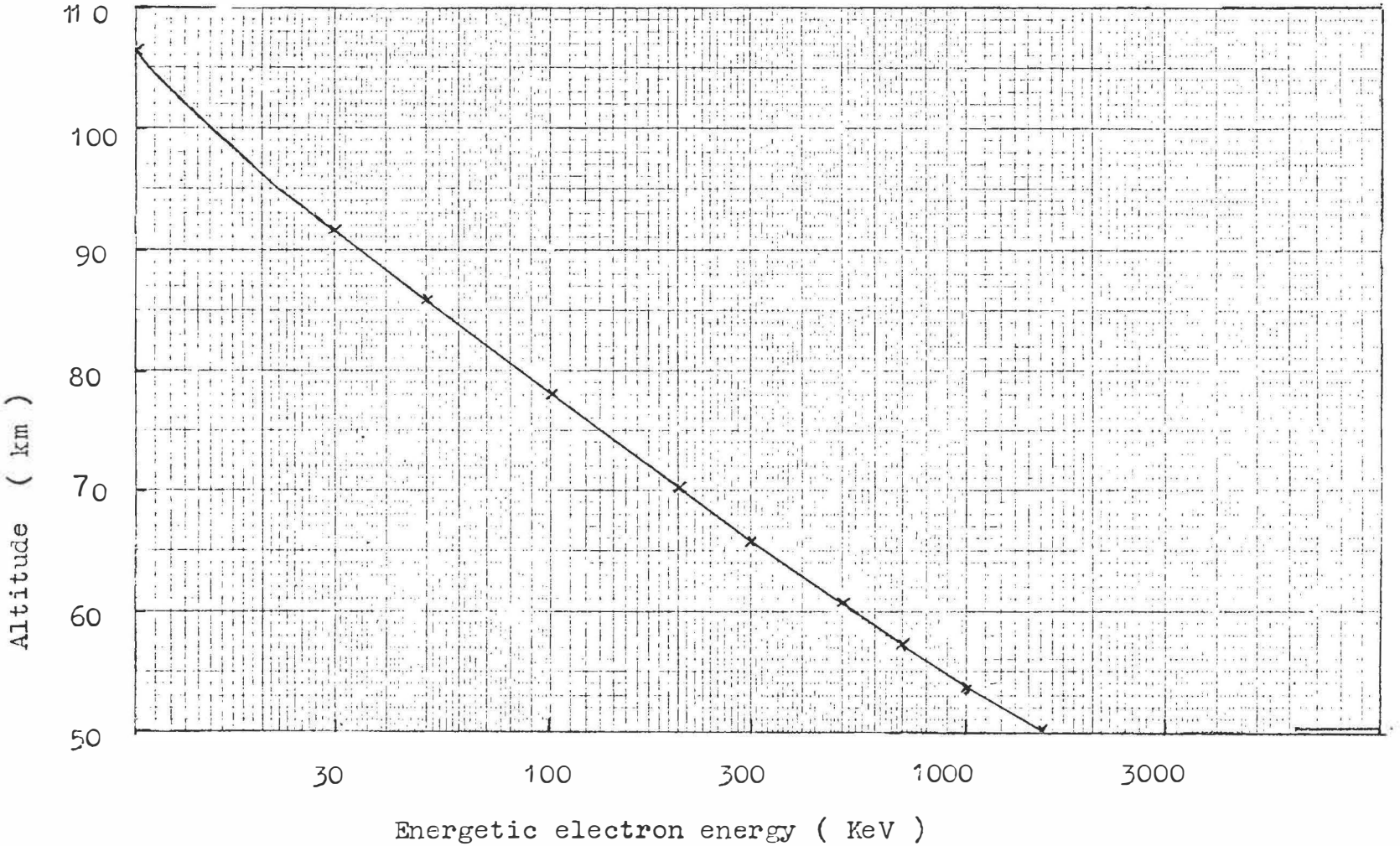

Fig 8.5: Lowest altitude of penetration of precipitating electrons.

The path of an energetic electron in the magnetic field of the earth is actually a spiral down a field line. Suppose the electron has pitch angle α and the field line is at an angle β to the vertical. Suppose that in one gyration around a field line the electron travels an actual distance ℓ. The vertical component of this distance will be

$$h = \ell \cos \alpha \cos \beta \qquad (8.4)$$

Using the theory of motion of relativistic charged particles in magnetic fields of Jackson (1962, page 393) it was found that in one gyration around a field line a 250 KeV electron over Christchurch would travel less than 0.20 km parallel to the field, or 0.19 km vertically. Since production rates will be calculated at height intervals of 1 km, negligible error will be introduced by using (8.4) to give the actual distance ds travelled corresponding to an arbitrary change in height dh.

$$ds = dh \sec \alpha \sec \beta \qquad (8.5)$$

The production at the height h_0 can be calculated by (8.3). At the height (h_0-dh) the electron will have energy (E_0-dE_0) where dE_0 is given by (8.2) and (8.5)

$$dE_0 = \rho \frac{dE_0}{dR} dh \sec \alpha \sec \beta. \qquad (8.6)$$

This new energy can be used to calculate the production at the new height. A production versus height profile can be built up by similar steps.

A profile from a typical calculation, using a height step of 1 km is shown as the "model 1" curve in figure 8.6. Unfortunately the maximum production occurs at a height just below the maximum range!

The reason for this is a false assumption implicit in the method. It is assumed that at the beginning of each height step the electrons are travelling parallel to their initial direction of incidence. This will not in general be true, because of scattering by collisions (both elastic and inelastic). This method has been used in the literature (e.g. Manson and Merry, 1970) and although the error will not be so bad in calculations for fluxes isotropic over pitch angles 0^{o} to 90^{o} as for the mono-directional fluxes discussed here, such calculations should be viewed with caution.

A more satisfactory method has been used by Rees (1963). The scattering of the beta particles as they travel through the air is accounted for by a "normalized energy dissipation distribution function", which has been measured experimentally by Grün (1957) and calculated experimentally by Spencer (1959). Both of these determinations were for a mono-energetic mono-directional beam of electrons incident on a homogeneous isotropic atmosphere.

Rees used the measurements of Grün to calculate the ionozation rate P_h at height h, for vertical incident electron flux $\mathcal{F}$ cm^{-2} sec^{-1}, neglecting the geomagnetic field, by the relation:

$$\frac{P_h}{\mathcal{F}} = \frac{E_0/r_0}{W} \lambda\left[\frac{Z}{R}\right] \frac{n(M)_Z}{n(M)_R} \qquad (8.7)$$

Here E_0 is the initial energy of the β-particle

W is the mean energy loss per ion formed (35 eV)

R is the range (g/cm^2) of electrons of energy E_0

Z is the atmospheric depth at height h ($Z = \frac{P(h)}{g}$ g/cm^2, where $P(h)$ = pressure ($dynes/cm^2$), g = gravitational acceleration (cm/sec^2)

$n(M)_Z$, $n(M)_R$ are the number densities of ionizable molecules at atmospheric depth Z and R.

$r_0 = \frac{R}{\rho(h_p)}$ where $\rho(h_p)$ is the density at the lowest altitude of penetration (h_p).

$\lambda(\frac{Z}{R})$ is the normalized energy dissipation distribution function from the measurements of Grün.

From the measurements of Grün, $\lambda(\frac{Z}{R})$ varies little with energy in the energy range 5 to 54 KeV. By considering the theoretical values of Spencer it appears that using this same distribution function up to energies of 250 KeV will lead to errors of less than 15% in the calculated ion-pair production rate, and the shape of the production profile will not be altered. At 1.5 MeV the predicted production rate could be about 25% too low, but again the shape would be all right. Because of the uncertainty in the flux data these errors are acceptable, and the distribution function given by Rees (1963) will be used for all energies.

It is assumed that the change in atmospheric density with height will not affect the dissipation distribution function.

The presence of the magnetic field of the earth is a further complication. For a particle with pitch angle α on a field line at the angle β to the vertical it is included in the following calculations by putting

$$dR = \rho dh \sec \alpha \sec \beta \tag{8.8}$$

The lowest altitude of penetration, h_p, is then found from the relation

$$P(h_p) = \int_{h_p}^{\infty} g dh = g \cos \alpha \cos \beta \int_{h_p}^{\infty} \rho \sec \alpha \sec \beta \, dh$$

$$\text{i.e. } P(h_p) = gR \cos \alpha \cos \beta \tag{8.9}$$

which gives the pressure at h_p in dynes/cm^2. From this pressure h_p can be found using model atmosphere data.

Also, Z is redefined as

$$Z = \frac{P(h)}{g} \sec \alpha \sec \beta \tag{8.10}$$

Since the mean molecular weight of the atmosphere is essentially constant below 100 km,

$$\frac{N(M)_Z}{N(M)_R} = \frac{\rho(h)}{\rho(h)_p} \tag{8.11}$$

The experimental measurements of beta particle range in air by Grün are only for energies up to 54 KeV, so the range energy relation of Katz and Penfold (8.1) was used. There is satisfactory agreement between the two sets of values between 20 and 54 KeV.

The 45^{o}N February atmosphere of Kantor and Cole (1965) was used for atmospheric parameters.

A typical ionization rate profile from this theory is shown by the curve labelled "model 2" in figure 8.6.

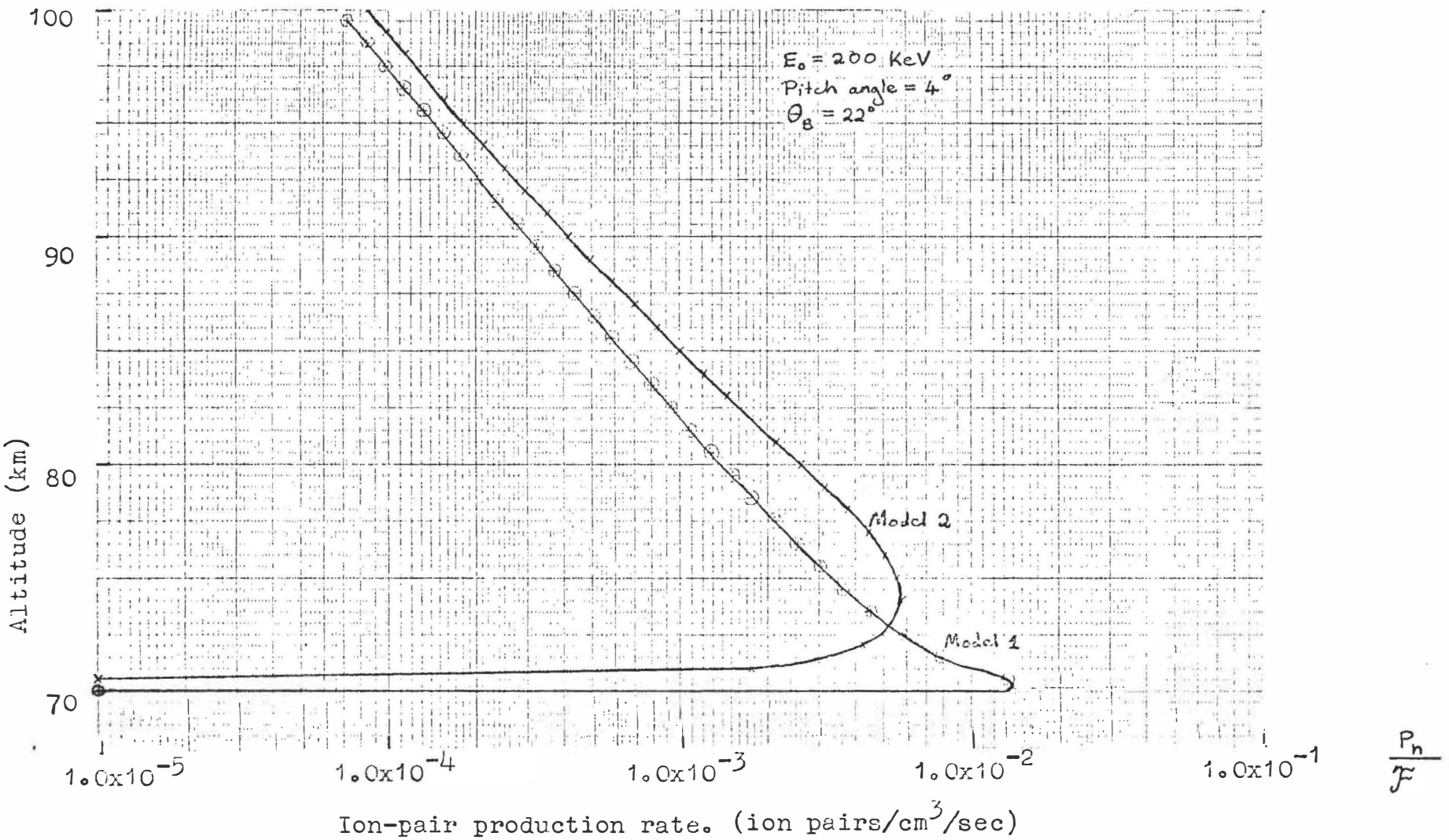

Fig 8.6: Ionization by energetic electrons- two models.

8.4 CALCULATIONS FROM THE ISIS-2 DATA

The pitch angle distribution at the Isis-2 satellite (altitude 1400 km) for a typical pass during the period of enhanced D-region electron densities is shown in figure 8.7 (Burrows, private communication). The specification of the detectors is as follows:

DE2L Solid state $e^- > 150$ KeV

Geometrical factor = 8.15×10^{-3} $cm^2 sr$,

collimator half-angle = 7^o

DE2H Solid state $e^- > 210$ KeV

Geometrical factor = 8.15×10^{-3} $cm^2 sr$,

collimator half-angle = 7^o

D3E Solid state $1.0 \text{ MeV} < e^- \leq 2.0 \text{ MeV}$

Geometrical factor = 3.45×10^{-1} $cm^2 sr$,

collimator half-angle = 45^o

It was assumed that the pitch angle distributions of figure 8.7 for DE2L and DE2H were typical of $\Lambda = 52^o$ for the disturbed period. Since the angular resolution of detector D3E was so poor, it was assumed that the D3E electrons had a similar pitch angle distribution to the DE2H ones. (This appears reasonable from the theoretical pitch-angle distributions of Lyons et al., 1972). It was also assumed that the pitch angle distribution and flux at 70-80 km could be calculated from the values at 1400 km allowing only for the change in pitch angle with height because of the changing magnetic field, and the absorption of energy by ionizing collisions. (This will perhaps not be true, since pitch angle diffusion due to the interactions with whistler mode waves mentioned earlier will take place in the 1400-100 km height range, but this should not change the order of magnitude

of the ionization.)

In using relation 8.7 the pitch angle α_h at height h km rather than the measured value α_{1400} at the space-craft must be used. As discussed earlier, $\frac{\sin^2\alpha}{B}$ is a constant along a field line so that

$$\frac{\sin^2\alpha_h}{\sin^2\alpha_{1400}} = \frac{B_h}{B_{1400}} \qquad (8.12)$$

A dipole field representation was used to calculate the field at height h from a known value at the earth's surface. For a dipole field (Davies 1966, P21)

$$B = B_0 (\frac{a}{r})^3 \{1 + 3\sin^2\phi_m\} \qquad (8.13)$$

where B_0 is the flux density at the dipole equator

a is the radius of the earth

(r,ϕ_m) are the dipole coordinates.

The lines of force of the dipole field are given by

$$r = ka\cos^2\phi \qquad (8.14) \qquad \text{(Davies 1966)}$$

Thus 8.13 can be written as

$$B = B_0 (\frac{a}{r})^3 \{1 + 3(1-(\frac{r}{ak})^2)\}^{\frac{1}{2}} \qquad (8.15)$$

If the McIlwain L-parameter is used, then for a dipole field $L \equiv k$. Thus the field at a height h vertically above the earth's surface is given by

$$B_h = B_s (\frac{a}{a+h})^3 \left\{\frac{1 + 3(1-(\frac{a+h}{aL})^2)}{1 + 3(1-(\frac{1}{L})^2}\right\}^{\frac{1}{2}} \qquad (8.16)$$

where B_s is the field on the earth's surface on the same field line.

(8.16) will be sufficiently accurate for h < 100 km. However, at 1400 km the deviations from a dipole field are important, and a direct field measurement from the satellite was used.

B_{1400} = 3.15 x 10^{-5} Tesla (0.315 gauss)

B_s = 5.893 x 10^{-5} Tesla (Kaye & Laby 1966, for Amberley 1972)

L = 2.6

a = 6.371 x 10^5m.

From (8.16) and (8.12) it was found that electrons with pitch angles at the satellite greater than 48.0° would mirror above 70 km, and those with pitch angles greater than 48.5° would mirror above 100km.

Table (8.1) was obtained from figure 8.7. Since the collimator half-angle was 7° values were taken at 14° intervals.

Typical counting rates at ISIS-2 at $\Lambda = 52^\circ$ during days 220 to 224 for mirroring particles ($\alpha_{1400} = 90^\circ \pm 7^\circ$) are:

D3E (90°) = 1600 sec^{-1} = 4.6 x 10^3 electrons sr^{-1} cm^{-2} sec^{-1}

DE2H(90°) = 2200 sec^{-1} = 2.7 x 10^5 electrons sr^{-1} cm^{-2} sec^{-1}

DE2L(90°) = 4100 sec^{-1} = 5.0 x 10^5 electrons sr^{-1} cm^{-2} sec^{-1}

(The geometrical correction factors given at the beginning of this section have been used.)

To use equation (8.7) the electron flux should be in cm^{-2} sec^{-1}. The electron fluxes in $sr^{-1}cm^{-2}sec^{-2}$ were calculated from the 90° counting rates above, and the pitch angle distribution of table 8.1.

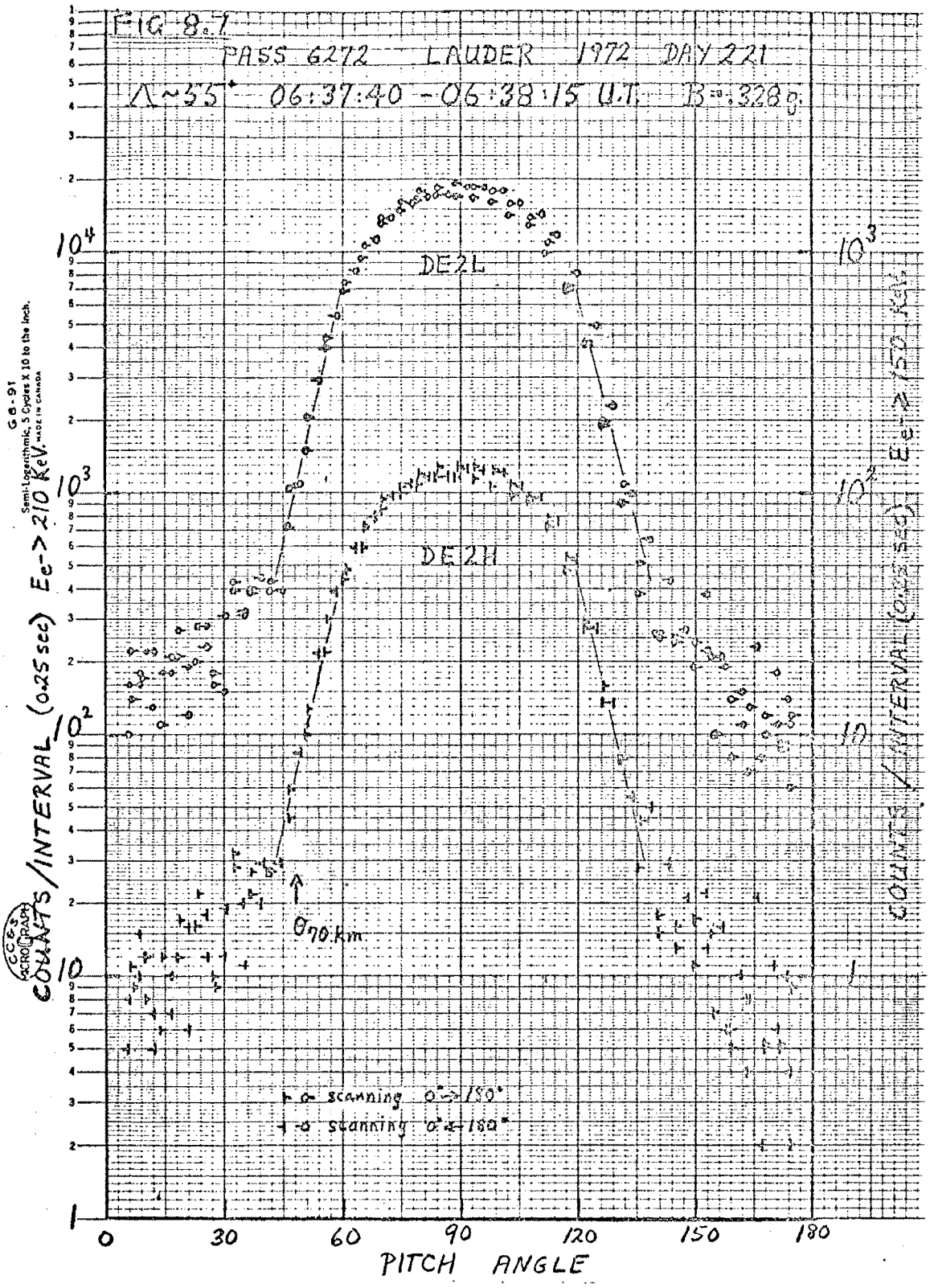

Fig 8.7: Pitch angle distribution at 1400 km.

(Burrows, private communication.)

Pitch angle (degrees) at 1400 km	Counts/interval (0.25 sec)			
	DE2H	$\frac{DE2H(\alpha)}{DE2H(90^{o})}$	DE2L	$\frac{DE2L(\alpha)}{DE2L(90^{o})}$
90^{o}(83- 97)	1.2×10^{3}	1.0	1.8×10^{3}	1.0
55^{o}(48- 62)	2.0×10^{2}	0.16(7)	3.4×10^{2}	0.18(9)
41^{o}(34- 48)	2.7×10^{1}	0.022(5)	4.1×10^{1}	0.022(8)
27^{o}(20- 34)	1.6×10^{1}	0.013(3)	2.3×10^{1}	0.012(8)
13^{o}(6- 20)	9	0.007(5)	1.8×10^{1}	0.010(0)
3^{o}(0- 7)	9	0.007(5)	1.8×10^{1}	0.010(9)
177^{o}(173-180)	6	0.005(0)	1.2×10^{1}	0.006(7)
167^{o}(160-174)	6	0.005(0)	1.2×10^{1}	0.006(7)
153^{o}(146-160)	1.4×10^{1}	0.011(7)	2.1×10^{1}	0.011(7)
139^{o}(132-146)	2.7×10^{1}	0.022(5)	3.8×10^{1}	0.021(1)
125^{o}(118-132)	2.0×10^{2}	0.16(7)	3.4×10^{2}	0.18(9)

Table 8.1 Pitch angle distribution for Pass 6722, $\Lambda \sim 55^{o}$ (The ranges in column one are given because of the 7^{o} half-angle of the collimator.)

(D3E was assumed to have the same pitch-angle distribution as DE2H.) The flux was converted to $cm^{-2}sec^{-1}$ by multiplying by $d\Omega = \sin\alpha\, d\alpha$ where $d\alpha$ was 14^{o} (.244 radians) or 6^{o} for $\alpha = 3^{o}$. Thus the entire flux between 6^{o} and 20^{o} was assumed to have a pitch angle of 13^{o} for example. This leads to table 8.2.

Pitch angle (degrees) at 1400 km	Electron flux (cm^{-2} sec^{-1})		
	DE2L	DE2H	D3E
41^{o}	$1.8(2)\times10^{3}$	$9.6(0)\times10^{2}$	$1.6(5)\times10^{1}$
27^{o}	$7(.1)\times10^{2}$	$3.9(9)\times10^{2}$	6.7(9)
13^{o}	$2.7(5)\times10^{2}$	$1.0(4)\times10^{2}$	1.7(7)
3^{o}	6(.5)	2.4(6)	4.2×10^{-2}

Table 8.2 Electron fluxes for various pitch angles.

Production of ionization by these fluxes was then calculated using equation (8.7). All of the electrons with energies between 150 and 210 KeV were assigned an energy of 180 KeV; those between 210 KeV and 1 MeV were assigned 250 KeV; and separate calculations were carried out assuming the 1.0-2.0 MeV electrons to have energies 1.0 and 1.5 MeV. The results are shown in table 8.3 and figure 8.8.

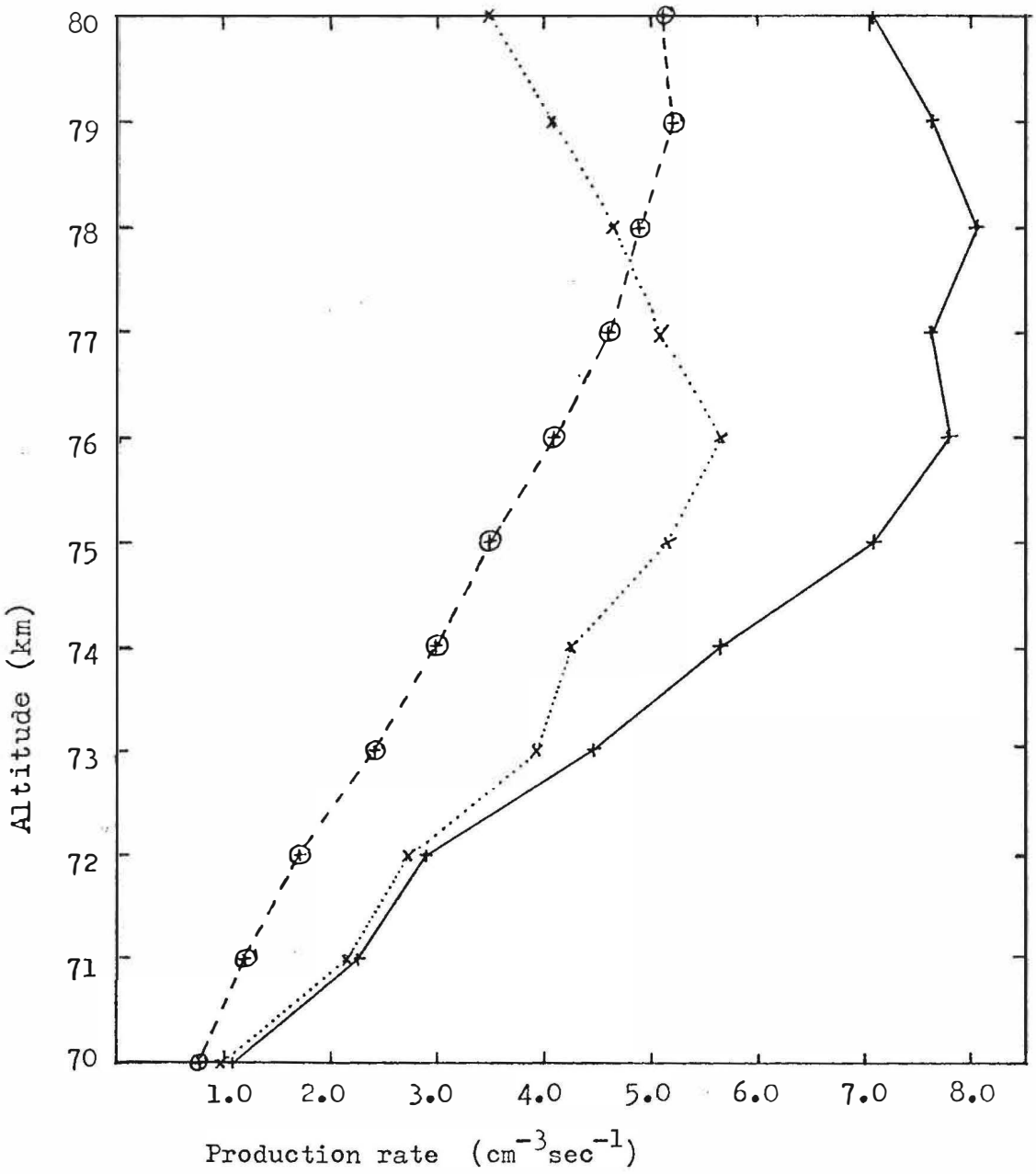

Fig 8.8: Ion-pair production rate profiles.

Height (km)	180 KeV	250 KeV	1 MeV	1.5 MeV	All E > 150 KeV
80	3.56	3.49	2.3×10^{-2}	2.0×10^{-2}	7.1
79	3.59	4.08	2.6×10^{-2}	2.3×10^{-2}	7.7
78	3.34	4.65	3.2×10^{-2}	2.7×10^{-2}	8.0
77	2.50	5.09	3.8×10^{-2}	3.2×10^{-2}	7.6
76	2.08	5.65	4.5×10^{-2}	3.8×10^{-2}	7.8
75	1.88	5.15	5.4×10^{-2}	4.5×10^{-2}	7.1
74	1.35	4.25	6.4×10^{-2}	5.3×10^{-2}	5.7
73	0.50	3.91	7.7×10^{-2}	6.3×10^{-2}	4.5
72	0.046	2.73	9.3×10^{-2}	7.6×10^{-2}	2.9
71	0.0	2.15	1.1×10^{-1}	9.0×10^{-2}	2.2
70	0.0	0.95	1.4×10^{-1}	1.1×10^{-1}	1.1
69	0.0	0.24			
68	0.0	0.0			

Table 8.3 Production rates (ion pairs/cm^2/sec) for the β-particle fluxes of energy greater than 150 KeV during days 220 to 224 of 1972.

8.5 DISCUSSION OF THE PRODUCTION RATE RESULTS

The major quiet time source of ionization in the mid-latitude D-region between 70 and 80 km is thought to be photoionization of nitric oxide by solar Lyman-α radiation (Sechrist 1972a). The production rate of electrons from this source is shown in figure 8.8, the theory for this calculation is given in section 9.3. The nitric oxide concentrations used were taken from Meira (1971) and the concentration of

molecular oxygen from the mean 45^{o}N atmosphere of CIRA 1965. The solar zenith angle is 60^{o}. (For most of the differential absorption runs of early August 1972 the solar zenith angle was about 62^{o}.) Before making comparisons with the β-particle production curve the following qualifications should be noted.

(1) The positive ion resulting from the photo-ionization of nitric oxide is NO^{+}, whereas all molecular species will be ionized by β-particles leading predominantly to ions formed from O_2 and N_2. Thus significant ionization production by β-particles may lead to differences in the positive ion chemistry and thus in the recombination coefficient. This means that the electron densities resulting from ionization by Lyman-α radiation, and those resulting from β-particle bombardment will not necessarily be simply related to the relative production rates of the two processes.

(2) There are large uncertainties in the nitric oxide profile below 80 km (Strobel, 1972b). These may be as large as a factor of ten.

(3) The assumptions used in calculating the energetic electron flux at 75 km from that at 1400 km may be inaccurate.

(4) The pitch angle and energy resolution of the ISIS-2 experiment is coarse. However, I think this would make little difference to the production except for shifting the profile up or down by a kilometer or so.

From figure 8.8, if the loss of electrons followed an attachment-type law (section 9.5) and the loss coefficient was the same whether Lyman-α radiation or beta particles produced the predominant ionization, an increase of from 2.3 times at 70 km to 3 times at 75 km would be expected in the electron

density at disturbed times compared to quiet times. However, a significant increase would also be expected from 76 to 79 km and this was not observed. A possible explanation for this is that the attachment of electrons to neutral molecules may be the rate-determining step in the loss of electrons below about 75 km, whereas above this height the reactions of positive ions amongst themselves or with electrons may determine the loss rate (Section 9.5). On the hypothesis that β-particle bombardment changes the positive ion composition but not the neutral composition it is possible that the loss rate above 75 km differs between quiet and stormy conditions, while that below 75 km does not. In fact Narcisi et al. (1972) have found significant differences at auroral latitudes (Churchill, L = 6) in positive ion composition between quiescent times and times of energetic particle bombardment. (In this case the precipitating particles were protons during a polar cap absorption event, rather than electrons. The overall effect was a decrease in recombination coefficient, whereas the present results require an increase.)

The theory that nitric oxide produced at aurural latitudes at the time of geomagnetic storms and transported to middle latitudes gives rise to the electron density increases does not satisfactorily explain the observed 70 to 75 km electron density increases. Nitric oxide is produced under normal conditions at heights above 90 km (Section 9.3.3) and the auroral enhancement of nitric oxide seen by Zipf et al. (1970) was at 110 to 130 km. Typical meridional velocities in the mesosphere could carry nitric oxide from the auroral zone to mid-latitudes in one or two days (section 9.8), but to

transport nitric oxide from 90 km down to 75 km in two days would require vertical transport of about 9 cm/sec which is higher than is likely in the mesosphere (section 9.2). Further, horizontal and vertical transport of nitric oxide should give rise to increases in electron density from 76 to 79 km as well as from 70 to 75 km, and this was not observed. However, as was noted earlier there is some indirect evidence that there was an electron density increase above 80 km following the onset of the August 1972 magnetic storm. It is conceivable that this increase was partly caused by nitric oxide transport, although any increase in the precipitating flux of electrons with energies above about 20 KeV would also be important.

8.6 CONCLUSIONS

An increase in electron density between 70 and 75 km in the D-region over Christchurch was observed during and following the solar disturbances in 1972. This increase can be accounted for by an increase in the high energy electron flux (electrons with energy between about 150 and 300 KeV) into the lower ionosphere following the filling of the electron slot between the two electron zones in the radiation belt at the time of the large magnetic storms. The occurrence and magnitude of the high energy electron flux was inferred from satellite measurements at a height of 1400 km. There was no significant increase in electron density observed between 76 and 79 km, and this may indicate that some modification of the positive ion chemistry occurred at this height.

The hypothesis that the observed storm after effects in the 70-75 km region are due to the transport of nitric oxide from the auroral regions is unsatisfactory. However, indirect evidence indicated a probable increase in electron density above 80 km, which may have been caused by particle precipitation or nitric oxide transport.

CHAPTER 9

THE THEORY OF ELECTRON DENSITY VARIATIONS IN THE MESOSPHERE

The electron density in the mesosphere shows considerable day to day variation. This is evident both from a review of the literature (Chapter 6) and from the results of the research undertaken for this thesis (Chapter 7). The purpose of this chapter is to consider the possible mechanisms which could give rise to this variation, and in particular to look at the effect of vertical transport of nitric oxide.

9.1 PRODUCTION AND LOSS OF IONIZATION

The electron number density in the mesosphere will satisfy the following equation

$$\frac{\partial N_e}{\partial t} = -\nabla\cdot(\underset{\sim}{v}\, N_e) + P - L \qquad (9.1)$$

where N_e = electron density

t is time

$\underset{\sim}{v}$ is the velocity of the electrons

P is the ion-pair production rate

L is the electron loss rate.

Thus a change in electron density could be due to a transport of electrons (the $\nabla\cdot(\underset{\sim}{v}\, N_e)$ term), or a change in the production or loss rates. To discuss the relative importance of these processes the concept of a lifetime (or relaxation time) of a species of ion or molecule in the atmosphere is useful (Whitten and Poppoff 1971, section 2.6.1).

Consider a reaction of the type:

$$X \rightarrow Y + Z \qquad \text{rate constant} = k \tag{9.2}$$

then

$$\frac{d[X]}{dt} = -k[X]$$

and (9.3)

$$[X] = [X(t=0)]e^{-kt}$$

In a time $\tau = \frac{1}{k}$ seconds the concentration of X will have decayed to a factor of $\frac{1}{e}$ of its initial value. For a more complicated reaction of the form

$$X + Y \rightarrow \text{products} \qquad \text{rate} = k_2$$

the lifetime τ of species X is defined as

$$\tau = \frac{1}{k_2[Y]} \tag{9.4}$$

To summarize, the lifetime τ is an indication of the time a particular species would last in the atmosphere if production of it was stopped, and there was no transport.

9.1.1 Transport of Electrons

Transport is represented by the $\nabla\cdot(\mathbf{v} N_e)$ term in equation 9.1. The loss of electrons in the absence of production or transport is thought to follow one of the following two equations (section 9.5).

$$\frac{dN_e}{dt} = -\alpha_{eff} N_e^2 \tag{9.5a}$$

or $$\frac{dN_e}{dt} = -B N_e \tag{9.5b}$$

Typical values for these parameters at 75 km are:

N_e = 230 cm^{-3} (Average winter value at Birdling's Flat)

α_{eff} = 7 x 10^{-6} cm^3 sec^{-1} (Aiken, 1972)

$B = 8 \times 10^{-3}$ sec^{-1} (Mechtly et al., 1972b)

Thus (9.5a) gives $\tau = 6 \times 10^2$ sec (10 minutes)

(9.5b) gives $\tau = 1.4 \times 10^2$ sec (2 minutes)

It is thought that vertical velocities w in the mesosphere are less than or of the order of 1 cm/sec. (Geisler and Dickinson, 1968). Thus if vertical transport of electrons is to be an important effect, there must be a significant change in electron densities within a height interval of $w\tau \simeq 600$ cm. However, rocket measurements (Mechtly et al., 1972a) show that the height interval for electron densities to change by a factor of e in the D-region is at least 1 km. Horizontal winds of perhaps up to 130 m/sec are found in the mid-latitude D-region (Murgatroyd, 1970). However, large differences in electron density over horizontal distances of $v\tau$ = 88 km are unlikely as they would indicate localized changes in production or loss rates.

Thus direct transport of electrons can be ruled out as a cause of day to day variability of D-region electron densities.

9.1.2 Changes in Production Rate

Figure 9.1 (Sechrist 1972a) shows ionization rates for the daytime mid-latitude D-region for a solar zenith angle of 60^o and solar minimum conditions. It can be seen that the major production mechanism between 70 and 90 km is the ionization of nitric oxide by solar Lyman-alpha radiation. (The curve labelled Ly-α is based on the rocket nitric oxide measurements of Meira (1971).)

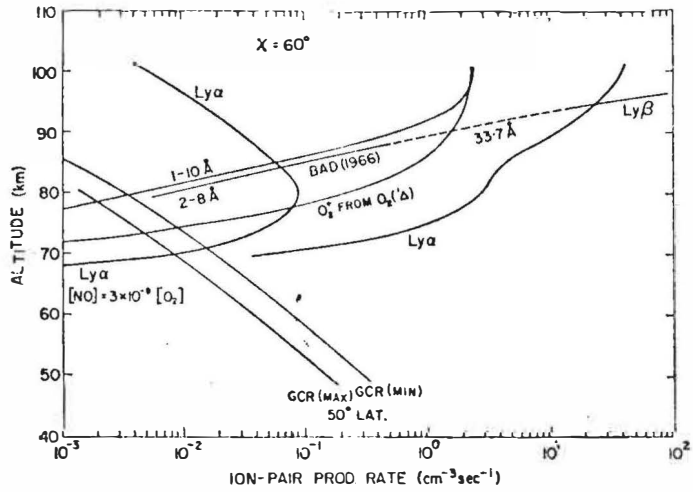

Fig 9.1: Ion-pair production rates from various sources of D-region ionization. (Sechrist, 1972a)

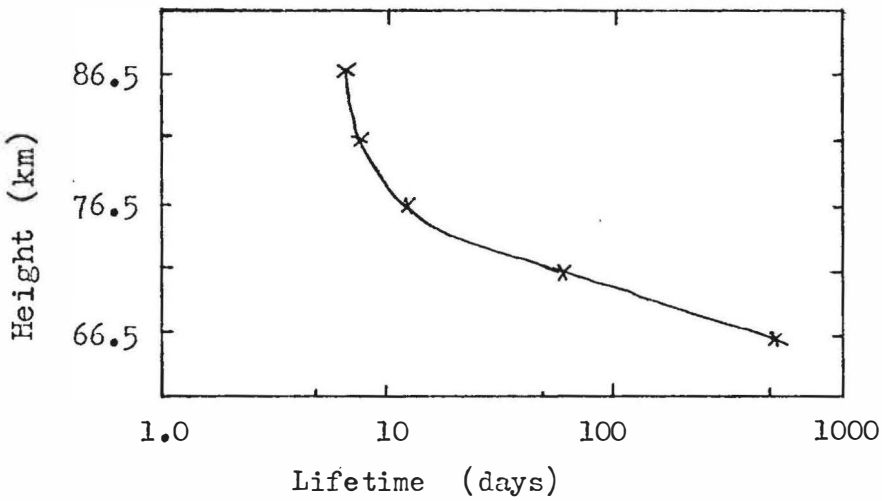

Fig 9.3: Photochemical lifetime of nitric oxide. (Winter)

The only source of nitric oxide below 90 km which does not involve transport from higher altitudes is via the photo-ionization of N_2 (Strobel, 1972a). It will be shown later that this source is insignificant compared to measured mesospheric nitric oxide concentrations. This means most of the nitric oxide in the mesosphere must be transported down from the thermosphere. Thus it is tempting to ascribe the electron density variations in the mesosphere to fluctuations in this transport process. It is also possible that temperature variations in the mesosphere could have some effect through the variation of reaction rates involving nitric oxide. A simple computer model of the photochemistry and transport of nitric oxide built up to investigate these possibilities is described in this chapter. Several computer studies of nitric oxide concentrations in the mesosphere involving transport have been made already (e.g. Hesstvedt & Janson 1969, Shimazaki & Laird 1972, Hunt 1973, Strobel 1971, Geisler and Dickinson 1968). However, these studies have attempted to explain the mean concentration of nitric oxide in the mesosphere rather than the day to day changes.

It was shown in chapter 8 that energetic particle precipitation could cause variation in D-region electron densities. However, Manson & Merry (1971) have shown that the extra attenuation radio waves are likely to suffer because of the ionization due to energetic electron precipitation cannot account for all of the day to day variation observed in absorption. Also chapter 6 discusses evidence for other causes of variation in addition to electron precipitation.

Another possible cause of a change in the rate of ionization production is a change in the flux of electromagnetic radiation from the sun. Such changes occur during solar flares, and the resultant increase in X-radiation can give rise to increases in ionization down to 60 km. However, these disturbances (called SID's, Collins and Herzburg 1965) are short-lived, lasting only 15 minutes to 2 hours, and also cannot explain the correlations between D-region absorption and stratospheric warmings (chapters 6,7) or the fact that radio wave absorption is anomalously large in winter (chapter 6).

9.1.3 Changes in the Loss Rate

The positive ion chemistry of the D-region is as yet poorly understood (Ferguson, 1971). Thus loss rates cannot yet be satisfactorily calculated from theory. (The question will be considered in more detail in section 9.5.) However, it is quite possible that changes in the loss rate, due either to temperature effects on the positive ion reaction rates (Reid 1970) or variations in water vapour transport (Sechrist 1970) are an important source of electron density variability.

9.2 NITRIC OXIDE TRANSPORT

All of the studies of nitric oxide transport in the mesosphere referred to earlier, except that of Geisler and Dickinson, have handled the motion by lumping all of the transport mechanisms together into an "eddy diffusion coefficient" (Strobel 1972a). This is used to calculate a mean nitric oxide profile. If such an approach were used to calculate day to day changes it would be necessary to include in the eddy diffusion coefficient only those processes which

have time scales of a day or less (e.g. 'turbulence' due to gravity waves and tides) while the longer scale variations are put in the model as vertical motions. It is shown in appendix D that this leads to a non-linear parabolic differential equation.

Because of the problem of deciding on appropriate eddy diffusion coefficients, the problem of deciding on upper and lower boundary conditions, and the general complexity of solving a time dependent non-linear second order partial differential equation it was thought best to begin with a simpler model. This model included the most important known chemical reactions involving nitric oxide, and considered the changes in an initially specified nitric oxide height profile caused by steady vertical motion lasting for periods of one up to ten days. The effect of changes in reaction rates due to temperature variations was also investigated. Thus transport by 'turbulent' processes (fluctuations with time scales less than a day) was neglected.

Measurements of the meteorological properties of the atmosphere in the height range 65-85 km are rare. However, there is some evidence for variations with time scales of several days at these heights. Pokrovskiy and Teptin (1970) found a peak in the spectral energy density of the zonal wind at a period of 3.5 days and a possible peak at ten days by analysing meteor wind data (80-100 km) at Kazan (56^{o}N) in the late winter of 1966-67. Also Muller (1972) found that the meteor winds over Sheffield (56^{o}N) at an average height of 97 km could not be accounted for fully by a harmonic series of fundamental period 24 hours (atmospheric tides) and suggested

that slower changes in the wind with time scales of several days were responsible. Justus and Woodrum (1973) found evidence in rocket data of disturbances in winds and density in the 65-85 km height range with vertical scales of about 20 km and periods (over a given point on the earth) somewhere in the range from several days up to about 24 days. Finally, from theoretical work on planetary waves (e.g. Dickinson 1969) it appears likely that there is some propagation of planetary scale variations up to the mesosphere from the lower atmosphere in winter and early spring.

These measurements suggest that there are synoptic scale variations in pressure and winds in the mesosphere. By analogy with the lower atmosphere one would expect vertical motion to be associated with these varations.

Christie (1970) pointed out features common to both the winter mesopause (particularly at low latitudes) and the mid-latitude tropopause. These similarities show up in thermal, flow and radiative temperature change distributions. He interpreted day to day variations in nitric oxide concentrations in the D-region by analogy with tracer transports near and through the tropopause. He suggested that subsidence of a few kilometers between 80 and 88 km would be sufficient to account for the observed sporadic increases in electron density in winter. However, later chemical models for the region (see the following work) suggest shorter photochemical lifetimes for nitric oxide than he assumed, so it is necessary to consider both the chemistry and the transport of the nitric oxide.

Estimates of the magnitude of the vertical motion likely to occur in the winter mesosphere are difficult due to the scarcity of data. Murgatroyd (1970) calculated that the net diabatic heating in winter (heating by absorption of solar radiation minus cooling by re-radiation) is about $-1^{o}K$ at $45^{o}N$. Thus for the temperature of the atmosphere to stay constant this heat must provided by another source. Heating of the atmosphere by adiabatic subsidence will follow the relation:

$$\frac{dT}{dt} = -\frac{(\gamma-1)}{\gamma}\left(\frac{w}{H}\right) T \qquad (9.6)$$

where $\gamma = \frac{c_p}{c_v}$; H = scale height,

T = temperature;

w = vertical velocity (positive upwards).

At 80 km $T \simeq 186^{o}K$, H ≃ 5.6 km (CIRA 1965). Thus (9.6) gives:

$$\frac{dT}{dt} \simeq 8.2\ w \quad {}^{o}K/day$$

where w is in cm/sec.

This would suggest that a mean vertical velocity of about 0.1 cm/sec would keep the temperature constant. Hesstvedt (1971) considered the emission and absorption of radiation and also heating due to the recombination of atomic oxygen with molecular oxygen and ozone. He found that even including an eddy diffusion coefficient that was independent of latitude a steady downward motion of about 0.5 cm/sec was still necessary at $45^{o}N$ in winter to keep the temperature constant (assuming no meridional transport of heat into the region).

The calculation of vertical velocities likely to be associated with transient fluctuations is even more uncertain. Geisler and Dickinson (1968) have suggested that vertical velocities of about 0.1 to 1 cm/sec could be associated with planetary waves in the mesosphere.

On this basis a steady downward motion of 0.1 to 1.0 cm/sec will be assumed, with transient fluctuations of about the same order superimposed.

9.3 THE CHEMISTRY OF NITRIC OXIDE

The large number of reactions used in the models of Hesstvedt and Jansson, Shimazaki and Laird, Strobel, and Hunt make the problem rather complex. Thus it was decided that in view of the uncertainties which exist in the concentrations of neutral constituents anyway, it would be better to follow the lead of Geisler and Dickinson (1968) and simplify the reaction scheme down to the most important reactions. However, because of the extra knowledge on reactions and rates which has accumulated since 1968 a check was made of the importance of the reactions shown in table 9.1, which were taken from the work of Shimazaki and Laird (1972), Geisler and Dickinson (1968), Turco and Sechrist (1970), Hesstvedt and Jansson (1969), and Strobel (1971). The original sources for the rate constants will be found in those papers.

Temperatures, where required, were taken from the January $45^{o}N$ values of Kantor and Cole (1965) for heights less than 80 km, and from the winter $45^{o}N$ values of Champion (1967) for heights above 80 km.

Reaction	Rate	Source
(1) $N(^4S)+O_2 \rightarrow NO+O$	$k_1 = 1.4\times10^{-11}\exp(-\frac{3600}{T})$	Shimazaki & Laird
(2) $N(^4S)+NO \rightarrow N_2+O$	$k_2 = 1.5\times10^{-12}T^{\frac{1}{2}}$	Geisler & Dickinson
(3) $NO+h\nu(\lambda\approx1216\text{Å}) \rightarrow NO^+ + e$	J_3	
(3a) $NO^+ + e \rightarrow N(^4S)+O(25\%)$ $\rightarrow N(^2D)+O(75\%)$	$k_{3a} = 1\times10^{-7}(\frac{T}{1000})^{-1.5}$	Strobel
(4) $NO+h\nu(1750\text{-}1900\text{Å}) \rightarrow N(^4S)+O$	J_4	
(5) $N_2+h\nu(1216\text{Å}) \rightarrow 2N(^4S)$	J_5	
(6) $N(^4S)+O+M \rightarrow NO+M$	$k_6 = 9\times10^{-33}$	Shimazaki & Laird
(7) $NO+O+M \rightarrow NO_2+M$	$k_7 = 1.1\times10^{-31}$	Shimazaki & Laird
(8) $O+NO_2 \rightarrow NO+O_2$	$k_8 = 3.2\times10^{-11}\exp(-\frac{0.6}{RT})$	Shimazaki & Laird
(9) $O_3+NO \rightarrow NO_2+O_2$	$k_9 = 9.5\times10^{-13}\exp(-\frac{2.46}{RT})$	Shimazaki & Laird
(10) $NO_2+h\nu(\lambda<3975\text{Å}) \rightarrow NO+O$	$J_{10} = 5.0\times10^{-3}$	Turco & Sechrist
(11) $N_2O+h\nu \rightarrow NO+N(^4S)$	*	Turco & Sechrist
(12) $N(^4S)+O_3 \rightarrow NO+O_2$	$k_{12} = 2.0\times10^{-12}T^{\frac{1}{2}}\exp(-\frac{1200}{T})$	Turco & Sechrist
(13) $N(^4S)+O \rightarrow NO+h$	$k_{13} = 2.0\times10^{-17}$	Turco & Sechrist
(14) $NO+O \rightarrow NO_2+h$	$k_{14} = 6.4\times10^{-17}$	Turco & Sechrist
(15) $N(^4S)+NO_2 \rightarrow 2NO$	$k_{15} = 3.0\times10^{-12}$	Turco & Sechrist
(16) $N(^4S)+OH \rightarrow NO+H$	†	Strobel
(17) $N_2+O \rightarrow N_2O+h$	*	Turco & Sechrist
(18) $N(^4S)+NO_2 \rightarrow N_2+O_2$	$k_{18} = 1.5\times10^{-11}$	Turco & Sechrist
(19) $N(^4S)+NO_2 \rightarrow N_2O+O$	$k_{19} = 1.5\times10^{-13}$	Turco & Sechrist
(20) $N+N+M \rightarrow N_2+M$	$k_{20} = 5\times10^{-33}(\frac{T}{300})^{-2.0}$	Turco & Sechrist
(21) $N(^2D)+O_2 \rightarrow NO+O$	$k_{21} = 6.0\times10^{-12}$	Strobel

* See section 9.3.1

† This reaction was neglected as no information on [OH] could be found.

Where a reaction contains temperature dependence:

T is in degrees Kelvin

$R = 1.99 \times 10^{-3}$ Kcal $(mole)^{-1}$ $(^{o}K)^{-1}$

All rate constants are in c.g.s. units. Concentrations should be in molecules cm^{-3}, then rates will be calculated in molecules cm^{-3} sec^{-1}.

Table 9.1 Reactions involving nitrogen constituents

Photo-dissociation and ionization rates were based on a solar zenith angle of 60^{o} and molecule number densities in general conforming to CIRA 1965. The production rate of electrons by reaction (3) is (Sechrist 1972b):

$$P = \sigma_i(NO)\ [NO]\ Q_\infty \exp(-\tau)$$

where $\sigma_i(NO)$ = ionization cross-section of nitric oxide (for $\lambda = 1216\text{Å}$) = 2.0×10^{-18} cm^2 (Manson & Merry, 1971)

Q_∞ = Lyman-α flux incident at the top of the atmosphere = 3×10^{11} cm^2 sec^{-1} (Manson & Merry, 1971)

τ = optical depth.

Since the major absorber of Lyman-α is molecular oxygen,

$$\tau = \sigma_a(O_2) \int_Z^\infty [O_2]\ \sec\chi\ dz$$

where $\sigma_a(O_2) = 8.5 \times 10^{-21}$ cm^2 (Manson & Merry, 1971)

χ = solar zenith angle (= 60^{o} here)

$\int_Z^\infty [O_2]dz$ was calculated using CIRA 1965 below 120 km, and Hinteregger et al. (1965) above 120 km.

J_3 $(= \sigma_i(NO)\ Q_\infty\ e^{-\tau})$ is plotted in figure 9.2.

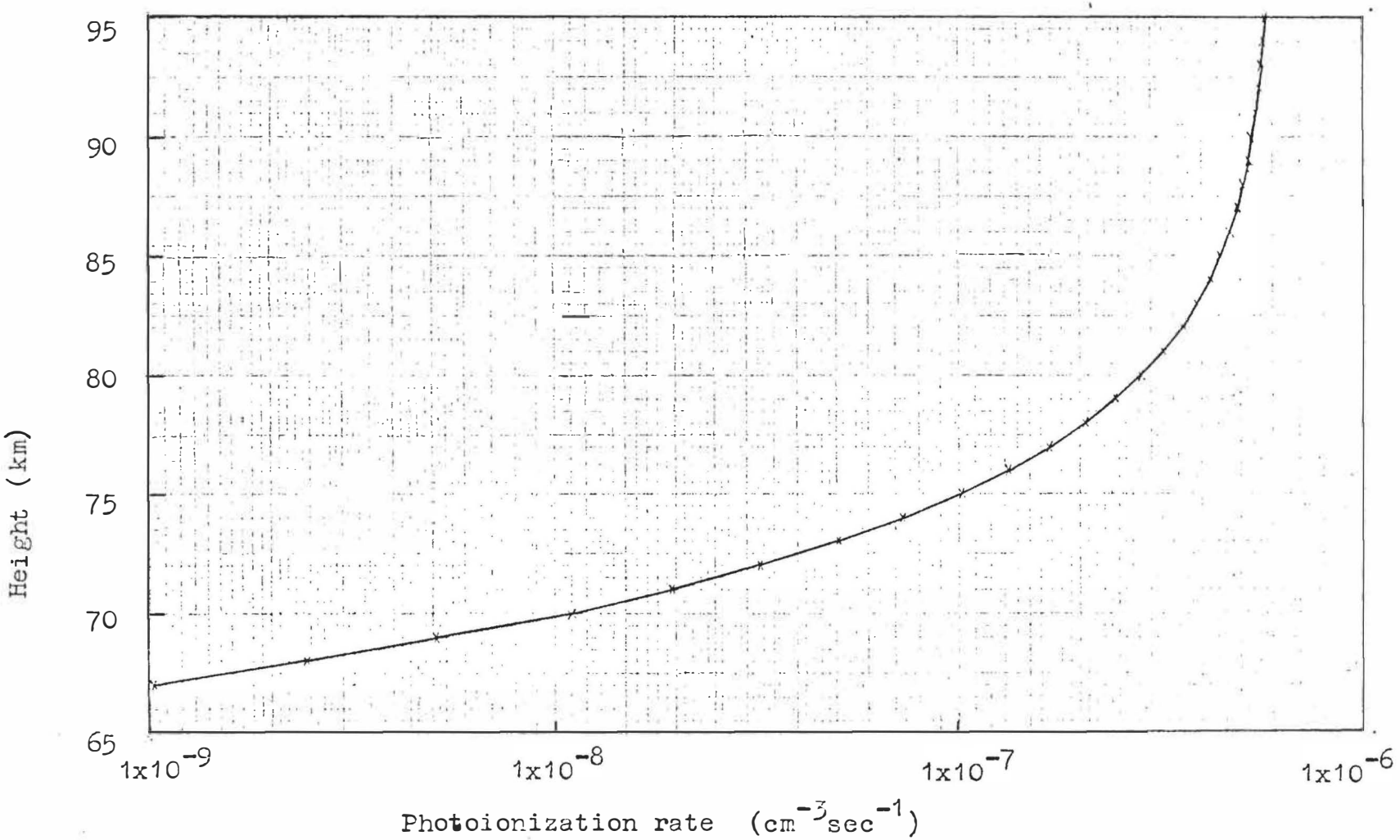

Fig 9.2: Photoionization rate of nitric oxide by solar Lyman-α. $\chi = 60$

The production rate of $N(^4S)$ by reaction (4) is difficult to calculate (Strobel 1971) because of the important attenuation of the 1750-1900 Å radiation by the Schumann-Runge bands of O_2. The curve labelled "$J_7 \times 10^4$ with σ_ℓ (O_2)" in figure 2 of Strobel (1971) was used, divided by a factor of two as suggested in that paper. This rate is about ten times that considered by Geisler and Dickinson (1968).

The production rate of $N(^4S)$ by the photoionization of molecular nitrogen (reaction 5) was calculated as follows (Geisler and Dickinson, 1968):

$$J_5 = 1 \times 10^{-12} e^{-\tau}$$

$$\tau = 3 \times 10^{-19} \sec(60^\circ) \int_Z^\infty [O_2] \, dz$$

The photochemical lifetimes of nitric oxide, atomic nitrogen, and nitrogen dioxide under the reactions of table 9.1 were calculated to see which reactions were important, so far as nitric oxide was concerned, and time scales under which constituents could be considered to be conserved. Where it was necessary to assume concentrations the following rules were applied:

(1) For N, NO_2 and N_2O the values given by Turco and Sechrist (1970) in their tables 4.4 (night) and 4.5 (day) were used. These are based on theoretical model calculations by Shimazaki and Laird, and Hesstvedt and Jansson.

(2) For major neutral concentrations the U.S. Standard Atmosphere values as in table 3.1 of Turco and Sechrist (1970) were used.

(3) The concentration of nitric oxide was taken from the measurements of Meira (1971).

(4) Concentrations for O, O_3 were taken from the curves for $O(^3P)$ and O_3 in figure 15 of Strobel (1971). These are for a theoretical model by Bowman et al. (1970).

The results are given in tables 9.2, 9.3, 9.4 and 9.5. The upper values are for day time conditions and the lower values are for night-time. The entry same means that daytime and night-time lifetimes are approximately equal.

In the following discussion the term odd nitrogen is used to refer to NO, N and NO_2, and the concentration of odd nitrogen is defined as:

$$[ON] \equiv [N] + [NO] + [NO_2]$$

9.3.1 Nitrous Oxide in the D-region

One possible source of nitric oxide in the D-region is the photolysis of nitrous oxide (reaction 11). Preston and Barr (1971) found that there are three possible photolysis processes of N_2O in the region near 1800 Å.

$$N_2O + h\nu \rightarrow N_2 + O(^1D) \qquad (a)$$

$$N_2O + h\nu \rightarrow N_2 + O(^3P) \qquad (b)$$

$$N_2O + h\nu \rightarrow N + NO \qquad (c)$$

Preston and Barr found that process (c), at 2288Å, 2139Å and 1849Å occurred in less than 1% of the photolysis processes if it occurred at all. They suggested that (a) might be the

Reaction	Lifetime (seconds)					
	65 km	70 km	75 km	80 km	85 km	90 km
(2) $N(^4S)+NO \rightarrow N_2+O$	2.8×10^{8} ∞	4.4×10^{7} ∞	2.0×10^{6} ∞	1.1×10^{6} ∞	8.4×10^{5} 3×10^{8}	6.7×10^{5} 2.3×10^{7}
(3) $NO+h\nu \xrightarrow{1216\text{Å}} NO^{+}+e \rightarrow N+O$	1.3×10^{9} ∞	5×10^{7} ∞	8×10^{6} ∞	3.5×10^{6} ∞	2.3×10^{6} ∞	1.9×10^{6} ∞
(7) $NO+O+M \rightarrow NO_2+M$	1×10^{6} $\sim1\times10^{14}$	5×10^{6} $\sim2.5\times10^{13}$	2×10^{7} ~same	7×10^{5} ~same	5×10^{5} ~same	1×10^{6} ~same
(9)* $O_3+NO \rightarrow NO_2+M$	3×10^{5} 9×10^{4}	3×10^{6} 7×10^{5}	3×10^{7} 6×10^{6}	6×10^{6} 6×10^{6}	2×10^{7} 2×10^{6}	5.5×10^{7} 5.5×10^{6}
(14) $NO+O \rightarrow NO_2+h$	8×10^{6} $\sim8\times10^{14}$	1.6×10^{7} $\sim8\times10^{13}$	3×10^{7} ~same	5×10^{5} ~same	2×10^{5} ~same	1.6×10^{5} ~same
(4) $NO+h\nu \xrightarrow{1900} N+O$	1.0×10^{6} ∞	6.7×10^{5} ∞	4.4×10^{5} ∞	4.0×10^{5} ∞	4.0×10^{5} ∞	3.4×10^{5} ∞

Table 9.2 Lifetime of NO under various reactions.

* The O_3 concentrations calculated by Shimazaki & Laird (Strobel 1972) are about ten times those of Bowman et al. which were used here. This would decrease the lifetime of NO under reaction by about a factor of ten.

Reaction	Lifetime (seconds)					
	65 km	70 km	75 km	80 km	85 km	90 km
(8) $NO_2+O \rightarrow NO+O_2$	55 5.5×10^{9}	110 5.5×10^{8}	210 ~same	4.4 ~same	1.4 ~same	1.4 ~same
(10) $NO_2+h\nu \rightarrow NO+O$	200 ∞	200 ∞	200 ∞	200 ∞	200 ∞	200 ∞
(15) $N+NO_2 \rightarrow 2NO$	9.5×10^{7} ∞	3.9×10^{7} ∞	1.5×10^{7} ∞	8.3×10^{6} ∞	6.0×10^{6} 2.1×10^{9}	4.8×10^{6} 1.7×10^{8}
(18) $N+NO_2 \rightarrow N_2+O_2$	6.6×10^{10} ∞	5.3×10^{10} ∞	2.1×10^{10} ∞	1.2×10^{10} ∞	1.0×10^{10} 3.5×10^{12}	9.4×10^{9} 3.3×10^{11}
(20) $N+NO_2 \rightarrow N_2O+O$	6.6×10^{12} ∞	5.3×10^{12} ∞	2.1×10^{12} ∞	1.2×10^{12} ∞	1.0×10^{12} 3.5×10^{14}	9.4×10^{11} 3.3×10^{13}

Table 9.3 Lifetime of NO_2 under various reactions.

Reaction	Lifetime (seconds)					
	65 km	70 km	75 km	80 km	85 km	90 km
(1) $N(^4S)+O_2 \rightarrow NO+O$*	3.5×10^{2} same	1.1×10^{3} same	6×10^{3} same	2.3×10^{4} same	1.5×10^{5} same	3.6×10^{5} same
(6) $N(^4S)+O+M \rightarrow NO+M$	1.6×10^{7} 1.6×10^{15}	6×10^{7} 3×10^{14}	2×10^{8} same	9×10^{6} same	7×10^{6} same	2×10^{7} same
(12) $N(^4S)+O_3 \rightarrow NO+O_2$†	8×10^{3} 3×10^{3}	7×10^{4} 2×10^{4}	9×10^{5} 5×10^{5}	1.7×10^{5} 1.7×10^{5}	5×10^{5} 5×10^{4}	2×10^{6} 2×10^{5}
(13) $N+O \rightarrow NO+h\nu$	2.5×10^{7} 2.5×10^{15}	5×10^{7} 3×10^{14}	8×10^{7} same	2×10^{6} same	5×10^{5} same	5×10^{5} same
(15) $N+O_2 \rightarrow 2NO$	4×10^{6} 4×10^{3}	1.7×10^{7} 5.1×10^{4}	3.5×10^{7} 5.5×10^{5}	6.7×10^{7} 4.8×10^{6}	1.7×10^{8} 3.5×10^{7}	6.7×10^{8} 3.3×10^{8}
(2) $N+NO \rightarrow N_2+O$	4×10^{3} 3.3×10^{4}	2.5×10^{3} 2.9×10^{3}	6.6×10^{2} same	1.3×10^{3} same	2.6×10^{3} same	5.7×10^{3} same
(18) $N+NO_2 \rightarrow N_2+O_2$	8.3×10^{5} 8.3×10^{2}	3.3×10^{6} 1.0×10^{4}	7.1×10^{6} 1.1×10^{5}	1.4×10^{7} 9.5×10^{5}	3.3×10^{7} 7.0×10^{6}	$>6.7\times10^{7}$ $>6.7\times10^{7}$
(19) $N+NO_2 \rightarrow N_2O+O$	8.3×10^{7} 8.3×10^{4}	3.3×10^{8} 1.0×10^{6}	7.1×10^{8} 1.1×10^{7}	1.4×10^{9} 9.5×10^{7}	3.3×10^{9} 7.0×10^{8}	$>6.7\times10^{9}$ $>6.7\times10^{9}$
(20) $N+N+M \rightarrow N_2+M$	1.0×10^{12} -	7.7×10^{12} -	5.1×10^{12} -	6.0×10^{12} -	9.9×10^{12} 3.5×10^{15}	2.0×10^{13} 7×10^{14}

Table 9.4 Lifetime of $N(^4S)$ under various reactions.

* Reaction (1) is strongly temperature dependent.

† Reaction (12) is strongly temperature dependent. Also Shimazaki & Laird's $[O_3]$ would reduce the lifetime be a factor of about 10 for reaction (12).

Reaction	Lifetime (seconds)					
	65 km	70 km	75 km	80 km	85 km	90 km
$N(^2D)+O_2 \rightarrow NO+O$	2.3×10^{-4} same	4.6×10^{-4} same	9.8×10^{-4} same	2.1×10^{-3} same	5.1×10^{-3} same	1.25×10^{-3} same

Table 9.5 Lifetime of $N(^2D)$

exclusive primary photolytic process throughout the wavelength range 2300-1800 Å. Shimazaki and Laird (1972) obtained their results before this paper was published, and assumed the photolysis reaction was $N_2O + h\nu \rightarrow N + NO$. Thus to assess the possible importance of N_2O photolysis as a source of NO a photolysis rate of 1% that used by Shimazaki and Laird will be used. From the N_2O concentrations of table 4.5 of Turco and Sechrist (1970) the production rate of nitric oxide from this source can be found. It will be shown shortly that the formation of NO_2 is unimportant in discussing daytime nitric oxide concentrations. Thus to estimate the importance of N_2O assume photochemical equilibrium between reactions 1, 2, 4 and 11. The photochemical equations for N and NO (assuming no transport of NO) will be:

$$\frac{d[NO]}{dt} = 0 = J_{11}[N_2O] + k_1[O_2][N] - k_2[N][NO] - J_4[NO]$$

$$\frac{d[N]}{dt} = 0 = J_{11}[N_2O] - k_1[O_2][N] - k_2[N][NO] + J_4[NO]$$

The solution for NO is:

$$[NO] = \left(\frac{k_1 J_{11}[O_2]}{k_2 J_4}[N_2O]\right)^{1/2}$$

This value is shown in table 9.6 under the heading "maximum [NO]". Also shown in table 9.6 are the measured nitric oxide concentrations of Meira (1971).

Height (km)	maximum [NO]	[NO] (Meira)
65	1.2×10^7 (cm^{-3})	
70	5.2×10^6	7×10^7 (cm^{-3})
75	2.0×10^6	4.5×10^7
80	8.7×10^5	3.5×10^7
85	2.8×10^5	1.2×10^7
90	1.1×10^5	2.7×10^7

Table 9.6 Production of NO from N_2O

From the table, if the N_2O concentrations of Turco and Sechrist (op. cit.) are realistic, N_2O is not an important source of nitric oxide in the D-region. It will be neglected in the present model.

9.3.2 Nitrogen Dioxide in the Mesosphere

In the daytime any nitrogen dioxide (which is formed from NO) will be rapidly reconverted to NO (lifetime $\lesssim$ 2 minutes, table 9.3). The loss of odd nitrogen to N_2 via $N+NO_2 \rightarrow N_2+O_2$ can be neglected, since the lifetime of NO_2 under this reaction is about 100 years.

The production rate of NO_2 from NO will be

$$\{k_7[O][M] + k_9[O_3] + k_{14}[O]\}[NO]$$

The rate at which NO_2 returns to NO will be

$$\{k_8[O] + J_{10}\}[NO_2]$$

Thus under photochemical equilibrium (a reasonable assumption since the lifetime of NO_2 is < 200 secs) between NO and NO_2:

$$\frac{[NO_2]}{[NO\ ]} = \frac{k_7[O] + k_9[O_3] + k_{14}[O]}{k_8[O] + J_{10}}$$

This leads to table 9.7.

Height(km)	65	70	75	80	85	90
$\frac{[NO_2]}{[NO]}$	$2x10^{-4}$	$4x10^{-5}$	$2x10^{-5}$	$2x10^{-5}$	$1x10^{-5}$	$1x10^{-5}$

Table 9.7 Relative concentrations of NO_2 and NO (daytime)

Thus NO_2 is unimportant to the daytime odd nitrogen chemistry between 65 and 90 km.

At low heights at night the situation is somewhat different, since NO_2 is formed from NO with a time constant of about one day, and the time constant to get from NO_2 back to NO again is about a year. Thus appreciable amounts of NO_2 will exist in the lower mesosphere at night. However, this will not be important to the daytime electron density since the NO_2 will rapidly reconvert to NO when the sun comes up, and any vertical transport which occurs during the night will shift the same amount of odd nitrogen regardless of whether it is as NO or NO_2.

9.3.3 Atomic Nitrogen in the Mesosphere

Suppose there is no transport of atomic nitrogen into the mesosphere. Then the only source of nitric oxide will be atomic nitrogen from the photolysis of N_2 (reaction 5). To estimate the importance of N_2 photolysis as a source of nitric oxide consider photochemical equilibrium between reactions 1, 2, 4 and 5. This will give

$$\frac{d[NO]}{dt} = 0 = (-k_2[NO] + k_1[O_2])[N] - J_4[NO]$$

$$\frac{d[N]}{dt} = 0 = (-k_2[NO] - k_1[O_2])[N] + J_4[NO] + 2J_5[N_2]$$

The solution to these two equations is:

$$[NO] = \frac{-b+a}{2k_2 J_4}$$

where $b = k_2 J_5 [N_2]$

$$a = (k_2^2 J_5^2 [N_2]^2 + 4k_1 k_2 J_4 J_5 [N_2][O_2])^{\frac{1}{2}}$$

These nitric oxide concentrations are given in table 9.8 under the heading "[NO] from nitrogen photolysis". The NO concentrations measured by Meira (1971) are also given.

Thus it can be seen that the photolysis of N_2 is an unimportant source of odd nitrogen below 90 km. This means that odd nitrogen must be transported into the region to maintain the observed nitric oxide concentrations.

Above 90 km atomic nitrogen is produced in important quantities from N_2 by a number of processes, such as photolysis, the splitting of the N_2 molecule by fast electrons, and reactions involving various positive ions (figure 1, Strobel 1971).

Height(km)	[NO] from nitrogen photolysis	[NO] (Meira)
65	$6x10^{-49}$ (cm^{-3})	
70	$4.9x10^{-19}$	$7x10^{7}$
75	$5.4x10^{-5}$	$4.5x10^{7}$
80	$3.4x10^{1}$	$3.5x10^{7}$
85	$7.9x10^{4}$	$1.2x10^{7}$
90	$2.1x10^{5}$	$2.7x10^{7}$

Table 9.8 Production of nitric oxide from N_2

This is the reason that the present study extends only up to 90 km, since a treatment of the production processes would add increased complexity.

From the list of reactions it can be seen that atomic nitrogen may exist in both the ^4S and ^2D states. The production rate of $N(^2D)$ via reactions (3) and (3a) is $0.75\ J_3[NO]$. (3a is much faster than 3 which is the rate determining step.) The loss rate of $N(^2D)$ is $k_{21}[N(^2D)][O_2]$. Thus photochemical equilibrium between $N(^2D)$ and NO (this is valid since the lifetime of $N(^2D)$ is only a fraction of a second, table 10.4) yields

$$\frac{[N(^2D)]}{[NO]} = \frac{0.75\ J_3}{k_{21}[O_2]}$$

This leads to table 9.9.

Height (km)	65	70	75	80	85	90
$\frac{[N(^2D)]}{[NO]}$	2.1×10^{-14}	3.8×10^{-12}	7.4×10^{-11}	4.4×10^{-10}	1.7×10^{-9}	5.1×10^{-9}

Table 9.9 Relative concentrations of $N(^2D)$ and NO.

Thus, since the only important reactions involving $N(^2D)$ are conversion from and reconversion to NO (reactions 3 and 22), $N(^2D)$ is unimportant to the odd nitrogen chemistry between 65 and 85 km.

9.3.4 The Introduction of Vertical Motion

Consider a parcel of air as it subsides in the atmosphere with velocity $\underset{\sim}{v}$. The concentration within the parcel of a constituent N_i will obey:

$$\frac{dN_i}{dt} = \frac{\partial N_i}{\partial t} + \underset{\sim}{v}\cdot\nabla N_i \tag{9.7}$$

Now $$\frac{\partial N_i}{\partial t} = P_i - L_i - \nabla\cdot(N_i\underset{\sim}{v}) \tag{9.8}$$

$$= P_i - L_i - (\nabla N_i)\cdot\underset{\sim}{v} - N_i(\nabla\cdot\underset{\sim}{v}) \tag{9.9}$$

(9.9),(9.7) $\rightarrow$ $$\frac{dN_i}{dt} = P_i - L_i - N_i\nabla\cdot\underset{\sim}{v} \tag{9.10}$$

Now consider the total number of atmospheric particles per unit volume, N. Assume this follows:

$$N = N_0\, e^{-(\frac{z-z_0}{H})} \tag{9.11}$$

where H is the scale height, z is height and N_0 is the particle concentration at height z_0.

Assume a vertical velocity w which does not vary with height, that is $\frac{\partial w}{\partial z} = 0$.

Also, assume that $\frac{\partial N}{\partial t} = 0$, $\frac{\partial N}{\partial x} = 0$, $\frac{\partial N}{\partial y} = 0$, $P = L = 0$.

Then since $\frac{\partial N}{\partial t} = P - L - \nabla\cdot(N\underset{\sim}{v})$

$$\nabla\cdot(N\underset{\sim}{v}) = 0 \qquad (9.12)$$

i.e. $N\nabla_h\cdot\underset{\sim}{v} + w\frac{\partial N}{\partial z} = 0$

(where $\nabla_h \equiv \hat{i}_x \frac{\partial}{\partial x} + \hat{i}_y \frac{\partial}{\partial y}$)

But by (9.11) $\frac{\partial N}{\partial z} = -\frac{N}{H}$

Thus $N\nabla_h\cdot\underset{\sim}{v} - \frac{wN}{H} = 0$

$$\nabla_h\cdot\underset{\sim}{v} = \frac{w}{H} \qquad (9.13)$$

Using (9.13) in (9.10)

$$\boxed{\frac{dN_i}{dt} = P_i - L_i - \frac{N_i w}{H}} \qquad (9.14)$$

9.3.5 Production and Loss Terms

From the lifetimes in tables 9.2 to 9.5 and the discussion following them, the important reactions in the 65 km to 95 km region are:

(2) $N(^4S) + NO \rightarrow N_2 + O$

(1) $N(^4S) + O_2 \rightarrow NO + O$

(4) $NO + h\nu\,(\lambda=1750\text{-}1900\mathring{A}) \rightarrow N(^4S) + O$

From table 9.4 the photochemical lifetime of $N(^4S)$ in this region is in the range 6 minutes to about 1½ hours. This can be compared to the lifetime of NO under transport processes (a rough estimate is $\frac{H}{w}$ where H is the scale height, Whitten & Popoff (1971) P137) of about 7 days for a downward velocity of 1 cm/sec. Thus it is reasonable to assume that $N(^4S)$ is in chemical equilibrium with NO and O_2.

i.e. $$\frac{\partial [N]}{\partial t} = (-k_1[O_2] - k_2[NO])[N] + J_4[NO] = 0$$

$$[N] = \frac{J_4}{k_1[O_2] + k_2[NO]}\,[NO] \qquad (9.15)$$

Applying (9.14) to nitric oxide gives

$$\frac{d[NO]}{dt} = k_1[N][O_2] - (J_4 + k_2[N])[NO] - \frac{w}{H}[NO] = 0$$

Substituting for [N] this gives

$$\boxed{\frac{d[NO]}{dt} = -\frac{2k_2 J_4}{k_1[O_2] + k_2[NO]}\,[NO]^2 - \frac{w}{H}\,[NO]} \qquad (9.16)$$

N.B. Equation (9.16) gives the rate of change of nitric oxide concentration within a parcel of air which is moving with vertical velocity w, not the rate of change at a fixed height.

9.4 THE SOLUTION OF THE NITRIC OXIDE EQUATION

To use equation 9.16 to predict day to day variability in nitric oxide concentrations an initial nitric oxide versus height profile was specified. The equation was then solved numerically for times of one up to ten days, and at heights from 66.5 to 86.5 km at 5 km intervals. Values for a given height were not calculated if the air parcel there at the time of interest would have been above 90 km at t = 0 days. The difference between the initial profile, and the solution after x days had elapsed indicated the variability due to x days of vertical motion.

A Runge-Kutta integration procedure was used. It was found that for vertical velocities w = 0, -1, -2 cm a time step of 0.25 days was sufficiently small for convergence.

The photochemical lifetime of nitric oxide (the time taken for the concentration to decay by a factor of e) was found from the w = 0 solution. This is shown in figure 9.3. A value for J_4 of one-third that given by Strobel (1971) for solar zenight angle of 60° was used, since photo-dissociation will only occur during daylight and also the solar zenith angle is greater than 60° for much of the day in winter. For molecular oxygen concentrations CIRA (1965) with $\frac{n(O_2)}{n_T} = 0.210$ below 80 km was used. Temperature is also from CIRA (1965). Curve b of figure 1 in Strobel (1972b) was used as an initial nitric oxide profile.

9.5 ELECTRON LOSS RATES

It was stated earlier in this chapter that loss rates for electrons in the D-region cannot yet be satisfactorily calculated from theory because the positive ion chemistry is poorly understood. The usual approach (Sechrist 1972a) has involved "effective recombination coefficients" as defined below. The following equation is often used to describe the ionization and loss processes (Whitten and Poppoff, 1971)

$$\frac{dN_e}{dt} = \frac{P}{1+\lambda} - (\alpha_d+\lambda\alpha_i)N_e^2 \qquad (9.17)$$

where P = ion-pair production rate

λ = number density ratio of negative ions to electrons

α_d = electron-ion recombination coefficient

α_i = ion-ion recombination coefficient.

When $\lambda\alpha_i << \alpha_d$, and $\frac{dN_e}{dt} = 0$

$$P = (1+\lambda)\alpha_D N_e^2$$

$$\text{i.e. } P = \alpha_{eff} N_e^2 \qquad (9.18)$$

where α_{eff} is the effective recombination coefficient.

Thus if α_{eff} could be measured in some way, (9.18) could be used to predict the electron densities resulting from a given ionization production rate.

One method which has been used is to measure the electron density by means of rockets sent up at intervals during a solar eclipse (Sechrist 1972b). It is assumed that $P = 0$, so that

$$\frac{\Delta N_e}{\Delta t} = -\alpha_{eff} N_e^2 \qquad (9.19)$$

This method has been used by Belrose et al. (1972a) and Mechtly et al. (1972b).

α_{eff} can also be calculated directly from an assumed production rate profile, and a measured electron density profile.

As stated earlier in this chapter, the major source of ionization in the mesosphere between 70 and 85 km is thought to be photoionization of nitric oxide by solar Lyman-α radiation. However, mass spectrometer measurements (Narcisi and Bailey, 1965) have shown that water cluster ions such as H_3O^+ and $H_5O_2^+$ are in greater concentration than NO^+ below about 82 km. The mechanism leading to the formation of these ions is not fully understood (Ferguson, 1971). However, the hydrated ions have considerably larger dissociative recombination coefficients (α_d) than has NO^+ (Aiken, 1972). Haug and Landmark (1970) have discussed the case of an atmosphere with two positive ions X_1^+ and X_2^+, which might tentatively be identified as NO^+ and a positive hydrated ion. In their model X_2^+ is formed from X_1^+ and also has a much faster recombination rate than X_1^+. They show that if the rate determining step is the conversion of X_1^+ to X_2^+ then an equation of type (9.18) is no longer followed. Instead the relation is:

$$P = (1+\lambda)\, BN_e \qquad (9.20)$$

where the rate of formation of X_2^+ from X_1^+ is given by $B[X_1]^+$.

In eclipse studies Mechtly et al. (1972b) found that their results appeared to be most consistent with (9.20) below a certain height Z_0 (82.5 km on 7 March 1970, 86.8 km on 12 Nov. 1966) where there was a steep increase in electron density. Above this height a recombination-like law of form (9.18) appeared more consistent. Landmark et al. (1970) also came to the conclusion that (9.20) was the best relation at 80 km from the solar eclipse of 20 May 1966.

Folkestead et al. (1972) took a different approach. They calculated $\frac{P}{1+\lambda}$ at times for which they had electron density data from ground-based radio measurements or rocket measurements. By considering the relationship between $\ell n(N_e)$ and $\ell n(\frac{P}{1+\lambda})$ they found that for altitudes of 74 and 80 km at mid-latitudes the observations were better described by a linear relation like (9.20) than a squared relation of form (9.18).

Below about 75 km the ratio λ of negative ions to electrons becomes greater than 1, according to calculations based on negative ion models (Thomas 1971). Thus at these heights attachment of electrons to neutrals may be the dominant loss process, which will also lead to a linear dependence of electron density on production rate.

In the following work it will be assumed that electron loss is by a linear type process of form (9.20). An assumed nitric oxide profile and an average winter electron density profile will be used to calculate a height profile for the coefficient $B(1+\lambda)$. This will be assumed to stay constant at a given height, and it will be used to predict electron densities resulting from the changed nitric oxide densities after vertical motion.

The assumption of a constant value for $B(1+\lambda)$ might not be very good, as B may well depend on concentration of constituents such as H_2O (Sechrist 1970) which might also be affected by the motion. Furthermore, it may be rather sensitive to temperature through the temperature dependence of the reaction rates of the hydrated positive ions (Reid 1970). Finally it is not definitely proven that this model is appropriate. However, it represents the best estimate that can be made at present.

9.6 THE RESULTS OF THE MODEL

For an initial electron density profile, the average winter electron density measured over Birdling's Flat by the differential absorption experiment in 1973 was used.

The choice of an initial nitric oxide profile was more difficult. The best measurements to date are those of Meira (1971), taken by rocket of emission by NO in the dayglow. However, Strobel (1972b) pointed out that these measurements are not very sensitive to NO in the mesosphere. Thus in the present work two possible initial profiles were considered, one being the profile obtained by Meira from rocket 14.390, and the other figure 1, curve b of Strobel (1972b) which was based on a theoretical model with eddy diffusion.

The results of running the model are shown in figures 9.4 and 9.5. The descriptions model a and model b mean:

Model a: Nitric oxide initial density from Meira (1971), flight 14.390. Temperature and scale height from CIRA 1965. Molecular oxygen density from CIRA 1965. Photo-ionization rate J4 one third of that from Strobel (1971).

Model b: Initial nitric oxide density from Strobel (1972b), figure 1, curve b. Other parameters as for model a.

The model was also run for the same set of parameters as model b, except for an increase of 40°C in temperature. The results for this (model c) after four days, together with model b after four days are shown in figure 9.6.

It was shown previously that $N(^4S)$ can be considered to be in photochemical equilibrium with NO and O_2. One possible effect of a sudden change in temperature would be a change in this equilibrium, using some of the nitrogen atoms to produce nitric oxide. However, the ratio $\frac{[N]}{[NO]}$ as given by equation 9.15 is less than 5×10^{-3} for all heights from 66.5 to 90 km, so the temperature variation would cause only an insignificant change in nitric oxide concentration through this effect. The other possibility is that a temperature change could affect the lifetime of nitric oxide through changes in the rate coefficient of reaction 2. This effect is shown in figure 9.6. For a temperature increase of 40°C this effect is small at most heights compared to the direct effects of the transport.

9.7 COMPARISON WITH OBSERVATIONS

9.7.1 Birdling's Flat Differential Absorption Electron Densities, 69 to 84 km

From the differential absorption observations at Birdling'S Flat (section 7.3.2) the electron density from 69 to 84 kilometers in the winter and spring can increase by a factor of up to 2.5 over four days. (That is a fluctuation with eight day quasi-period.) This is about the size of the

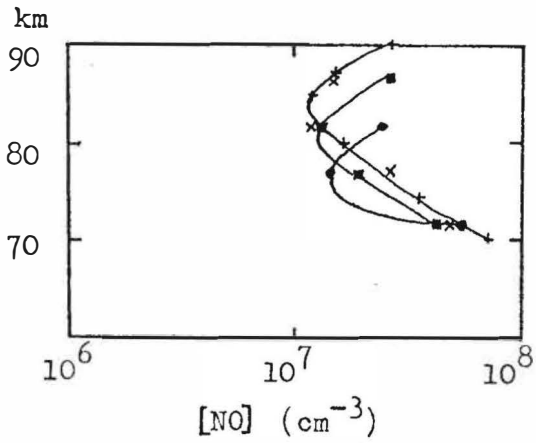

Model a, w= -1.0 cm/sec

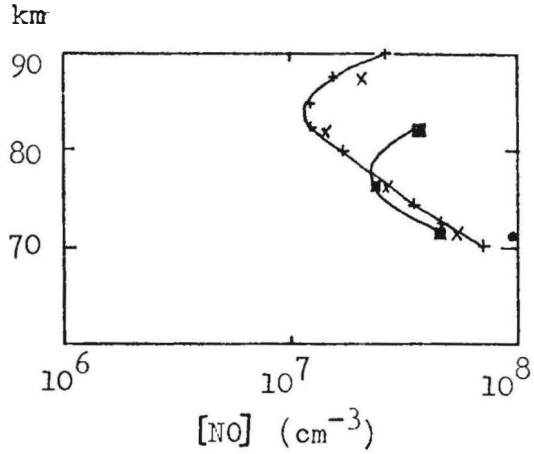

Model a, w= -2.0 cm/sec

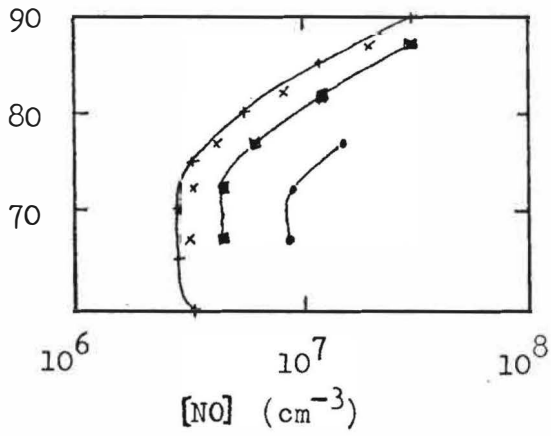

Model b, w= -1.0 cm/sec

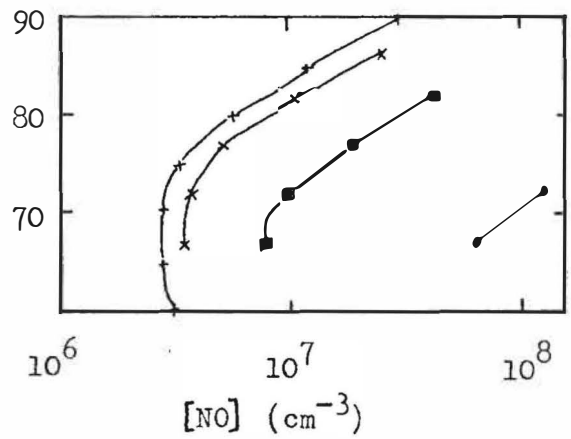

Model b, w=-2.0 cm/sec

KEY

\+ 0 days

× 1 day

■ 4 days

• 10 days

Fig 9.4: The effect of 1, 4, and 10 days of vertical motion on the nitric oxide profile.

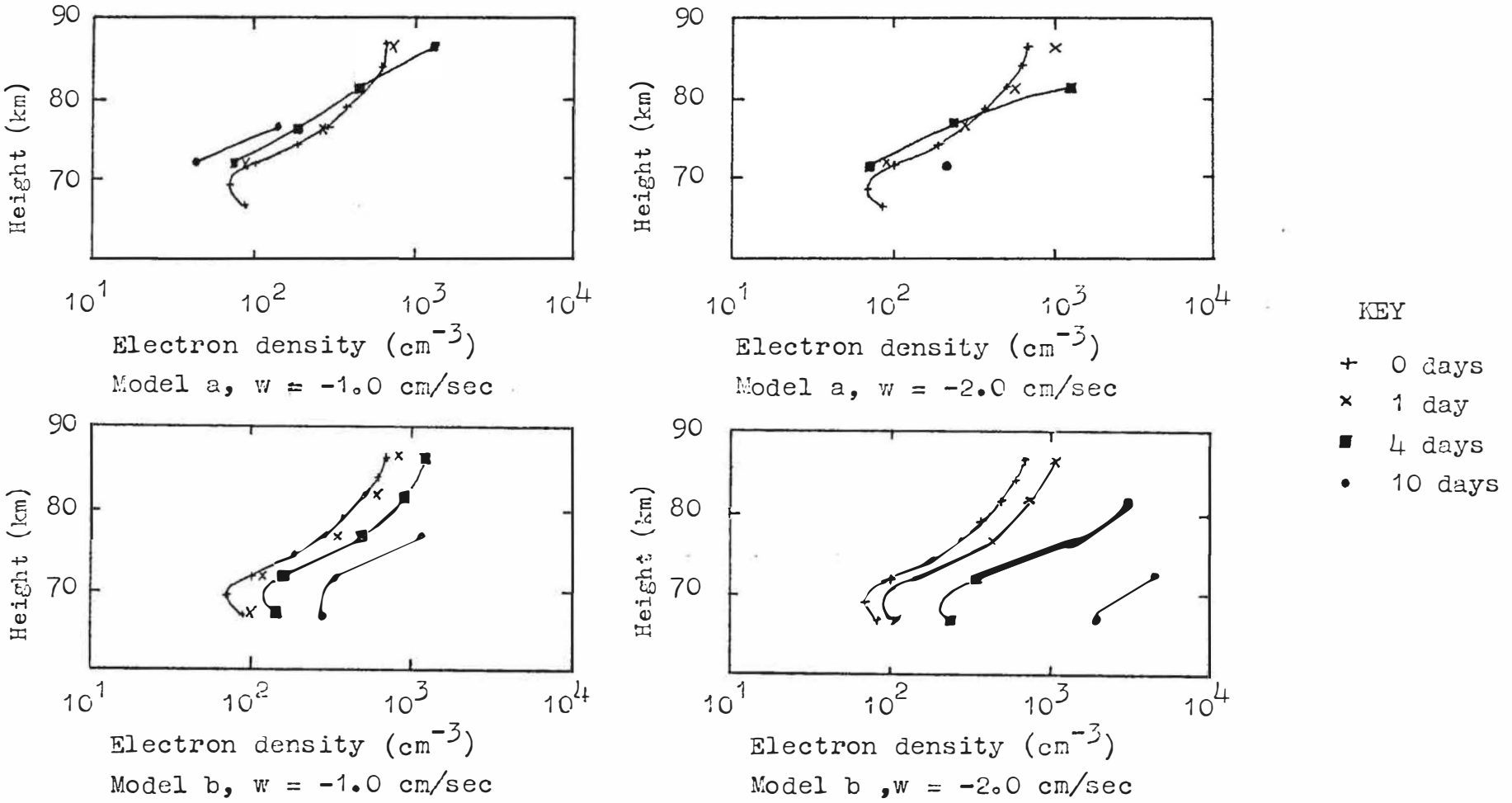

Fig 9.5: The effect of 1, 4, and 10 days of vertical motion on the electron density.

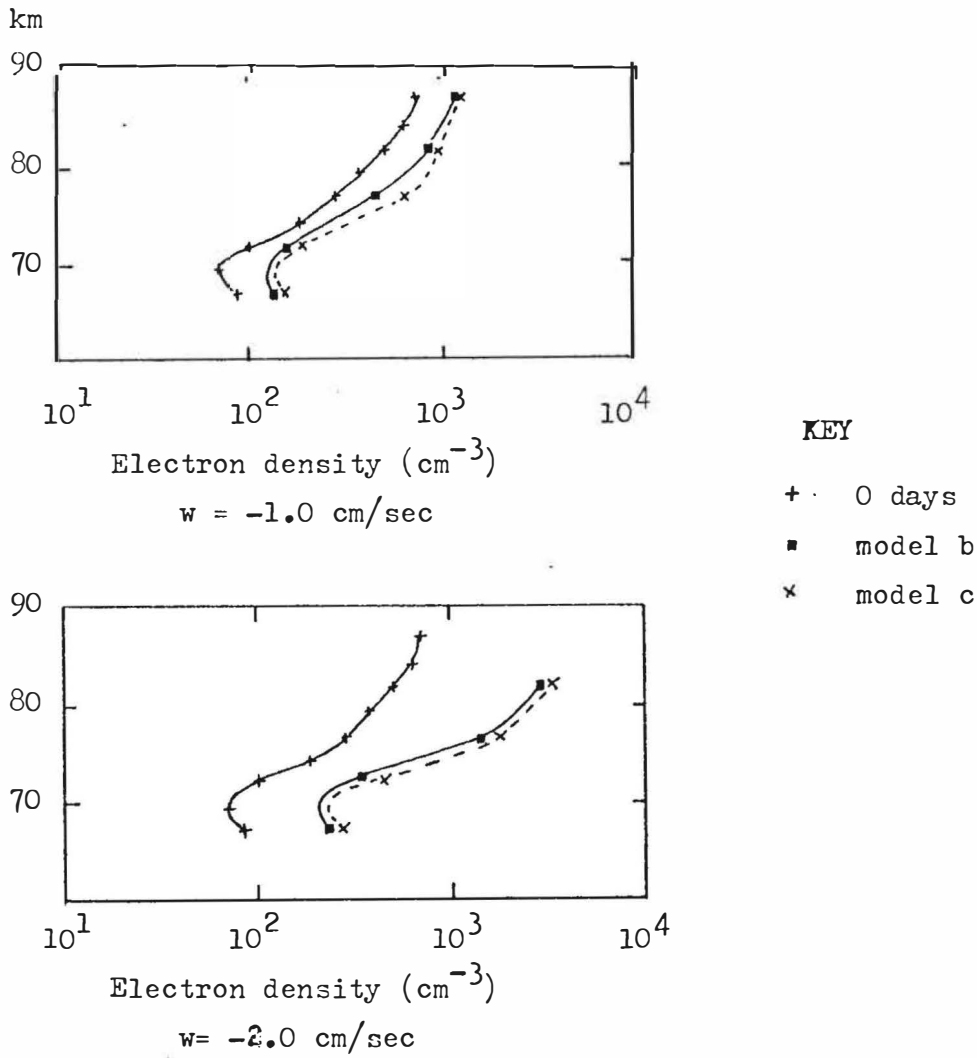

Fig 9.6: Effects of different temperature- models b and c after 4 days.

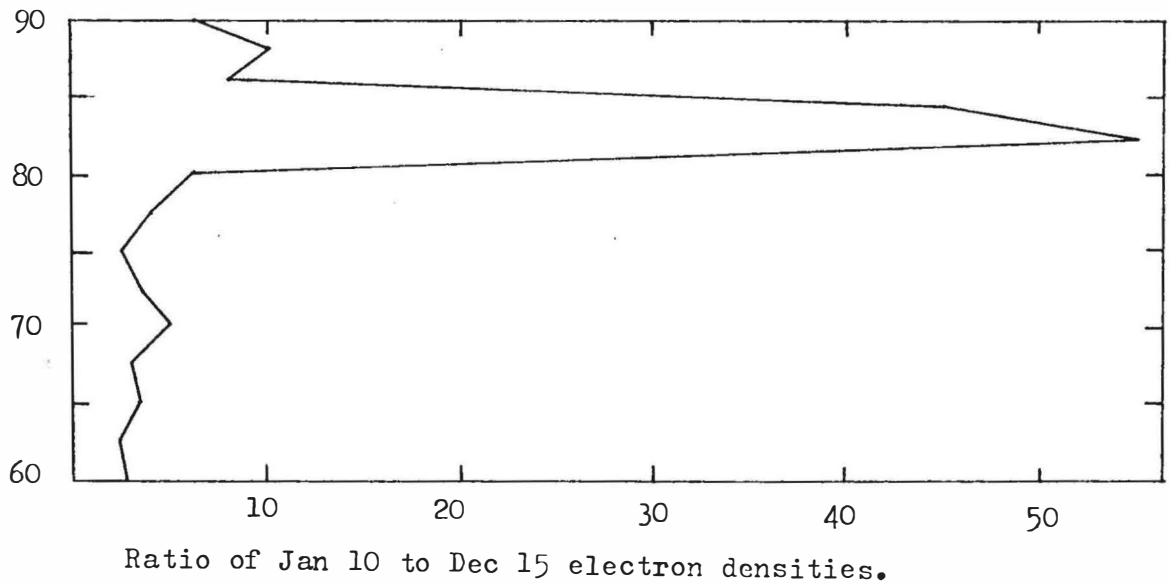

Fig 9.7: Electron density ratios.

electron density increase predicted by model b with a downward velocity of 2 cm/sec, which is at the upper limit of velocities expected in the D-region.

As is discussed in section 7.3.2 it is not possible to estimate the electron density variation for shorter time scales from the experimental data.

9.7.2 Rocket Measurements of Electron Densities

Figure 9.7 shows the ratio of electron densities for December 15th, 1965 (a day which showed "normal" radio absorption on 3.0 MHz) and January 10th, 1966 (which showed high absorption on 3.0 MHz) (Mechtly and Shirke, 1968). The solar zenith angle was 60^{o} in both cases.

From figure 9.5 the increase by a factor of about three in the 65 to 80 km electron densities between the two measurements (which were separated by 25 days) could be caused by downward motion of 1 to 2 cm/sec for a few days before January 10th, carrying down nitric oxide. However, nitric oxide transport cannot account for the increase by a factor of about 50 in the electron density which is localized within about 3 km centered about 82 km.

An examination of the two electron density profiles shows that the large ratio at 82 km is due to a sharp increase in the January 10th electron density (by about a factor of ten over about 1 kilometer) at this height. The December 15 density also shows a sharp increase but not until about 85 km. This sharp increase seems to be a characteristic of most rocket electron density measurements (e.g. see Sechrist 1972b). It has been suggested that it is due to the abrupt decrease in the relative abundance of hydrated positive ions above this

height seen by Narcisi and Bailey (1965), since as was stated earlier the hydrated ions have much larger recombination coefficients than NO^+. A change in the height at which the abrupt decrease of hydrated positive ions occurs (due perhaps to temperature dhanges and resulting effects on reaction rates, or transport of constituents important in the reactions) is a possible cause of the large electron density ratio at 82 km of fig. 9.7. (Geller and Sechrist (1971) decided that this was the most likely cause.)

If this is true, then the discussion on electron loss rates would suggest that above 85 km the electron density is proportional to the square root of the nitric oxide concentration (equation 9.18). Thus the increase of about eight times in the 86 to 90 km electron densities would require a nitric oxide concentration increase of about sixty times. Whether such increases are feasible is not apparent from the model, since at 86 km and above varying production of odd nitrogen above 90 km will be very important as well as the transport processes.

9.7.3 The Winter Anomaly in Ionospheric Absorption

The so called "winter anomaly" in ionospheric absorption at mid latitudes can be summed up by three characteristics (Schwentek 1971). These are that if high frequency radiowave absorption values are adjusted to be characteristic of a constant solar zenith angle ($\cos \chi = 0.1$)

(i) On a few days the absorption is as small as in summer.

(ii) There are a considerable number of days when the absorption follows a regular trend, increasing from the end of September to the winter solstice, then decreasing until the

end of March. (Northern hemisphere). Schwentek terms this the "normal" winter anomaly.

(iii) There is a greater number of groups of days (ranging from about three days to 20 or more days) when the absorption is very high. Schwentek calls this the "anomalous" winter anomaly.

Studies of the absorption which occurs on various frequencies suggest that most of the anomalous absorption in case (iii) takes place in the region 80 to 100 km above the ground (Thomas, 1968) although increased ionization below 80 km may have some effect.

Measurements of absorption on 2.4 MHz at Birdling's Flat have shown the occurrence of the winter anomaly in absorption there (Thorpe 1970). Measurements taken by Thorpe in the winter of 1967 show fluctuations of up to 18 db in the 2.4 MHz absorption.

The ordinary mode absorption on 2.4 MHz was calculated from the predictions of the nitric oxide transport model, using the Sen-Wyller refractive index (Budden, 1965) to see what effect nitric oxide transport could have on ionospheric absorption.

(a) The "anomalous" winter anomaly

The ordinary mode absorption between 66.5 and 81.5 km for the 1973 winter average electron density profile used as a starting point for the model is 1.5 db. (This is the two-way absorption, for a wave going up through the region and returning back through it.) The absorption from the same height range for model b with four days of downward motion at

1.0 cm/sec is 2.5 db, while model b with four days of downward motion at 2.0 cm/sec gives rise to 6.8 db of attenuation between 66.5 and 81.5 km. However, four days of vertical transport at 2 cm/sec gives rise to higher electron densities than were observed in the Birdling's Flat measurements. Thus vertical transport of nitric oxide to below 81.5 km can be ruled out as a significant cause of the "anomalous" winter anomaly.

The 81.5 to 86.5 km two-way absorption at 2.4 MHz for the 1973 average winter profile is 0.5 db, while the 81.5 to 86.5 km absorption for model b after four days of downward motion at 1 cm/sec is 0.9 db.

To check the influence of the large increase around 82 km shown between the two Mechtly and Shirke profiles, (fig. 9.7), absorption due to these profiles was calculated between 80 and 86 km, and 86 and 90 km. The results are in table 9.10.

Height range (km)	Absorption (two-way, 2.4 MHz)		
	Dec 15,1965	Jan 10,1966	Difference
80 → 86	0.9 db	21.6 db	20.7 db
86 → 90	1.5 db	15.8 db	14.3 db

Table 9.10 2.4 MHz absorption for the Mechtly & Shirke profiles.

Thus both the height range 80-86 km (where it has been suggested that a change in electron loss rate led to the electron density increase) and the interval 86-90 km (where it is possible that a change in nitric oxide concentration led to

the increase) are important for the anomalous absorption on Jan 10th.

(b) The "normal" winter anomaly

In the summer mesosphere the net diabatic heating rate is positive (Murgatroyd, 1970). This suggests a net upward motion rather than a downward motion of the atmosphere, and Hesstvedt (1971) calculated a net upward flow at 45^{o}N ranging from about 1 cm/sec at 75 km until a changeover to downward motion occurs at about 90 km. Geisler and Dickinson (1968) suggested that the summer mesosphere is supplied with nitric oxide from the winter mesosphere - the nitric oxide transported down from the source region in winter being transported to the summer hemisphere by the meridional circulation below 70 km where the nitric oxide lifetime is long (figure 9.3).

It would seem likely that this is too simplified a picture - some of the nitric oxide in the 85 to 90 km region in summer is probably supplied by eddy mixing from the source region above 90 km. A further point is that the photolysis rate of NO by reaction (4), J4 will be higher in summer, so that the photochemical lifetime of nitric oxide will be less in summer than winter. Thus it is likely that the nitric oxide concentration in the mesosphere is lower in summer than in winter. From the calculations on absorption, the normal winter absorption below 90 km is about 4 db. However, from Schwentek (1971) the "normal" winter anomaly at 53^{o}N is about 10 db for 2.61 MHz (reduced to a solar zenith angle of 60^{o}). Thus it seems likely that the "normal" winter anomaly is due to a phenomenon occurring above 90 km, and this belief is strengthened by the fact that Schwentek says similar behaviour is seen on the higher frequencies of 6.09 and 27.6 MHz.

However measurements at Birdling's Flat, (Chapter 8, also Gregory and Manson 1969b) indicate that in some parts of the mesosphere the electron density is higher at mid-day in winter than at mid-day in summer. This is consistent with reduced nitric oxide concentrations in summer.

9.8 THE MERIDIONAL TRANSPORT OF NITRIC OXIDE

Manson (1971) has pointed out that meridional transport of nitric oxide could be important as well as vertical transport. He points out the observations of Zipf et al. (1970) of very high concentrations of nitric oxide in auroral arcs near 114 km. If the meridional component of the wind at 70-90 km is similar to that at 60 km (25 m/sec, Murgatroyd 1970) nitric oxide could be transported from auroral latitudes to above Christchurch in a day or so if the direction was favourable. Thus a combination of vertical and meridional motion is probably important in the transport of nitric oxide. In this connection, Rusch and Barth (1972) in spectrometer measurements of nitric oxide emission at twilight from the satellite OGO IV found a general increase in the nitric oxide emission rate from the equator to 60^{o} latitude in both winter and summer, but not in spring or autumn. They also found an enhancement at mid-latitudes from 65 to 90 km on April 6, 1968.

9.9 CONCLUSIONS

If the increase in electron density between 70 and 75 km in early August 1972 which was probably caused by energetic particle precipitation (Chapter 9) is excluded, the transport of nitric oxide could account for the increases in electron

density which took place over periods of four or more days above Birdling's Flat in the 1972 and 1973 winter-spring periods. This is provided the electron density is linearly proportional to the nitric oxide concentration, and the nitric oxide initial density and vertical velocity assumed are in fact typical of the D-region. This does not rule out changes in electron loss rate as a further contribution to this variation. The Birdling's Flat measurements over shorter time scales are too uncertain to come to any conclusion on the electron density variation from one day to the next.

To account for the large variation in electron density near 82 km found in the rocket measurements of Mechtly and Shirke it is necessary to assume a large variation in the electron loss rate near this height.

The large variations in high-frequency radio wave absorption which take place in winter are due to electron density increases above 80 km. Because the model does not take into account variations in nitric oxide production, which occur above 90 km, it is not certain whether changes in production and transport of nitric oxide can account for the winter anomaly in ionospheric absorption. However, it seems likely that the anomaly is due to a combination of the effects of variation in transport and production of nitric oxide, and variations in the electron loss rate.

The differences between summer and winter electron densities from 69 to 84 kilometers can be qualitatively explained in terms of the differences in transport of nitric oxide.

Meridional transport, as well as vertical transport, may be important to the nitric oxide density.

A full treatment of electron density variations in the mesosphere due to transport processes would involve a model which included eddy diffusion due to motions of time scales of a day or less (appendix C), the production of nitric oxide in the region above 90 km, both vertical and horizontal motion, and a theoretical treatment of the electron loss processes.

The development of such a model is probably impractical at present because

(i) There has been no reliable measurement of nitric oxide concentrations below about 85 km.

(ii) The photoionization rate of reaction (4) is uncertain because of the uncertainty in the 1750 to 1900 Å solar flux.

(iii) The present knowledge of synoptic scale motions in the mesosphere is extremely limited.

(iv) The latitudinal variation of nitric oxide concentration is unknown.

(v) The positive ion reaction scheme in the mesosphere, and hence the electron loss processes are not yet understood.

Points (i), (iii) and (v) probably represent the major problems still outstanding in understanding the mesosphere.

CHAPTER 10

CONCLUSIONS

The present uncertainty about the processes of reflection of high frequency radio waves in the D-region is not a serious difficulty in the calculation of electron densities from differential absorption and differential phase measurements for short pulsewidths (25 microseconds), as the experimental uncertainties are as great. These experimental uncertainties lead to difficulties in estimating the day to day changes in electron densities in the mesosphere, but large changes (of the order of 100%) do show up clearly, particularly for heights between about 70 and 80 kilometers.

The differential phase experiment, using the measurement of the complex correlation coefficient, gives electron densities which agree well with those of the differential absorption experiment at heights near 74 kilometers. However, the method is more prone to uncertainty than the differential absorption method. Thus the differential absorption method is the better one for routine measurements.

Energetic electron precipitation can lead to increases in electron density in the mid-latitude D-region. However, both the present experiments and a literature search lead to the conclusion that while stratospheric warmings are associated at times with increases in D-region electron density there is no clear proof of direct co-variation of stratospheric parameters and D-region electron densities at other times.

In future studies of D-region electron density it is felt that total absorption measurements on H.F. radio reflections from the E-region would be a valuable addition to differential absorption results. This would extend information on electron density variations to the 85-90 km region which would be valuable for particle precipitation studies. and could clarify the relationship of electron density variations in the lower D-region to the winter anomaly in ionospheric absorption.

The major result of the studies of the photochemistry and transport of nitric oxide in the mesosphere was the realization of how much is still unknown about this part of the atmosphere. The height distribution of nitric oxide, which is the main ionizable constituent, is still not properly known, and there are large gaps in the knowledge of the positive-ion chemistry and the electron loss processes. It is to be hoped that the coordinated series of rocket experiments at Wallops Island in June 1974 will lead to some illumination on these problems. The formulation of models to describe the variation in D-region electron densities is thus a rather uncertain task. However, it is felt that the conclusion that variations in nitric oxide concentrations alone do not account for all of the observed variation in electron density is valid.

APPENDIX A

ELECTROMAGNETIC THEORY

The W.K.B. Solution for a Slowly Varying Ionosphere

Consider a slowly varying, horizontally stratified ionosphere. Let the z axis be vertically upward, and the magnetic field of the earth be in the x-z plane at an angle θ to the z axis. Then it can be shown (Budden 1961) that in many cases there are four independent plane wave solutions to Maxwell's equations and the constitutive relations. These may be regarded as the upgoing ordinary, downgoing ordinary, upgoing extraordinary and downgoing extraordinary waves. (Levels where the independence breaks down are levels of reflection, or of coupling between modes). These W.K.B. solutions are as follows (Budden, op. cit., section 18.14): (for vertical incidence, time factor $e^{j\omega t}$ omitted)

Upgoing ordinary mode

$$E_x = -\{2(\rho_0^2-1)n_0\}^{-\frac{1}{2}}\exp\{-jk\int^z n_0 dz\} \qquad (A1)$$

Downgoing ordinary mode

$$E_x = -j\{2(\rho_0^2-1)n_0\}^{-\frac{1}{2}}\exp\{jk\int^z n_0 dz\} \qquad (A2)$$

Upgoing extraordinary mode

$$E_x = -j\rho_0\{2(\rho_0^2-1)n_X\}^{-\frac{1}{2}}\exp\{-jk\int^z n_X dz\} \qquad (A3)$$

Downgoing extraordinary mode

$$E_x = -\rho_0\{2(\rho_0^2-1)n_X\}^{-\frac{1}{2}}\exp\{jk\int^z n_X dz\} \quad (A4)$$

The other components of the electric and magnetic fields of the waves in the x and y directions are given by:

$$E_y = \rho E_x \quad (A5)$$

$$\mathcal{H}_X = \mp \rho n E_x \quad (A6)$$

$$\mathcal{H}_y = \pm n E_x \quad (A7)$$

where the upper sign is for a wave propagating upwards, and the lower sign is for a downwards wave.

$\rho = \rho_0, \rho_X$; $n = n_0, n_X$ for the ordinary and extraordinary waves respectively.

Here ρ = Wave polarization = $\frac{E_y}{E_x}$

n = Complex refractive index

$k = \frac{\omega}{c}$ where ω = angular frequency of wave

c = velocity of light in free space

$\underset{\sim}{E}$ = electric field of wave

$\underset{\sim}{\mathcal{H}} = Z_0 \underset{\sim}{H}$ where $\underset{\sim}{H}$ = magnetic intensity in wave

$Z_0 = (\frac{\mu_0}{\varepsilon_0})$ = characteristic impedance of free space

Also, $\rho_0 \rho_X = 1$ (Budden, 1965).

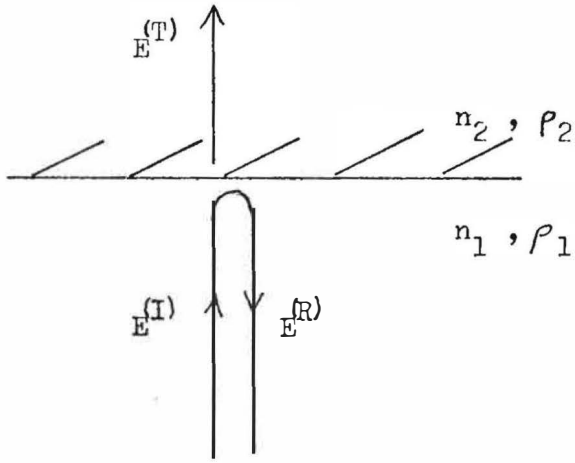

Fig A1: Partial reflection of a radio wave.

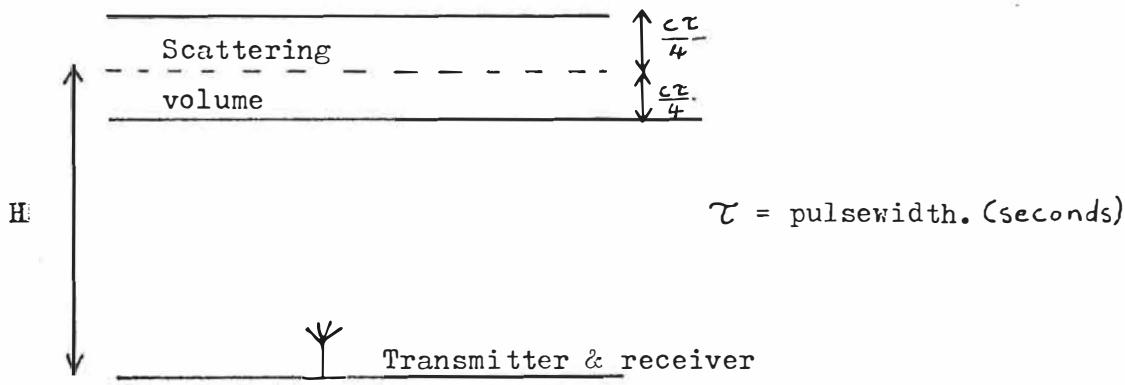

Fig A2: Volume scatter geometry.

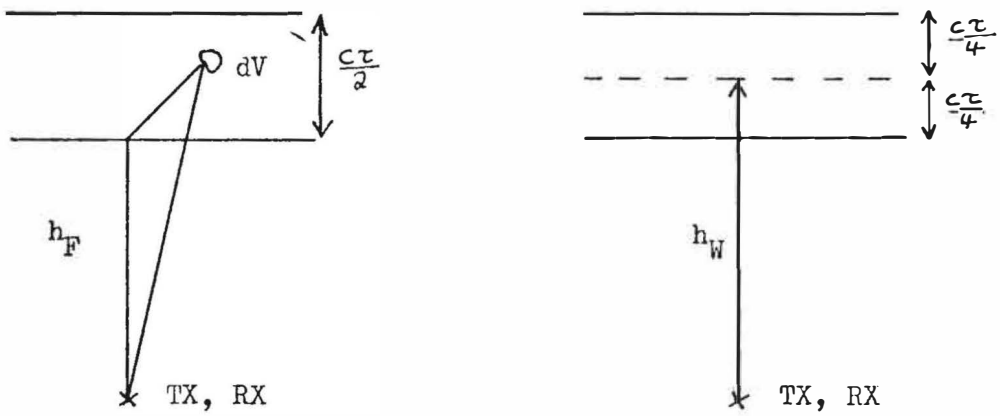

Flood's geometry

Geometry for equation A20.

Fig A3: The reference height in the volume scatter theory.

Reflection of a Plane Characteristic Wave at a Sharp Horizontal Boundary

Denote the two characteristic modes in the medium by subscripts a and b. Suppose a plane wave of mode a is incident on a sharp horizontal boundary from below. Then the tangential components of electric field intensity and magnetic field intensity will be continuous across the boundary (Jackson, 1962). The notation to be used is as in the previous section, and the incident, reflected and transmitted waves will be denoted by superscripts I, R and T. Subscripts 1 and 2 denote the medium below and above the boundary (Figure A1). Using equations (1) to (7), and neglecting common factors, the continuity of E_x, E_y, $\mathcal{H}_x$, $\mathcal{H}_y$ across the boundary gives rise to the following set of equations. (Remember that mode a only is incident.) ($E_a \equiv E_x$ in A1).

$$E_a^{(T)} + E_b^{(T)} - E_a^{(R)} - E_b^{(R)} - E_a^{(I)} = 0 \qquad \text{(A8)}$$

$$\rho_{a_2} E_a^{(T)} + \rho_{b_2} E_b^{(T)} - \rho_{a_1} E_a^{(R)} - \rho_{b_1} E_b^{(R)} - \rho_{a_1} E_a^{(I)} = 0 \qquad \text{(A9)}$$

$$-n_{a_2}\rho_{a_2} E_a^{(T)} - n_{b_2}\rho_{b_2} E_b^{(T)} - n_{a_1}\rho_{a_1} E_a^{(R)} - n_{b_1}\rho_{b_1} E_b^{(R)} + n_{a_1}\rho_{a_1} E_a^{(I)} = 0 \qquad \text{(A10)}$$

$$n_{a_2} E_a^{(T)} + n_{b_2} E_b^{(T)} + n_{a_1} E_a^{(R)} + n_{b_1} E_b^{(R)} - n_{a_1} E_a^{(I)} = 0 \qquad \text{(A11)}$$

These four equations were solved for typical electron density profiles and collision frequency profiles, using the Sen-Wyller theory for the refractive indices and polarizations.

Some of the results are given in table 2.2. It was found that for the region of interest (60-90 km) the coupling terms (those with subscript b in the equations) were less than the other terms by at least a factor of 100. Thus the coupling terms can be neglected and the following simplified system of equations used to obtain the reflection coefficients.

$$\text{(From A8)} \qquad E_a^{(T)} - E_a^{(R)} - E_a^{(I)} = 0 \tag{A12}$$

$$\text{(From A11)} \qquad n_{a_2} E_a^{(T)} + n_{a_1} E_a^{(R)} - n_{a_1} E_a^{(I)} = 0 \tag{A13}$$

$$\text{Thus} \qquad \frac{E_a^{(R)}}{E_a^{(I)}} = \frac{n_{a_1} - n_{a_2}}{n_{a_1} + n_{a_2}} \tag{A14}$$

$$\text{The incident wave is } \underset{\sim}{E}^{(I)} = E_a^{(I)} (\hat{i}_x + \rho_{a_1} \hat{i}_y) \tag{A15}$$

$$\text{The reflected wave is } \underset{\sim}{E}^{(R)} = E_a^{(R)} (\hat{i}_x + \rho_{a_1} \hat{i}_y) \tag{A16}$$

Thus the Fresnel reflection coefficient for mode a, which is the ratio of the reflected to the incident field, is:

$$R_a = \frac{n_{a_1} - n_{a_2}}{n_{a_1} + n_{a_2}} \tag{A17}$$

A Volume Scattering Model

Suppose that any reflection from a given irregularity satisfies the Fresnel conditions, so that equation (A17) holds. However, suppose that over the time of an experimental run reflections arise equally often from all heights within the scattering volume (figure A2). Assume that the difference in the group velcoity between the O and X waves is sufficiently small that they have a common scattering volume. For 25 μs

pulses this is reasonable below 85 km. Define the real and imaginary parts of the refractive index by

$$n = \mu + j\chi$$

Let $\kappa = -k\chi$.

Assume that the irregularities are small perturbations on a basic electron density which is constant throughout the volume, and that the Fresnel reflection coefficients R_X, R_O are constant through the scattering volume. Then the power received at the ground, averaged over the time of the experiment, divided by the power transmitted averaged over the same time will be (using A1 → A4)

$$\frac{\langle P_R \rangle}{\langle P_T \rangle} = \frac{1}{(2H)^2} \frac{1}{\frac{c\tau}{2}} \int_{-\frac{c\tau}{4}}^{\frac{c\tau}{4}} |R_{X,O}|^2 \, e^{-4\kappa_{X,O} z} \, dz$$

$$\times \text{ (absorption which occurs below H)}$$

where $\frac{1}{(2H)^2}$ is a geometrical factor to allow for a point source.

$$\text{i.e. } \frac{\langle P_R \rangle}{\langle P_T \rangle} = \frac{|R_{X,O}|^2}{c\tau\kappa_{X,O}} \left[\sinh(c\tau\kappa_{X,O})\right] \times \frac{1}{(2H)^2}$$

$$\times \text{ (absorption which occurs below H)} \qquad \text{(A18)}$$

Thus the "scattering cross-sections" in this case are

$$\boxed{\sigma_{X,O} = \frac{|R_{X,O}|^2}{c\tau\kappa_{X,O}} \sinh(c\tau\kappa_{X,O})} \qquad \text{(A19)}$$

and

$$\frac{\sigma_X}{\sigma_O} = \left|\frac{R_X}{R_O}\right|^2 \left(\frac{\sinh(c\tau\kappa_X)}{c\tau\kappa_X}\right) \left(\frac{c\tau\kappa_O}{\sinh(c\tau\kappa_O)}\right) \qquad \text{(A20)}$$

Flood's model for the partial reflection of radio waves from dielectric fluctuations gives (Flood's equation 14, Flood 1968)

$$\frac{\sigma_X}{\sigma_O} = \frac{\overline{\Delta\varepsilon(q_X)^2}}{\overline{\Delta\varepsilon(q_O)^2}} \frac{n_O{}^i}{n_X{}^i} \left\{\frac{1 - \exp[-(4\pi n_X{}^i/\lambda)c\tau]}{1 - \exp[-(4\pi n_o{}^i/\lambda)c\tau]}\right\} \qquad \text{(A21)}$$

To account for the different reference height (h_F as compared with h_W, figure A3), Flood's result must be multiplied by a factor of

$$\frac{\exp\left(\frac{4\pi n_X}{\lambda}\frac{c\tau}{2}\right)}{\exp\left(\frac{4\pi n_O}{\lambda}\frac{c\tau}{2}\right)}$$

which changes the final factor in A21 to

$$\frac{\sinh(\omega\tau n_X{}^i)}{\sinh(\omega\tau n_O{}^i)}$$

Also, if the dielectric fluctuations $\overline{|\Delta\varepsilon(q)|^2}$ are caused only by fluctuations in electron density and not in collision frequency, (Flood 1968)

$$\frac{\overline{\Delta\varepsilon(q_X)^2}}{\overline{\Delta\varepsilon(q_O)^2}} = \frac{y_X{}^2 \mathcal{L}^2_{3/2}(y_X) + \frac{25}{4}\mathcal{L}^2_{5/2}(y_X)}{y_O{}^2 \mathcal{L}^2_{3/2}(y_O) + \frac{25}{4}\mathcal{L}^2_{5/2}(y_O)} \qquad \text{(A22)}$$

This assumes the quasi-longitudinal approximation to the Sen-Wyller refractive indices (Sen & Wyller, 1960)

$$n^2 = 1 - \frac{\omega_0^2}{\omega\nu}\left\{y\,\mathcal{C}_{3/2}(y) - j\,\frac{5}{2}\,\mathcal{C}^2_{5/2}(y)\right\} \qquad (A23)$$

where ω_0^2 is the plasma frequency, ν the collision frequency and $y_0 = \frac{\omega+\omega_L}{\nu}$, $y_X = \frac{\omega-\omega_L}{\nu}$ for ω_L the gyrofrequency. $\mathcal{C}_{3/2}(y)$ and $\mathcal{C}_{5/2}(y)$ are the semi-conductor integrals (Hara, 1963). A23 can be differentiated with respect to N, the electron density, to give

$$2n\,\frac{\delta n}{\delta N} = -\frac{\omega_0^2}{N\omega\nu}\left\{y\,\mathcal{C}_{3/2}(y) + j\,\frac{5}{2}\,\mathcal{C}_{5/2}(y)\right\} \qquad (A24)$$

If it is assumed that $n_X, n_O \approx 1$, (17) can be written

$$R = -\frac{\delta n}{2}$$

Thus (25) and (24) give

$$\left|\frac{R_X}{R_O}\right|^2 = \frac{y_X^2\mathcal{C}^2_{3/2}(y_X) + \frac{25}{4}\,\mathcal{C}^2_{5/2}(y_X)}{y_O^2\mathcal{C}^2_{3/2}(y_O) + \frac{25}{4}\,\mathcal{C}^2_{5/2}(y_O)} = \frac{\overline{\Delta\varepsilon(q_X)^2}}{\overline{\Delta\varepsilon(q_O)^2}} \qquad (A26)$$

Using this in A21, and putting $\kappa = -\frac{\omega}{c}\,n^i$

$$\frac{\sigma_X}{\sigma_O} = \left|\frac{R_X}{R_O}\right|^2 \left\{\frac{\sinh(c\tau\kappa_X)}{(c\tau\kappa_X)}\right\}\left\{\frac{(c\tau\kappa_O)}{\sinh(c\tau\kappa_O)}\right\} \qquad (A27)$$

which is exactly the same as (A20).

Thus Flood's model leads to exactly the same result as is obtained from the extension to the simple Fresnel model.

It is clear from A20 that as the pulsewidth τ tends to zero, $\frac{\sigma_X}{\sigma_O} \to \left|\frac{R_X}{R_O}\right|^2$ which is the simple Fresnel expression used by most experimenters. This will also occur if the scattering irregularities occupy only a small height range within the scattering volume.

The Differential Absorption and Phase Theory

Assume that a radio wave undergoes a partial reflection at height h, and the reflection coefficients are $\mathcal{R}_X$, $\mathcal{R}_O$ for the extraordinary and ordinary components. Then using equations A1-A7 with a factor of $\frac{1}{2h}$ to allow for the fact that the transmitter is effectively a point source, the reflected extraordinary and ordinary components at the ground will be:

$$E_X = \frac{B\mathcal{R}_X}{4jh} \exp\{(-2jk\int_o^h n_X dz) + j\phi_X\} \tag{A28}$$

$$E_O = -\frac{B\mathcal{R}_O}{4jh} \exp\{(-2jk\int_0^h n_O dz) + j\phi_O\} \tag{A29}$$

where ϕ_O and ϕ_X are the initial phases of the O and X waves, which are transmitted with equal power represented by the constant B, and $n_O = n_X = 1$ at the ground, $\rho_O{}^2 = \rho_X{}^2 = -1$ at the ground.

Let

$$n_{X,O} = \mu_{X,O} + j\chi_{X,O}$$

and put

$$\kappa_{X,O} = -k\chi_{X,O}$$

$$\mathcal{R}_{X,O} = |\mathcal{R}_{X,O}|\exp(j\alpha_{X,O})$$

Then

$$E_O = \frac{B}{4h}|\mathcal{R}_O| \exp(-2\int_0^h \kappa_0 dz)\exp\{j(-2k\int_0^h \mu_0 dz + \alpha_O + \phi_O - \frac{\pi}{2})\} \tag{A30}$$

$$E_X = \frac{B}{4h}|\mathcal{R}_X| \exp(-2\int_0^h \kappa_X dz)\exp\{j(-2k\int_0^h \mu_X dz + \alpha_X + \phi_X - \frac{\pi}{2})\} \tag{A31}$$

The Complex Correlation Coefficient

This section assumes the same scattering model as that used earlier to obtain $\sigma_{X,O}$.

Suppose E_X, E_O are the ordinary and extraordinary component electric fields of a pulse scattered from the scattering volume centred at height h. The complex correlation coefficient is (von Biel et al., 1970)

$$\rho(h) = \frac{\langle E_X E_O^* \rangle}{(\langle |E_O|^2 \rangle \langle |E_X|^2 \rangle)^{\frac{1}{2}}} \tag{A32}$$

where < > denotes time averaging over the period for which the experiment is run. Then

$$E_X = -\frac{jB}{4h}\left[\sum_{scatt} R_X \exp(-2jkn_X z)\right]\exp\left(-2jk\int_0^h n_X dz + j\phi_X\right) \tag{A33}$$

$$E_O = +\frac{jB}{4h}\left[\sum_{scatt} R_O \exp(-2jkn_O z)\right]\exp\left(-2jk\int_0^h n_O dz + j\phi_O\right) \tag{A34}$$

(Using A28, A29, where $\sum_{scatt}$ means the sum from all of the Fresnel reflectors within the scattering volume at a given instant.)

Assuming that the sum over the scattering volume is statistically independent of the integral up to the reflecting height,

$$\langle E_X E_O^* \rangle = \left\langle \sum_{scatt} R_X R_O^* \exp(-2jk(n_X - n_O)z) \right\rangle \frac{B}{4h^2} \times \left\langle \exp\left\{-2jk\int_0^z (n_X - n_O)dz\right\}\right\rangle \exp\{j(\phi_X - \phi_O)\} \tag{A35}$$

If it is now assumed that over the averaging period reflections arise equally often from all heights within the scattering

volume,

$$\left\langle \sum_{\text{scatt}} R_X R_O^* \exp(-2jk(n_X-n_O)z) \right\rangle = \frac{R_X R_O^*}{\frac{c\tau}{2}} \int_{-\frac{c\tau}{4}}^{\frac{c\tau}{4}} \{\exp(-2jk(n_X-n_O)z\}dz$$

$$= R_X R_O^* \frac{\sin\left\{\frac{k(n_X-n_O)c\tau}{2}\right\}}{\left\{\frac{k(n_X-n_O)c\tau}{2}\right\}}$$

Thus

$$\langle E_X E_O^* \rangle = \frac{B}{4h^2} R_X R_O^* \frac{\sin\left\{\frac{k(n_X-n_O)c\tau}{2}\right\}}{\left\{\frac{k(n_X-n_O)c\tau}{2}\right\}} \times \left\langle \exp\{-2jk\int_0^h (n_X-n_O)dz\} \right\rangle e^{i(\phi_X-\phi_O)} \quad \text{(A36)}$$

Similarly,

$$\langle |E_X|^2 \rangle = \frac{B}{4h^2} |R_X|^2 \left[\frac{\sinh(c\tau\kappa_X)}{c\tau\kappa_X}\right] \langle \exp\{-4\int_0^h \kappa_X dz\} \rangle \quad \text{(A37)}$$

$$\langle |E_O|^2 \rangle = \frac{B}{4h^2} |R_O|^2 \left[\frac{\sinh(c\tau\kappa_O)}{c\tau\kappa_O}\right] \langle \exp\{-4\int_0^h \kappa_O dz\} \rangle \quad \text{(A38)}$$

If $\rho(h) = F(h) \exp(j\eta(h))$ (A39)

where $F(h)$, $\eta(h)$ are real, then

$$\eta(h) = \beta(h) - 2k\int_0^h (\mu_X-\mu_O)dz + (\phi_X-\phi_O) + \mathcal{E}(h) \quad \text{(A40)}$$

Here $R = |R|e^{j\alpha}$, $\beta = \alpha_X-\alpha_O$

and

$$\mathcal{E}(h) = \text{Arg}\left[\frac{\sin\left\{\frac{k(n_X-n_O)c\tau}{2}\right\}}{\frac{k(n_X-n_O)c\tau}{2}}\right] \quad \text{(A41)}$$

Epstein's Theory

Suppose the variable E satisfies the equation

$$\frac{d^2E}{dz^2} + k^2n^2E = 0 \qquad \text{(A42)}$$

where

$$n^2 = \varepsilon_1 + \frac{e^u}{(e^u+1)^2}\{(\varepsilon_2-\varepsilon_1)(e^u+1) + \varepsilon_3\} \qquad \text{(A43)}$$

(Here $u = \frac{z}{\sigma}$ and $\varepsilon_1, \varepsilon_2, \varepsilon_3$ and σ are constants chosen to fit a particular model.)

Epstein (1939) showed that (A42) is a transformation of the hypergeometric equation, and can be solved in terms of hypergeometric series. (A detailed description of the method is given in Budden, 1961).

But (A42) represents the passage of a vertically propagating electromagnetic wave through a horizontally stratified medium of refractive index n.

By considering the connection formulae between solutions to the hypergeometric equation for very large negative and very large positive values of $\xi = -e^{-u}$, Budden shows that the reflection coefficient referred to a level z is

$$\boxed{\mathcal{R} = \frac{(c-2)!(b-c)!}{(c-a-1)!(b-1)!(-c)!}\, e^{2ikn_1z_1}} \qquad \text{(A44)}$$

where n_1^2 is the value of n^2 by (A43) when $e^u \to 0$,

$$(c-1) = -2jk\sigma n_1$$

$$(a-b) = -2jk\sigma n_2$$

$$a+b-c = \pm(4k^2\sigma^2\varepsilon_3+1)^{\frac{1}{2}}$$

and n_2^2 is the value of n^2 by (A43) when $e^u \to \infty$.

(a) The Epstein "tanh" profile

If in (A43) ε_3 is put to zero,

$$n^2 = n_1^2 + \frac{e^u}{(e^u+1)}(n_2^2-n_1^2) \qquad (A45)$$

or $$n^2 = \tfrac{1}{2}(n_1^2+n_2^2) + \tfrac{1}{2}(n_2^2-n_1^2)\tanh(\frac{z}{2\sigma})$$

In this case, the reflection coefficient referred to the level z = 0 (the centre of the transition layer) is

$$\mathscr{R} = \frac{n_1-n_2}{n_1+n_2} \frac{(-2jk\sigma n_1)!}{(2jk\sigma n_1)!} \frac{[\{jk\sigma(n_2+n_1)\}!]}{[\{jk\sigma(n_2-n_1)\}!]} \qquad (A46)$$

(b) The Epstein "sech^2" profile

In (A43) put $\varepsilon_1 = \varepsilon_2 = n_1^2$

Then $$n^2 = n_1^2 + \frac{e^u}{(e^u+1)^2}\varepsilon_3 \qquad (A47)$$

or $$n^2 = n_1^2 + \tfrac{1}{4}\varepsilon_3 \operatorname{sech}^2(\frac{z}{2\sigma})$$

Note: If n_3 is the refractive index at the peak of the layer, $\varepsilon_3 = 4(n_3^2-n_1^2)$.

Put $4\gamma^2 = 1+4k^2\sigma^2\varepsilon_3$

Then

$$\mathscr{R} = \frac{(-2jk\sigma n_1)!}{(2jk\sigma n_1)!} \frac{(2jk\sigma n_1-\gamma-\tfrac{1}{2})!(2jk\sigma n_1+\gamma-\tfrac{1}{2})!}{(-\gamma-\tfrac{1}{2})!(\gamma-\tfrac{1}{2})!} \qquad (A48)$$

APPENDIX B

COLLISION FREQUENCY PROFILES

In this work the relation for collision frequency

$$\nu = 6.4 \times 10^{7} \; p \; sec^{-1}$$

was used. p is air pressure in millibars. The reference is Gregory and Manson (1969a) who give

$$\nu = (6.4 \pm 0.4) \times 10^{7} \; p \; sec^{-1}.$$

Mean pressures were obtained from Kantor and Cole (1965) for below 80 km and Champion (1967) for above 80 km for the following seasons: Summer (December to February), Winter (June to August) and equinox (March to May and September to November). For $43^{o}50'S$ the values for the corresponding northern hemisphere season at $43^{o}50'N$ were obtained by linear interpolation between $30^{o}N$ and $45^{o}N$. These values are given in table B1 - values for intermediate heights can be obtained by logarithmic interpolation.

Height (km)	Pressure (millibars)		
	Summer	Equinox	Winter
55	4.669×10^{-1}	3.999×10^{-1}	3.455×10^{-1}
60	2.430×10^{-1}	2.053×10^{-1}	1.775×10^{-1}
65	1.213×10^{-1}	1.017×10^{-1}	8.820×10^{-2}
70	5.672×10^{-2}	4.813×10^{-2}	4.252×10^{-2}
75	2.447×10^{-2}	2.158×10^{-2}	1.966×10^{-2}
80	1.180×10^{-2}	1.090×10^{-2}	1.030×10^{-2}
85	4.475×10^{-3}	4.520×10^{-3}	4.553×10^{-3}
90	1.642×10^{-3}	1.866×10^{-3}	1.975×10^{-3}
100	2.660×10^{-4}	3.608×10^{-4}	4.149×10^{-4}

Table B1 Mean seasonal pressure data.

APPENDIX C

THE MODIFIED MAGNETIONIC THEORY OF SEN AND WYLLER (1960)

It was briefly noted in chapter 2 that when the fact that the collision frequency of electrons with neutral molecules is proportional to the square of the electron velocity is taken into consideration, the Appleton-Hartree formula must be modified. A full discussion is contained in Budden (1965): this appendix simply gives the formulae used.

Notation:

e = charge on electron

N = electron density

ε_0 = permittivity of free space

m = electron rest mass

B = geomagnetic field

ω = 2π x frequency of wave

ν_m = "effective" collision frequency, given by appendix B

θ = angle between geomagnetic field and wave-normal

$$X = \frac{Ne^2}{\varepsilon_0 m\omega^2}$$

$$Y = \frac{eB}{m\omega}$$

$$w = \frac{\omega}{\nu_m}$$

Refractive index

The refractive index of a radio wave of angular frequency ω in a medium of electron density N is given by:

$$n^2 = \frac{\varepsilon_1\varepsilon_2\sin^2\theta + \tfrac{1}{2}\varepsilon_3(\varepsilon_1+\varepsilon_2)(1+\cos^2\theta) \pm [\sin^4\theta\{\varepsilon_1\varepsilon_2 - \tfrac{1}{2}\varepsilon_3(\varepsilon_1+\varepsilon_2)\}^2 + \cos^2\theta\varepsilon_3{}^2(\varepsilon_1-\varepsilon_2)^2]^{\frac{1}{2}}}{(\varepsilon_1+\varepsilon_2)\sin^2\theta + 2\varepsilon_3\cos^2\theta} \qquad (C1)$$

where, for the D-region, the + sign gives the ordinary mode and the - sign the extraordinary mode, and:

$$\varepsilon_1 = 1 - X[(1+Y)w^2\mathcal{C}_{3/2}\{w(1+Y)\} + \frac{5}{2}\,iw\mathcal{C}_{5/2}\{w(1+Y)\}]$$

$$\varepsilon_2 = 1 - X[(1-Y)w^2\mathcal{C}_{3/2}\{w(1-Y)\} + \frac{5}{2}\,iw\mathcal{C}_{5/2}\{w(1-Y)\}]$$

$$\varepsilon_3 = 1 - X[w^2\mathcal{C}_{3/2}(w) + \frac{5}{2}\,iw\mathcal{C}_{5/2}(w)] \qquad (C2)$$

and $$\mathcal{C}_p(w) = \frac{1}{p!}\int_0^\infty \frac{u^p e^{-u}}{u^2+w^2}\,du \qquad (C3)$$

The $\mathcal{C}$ integrals are most easily calculated by using the approximations, in the form of a ratio of two polynomials, given by Hara (1963).

Polarization

The polarization, ρ, of a characteristic mode is given by

$$\rho = \frac{-\alpha \pm \sqrt{\alpha^2-4}}{2} \qquad (C4)$$

where the positive sign gives the ordinary mode polarization, and the negative sign the extraordinary mode polarization in the D region, and

$$\alpha = \frac{i\sin^2\theta\{2\varepsilon_1\varepsilon_2 - \varepsilon_3(\varepsilon_1+\varepsilon_2)\}}{\cos\theta\,\varepsilon_3(\varepsilon_1-\varepsilon_2)} \qquad (C5)$$

APPENDIX D

RATE OF CHANGE OF CONCENTRATION OF AN ATMOSPHERIC CONSTITUENT IN AN ATMOSPHERE WITH EDDY DIFFUSION, MEAN MOTION, AND PHOTOCHEMICAL PROCESSES

Consider a constituent with concentration N_i, photochemical production rate P_i, loss rate L_i. Then at a given height,

$$\frac{\partial N_i}{\partial t} = P_i - L_i - \nabla\cdot(N_i \underset{\sim}{v}_i) \tag{D1}$$

where $\underset{\sim}{v}_i$ is velocity.

The total number density of particles in the atmosphere, N, may be considered to be conserved. Assume that $\frac{\partial N}{\partial x} = \frac{\partial N}{\partial y} = 0$ Also assume

$$N = N_0 \, e^{-\frac{(Z-Z_0)}{H}}$$

where N_0 is the number of particles at height Z_0, H is the mean scale height. Thus

$$\frac{\partial N}{\partial z} = -\frac{N}{H} \tag{D2}$$

For a simplified model, assume that the vertical component of velocity w is independent of height.

The equation of conservation for N is:

$$\frac{\partial N}{\partial t} + \nabla\cdot(N\underset{\sim}{v}) = 0$$

For the model, assume $\frac{\partial N}{\partial t} = 0$. Thus

$$\nabla\cdot(N\underset{\sim}{v}) = 0$$

$$\frac{\partial N}{\partial z} w + N\nabla_h\cdot\underset{\sim}{v} = 0 \qquad \text{(D3)}$$

(where $\nabla_h = \hat{i}_x \frac{\partial}{\partial x} + \hat{i}_y \frac{\partial}{\partial y}$)

From (D2) and (D3)

$$\nabla_h\cdot\underset{\sim}{v} = \frac{w}{H} \qquad \text{(D4)}$$

So far, only mean motion $\underset{\sim}{v}$ has been considered. Turbulent mixing can be included by a term

$$\frac{\partial}{\partial z}\{K(\frac{\partial N_i}{\partial z} + \frac{N_i}{H})\} \qquad \text{(Whitten \& Poppoff 1971, p180)}$$

This leads to an alteration of (D1) to give

$$\frac{\partial N_i}{\partial t} = P_i - L_i + \frac{\partial}{\partial z}\{K(\frac{\partial N_i}{\partial z} + \frac{N_i}{H})\} - \nabla N_i\cdot\underset{\sim}{v} - N_i\nabla\cdot\underset{\sim}{v} \qquad \text{(D5)}$$

Expanding the last two terms in (D5) gives

$$-\left(\frac{\partial N_i}{\partial x} v_x + \frac{\partial N_i}{\partial y} v_y + \frac{\partial N_i}{\partial z} v_z + N_i\nabla_h\cdot\underset{\sim}{v} + N_i \frac{\partial w}{\partial z}\right)$$

Assume that $\frac{\partial N_i}{\partial x} = \frac{\partial N_i}{\partial y} = 0$. Thus (D5) becomes:

$$\boxed{\frac{\partial N_i}{\partial t} = P_i - L_i + \frac{\partial}{\partial z}\{K(\frac{\partial N_i}{\partial z} + \frac{N_i}{H})\} - w(\frac{\partial N_i}{\partial z} + \frac{N_i}{H})}$$

APPENDIX E

THE ABSORPTION SUFFERED BY A RADIO WAVE TOTALLY REFLECTED IN THE E-REGION

The Appleton-Hartree formula for the refractive index n of a radio wave of angular frequency ω incident normally in a medium of electron density N is given by (Budden 1961, section 6.1)

$$n^2 = 1 - \frac{X}{1 - iZ - \frac{\frac{1}{2}Y_T^2}{1-X-iZ} \pm \left\{ \frac{\frac{1}{4}Y_T^4}{(1-X-iZ)^2} + Y_L^2 \right\}^{\frac{1}{2}}} \qquad \text{(E1)}$$

where the notation is as in appendix C and

$$Z = \frac{\nu_m}{\omega}$$

$$Y_L = Y \cos\theta$$

$$Y_T = Y \sin\theta$$

It is shown by Budden (1965) that the Sen-Wyller expression for refractive index (C1) gives the same value as (E1) for very small values of $\frac{\nu_m}{\omega}$ provided Z in (E1) is replaced by $Z_{eff} = \frac{5}{2}\frac{\nu_m}{\omega}$. At reflection levels for a 2.4 MHz wave, which are typically near or above 100 km, $\frac{\nu_m}{\omega} \approx 2 \times 10^{-3}$. This is sufficiently small for (E1) to be an accurate expression for the refractive index near the reflection point.

Consider (E1) with Z = 0. Then n^2 has zeroes at:

$$X = 1 \qquad \text{(+ sign in E1)} \qquad \text{(E2)}$$

$$X = 1 \pm Y \qquad \text{(- sign in E1)}$$

These are the conditions for reflection of the ordinary wave and the extraordinary wave respectively in the absence of collisions (Davies 1966, P73). For a 2.4 MHz wave at Christchurch, Y < 1, so the extraordinary mode is reflected when

$$X = 1 - Y \tag{E3}$$

Under the WKB approximation (appendix A), the absorption (nepers) for a wave which travels vertically upwards from the ground to the E-region where it is reflected back to the ground is:

$$A = -2k\, \mathcal{I}m\left(\int_0^{h_0} n\, dh\right) \tag{E4}$$

where h_0 is the height at which the complex refractive index given by (E1) is zero. Thorpe (1971) discusses the decomposition of (E4) into two integrals:

$$A_1 = -2k\, \mathcal{I}m\left(\int_0^{h_r} n\, dh\right) \tag{E5}$$

$$A_2 = -2k\, \mathcal{I}m\left(\int_{h_r}^{h_0} n\, dh\right) \tag{E6}$$

where h_r is the height where the refractive index would be zero for no collisions. A_2 is known as the "phase-integral" correction.

The absorption A_1 was calculated by integrating the imaginary part of the Sen-Wyller refractive index (C1) for the ordinary and extraordinary waves up to the heights where equations (E2) and (E3) hold respectively. The electron density profile used (figure E1) was from rocket measurements

by Mechtly et al. (1972a) at 38°N, solar zenith angle 60°, for quiet sun conditions (15 Sept, 1965). The results were:

Ordinary mode: attenuation = 12.6 db, reflection height = 99.7 km

Extraordinary mode: attenuation = 98.8 db, reflection height = 96.5 km

(This is the total attenuation from the ground to the E-region and back.)

Thorpe (1971) found that the phase integral correction to the ordinary mode was typically an extra attenuation of the order of 5% of the attenuation calculated by (E5) at 2.4 MHz. Thus even if the phase integral correction for the extraordinary wave was zero, the extraordinary wave would still suffer about 86 db more attenuation than the ordinary wave.

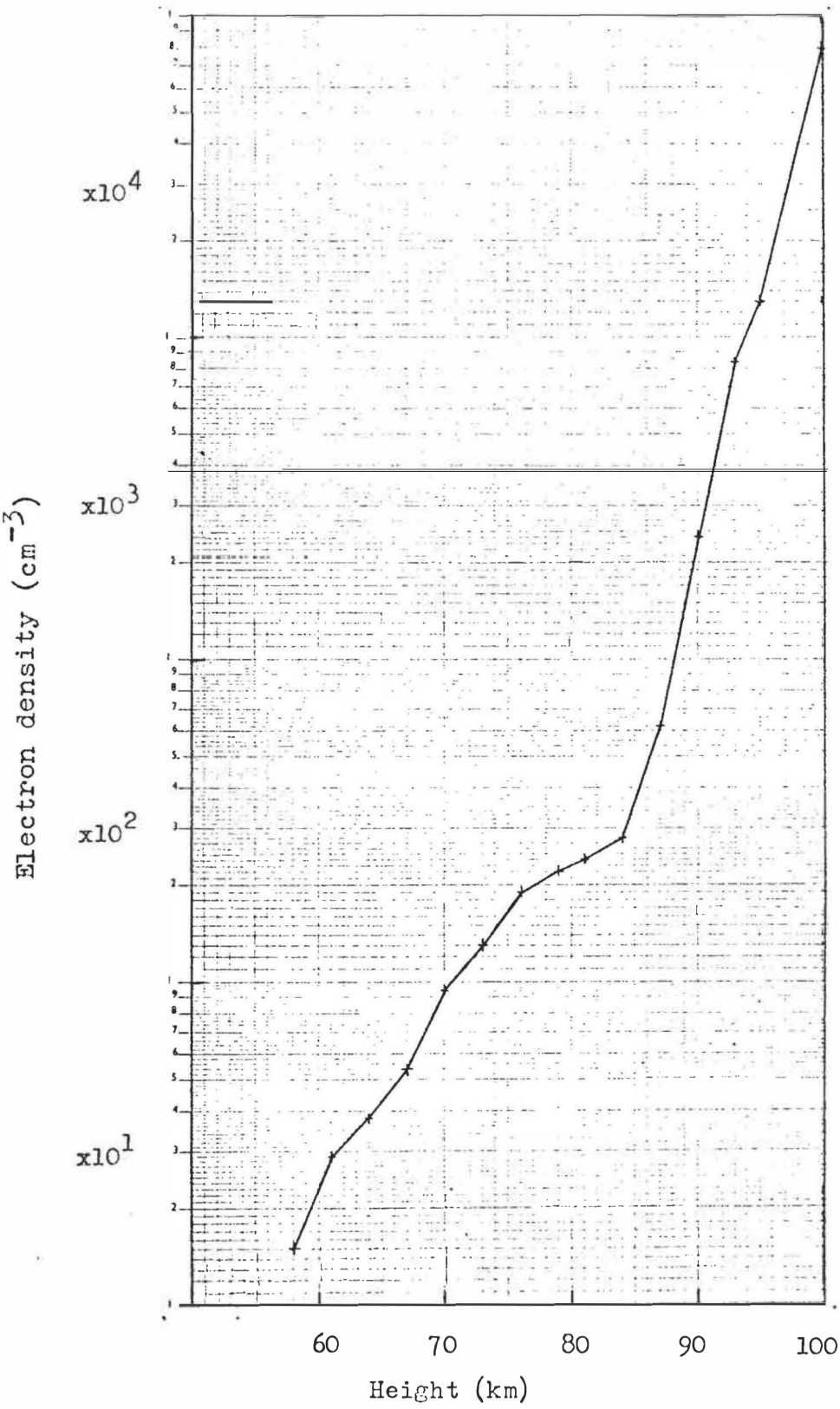

Fig El: Electron density profile used in absorption calculation.

APPENDIX F

UNCERTAINTY CONSIDERATIONS

1. The Uncertainty in a Mean Square Value

Consider a random variable x which is not necessarily normally distributed. Then the Central Limit theorem (Bendat and Piersol, 1971, P111) implies that as the sample size N becomes large ($N \geq 10$) the sampling distribution of the sample mean $\bar{x}$ approaches a normal distribution.

It is shown by Bendat and Piersol (op cit., section 4.1) that

$$S^2 = \frac{1}{N-1} \sum_{i=1}^{N} (x_i - \bar{x})^2 \qquad (F1)$$

is an unbiased estimator for the population variance, σ^2. The variance of the sample mean is $\frac{\sigma^2}{N}$. Thus if

$$S_b^2 \approx \frac{1}{N} \sum_{i=1}^{N} (x_i - \bar{x})^2 = (\overline{x^2} - \bar{x}^2) \qquad (F2)$$

an unbiased estimator for the variance of the sample mean will be:

$$\hat{\sigma}_X^2 = \frac{N}{N-1} \frac{S_b^2}{N} = \frac{S_b^2}{N-1} \qquad (F3)$$

If $w = x^2$ is considered to be a random variable, then $\bar{w} = \overline{x^2}$ will be approximately normally distributed with a standard deviation (F3) of

$$\boxed{\sigma = \left\{ \frac{\overline{x^4} - (\overline{x^2})^2}{N-1} \right\}^{\frac{1}{2}}} \qquad (F4)$$

Thus the standard error of a mean square value is given by (F4).

2. The Use of the Standard Error as an Estimate of the Uncertainty in Deduced Electron Densities due to the Scatter in the Data

Consider two time series A(t), B(t). (These two series could be $|E_X(t)|^2$, $|E_O(t)|^2$ of section 4.3.) Suppose n samples are taken from each series to give the series A_i, B_i, i = 1,n.

Define

$$\langle A\rangle = \frac{1}{n}\sum_{i=1}^{n} A_i \qquad e_A^2 = \frac{1}{n^2}\sum_{i=1}^{n} (A_i-\langle A\rangle)^2 \qquad \text{(F5)}$$

$$\langle B\rangle = \frac{1}{n}\sum_{i=1}^{n} B_i \qquad e_B^2 = \frac{1}{n^2}\sum_{i=1}^{n} (B_i-\langle B\rangle)^2 \qquad \text{(F6)}$$

The standard error of the ratio $\frac{\langle A\rangle}{\langle B\rangle}$ is defined as (cf. equation 4.7)

$$e = \left(\frac{e_A^2\langle A\rangle^2 + e_B^2\langle B\rangle^2}{\langle B\rangle^4}\right)^{\frac{1}{2}} \qquad \text{(F7)}$$

The use of the standard error as an indication of the uncertainty in $\frac{\langle A\rangle}{\langle B\rangle}$ due to the scatter in A_i and B_i is based on the theory that provided:

(i) The series A(t), B(t) are random and stationary

(ii) The values A_i, A_{i+1} are independent

(iii) n is sufficiently large ($n \geq 30$)

(iv) The values of A_i and B_i are independent

then the true value of $\frac{A}{B}$ (the value which would be found for

$\frac{\langle A \rangle}{\langle B \rangle}$ as $n \to \infty$) is within $\pm e$ of the experimental value of $\frac{\langle A \rangle}{\langle B \rangle}$ found from n samples.

However, in the experimental case of measuring $\frac{\langle |E_X|^2 \rangle}{\langle |E_O|^2 \rangle}$ some of these assumptions are violated. For example there may be an echo present at some height for two or three minutes (the amplitude rising and falling about some mean value), which vanishes over the next two or three minutes. This effectively makes the series non-stationary. Also $|E_X(t)|$ and $|E_O(t)|$ may fade in phase, violating condition (ii). Suppose the series A(t) and B(t) are perfectly correlated, i.e. A(t) = kB(t), k constant. Suppose also that A_i and B_i are measured at the same times. Then $\frac{\langle A^2 \rangle}{\langle B^2 \rangle} = k^2$ and there is no uncertainty in this ratio (that is, it is equal to the "true" value). However, if A is a random series the standard error e calculated by (F7) will be non-zero, so that in this case the standard error is not a true estimate of the uncertainty.

The actual experimental case is somewhat different. $|E_X|_i$ and $|E_O|_i$ are measured about one second apart from each other. However, at some heights (e.g. 74 km) it may take six seconds or more for the autocorrelation function of $|E_O(t)|$ to fall below 0.5 (Noonan, 1969, P47). Also at some heights there is significant correlation between the ordinary and extraordinary signals. (The manual method of adding attenuation to one mode until the two modes line up on the oscilloscope display depends on similar fading of the two modes.) Thus the situation is somewhat similar to the simple situation outlined above, and it is quite possible that the calculated standard error is an overestimate of the uncertainty.

An echo which was present over several sampling cycles and then absent for several cycles could also lead to a standard error which overestimated the uncertainty.

Similar arguments can be applied to the calculation of the uncertainty in the differential phase measurement at a given height.

APPENDIX G

SWITCHING LOGIC AND CIRCUITS

G.1 Station Control Register (SCR)

The station control register is a twelve bit register loaded from the accumulator of the PDP8, which controls the operation of various devices (for example the transmitter) (Figure G1).

Decoded outputs: Bits 8-11 are decoded to give 16 outputs. For SCR bits 8-11 zero all of the decoder outputs are HIGH. Setting given SCR bits to 1 causes the appropriate decoded output to go from HIGH to LOW.

e.g. SCR = 14_8 causes 12^{th} decoder output to go LOW.

The following decoder outputs were used:

13_8 Aerial lead switching clock

14_8 Attenuator switching clock

15_8 Turns on transmitter filaments

16_8 Turns on transmitter H.T.

17_8 Switches off the transmitter.

Normal outputs: Bits 2-7 go to the devices to be controlled.

Bit x = 1 implies output x is HIGH

Bit x = 0 implies output x is LOW

The outputs are via 7400 series TTL logic.

HIGH means 2.4 - 5.0 volts

LOW means 0.0 - 0.4 volts.

G.2 Signal switching

The RF signals from the receiving aerials were switched using Hamlin magnetic reed switches (type MRR-2). These were operated by coils of 750±5 turns of 34 s.w.g. copper wire, which required a current of about 100 mA to turn the reeds on. The coils were driven by switching transistors (figure G3) which were controlled from the switching logic.

G.3 Switching Logic

The values of SCR bits 4-7 were gated into the switching logic for a given device by the relevant clock pulse from the decoder (figure G2). The clock pulse was delayed slightly to allow the D inputs of the flip-flops to settle.

In the "hardware controlled" method the circuit of figure G2 was replaced by that of figure G4. The outputs were fed through further logic circuits to turn on the relays for the various aerial modes in sequence.

Figures G5-G10 give detailed logic and circuit diagrams for the aerial switching and switched attenuator circuits. The actual integrated circuits used were from the TTL 7400 series.

D type flip-flops	7474
NAND gates	7400, 7420
Delay (using monostable)	74121
Inverter	7404

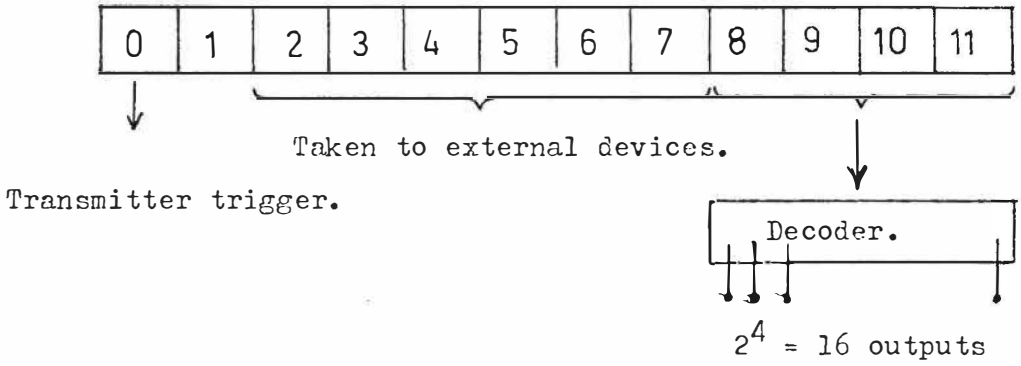

Fig G1 Station control register.

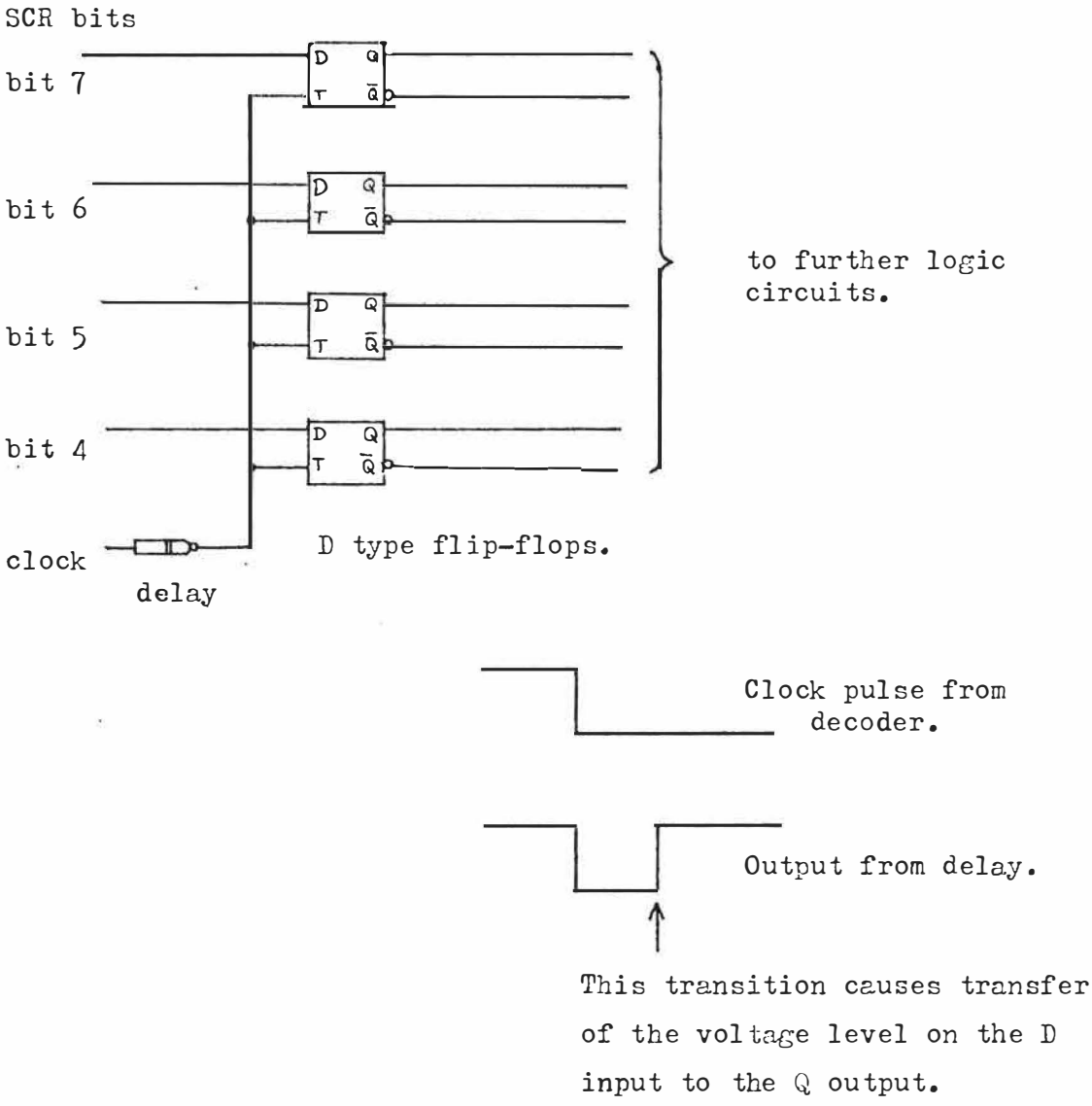

Fig G2 Circuit to gate SCR bits into switching logic.

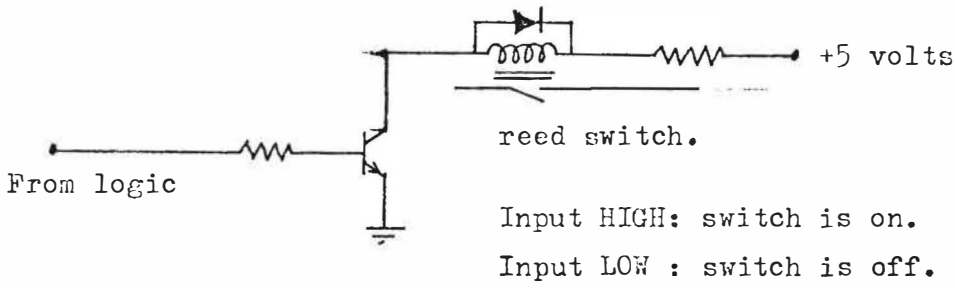

Fig G3: Relay switching.

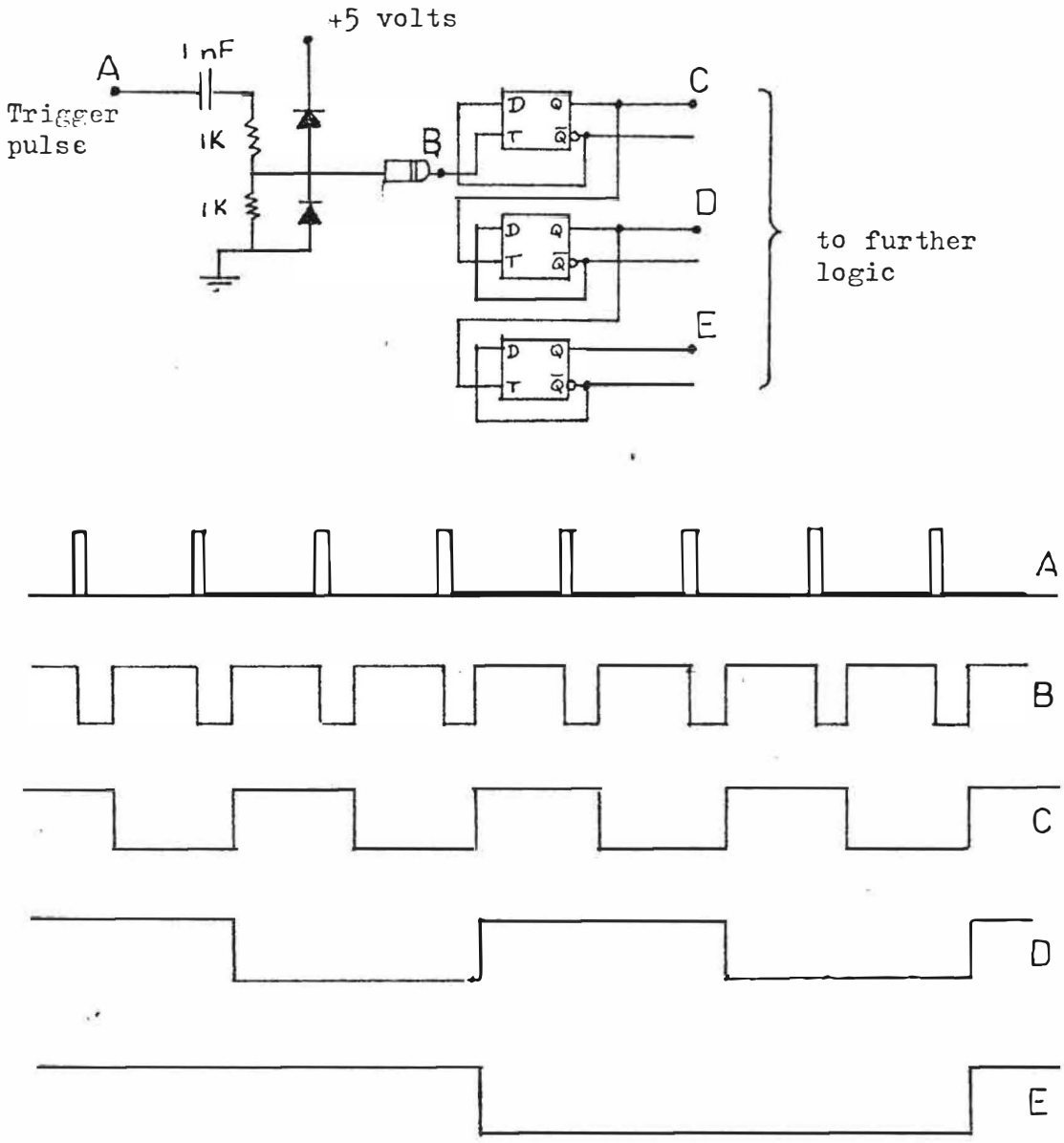

Fig G4: Circuit to set up operations sequence in the "hardware controlled" method.

N	transistors on	mode
0	A, F	M_1
1	A, G	M_2
2	C, F	A_X
3	C, G	A_O
4	D, F	V_1
5	E, G	V_2
6	B	Signal gen.

N is the octal value for bits 5-7.

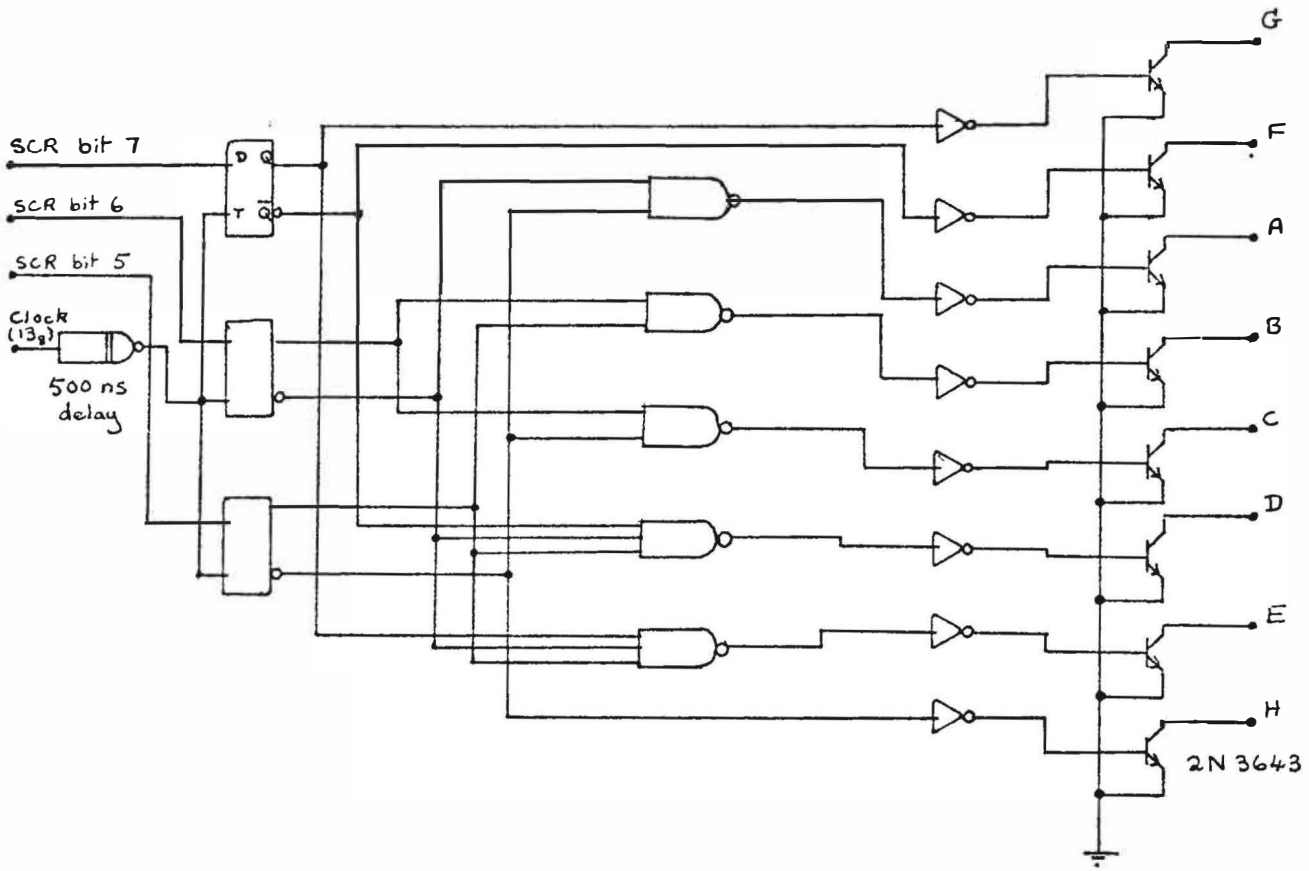

Fig G5 Logic for receiving aerial switching.

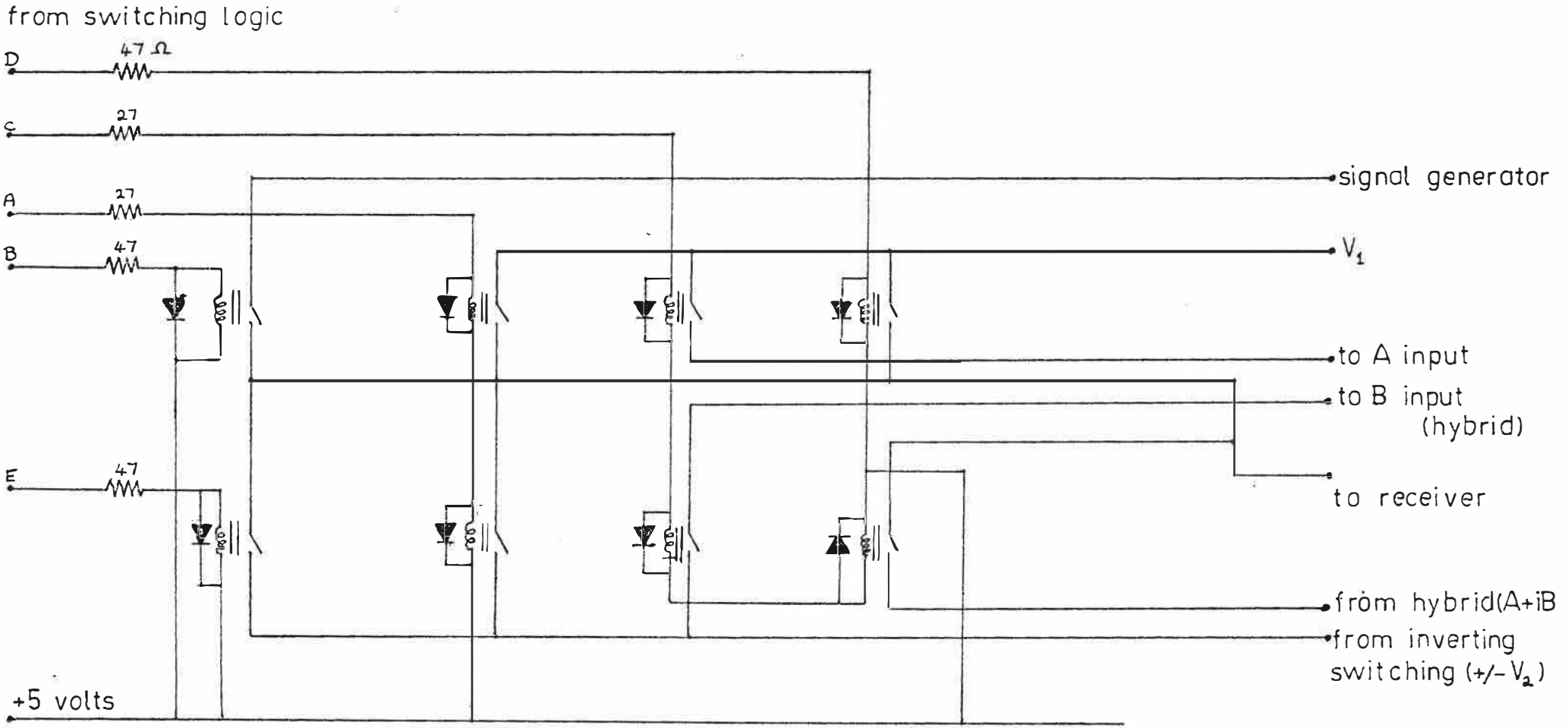

Fig G6 Aerial lead switching.

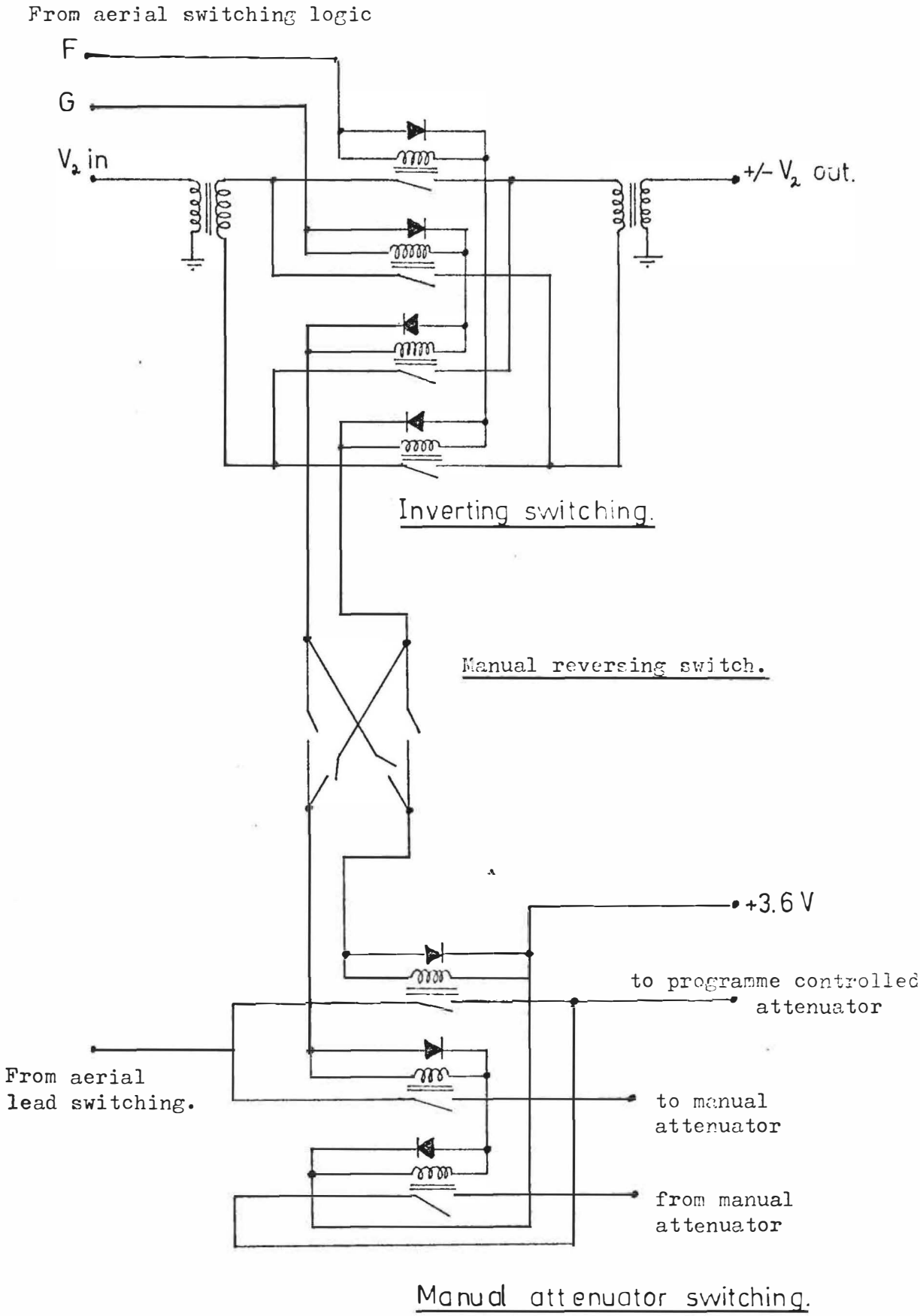

Fig G7. Reversing and manual attenuator switching.

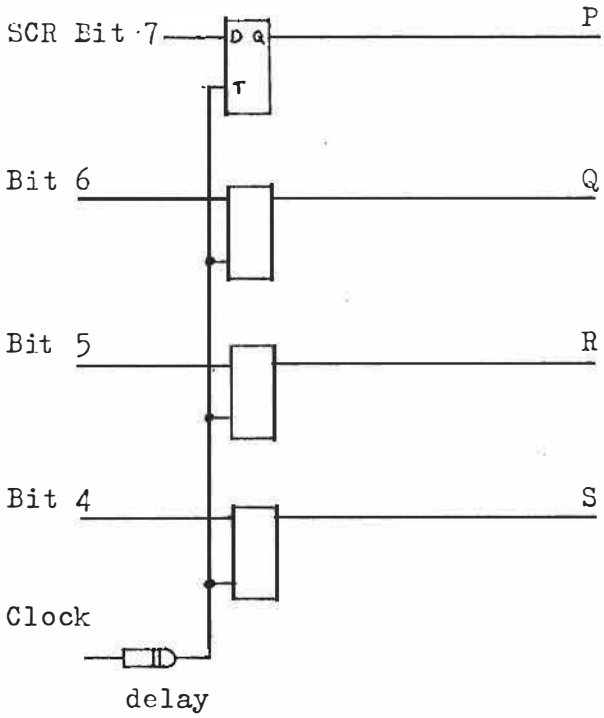

Bit 7 high switches in the 5 db attenuator.
Bit 6 high switches in the 10 db attenuator.
Bit 5 high switches in the 20 db attenuator.
Bit 4 high switches in the 40 db attenuator.

If N is the octal value of SCR bits 4-7 , then $(5xN)_8$ decibels of attenuation are switched in. (This only works up to 45 db.)

Fig G8: Switching logic for the programme controlled attenuator.

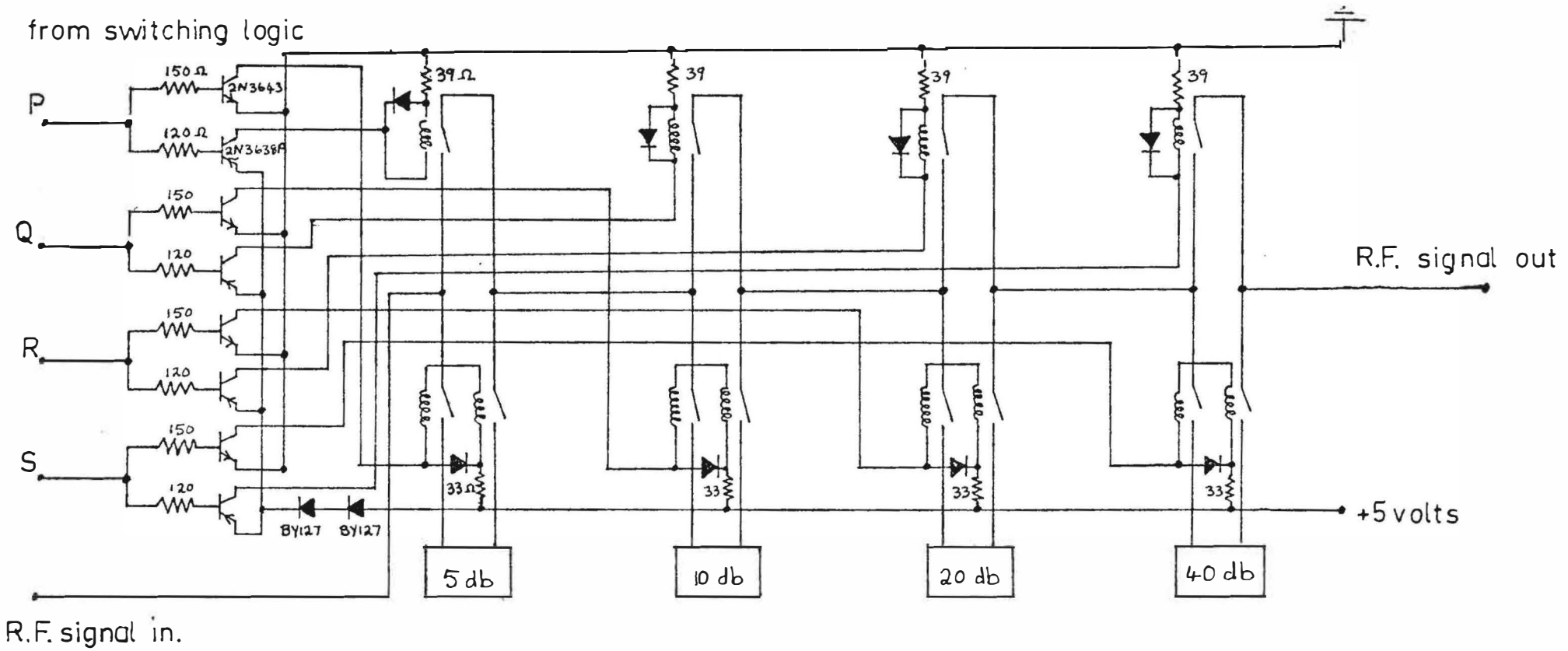

Fig G9. Programme controlled attenuator.

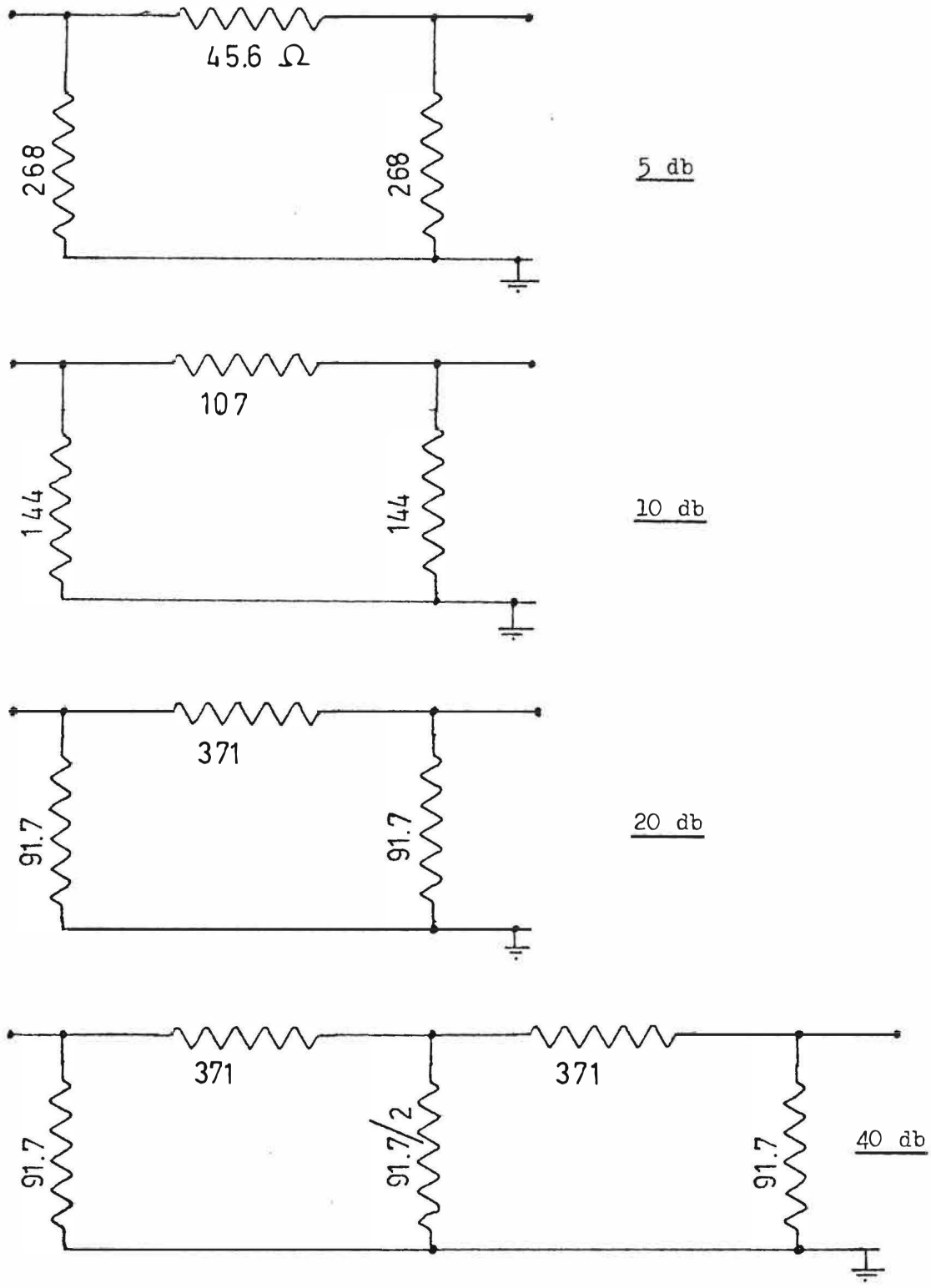

Input impedance = Output impedance = 75 ohms.

Fig G10 Attenuator circuits.

APPENDIX H Programmes for the software controlled differential absorption and phase experiment.

```
C       DAPE SEGMENT ONE- RECEIVER CALIBRATION AND NOISE RECORDING
C       STORE ON SYS AS NPR1.SV
C       REQUIRES SUBROUTINES RCAL,CALIB,DAEXP,ATTEN,DELAY,
C       TXHT,FNAME,TXOFF,AND ADNOT
C
C       TURN ON EXCITER STAGE OF TRANSMITTER.
C
        COMMON IDATA,CAL,NA,NB,ITIME,IDAY,IYEAR,SUMN2,SUMN4,SUMM2,
     1  SUMM4,IT,IST,M,DNAM,IPER,MEXP,ISTART
        DIMENSION IDATA(57),CAL(7),SUMN2(6),SUMN4(6),SUMM2(6),
     1  SUMM4(6),MEXP(6)
        CALL TXOFF
        CALL DELAY(20)
C       SET SWITCH REGISTER TO 1 FOR FIRST RUN
        IF(IRDSW(0)-1) 400,401,400
 400    IT=IT+1
        IT=IABS(IT)
        IF(IT-100) 51,202,202
 202    IT=0
C       SET THE SWITCH REGISTER TO 4 IF YOU WISH TO CHANGE THE
C       ATTENUATION OR THE TIME BETWEEN RUNS
 51     IF(IRDSW(0)-4) 53,52,53
 52     READ(1,54) NA,NB,IPER
 54     FORMAT('NA,NB,IPER,(3I2)=',3I2)
        GO TO 53
 401    IT=0
        WRITE(1,101)
 101    FORMAT('WRITE NA,NB,ISTART,IDAY,IYEAR,M,IPER-2I2,I4,I3,2I4,I2
        READ(1,100) NA,NB,ISTART,IDAY,IYEAR,M,IPER
 100    FORMAT(2I2,I4,I3,2I4,I2)
C       M IS NOISE PEAK FILTER,IPER IS TIME BETWEEN RUNS
        READ(1,500) (MEXP(I),I=1,6)
 500    FORMAT('RUN TIMES:',6I5)
C       CHANGE RUN TIMES TO MINUTES FROM MIDNIGHT
        DO 501 I=1,6
        IHR=MEXP(I)/100
        IMN=MEXP(I)-IHR*100
 501    MEXP(I)=IHR*60+IMN
        IHR=ISTART/100
        IMN=ISTART-IHR*100
        ISTART=IHR*60+IMN
S       CLA
S       6711            /LOAD MINUTES INTO AC
S       6713            /CLEAR OVERFLOW
S       DCA \IST        /IST IS STARTING TIME
C       WAITING PORTION
 53     CONTINUE
S       CLA
S       6711            /READ MINUTE CLOCK
S       DCA \KOUNT
        ITIME=(KOUNT-IST)+ISTART
C       PUT THE SWITCH REGISTER TO 2 TO RETURN TO THE KEYBOARD
C       MONITOR
        IF(IRDSW(0)-2) 55,56,55
 56     STOP
```

```
 55      IF(ITIME) 57,53,57
 57      IF(ITIME-1440) 58,59,58
 59      ISTART=0
         IST=KOUNT
         IDAY=IDAY+1
C        THIS WAS FOR A NEW DAY
         GO TO 53
 58      DO 60 I=1,6
         IF(ITIME-MEXP(I)) 60,111,60
 60      CONTINUE
C        ITIME IS THE ACTUAL TIME OF THE RUN
C        PUT SWITCH REGISTER TO SOME NON-ZERO NUMBER TO CHECK
C        THE SIGNAL GENERATOR LEVEL
         GO TO 53
 111     IF(IRDSW(0)-0) 403,402,403
 403     CALL DAEXP(6)
         CALL DELAY(20)
         CALL ATTEN(0)
         CALL DELAY(20)
         PAUSE 2047
 402     CALL RCAL
C        DOES A CALIBRATION RUN
C        INITIALIZE THE ARRAYS
         DO 200 I=1,6
         SUMN2(I)=0.0
         SUMN4(I)=0.0
         SUMM2(I)=0.0
 200     SUMM4(I)=0.0
C        DO NOISE RUN
         CALL ATTEN(0)
         CALL DELAY(20)
         NN=0
 4       DO 110 I=1,6
 3       CALL DAEXP(I-1)
         CALL DELAY(20)
         CALL ATTEN(NA)
 103     CALL DELAY(100)
         CALL ADNOT(51,1,0)
         K=IDATA(14)+IDATA(17)+IDATA(20)
C        REJECT NOISE PEAKS
         IF(K-M) 102,102,103
 102     DO 104 K=14,50,3
C        THIS SHOULD BE 55KM TO 85 KM IN 2.5 KM STEPS
         D=CALIB(IDATA(K),CAL)
         D2=D*D
         D4=D2*D2
         SUMN2(I)=SUMN2(I)+D2
 104     SUMN4(I)=SUMN4(I)+D4
         CALL ATTEN(NB)
 108     CALL DELAY(100)
         CALL ADNOT(51,1,0)
         K=IDATA(14)+IDATA(17)+IDATA(20)
         IF(K-M) 107,107,108
 107     DO 109 K=14,50,3
         D=CALIB(IDATA(K),CAL)
         D2=D*D
         D4=D2*D2
         SUMM2(I)=SUMM2(I)+D2
 109     SUMM4(I)=SUMM4(I)+D4
 110     CONTINUE
```

```
      NN=NN+1
      IF(NN-30) 4,105,105
105   DO 106 I=1,6
      SUMN2(I)=SUMN2(I)/390.0
      SUMN4(I)=SUMN4(I)/390.0
      SUMM2(I)=SUMM2(I)/390.0
106   SUMM4(I)=SUMM4(I)/390.0
      CALL TXHT
C     NON-ZERO SWITCH REGISTER GIVES PAUSE TO CHECK TX
      IF(IRDSW(0)-0) 405,404,405
405   PAUSE 0001
404   CALL FNAME(DNAM)
      CALL CHAIN('NPR2')
      END
```

```
C     DAPE SEGMENT 2
C     DOES A DATA RUN AND WRITES RESULTS ONTO SYS:DAPE.DA
C     STORE ON SYS AS NPR2.SV
C     REQUIRES SUBROUTINES CALIB,ADCOM,DELAY,ATTEN,DAEXP
C     CONTAINS DEVICE INDEPENDANT I/O, SO REQUIRES /I AND /O
C     OPTIONS TO LINKING LOADER
C
      COMMON IDATA,CAL,NA,NB,ITIME,IDAY,IYEAR,SUMN2,SUMN4,SUMM2,
     1 SUMM4,IT,IST,M,TITLE,IPER,MEXP,ISTART
      DIMENSION CAL(7),ASUM2(13,6),ASUM4(13,6),BSUM2(13,6),
     1 BSUM4(13,6),SUMN2(6),SUMN4(6),SUMM2(6),SUMM4(6),IDATA(57),
     2 NAH(13,6),NBH(13,6),MEXP(6)
      ICAL1=IFIX(CAL(1))
      K=1
      DO 200 I=1,6
      DO 200 J=1,13
      ASUM2(J,I)=0.0
      ASUM4(J,I)=0.0
      NAH(J,I)=0.0
      NBH(J,I)=0.0
      BSUM2(J,I)=0.0
200   BSUM4(J,I)=0.0
7     I=1
6     CALL ATTEN(NA)
      CALL DELAY(20)
      CALL DAEXP(I-1)
      CALL DELAY(20)
      CALL ADCOM(57,1,0)
      IF(IDATA(14)-800) 234,6,6
C     REJECTS BAD NOISE
234   DO 107 J=1,13
      JD=17+3*J
      IF(IDATA(JD)-ICAL1) 108,109,109
109   NAH(J,I)=NAH(J,I)+1
      GO TO 107
108   D=CALIB(IDATA(JD))
      D2=D*D
      D4=D2*D2
      ASUM2(J,I)=ASUM2(J,I)+D2
      ASUM4(J,I)=ASUM4(J,I)+D4
107   CONTINUE
```

```
120     CALL ATTEN(NB)
        CALL DELAY(20)
        CALL ADCOM(57,1,0)
        IF(IDATA(14)-800) 235,120,120
235     DO 110 J=1,13
111     JD=17+3*J
        IF(IDATA(JD)-ICAL1) 112,113,113
113     NBH(J,I)=NBH(J,I)+1
        GO TO 110
112     D=CALIB(IDATA(JD))
        D2=D*D
        D4=D2*D2
        BSUM2(J,I)=BSUM2(J,I)+D2
        BSUM4(J,I)=BSUM4(J,I)+D4
110     CONTINUE
        I=I+1
        IF(I-6) 6,6,114
114     K=K+1
        IF(K-75) 7,7,115
115     CALL OOPEN('SYS',TITLE)
        WRITE(4,117) ITIME,IDAY,IYEAR,NA,NB
117     FORMAT(I4,I3,I4,2I2)
        DO 11 I=1,6
        WRITE(4,118) I,SUMN2(I),SUMN4(I),SUMM2(I),SUMM4(I)
118     FORMAT(I2,2E11.4,/2X,2E11.4)
        DO 11 J=1,13
        IF(NAH(J,I)-74) 10,12,12
10      AK=FLOAT(75-NAH(J,I))
        ASUM2(J,I)=ASUM2(J,I)/AK
        ASUM4(J,I)=ASUM4(J,I)/AK
12      IF(NBH(J,I)-74) 13,11,11
13      AK=FLOAT(75-NBH(J,I))
        BSUM2(J,I)=BSUM2(J,I)/AK
        BSUM4(J,I)=BSUM4(J,I)/AK
11      WRITE(4,119) ASUM2(J,I),ASUM4(J,I),NAH(J,I),
    1   BSUM2(J,I),BSUM4(J,I),NBH(J,I)
119     FORMAT(2E11.4,I3)
        CALL OCLOSE
        CALL CHAIN('NPR1')
        END
```

```
        SUBROUTINE DAEXP(N)
C       SETS DAE CONTROL REGISTER TO N
S       CLA CLL
S       6726                /CLEAR THE SCR
S       TAD I \N
S       RTL
S       RTL
S       TAD (13
S       AND (3777
S       6726
S       CLA
        RETURN
        END
```

```
      SUBROUTINE ATTEN(N)
C     SETS ATTENUATOR REGISTER TO N
S     CLA CLL
S     6726              /CLEAR THE SCR
S     TAD I \N
S     RTL
S     RTL
S     TAD (14           /SET ATTEN TRIGGER CODE
S     AND (3777         /JUST IN CASE!
S     6726              /LOAD SCR
S     CLA
      RETURN
      END
```

```
      SUBROUTINE RCAL
      COMMON IDATA,CAL
      DIMENSION CAL(7),AV(10),IDATA(57)
      CALL DAEXP(6)
C     SWITCHES SIGNAL GENERATOR TO INPUT
      CALL DELAY(20)
      CALL ATTEN(0)
      L=1
      CALL DELAY(20)
 4    CALL ATTEN(L-1)
C     ATTENUATION SET IN=(L-1)*5 DB
      J=1
      AV=0.0
 2    CALL DELAY(20)
      CALL ADNOT(51,1,0)
      DO 1 K=23,50,3
 1    AV=AV+FLOAT(IDATA(K))
      J=J+1
      IF(J-40) 2,2,3
 3    CAL(L)=AV/400.0
      L=L+1
      IF(L-7) 4,4,5
 5    RETURN
      END
```

```
      SUBROUTINE TXHT
C     SWITCHES ON THE TRANSMITTER H.V. SUPPLY
S     CLA
S     6726              /CLEAR SCR
S     TAD (0016
S     6726              /SCR = 0016(8)
S     CLA
      RETURN
      END
```

```
      FUNCTION CALIB(ID)
C     USES CAL(7) TO APPROXIMATE RECEIVER CHARACTERISTICS BY
C     A PIECEWISE LINEAR CURVE.CALIB GIVES THE RX INPUT ON
C     A LINEAR SCALE [0,1] CORRESPONDING TO THE A-D OUTPUT
C     ID
      COMMON IDATA,CAL
      DIMENSION CAL(7),ORD(7),IDATA(57)
C     ORD(1),...,ORD(7) ARE THE VOLTAGE RATIOS CORRESPONDING
C     TO NATT=0,...,6 IN THE SUBROUTINE ATTEN(N)
      ORD(1)=1.0
      ORD(2)=0.5623
      ORD(3)=0.3162
      ORD(4)=0.1778
      ORD(5)=0.1000
      ORD(6)=0.05623
      ORD(7)=0.03162
      D=FLOAT(ID)
      IF(D-CAL(1)) 2,1,1
1     CALIB=1.0
      GO TO 100
2     DO 7 I=2,7
      IF(D-CAL(I)) 7,7,3
7     CONTINUE
6     CALIB=0.015811
      GO TO 100
3     FACTU=ORD(I-1)
      FACTL=ORD(I)
      CALIB=(FACTU-FACTL)*(D-CAL(I))/(CAL(I-1)-CAL(I))+FACTL
100   RETURN
      END
```

```
      SUBROUTINE FNAME(TITLE)
C     PROGRAMME TO ALTER FILE NAME
      COMMON IDATA,CAL,NA,NB,ITIME,IDAY,IYEAR,SUMN2,SUMN4,SUMM2,
     1 SUMM4,IT
      DIMENSION IDATA(57),CAL(7),SUMN2(6),SUMN4(6),SUMM2(6),
     1 SUMM4(6)
      EQUIVALENCE (IA,TOTLE)
      TOTLE=0.0
      IAA=IT
      IAL=IAA/10
      IAR=IAA-IAL*10+48
      IAL=IAL+48
S     CLA CLL
S     TAD \IAL
S     RTL;RTL;RTL
S     TAD \IAR
S     DCA \IA
      TITLE=TOTLE
      RETURN
      END
```

```
      SUBROUTINE TXOFF
C     SWITCHES OFF THE TRANSMITTER
S     CLA
S     6726              /CLEAR SCR
S     TAD (0017
S     6726              /SCR = 0017(8)
S     CLA
      RETURN
      END



      SUBROUTINE ADCOM(LAD, IMARK, INCH)
C     ADCOM.FS          27 JUNE 1973
C     FORTRAN/SABR ROUTINE FOR THREE-CHANNEL A/D CONVERTER
C
C     LAD = LENGTH OF A/D INPUT ARRAY IN COMMON
C     **** LAD MUST BE A MULTIPLE OF 3 ****
C          AND IS NOT ALLOWED TO EXCEED 255
C
C     IMARK : A/D CONVERSION STARTS ON THE IMARK-TH 1 MS (=150 KM)
C             MARKER.  THE 0-TH MARKER IS SET TO
C             AN ARBITRARY POSITION BECAUSE IT
C             IS UDED TO TIME THE TRANSMITTER TRIGGER.
C
C     INCH = 0 : A/D SAMPLING EVERY 2.5 KM
C          = 1 : "      "        "   5.0 "
C          = 2 : "      "        "    10 "
C
C
C     THE FIRST WORD IN COMMON IS RUBBISH,
C     SO ONLY 2 CHANNELS ARE READ FOR THE LAST HEIGHT
C
C
C     THE TRACK/HOLD CIRCUITS TAKE ABOUT 2 SAMPLES TO SETTLE
C     DOWN FROM THE EXTREMES TO WHICH THEY DRIFTED DURING THE
C     PREVIOUS HOLD, AFTER THE PREVIOUS SCAN.
C
C
S     OPDEF   LSCR    6726    /LOAD STATION CONTROL REG FROM ACC
C
C
S     OPDEF   AD02    6715    /START SAMPLING AT 2.5 KM INTERVALS
S     OPDEF   AD05    6716    /  "          "   " 5.0 KM     "
S     OPDEF   AD10    6717    /  "          "   "  10 KM     "
S     SKPDF   SKAD    6724    /SKIP WHEN A/D CONVERSION FINISHED
S     OPDEF   ADCF    6722    /CLEAR A/D DONE FLAG
C
C
S     OPDEF   CLF     6725    /CLEAR INTERFACE FLAGS
S     OPDEF   CLT     6712    /CLEAR MORE INTERFACE FLAGS
S     OPDEF   LCAR    6703    /LOAD INTERFACE CURRENT ADDRESS
S     OPDEF   LWCR    6701    /LOAD INTERFACE WORD COUNT REGISTER
S     OPDEF   LCMR    6705    /LOAD INTERFACE COMMAND REGISTER
C
C
S     SKPDF   CLSK    6727    /SKIP ON 1 MSEC CLOCK FLAG
S     OPDEF   CLCF    6707    /CLEAR 1 MSEC CLOCK FLAG
C
C     TRUNCATE LAD TO A MULTIPLE OF 3
      LAD = (LAD/3)*3
C
```

```
SGOSAB, NOP
S       CLT
S       CLF
S       CLA IAC
S       TAD I \IMARK      /GET FIRST 1 MSEC NEEDED
S       CIA
S       DCA GAP           /GAP = -IMARK-1
S       CLA IAC           /ACC = +1
S       TAD I \INCH       /GET THE HT INCREMENT
S       AND KMASK         /JUST IN CASE IT WASN'T VALID, I.E. 0,1,2
S       TAD (-1           /SUBTRACT THE -1
S       TAD ADIN
S       DCA AD            /AND SET UP THE INSTRUCTION
S       TAD (200          /COMMON IS AT 200
S       LCAR              /LOAD CURRENT ADDRESS
S       CLA IAC           /IN FIELD 1
S       LCMR
S       CLA CLL
S       TAD I \LAD
S       AND LMASK         /NOT > 255!
S       CIA
S       LWCR              /LOAD WORD COUNT REGISTER
S       CLCF              /CLEAR CLOCK
SA,     CLSK              /AND WAIT
S       JMP A
S       CLA CLL CML RAR   /ACC=4000
S       LSCR              /TRIGGER TRANSMITTER (SCR BIT 0 = 01)
S       CLA
S       LSCR              /CLEAR THE SCR
SAG,    CLSK
S       JMP AG
S       CLCF
S       ISZ GAP
S       JMP AG
S       TAD DEL
S       CIA
S       DCA DUMP
SDE,    ISZ DUMP
S       JMP DE
SAD,    AD05              /UNLESS MODIFIED BY INCH
S       ADCF              /CLEAR A/D FLAG
SB,     SKAD              /SCAN COMPLETE?
S       JMP B             /NO
S       CLCF              /WAIT FOR ABOUT 16 MILLISECONDS
S       CLA CLL IAC
S       TAD N
S       CIA               /ACC = -N-1
S       DCA KOUNT
SAW,    CLSK
S       JMP AW
S       CLCF
S       ISZ KOUNT         /TIME UP?
S       JMP AW            /NO
S       CLA               /YES, EXIT WITH ACC = 0!
S       JMP \1
SN,     20                /16 MILLISECOND DELAY
SKOUNT, 0
SGAP,   0
SADIN,  AD02
SLMASK, 377
SKMASK, 0003
SDEL,   0011
SDUMP,  0
1       RETURN
        END
```

```
      SUBROUTINE DELAY(N)
C     CAUSES A DELAY OF N MILLISECONDS(N<1024)
C
S     OPDEF     CLCF     6707     /CLEAR 1 MSEC CLOCK FLAG
S     SKPDF     CLSK     6727     /SKIP ON 1 MSEC CLOCK FLAG
S     CLA
S       TAD I \N
S     CIA
S       CLCF
SA,     CLSK
S     JMP A
S       CLCF
S     IAC
S     SZA
S     JMP A
      CONTINUE
      RETURN
      END
```

SUBROUTINE ADNOT(LAD, IMARK, INCH)

This subroutine takes the same arguments as ADCOM. It is identical to ADCOM except that the two statements:

```
S     CLA CLL CML RAR        /ACC = 4000
S     LSCR                   /TRIGGER TRANSMITTER
```

Are not included. It is used to sample the background signal without triggering the transmitter.

Subroutine ADCOM was written by Dr Fraser.

APPENDIX I

TIME SERIES OF D-REGION ELECTRON DENSITIES, METEOROLOGICAL VARIABLES IN THE STRATOSPHERE, AND GEOMAGNETIC INDICES

MAGNETIC INDEX (ΣK) FØR AMBERLEY — WINTER 1972

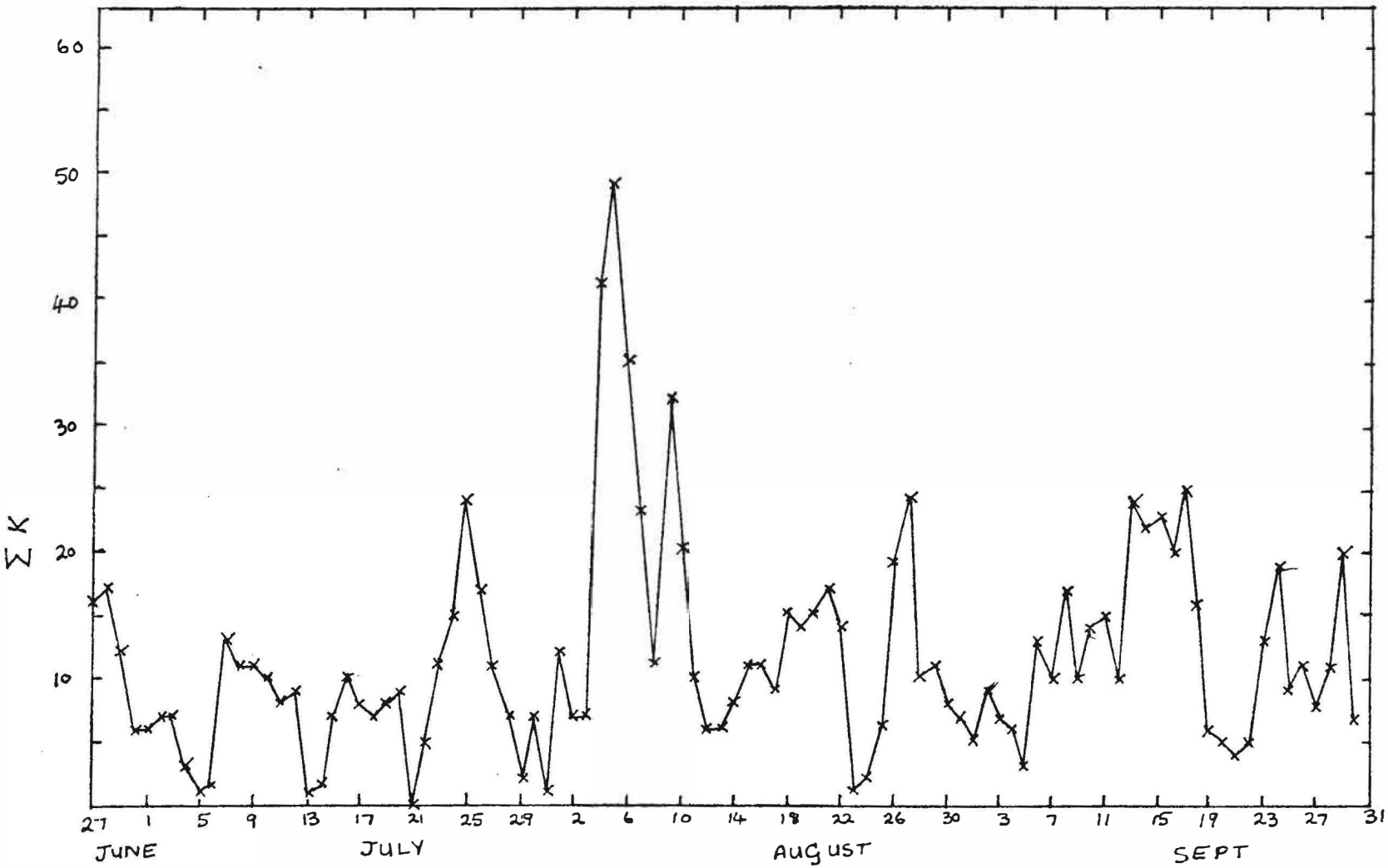

FIG I1

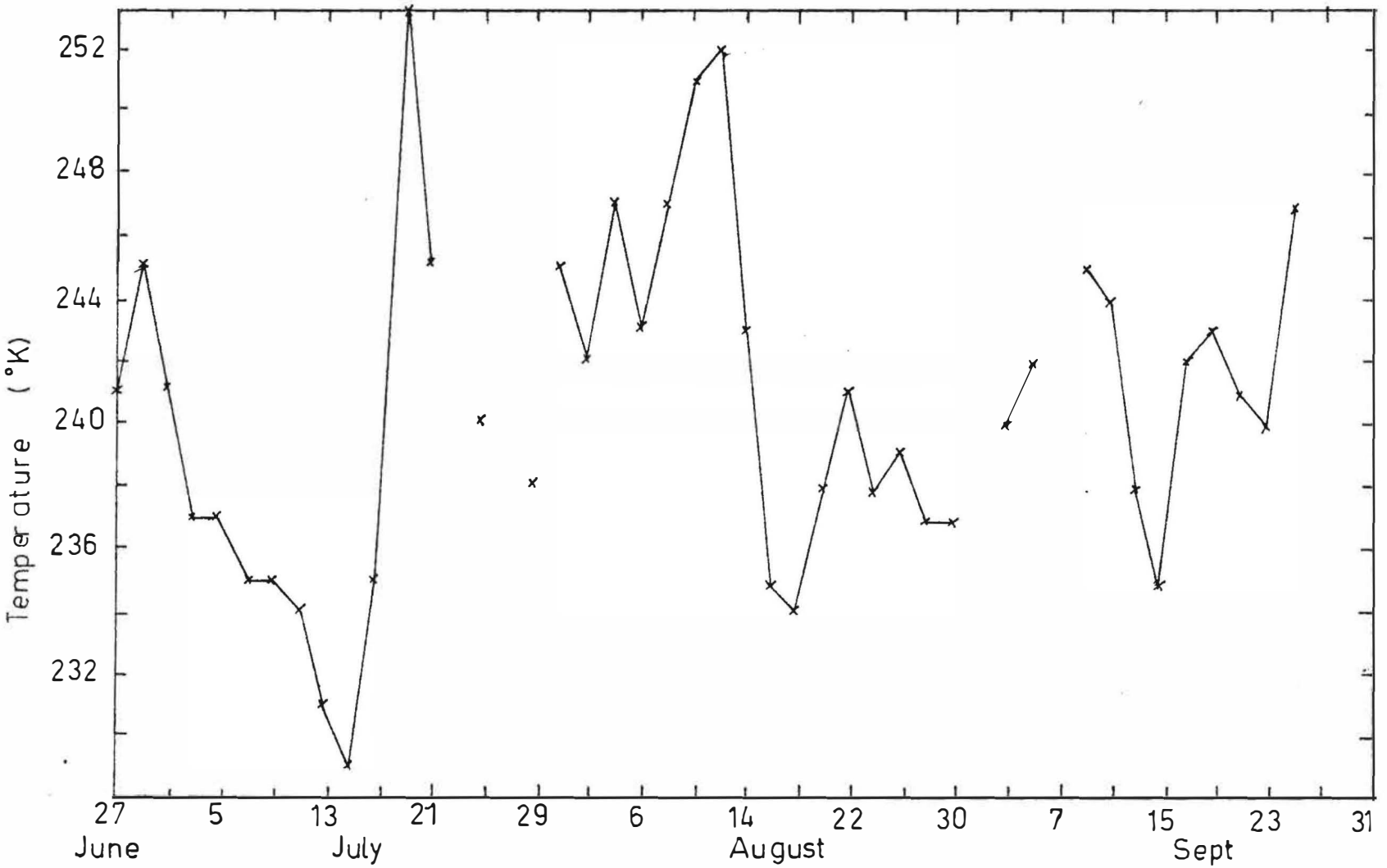

Fig I2 Nimbus IV S.C.R. : Channel A. 1972.

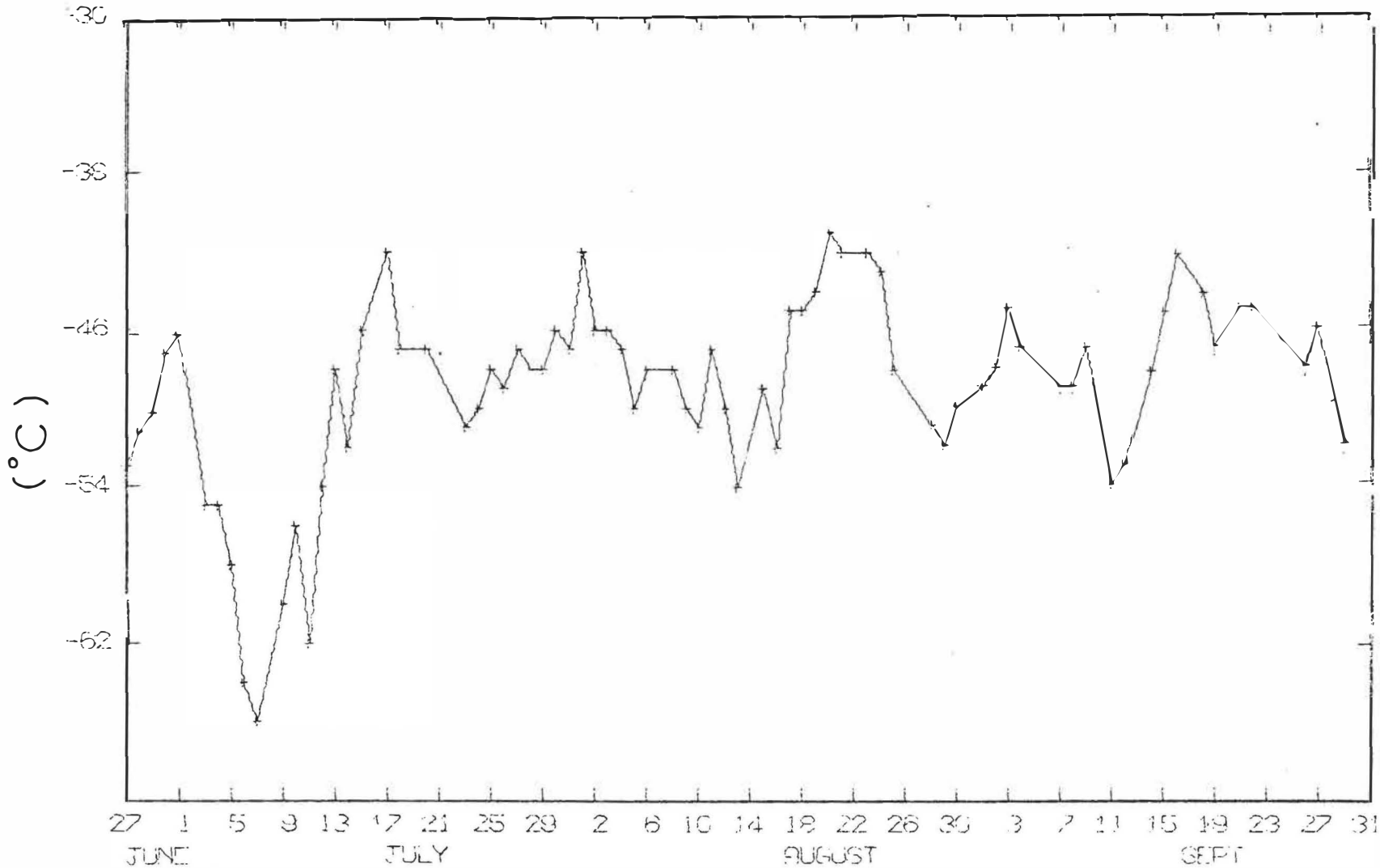

Fig I3 DAILY TEMP FOR 20 MB SURFACE, 1972

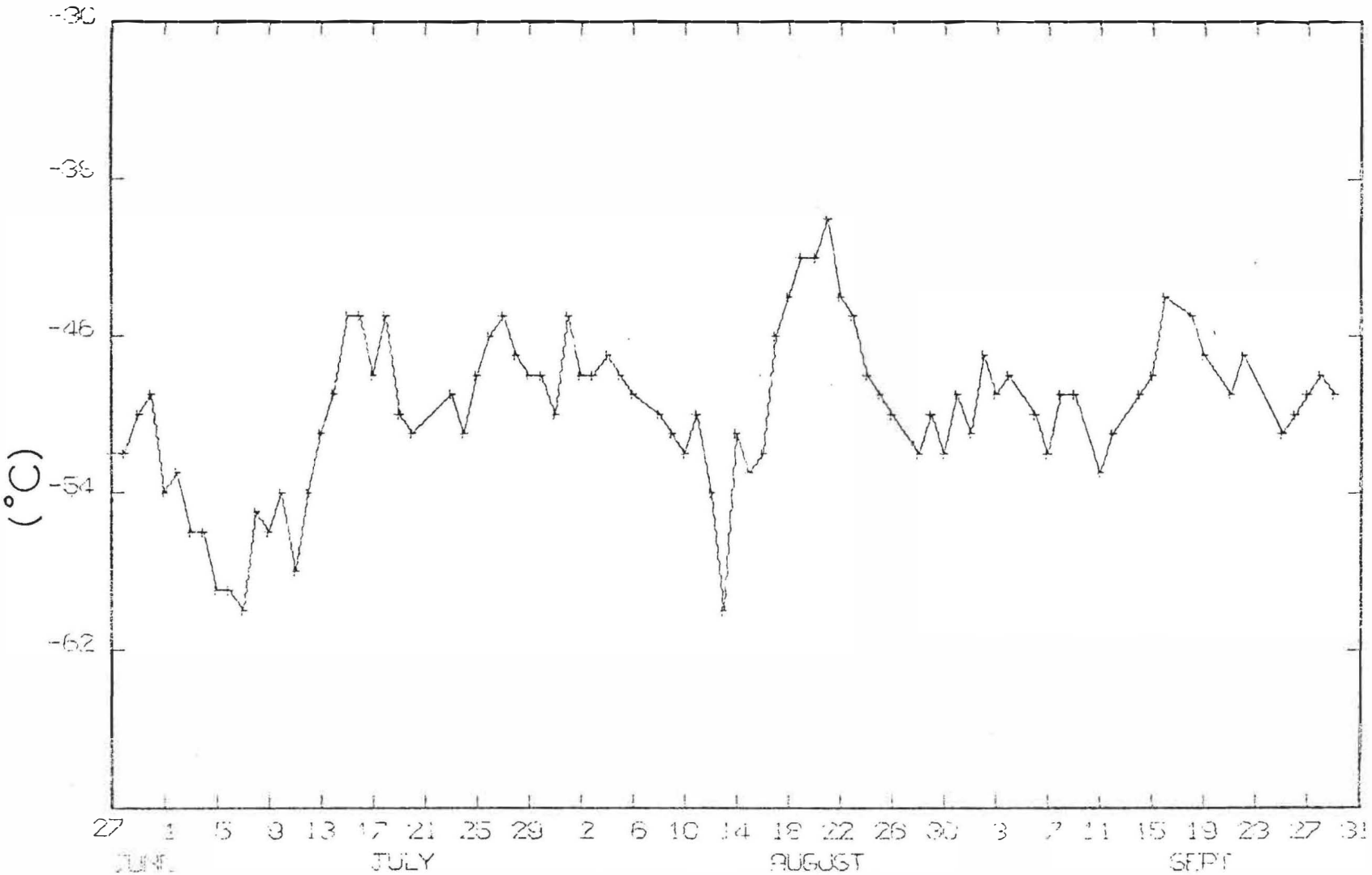

Fig I4 DAILY TEMP FOR 30 MB SURFACE, 1972

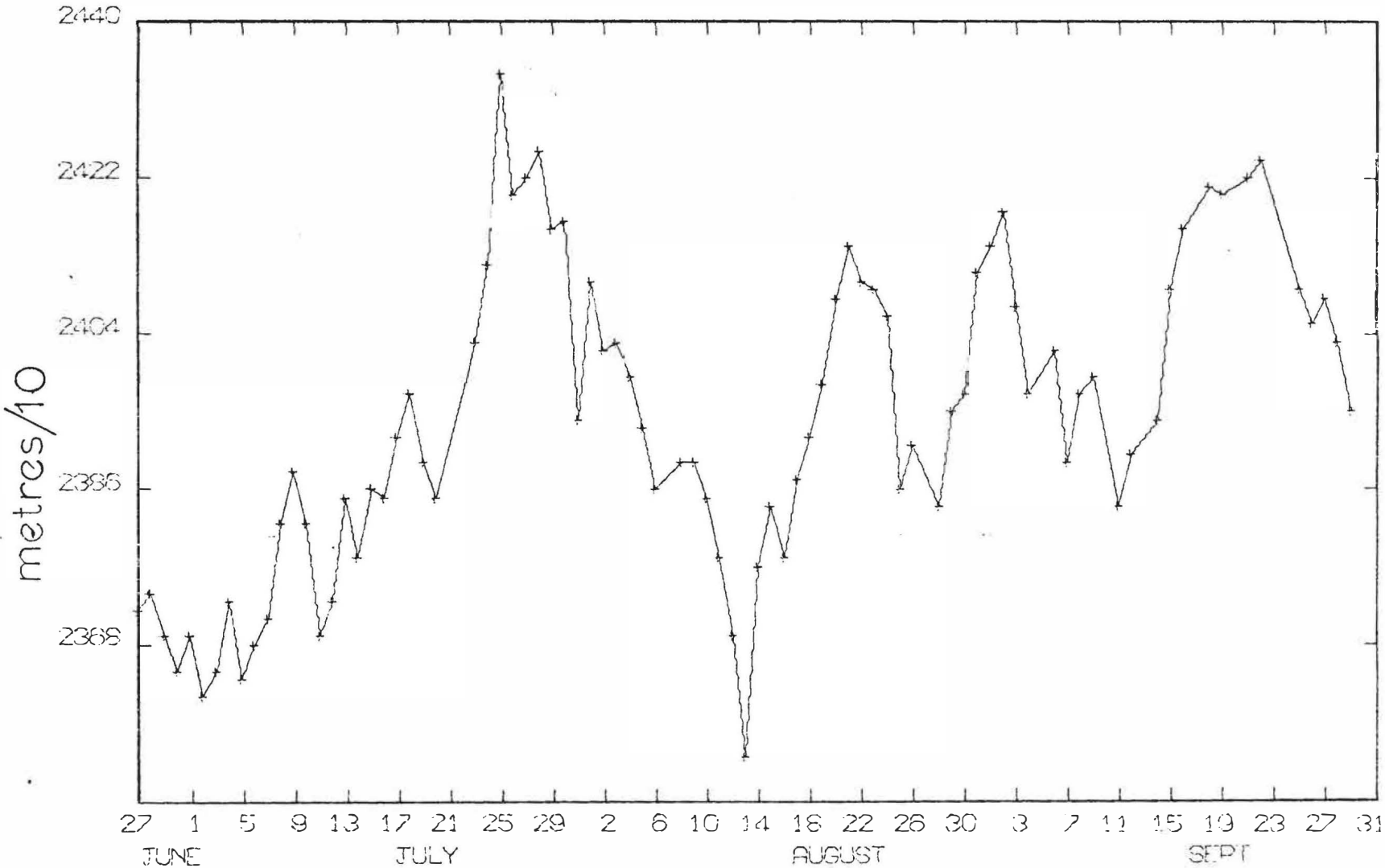

Fig I5 DAILY HEIGHT FOR 30 MB SURFACE, 1972

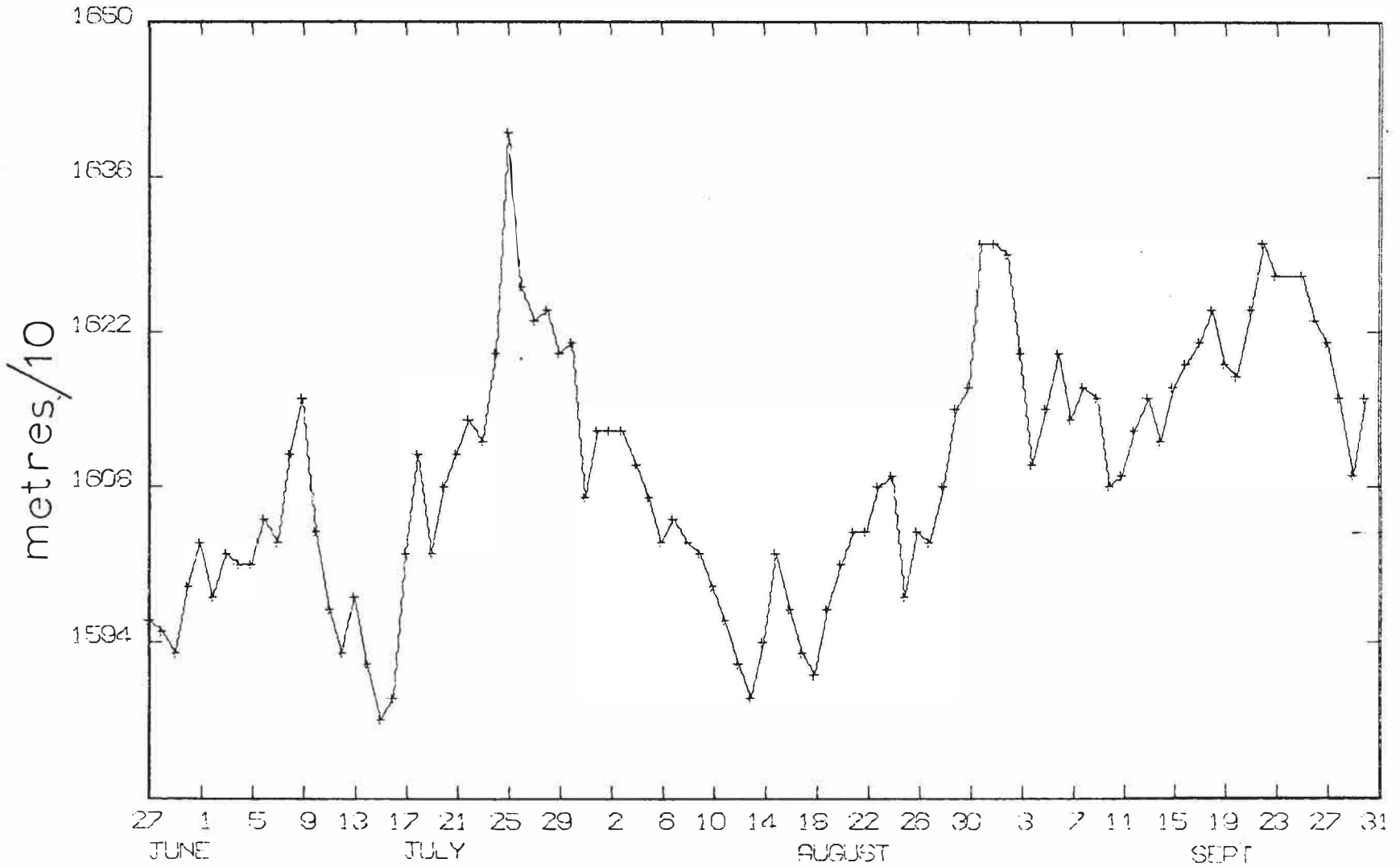

Fig I6 DAILY HEIGHT FOR 100 MB SURFACE, 1972

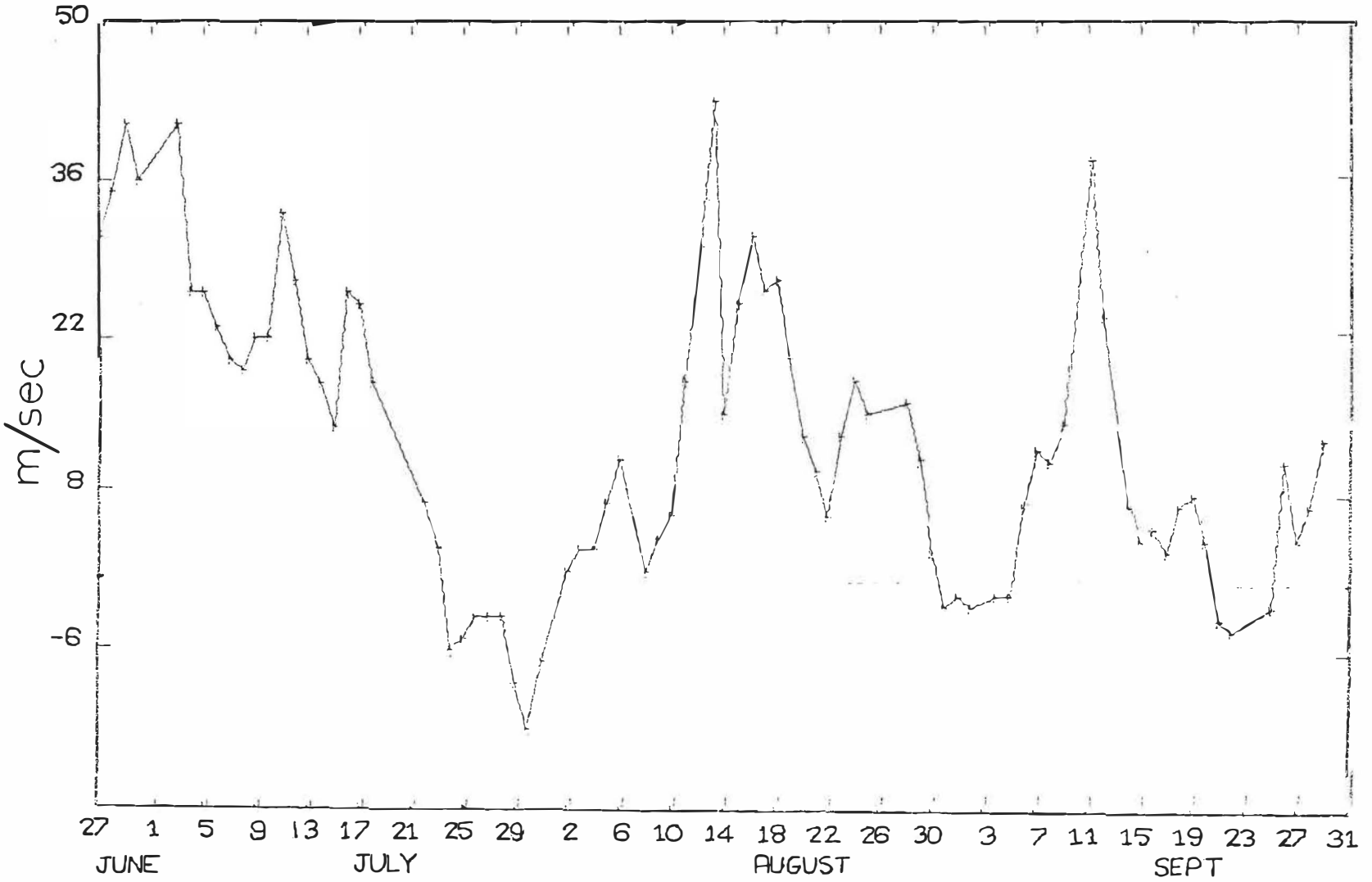

Fig I7 DAILY ZONAL WINDS AT 25 KM, 1972

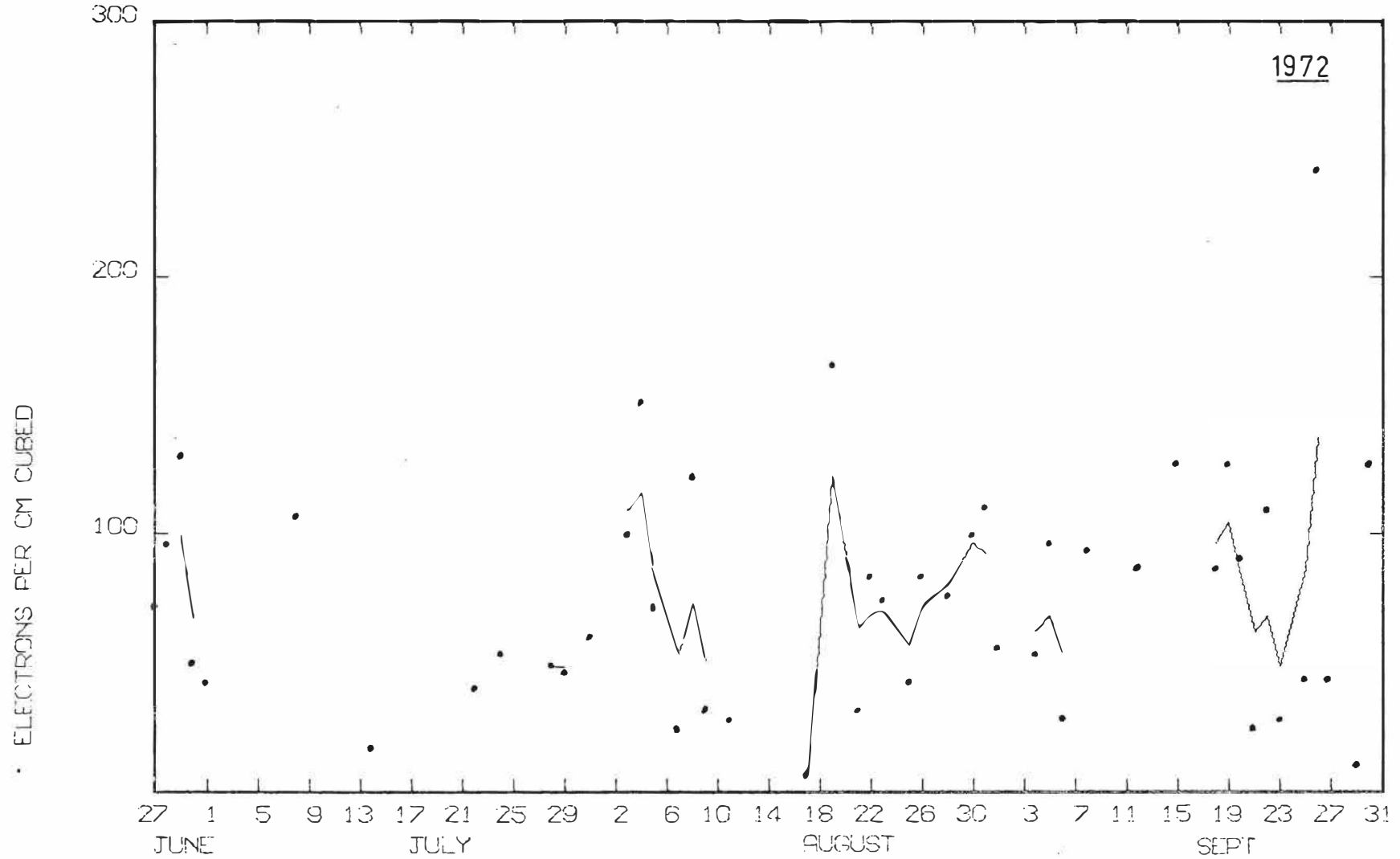

Fig I8 DAILY ELECTRON DENSITIES FOR 66.5 TO 69.0 KM

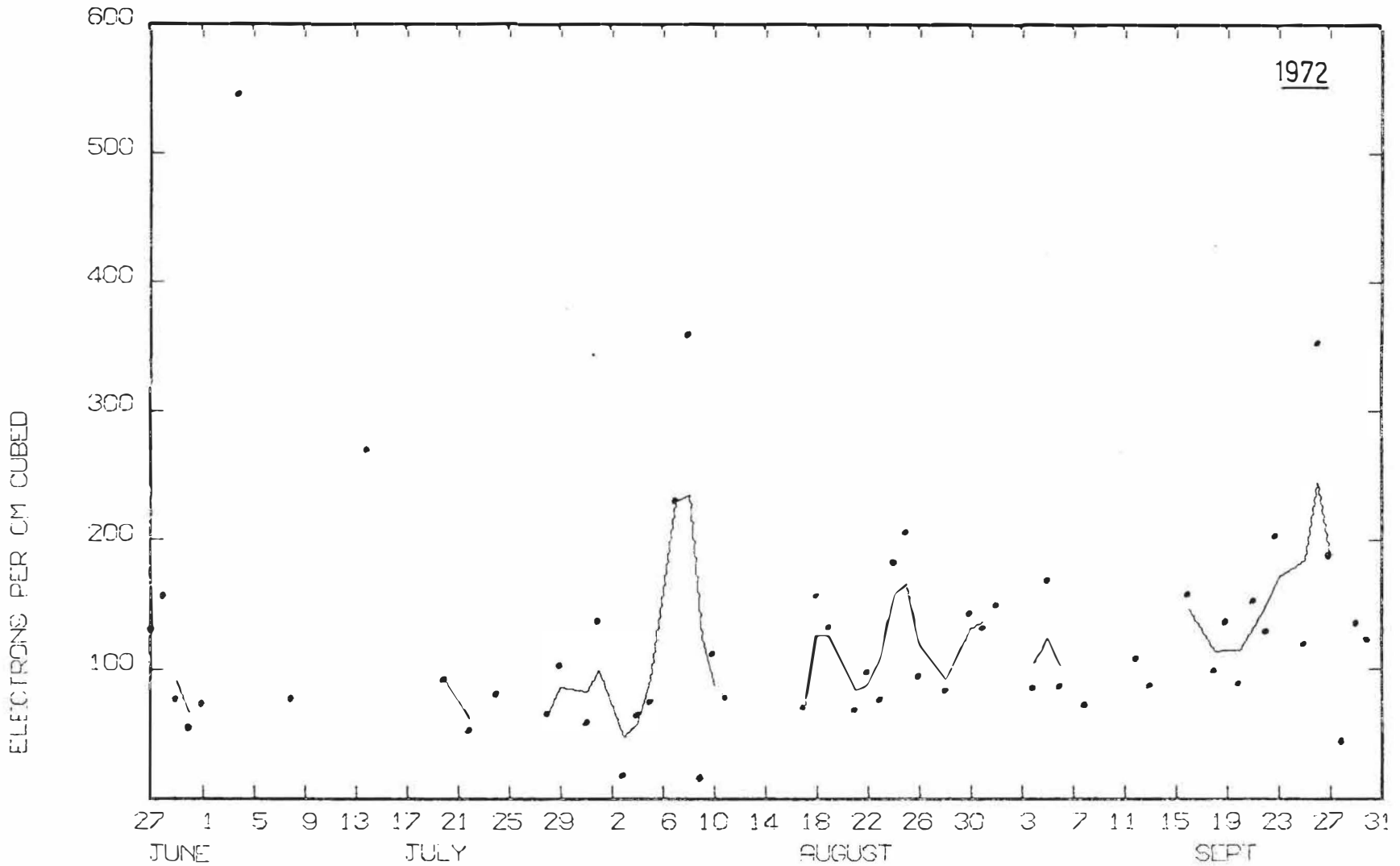

Fig I9 DAILY ELECTRON DENSITIES FOR 69.0 TO 71.5 KM

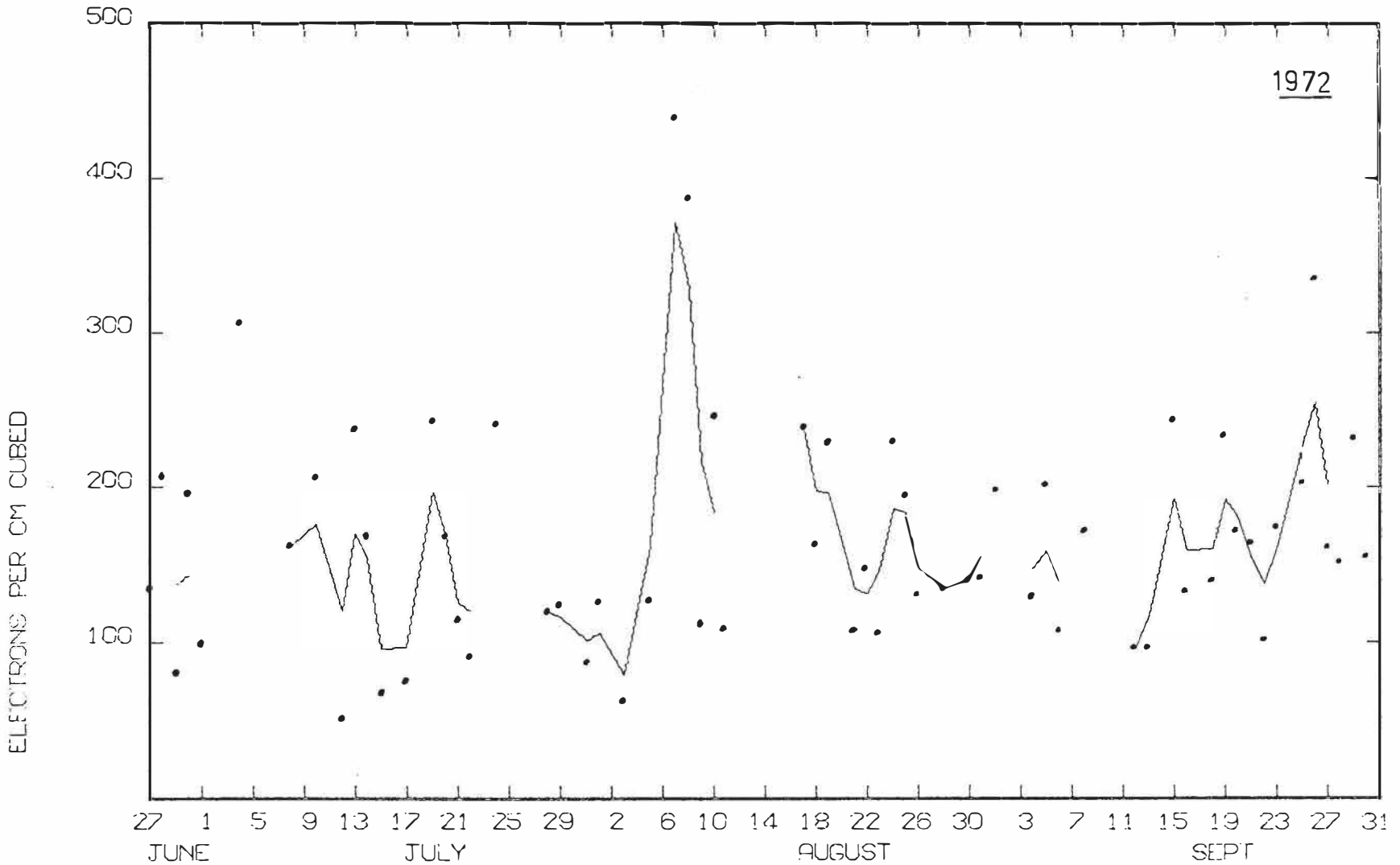

Fig I10 DAILY ELECTRON DENSITIES FOR 71.5 TO 74.0 KM

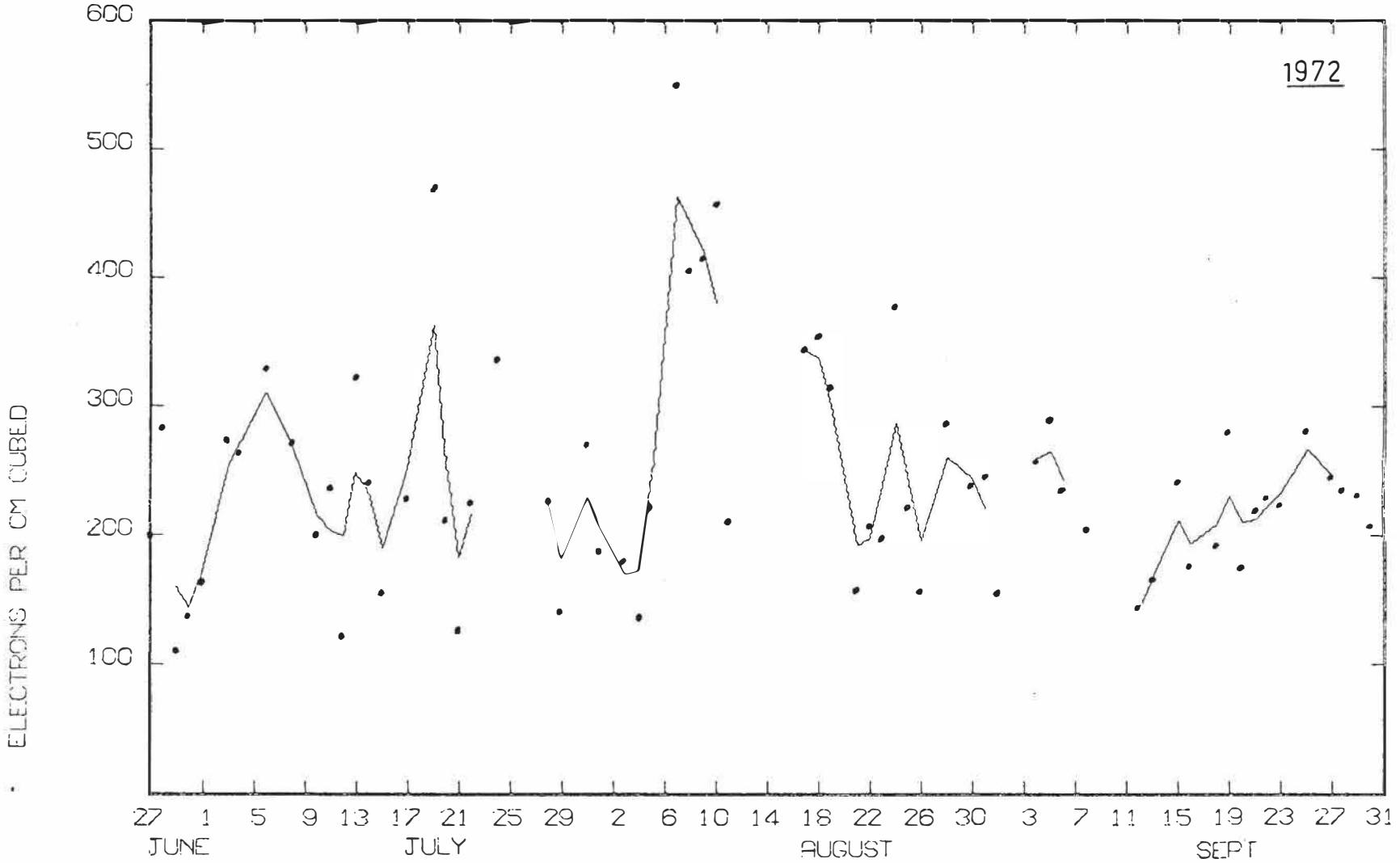

Fig I11 DAILY ELECTRON DENSITIES FOR 74.0 TO 76.5 KM

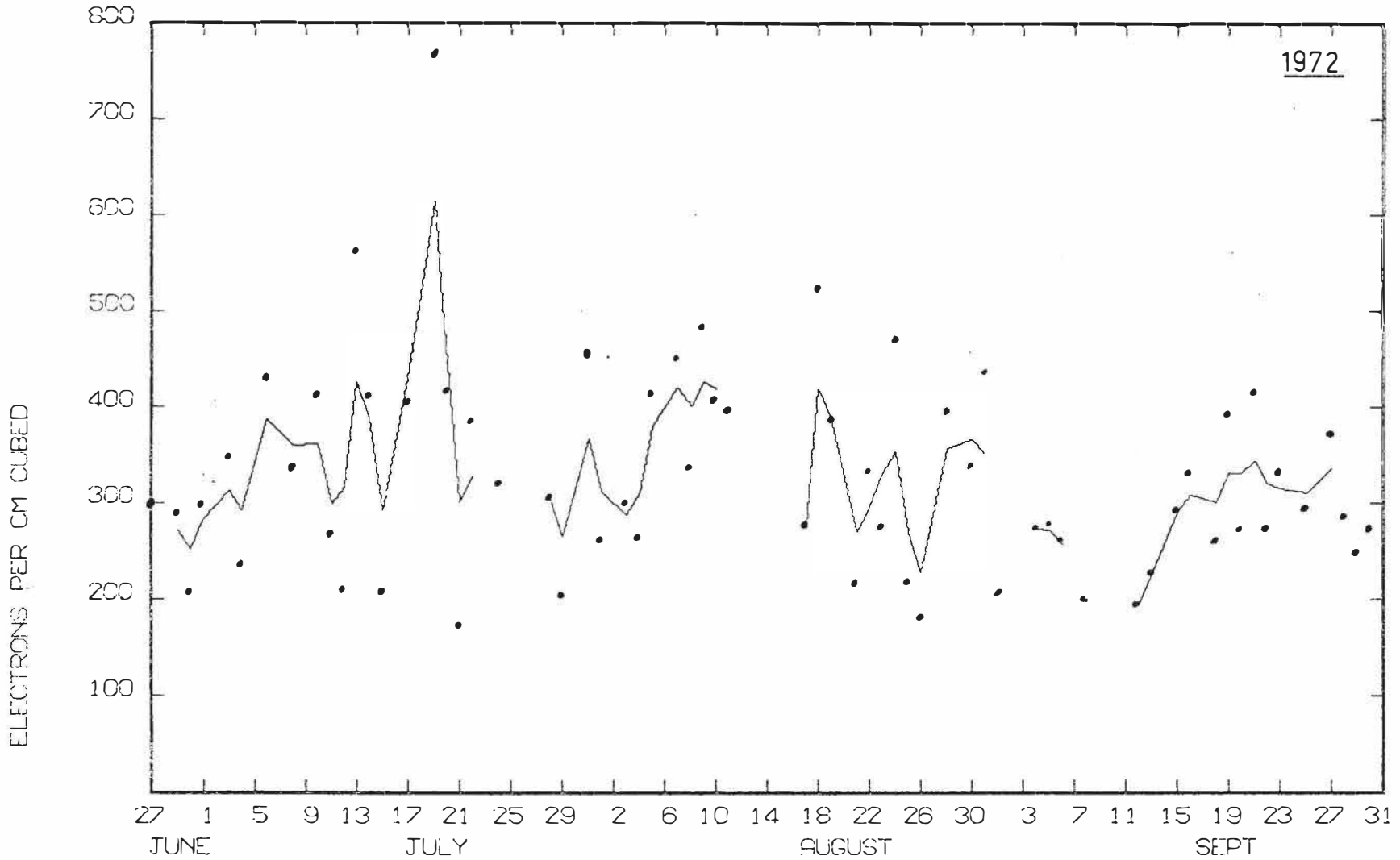

Fig I12 DAILY ELECTRON DENSITIES FOR 76.5 TO 79.0 KM

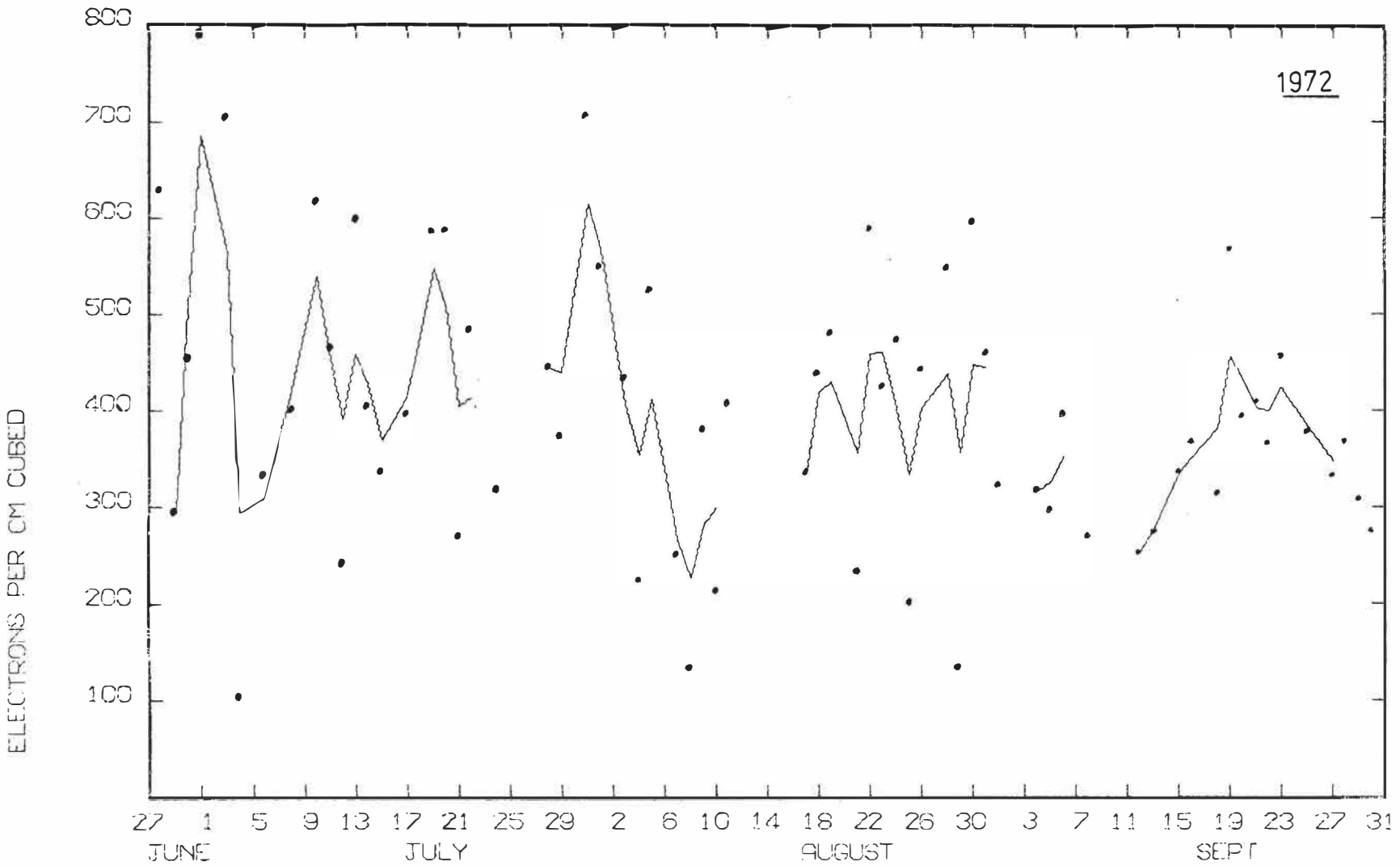

Fig I13 DAILY ELECTRON DENSITIES FOR 79.0 TO 81.5 KM

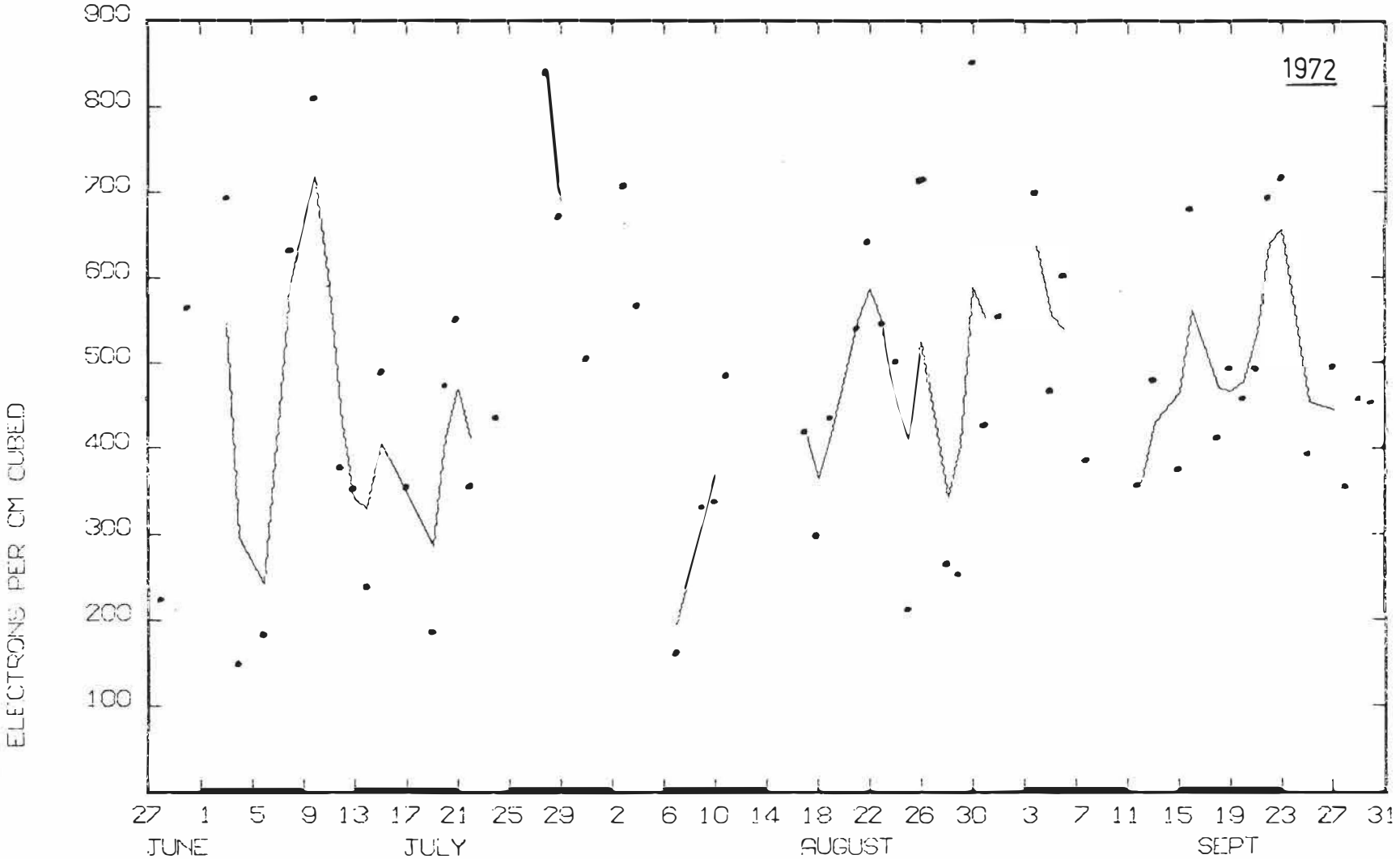

Fig I14 DAILY ELECTRON DENSITIES FOR 81.5 TO 84.0 KM

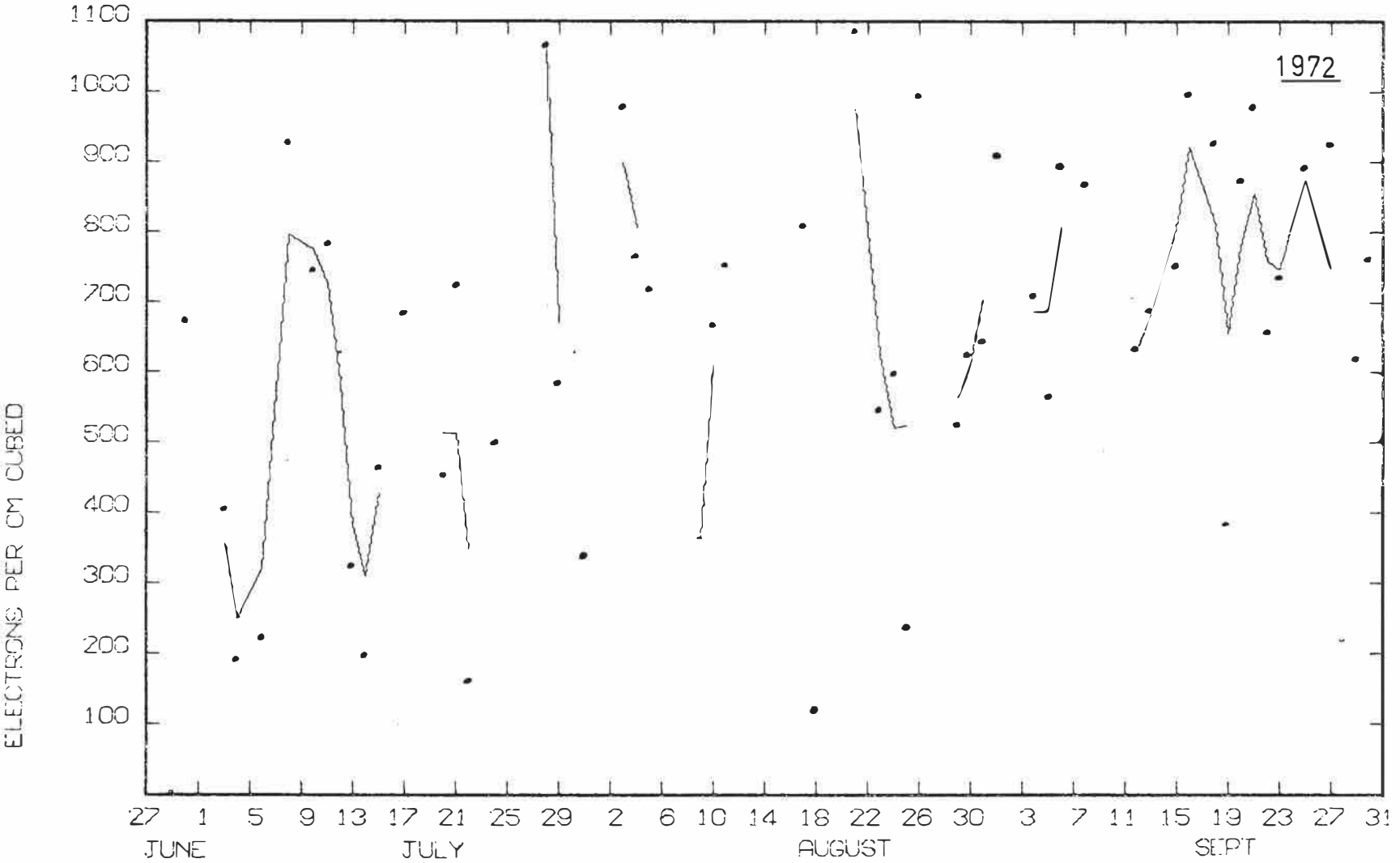

Fig I15 DAILY ELECTRON DENSITIES FOR 84.0 TO 86.5 KM

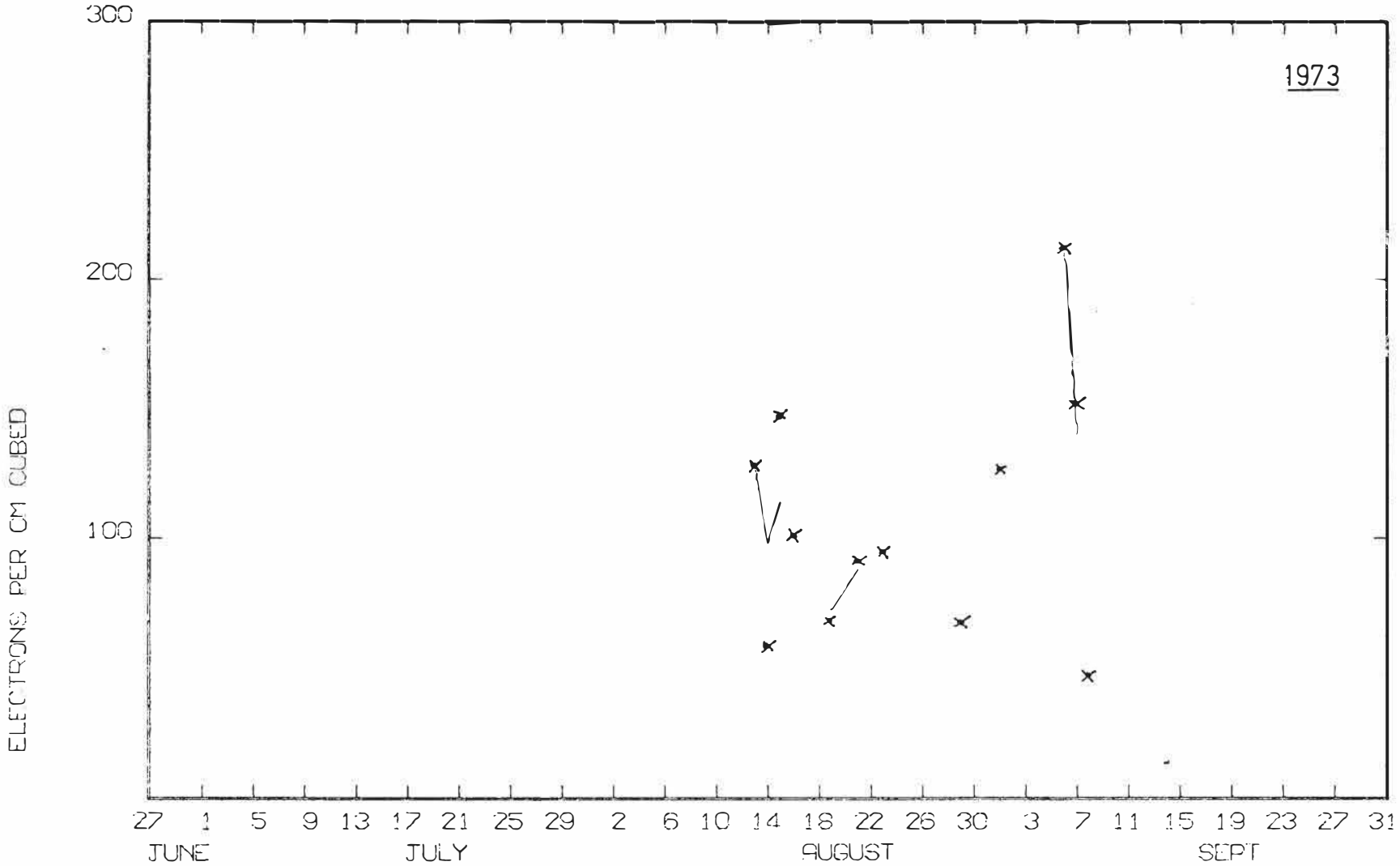

Fig I16 DAILY ELECTRON DENSITIES FOR 69.0 TO 71.5 KM

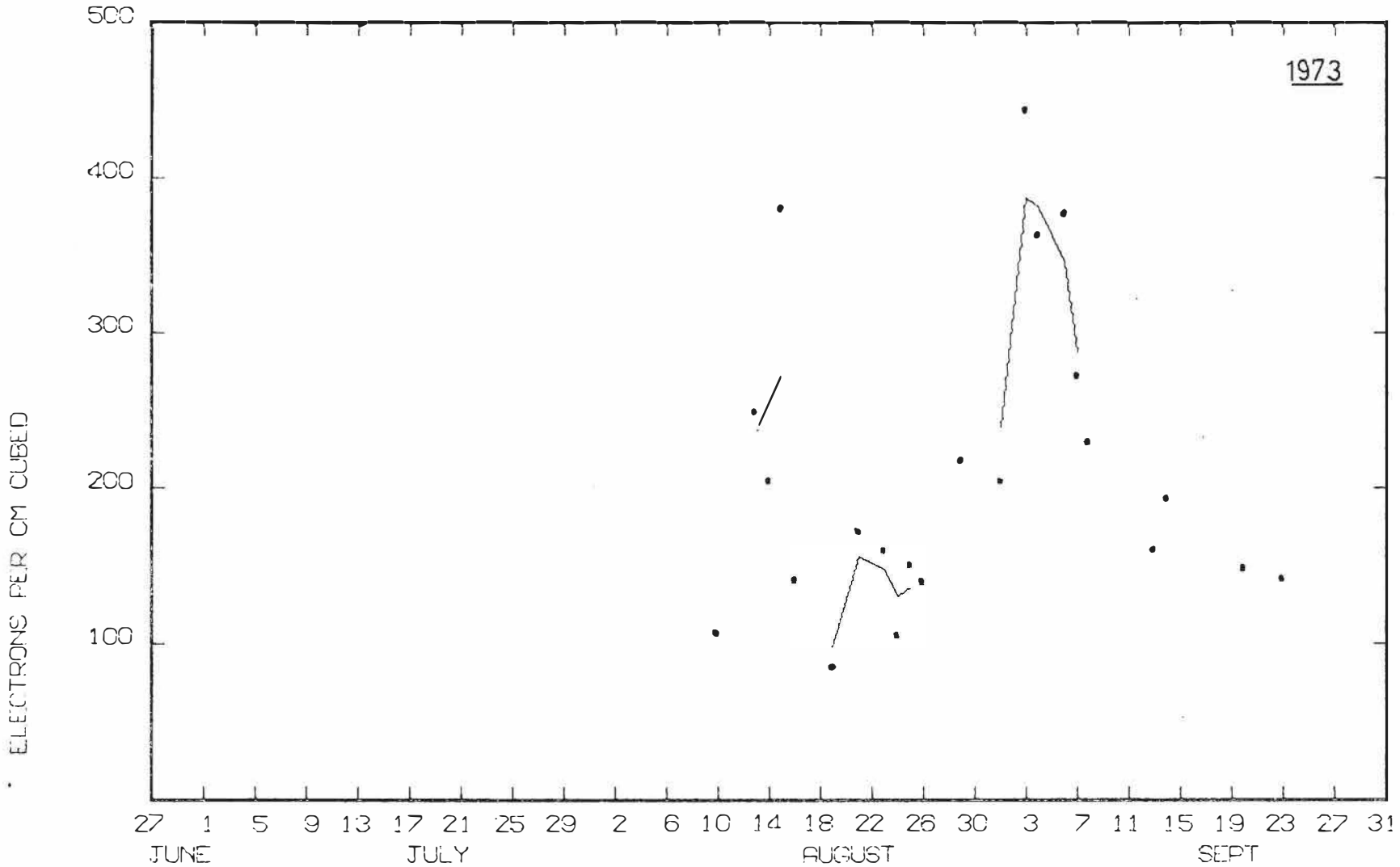

Fig I17 DAILY ELECTRON DENSITIES FOR 71.5 TO 74.0 KM

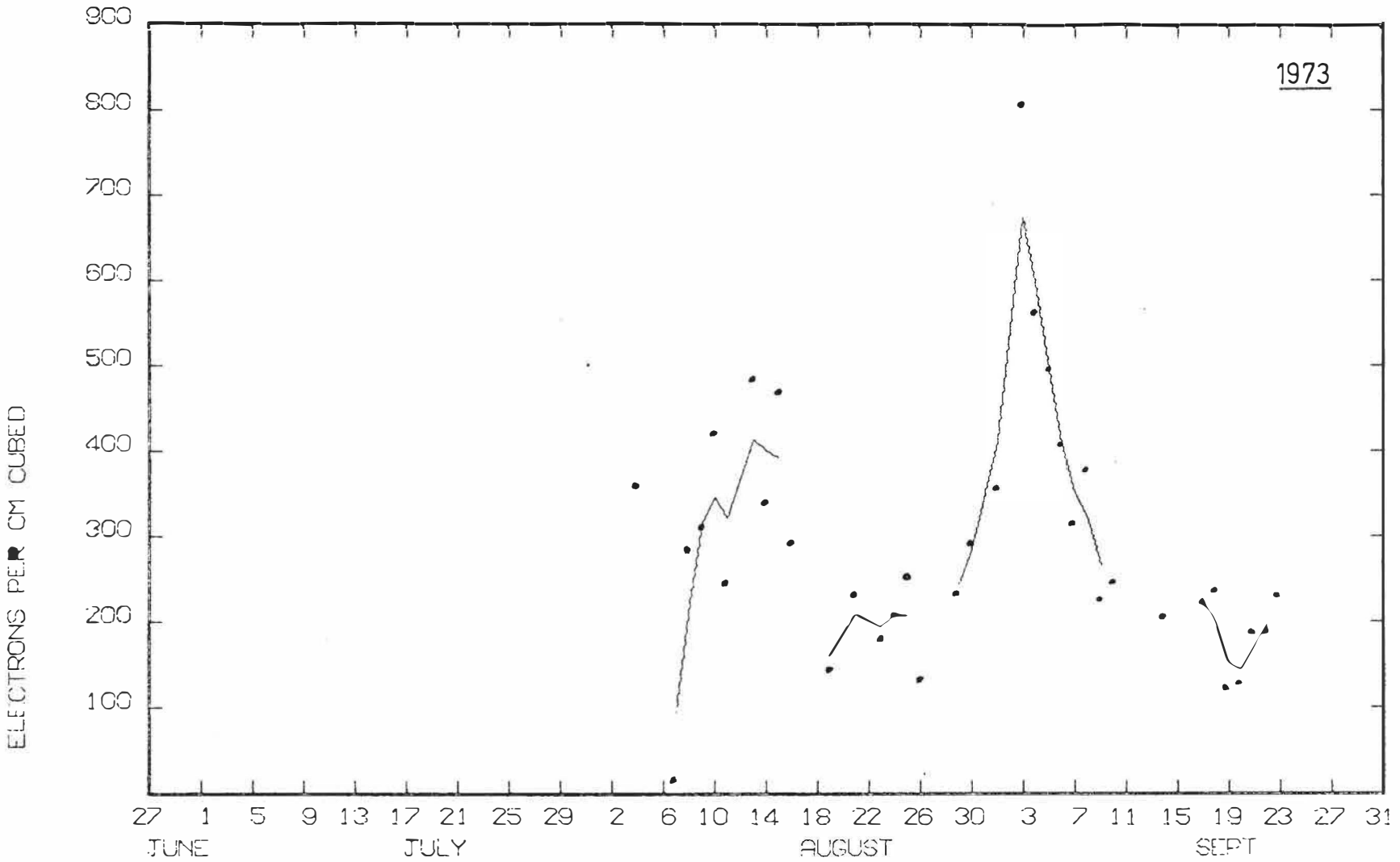

Fig I18 DAILY ELECTRON DENSITIES FOR 74.0 TO 76.5 KM

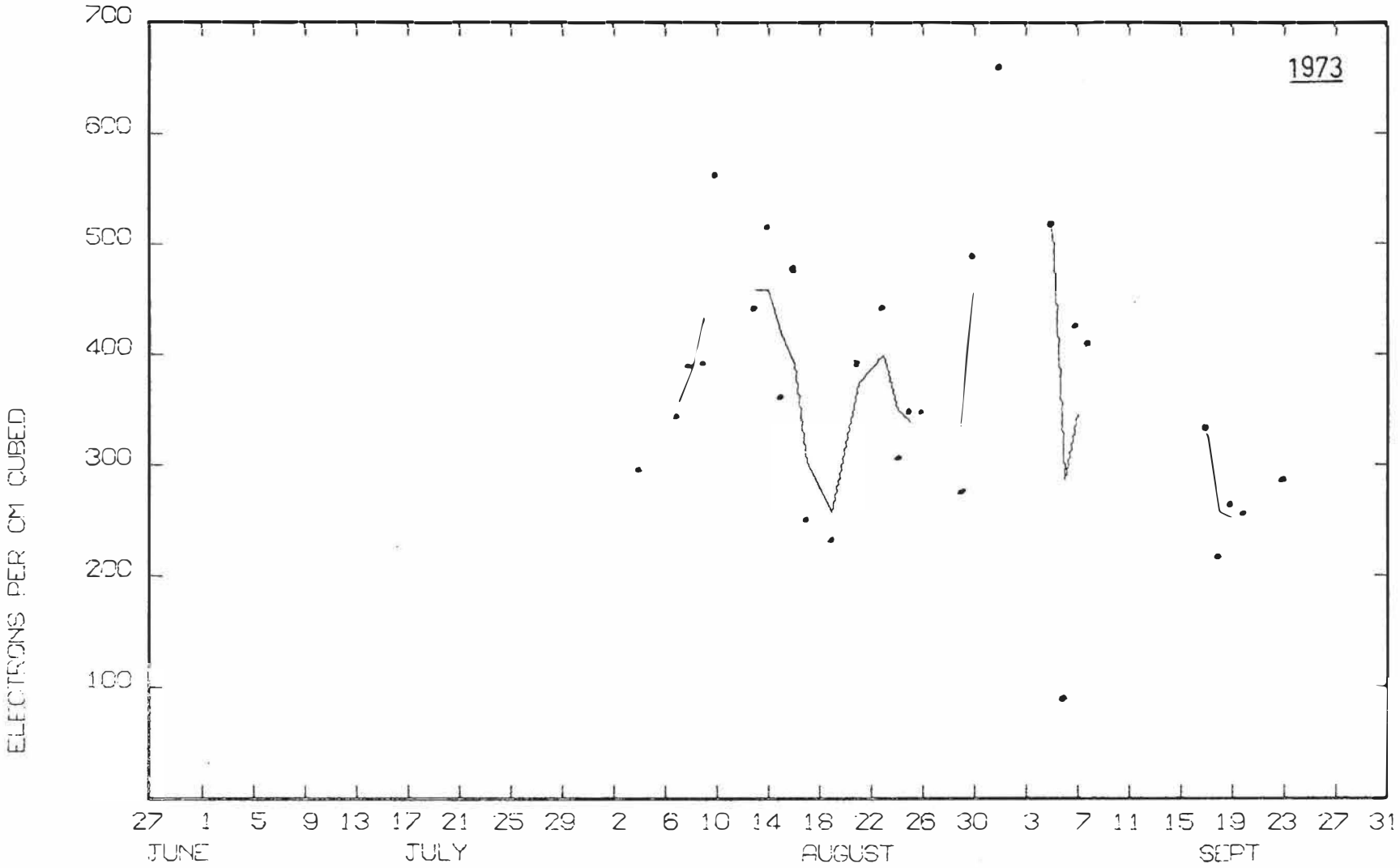

Fig I19 DAILY ELECTRON DENSITIES FOR 76.5 TO 79.0 KM

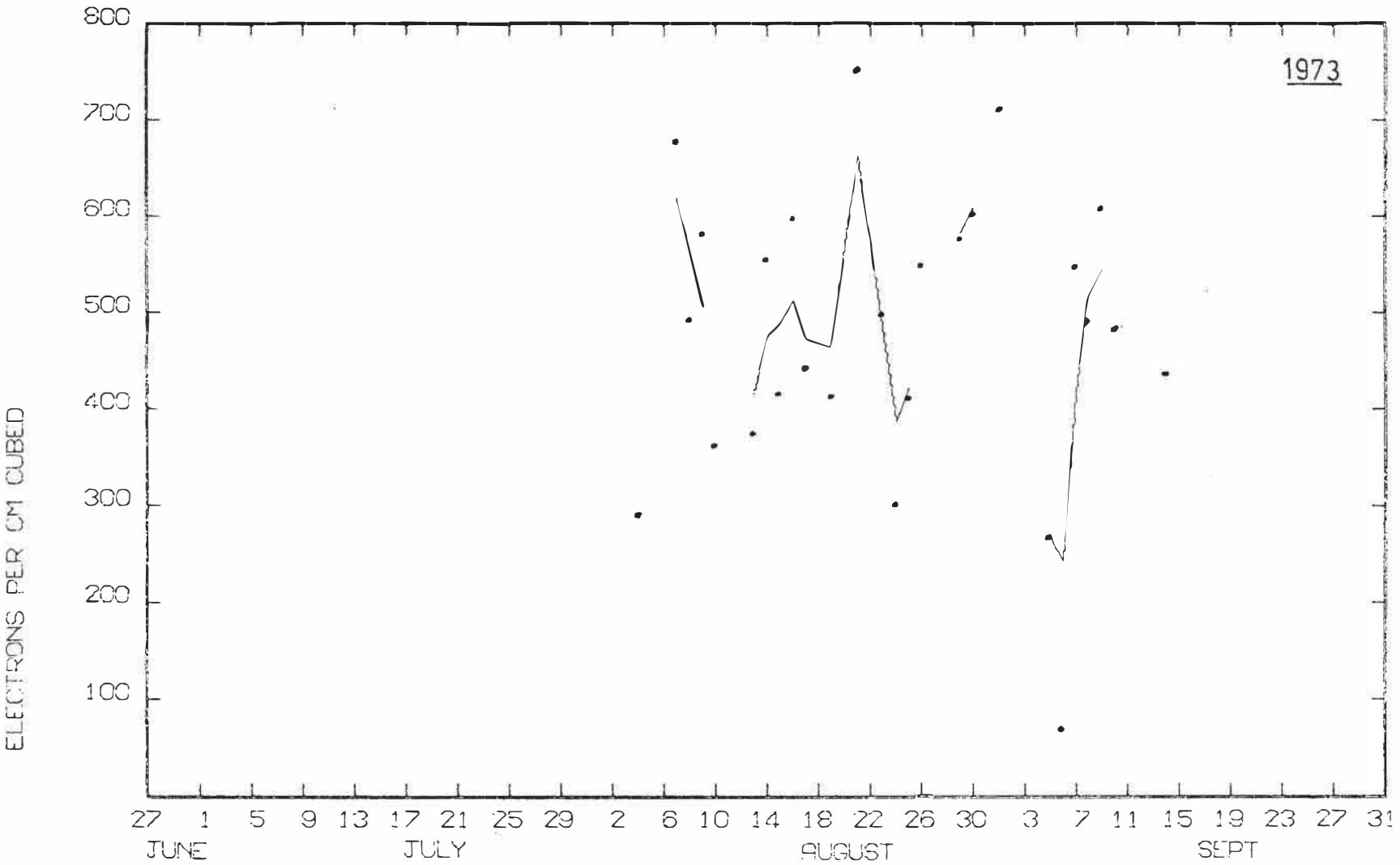

Fig I20 DAILY ELECTRON DENSITIES FOR 79.0 TO 81.5 KM

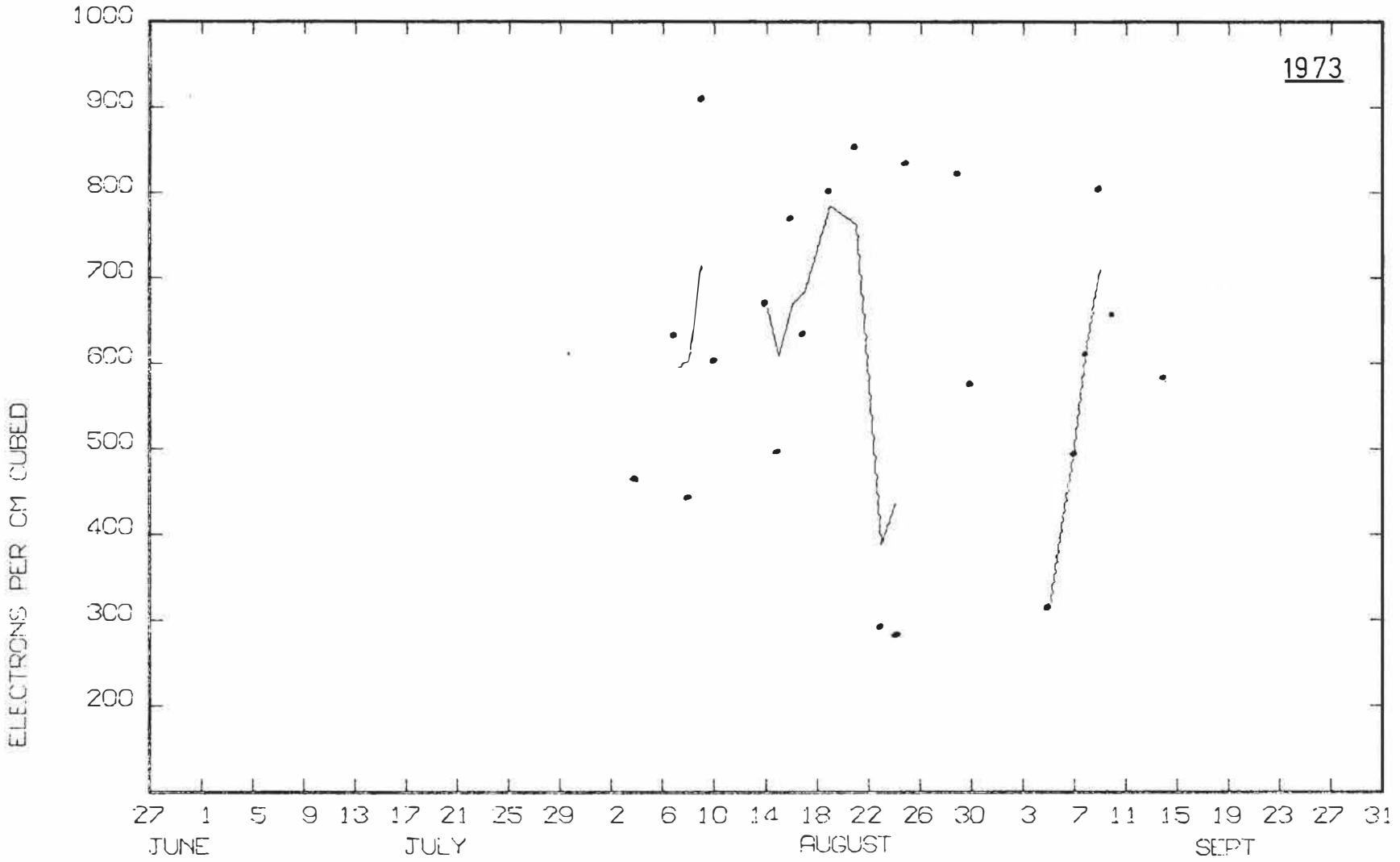

Fig I21 DAILY ELECTRON DENSITIES FOR 81.5 TO 84.0 KM

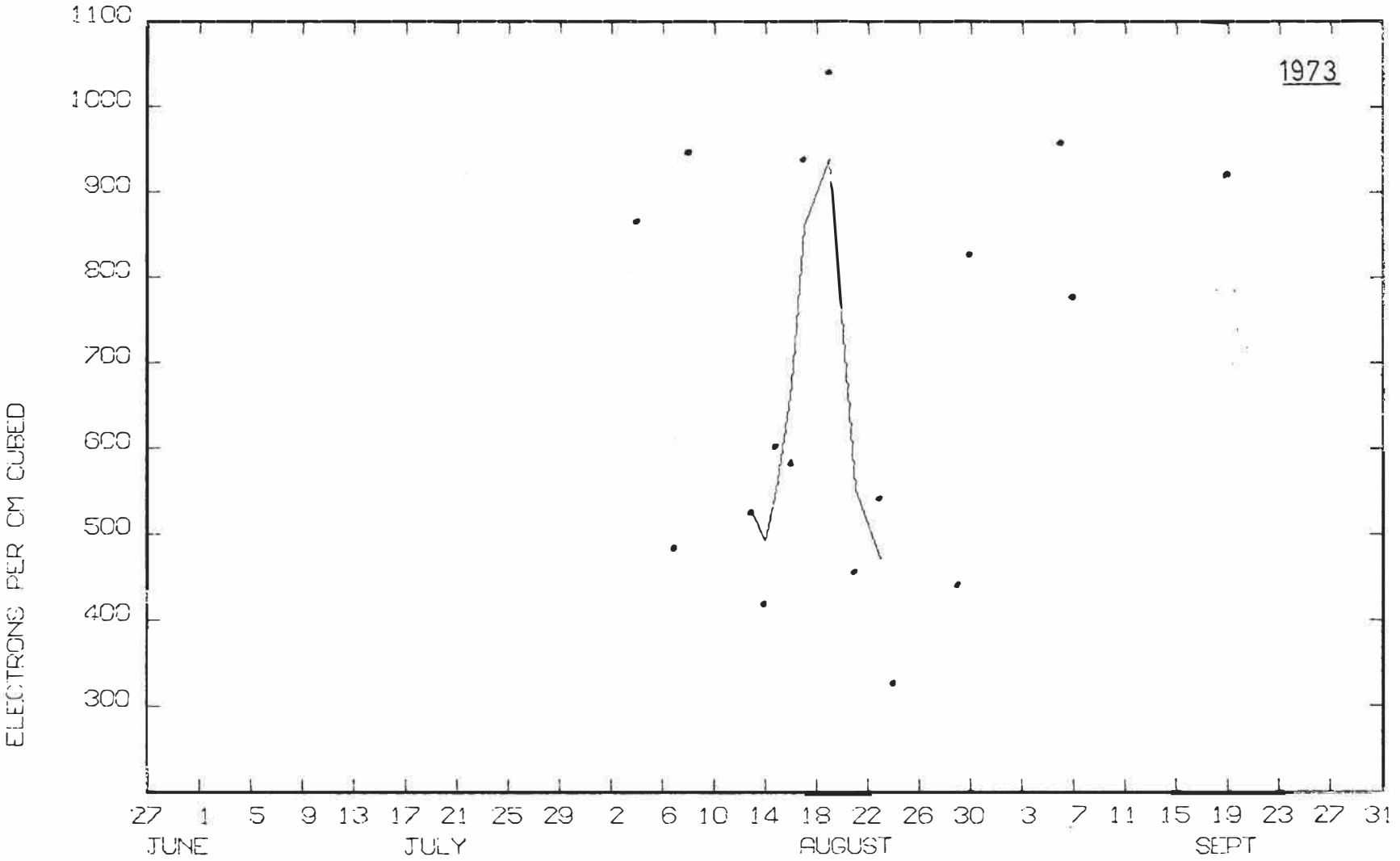

Fig I22 DAILY ELECTRON DENSITIES FOR 84.0 TO 86.5 KM

REFERENCES

AIKEN A.C. 1972 : The relationship of theory and experiment in the D-region. J. Atmos. Terr. Phys. 34, 1591.

APPLETON E.V. 1937 : Regularities and irregularities in the ionosphere - I. Proc. R. Soc. A162, 451.

APPLETON E.V. and PIGGOT W.R. 1954 : Ionospheric absorption measurements during a sunspot cycle. J. Atmos. Terr. Phys. 5, 141.

AUSTIN G.L. 1966 : Measurements of lower ionosphere refractive indices. Thesis, M.Sc., University of Canterbury.

AUSTIN G.L. 1969 : Studies of irregularities in electron concentration in the upper atmosphere. Thesis, Ph.D., University of Canterbury.

AUSTIN G.L. 1971 : A direct measuring differential phase experiment. J. Atmos. Terr. Phys. 33, 1667.

AUSTIN G.L. and MANSON A.H. 1969 : On the nature of the irregularities that produce partial reflections of radio waves from the lower ionosphere (70-100 km). Radio Sci. 4, 35.

BARNETT J.J., CROSS M.J., HARWOOD R.S., HOUGHTON J.T., MORGAN C.G., PECKHAM G.E., RODGERS C.D., SMITH S.D., WILLIAMSON E.J. 1972 : The first year of the selective chopper radiometer on Nimbus 4. Q. Jl. R. Met. Soc. 98, 17

BELROSE J.S. 1963 : AGARDograph 74 : Propagation of radio waves at frequencies below 300 kc/s. (W.T. Blackband editor). Pergamon Press, Oxford.

BELROSE J.S. 1967 : The "Berlin" warming. Nature 214, 660.

BELROSE J.S. 1970 : Radio wave probing of the ionosphere by the partial reflection of radio waves. J. Atmos. Terr. Phys. 32, 567.

BELROSE J.S. and BURKE M.J. 1964 : Study of the lower ionosphere using partial reflection - I. Experimental technique and method of analysis. J. Geophys. Res. 69, 2799.

BELROSE J.S., BURKE M.J., COYNE T.N.R., REED J.E. 1972b : D-region measurements with the differential-absorption differential-phase partial reflection experiment. J. Geophys. Res. 77, 4829.

BELROSE J.S., ROSS D.B., McNAMARA A.G. 1972a : Ionozation changes in the lower ionosphere during the solar eclipse of 7 March 1970. J. Atmos. Terr. Phys. 34, 627.

BELROSE J.S., THOMAS L. 1968 : Ionization changes in the middle latitude D-region associated with geomagnetic storms. J. Atmos. Terr. Phys. 30, 1397.

BENDAT J.S. and PIERSOL A.G. 1971 : Random data : Analysis and measurement procedures. John Wiley & Sons, New York, 1971.

BETHE H.A. and ASHKIN J. 1953 : Passage of radiations through matter. In Experimental nuclear physics volume 1 (E. Segrè editor). Wiley, New York.

BEYNON W.J.G. and JONES E.S.O. 1965a : Seasonal variations in the lower and upper atmosphere. Nature 206, 1243.

BEYNON W.J.G. and JONES E.S.O. 1965b : Meteorological influences in ionospheric absorption measurements. Proc. R. Soc. A288, 558.

BOSSALASCO M. and ELENA A. 1963 : Absorption de la couche D et temperature de la mesosphere. C. R. Hebd. Seanc. Acad. Sci. Paris 256, 4491.

BOURNE I.A. and HEWITT L.W. 1968 : The dependence of ionospheric absorption of MF radio waves at mid-latitudes on planetary magnetic activity. J. Atmos. Terr. Phys. 30, 1381.

BOWMAN M.R., THOMAS L., GEISLER J.E. (1970) : The effect of diffusion processes on the hydrogen and oxygen constituents in the mesosphere and lower thermosphere. J. Atmos. Terr. Phys. 32, 1661.

BROWN G.M. and WILLIAMS D.C. (1971) : Pressure variations in the stratosphere and ionosphere. J. Atmos. Terr. Phys. 33, 1321.

BUDDEN K.G. 1961 : Radio waves in the ionosphere. Cambridge University Press, London.

BUDDEN K.G. 1965 : Effect of electron collisions on the formulas of magnetoionic theory. Radio Sci. 69D, 191.

CAMPBELL W.H. and MATSUSHITA S. 1967 : World maps of conjugate coordinates and L contours. J. Geophys. Res. 72, 3519.

CHAMBERLAIN J.W. 1961 : Physics of the aurora and airglow, Academic Press, London and New York.

CHAMPION K.S.W. 1967 : The lower thermosphere. Space Research VII, 1101. North Holland Publ. Co., Amsterdam.

CHARNEY J.G. and DRAZIN P.G. 1961 : Propagation of planetary-scale disturbances from the lower into the upper atmosphere. J. Geophys. Res. 66, 83.

CHRISTIE A.D. 1970 : D-region winter anomaly and transport near the mesopause. J. Atmos. Terr. Phys. 32, 35.

CIRA 1965 : COSPAR international reference atmosphere. North Holland Publ. Co., Amsterdam.

CLARK J.H.E 1972 : The vertical propagation of forced atmospheric planetary waves. Jnl. Atmos. Sci. 29, 1430.

COLLINS W.C., HERZBERG L. 1965 : Solar activity and short lived terrestrial effects (SID). In Physics of the earths upper atmosphere (ed. Hines and others). Page 198. Prentice Hall, Englewood Cliffs, N.J.

CONNOLLY D.J., TANENBAUM R.S. 1972a : Partial reflection of radio waves from the lower ionosphere. NASA TN D-6742.

CONNOLLY D.J., TANENBAUM R.S. 1972b : Mode coupling in partial reflections from the ionosphere at vertical incidence. Radio Sci. 7, 457.

COYNE T.N.R., BELROSE J.S. 1973 : An investigation into the effects of limited height resolution in the differential absorption partial reflection experiment. J. Geophys. Res. 78, 8276.

DAVIES K. 1966 : Ionospheric radio propagation. Dover, New York.

DELAND R.J., CAVALIERI D.J. 1973 : Planetary scale fluctuations of pressure in the E-layer, f_{min}, and pressure in the stratosphere. J. Atmos. Terr. Phys. 35, 125.

DELAND R.J., FRIEDMAN R.M. 1972 : Correlation of fluctuations of ionospheric absorption and atmospheric planetary scale waves. J. Atmos. Terr. Phys. 34, 295.

DELAND R.J., JOHNSON K.W. 1968 : A statistical study of the vertical structure of travelling planetary-scale waves. Mon. Weather Rev. 96, 12.

DICKINSON R.E. 1969 : Vertical propagation of planetary Rossby waves through an atmosphere with Newtonian Cooling. J. Geophys. Res. 74, 929.

DIEMINGER W. 1952 : Über die Ursache der exzessiven Absorption in der Ionosphäre an Wintertagen. J. Atmos. Terr. Phys. 2, 340.

EPSTEIN P.S. 1939 : Reflection of waves in an inhomogeneous absorbing medium. Proc. Natn. Acad. Sci. U.S.A. 16, 627.

FERGUSON E.E. 1971 : D-region ion chemistry. Rev. Geophys. & Space Phys. 9, 997.

FLOOD W.A. 1968 : Revised theory for partial reflection D-region measurements. J. Geophys. Res. 73, 5585.

FLOOD W.A. 1969 : Reply. J. Geophys. Res. 74, 5183.

FOLKSTEAD K., THRANE E.V., LANDMARK B. 1972 : A study of ion-pair production rates and electron densities in the ionospheric D-region. J. Atmos. Terr. Phys. 34, 963.

FRASER G.J. 1968 : Seasonal variation of southern hemispheric mid-latitude winds at altitudes of 70-100 km. J. Atmos. Terr. Phys. 30, 707.

GANGULY S. 1974 : Ionization balance in the D-region. J. Geophys. Res. 79, 267.

GARDNER F.F. and PAWSEY J.L. 1953 : Study of the ionospheric D-region using partial reflections. J. Atmos. Terr. Phys. 3, 321.

GEISLER J.E. and DICKINSON R.E. 1968 : Vertical motions and nitric oxide in the upper mesosphere. J. Atmos. Terr. Phys. 30, 1505.

GELLER M.A., SECHRIST C.F. (Jr) 1971 : Coordinated rocket measurements on the D-region winter anomaly - II. Some implications. J. Atmos. Terr. Phys. 33, 1027.

GREGORY J.B. 1965 : The influence of atmospheric circulation on mesospheric electron densities in winter. Jnl Atmos. Sci. 22, 18.

GREGORY J.B. and MANSON A.H. 1969a : Seasonal variations of electron densities below 100 km at mid-latitudes - I: Differential absorption measurements. J. Atmos. Terr. Phys. 31, 683.

GREGORY J.B. and MANSON A.H. 1969b : Seasonal variations of electron densities below 100 km at mid-latitudes - II: Electron densities and atmospheric circulation. J. Atmos. Terr. Phys. 31, 703.

GREGORY J.B. and MANSON A.H. 1970 : Seasonal variations of electron densities below 100 km at mid-latitudes. - III: Stratospheric-ionospheric coupling. J. Atmos. Terr. Phys. 32, 837.

GRÜN A.E. 1957 : Z. Naturf. 12a, 89.

HARA E.H. 1963 : Approximations to the semi-conductor integrals for use with the generalized Appleton-Hartree magneto-ionic formulas. J. Geophys. Res. 68, 4388.

HARE F.K., BOVILLE B.W. 1965 : The polar circulations. In The circulation in the stratosphere and mesosphere. W.M.O. Tech. Note no. 70, Geneva.

HARWOOD R. 1971 : Mapping the atmosphere from space. New Sci. & Sci. J. 51, 622.

HAUG A., LANDMARK B. 1970 : A two ion model of electron-ion recombination in the D-region. J. Atmos. Terr. Phys. 32, 405.

HESS S.L. 1959 : Introduction to theoretical meteorology. Holt, Rinehart and Winston, New York.

HESSTVEDT E. 1971 : A meridional model of the oxygen-hydrogen atmosphere. In Mesospheric models and related experiments. (G. Fiocco editor). D. Reidel Publ. Co., Dordrecht.

HESSTVEDT E., JANSSON U.B. 1969 : On the effects of vertical eddy transport on the distribution of neutral nitrogen components in the D-region. In Meteorological and chemical factors in D-region aeronomy. (C.F. Sechrist editor), Aeronomy Report no. 32, University of Illinois, Urbana.

HINES C.O. 1972 : Motions in the ionospheric D and E regions. Phil. Trans. R. Soc. A271, 457.

HINES C.O., REDDY C.A. 1967 : On the propagation of atmospheric gravity waves through regions of wind shear. J. Geophys. Res. 72, 1015.

HINTEREGGER H.E., HALL L.A., SCHMIDTKE G. 1965 : Solar XUV radiation and neutral particle distribution in July 1963 thermosphere. Space Res. V, 1175.

HOLLOWAY J.L. (Jr) 1958 : Smoothing and filtering of time series and space fields. Adv. Geophys. 4, 351.

HOLT O. 1969 : Discussion of paper by W.A. Flood, 'Revised theory for partial reflection D-region measurements'. J. Geophys. Res. 74, 5179.

HOUGHTON J.T., SMITH S.D. 1970 : Remote sounding of atmospheric temperatures from satellites. I. Introduction. Proc. R. Soc. A320, 23.

HUNT B.G. 1973 : A generalized aeronomic model of the mesosphere and lower thermosphere including ionospheric processes. J. Atmos. Terr. Phys. 35, 1775.

HUNTEN D.M., GODSON W.L. 1967 : Upper atmosphere sodium and stratospheric warmings at high latitudes. Jnl. Atmos. Sci. 24, 80.

JACKSON J.D. 1962 : Classical Electrodynamics. John Wiley & Sons, New York.

JUSTUS C.G., WOODRUM A. 1973 : Short and long period atmospheric variations between 25 and 200 km. NASA CR-2203.

KANTOR A.J., COLE A.E. 1965 : Monthly atmospheric structure, surface to 80 km. Jnl Appl. Met. 4, 228.

KATZ L., PENFOLD A.S. 1952 : Range-energy relations for electrons and the determination of beta-ray end point energies by absorption. Rev. Mod. Phys. 24, 28.

KAYE G.W.C., LABY T.H. 1966 : Tables of physical and chemical constants and some mathematical functions. Longmans, London.

KING G.A.M. 1967 : Discussion of paper by Bernt Maehlum, 'On the winter anomaly in the mid-latitude D-region'. J. Geophys. Res. 72, 6118.

LABITZKE K. 1972a : Temperature changes in the mesosphere and stratosphere connected with circulation changes in winter. Jnl. Atmos. Sci. 29, 756.

LABITZKE K. 1972b : The interaction between stratosphere and mesosphere in winter. Jnl. Atmos. Sci. 29, 1395.

LANDMARK B., HAUG A., THRANE E.V., HALL J.E., WILLMORE A.P., JESPERSEN M., PEDERSEN B.M., ANASTASSIADES M., TSAGAKIS E., KANE J.A. 1970 : Ionospheric observations during the annular solar eclipse of 20 May 1966 - V: Interpretation of observed results. J. Atmos. Terr. Phys. 32, 1873.

LARSEN T.R. 1971 : Short path V.L.F. phase and amplitude measurements during a stratospheric warming in February 1969. J. Atmos. Terr. Phys. 33, 1251.

LAUTER E.A., KNUTH R. 1967 : Precipitation of high energy particles into the upper atmosphere at medium latitudes after magnetic storms. J. Atmos. Terr. Phys. 29, 411.

LINDZEN R.S. 1967 : Planetary waves on beta-planes. Mon. Weather Rev. 95, 441.

LYONS L.R., THORNE R.M., KENNEL C.F. 1972 : Pitch angle diffusion of radiation belt electrons within the plasmasphere. J. Geophys. Res. 77, 3455.

MANSON A.H. 1968 : Coupling effects between the ionosphere and stratosphere in Canada (45^{o}N, 75^{o}W), 1962-66. J. Atmos. Terr. Phys. 30, 627.

MANSON A.H. 1971 : Ionospheric absorption and transport of minor constituents in the mesosphere and lower thermosphere (70-110 km) during periods of anomalous absorption. J. Atmos. Terr. Phys. 33, 715.

MANSON A.H., MERRY M.W.J. 1970 : Particle influx and the 'winter anomaly' in the mid-latitude (L ≈ 2.5-3.5) lower ionosphere. J. Atmos. Terr. Phys. 32, 1169.

MANSON A.H., MERRY M.W.J. 1971 : Seasonal variation of electron densities below 100 km at mid-latitudes - IV. Preliminary model calculations. J. Atmos. Terr. Phys. 33, 413.

MANSON A.H., MERRY M.W.J., VINCENT R.A. 1969 : Relationship between the partial reflection of radio waves from the ionosphere and irregularities as measured by rocket probes. Radio Sci. 4, 955.

MATSUNO T. 1971 : A dynamical model of the stratospheric warming. Jnl. Atmos. Sci. 28, 1479.

McILWAIN C.E. 1961 : Coordinates for mapping the distribution of magnetically trapped particles- J. Geophys. Res. 66, 3681.

MECHTLY E.A., BOWHILL S.A., SMITH L.G. 1972a : Changes of lower ionosphere electron content with solar activity. J. Atmos. Terr. Phys. 34, 1899.

MECHTLY E.A., SECHRIST C.F.(Jr), SMITH L.G. 1972b : Electron loss coefficients for the D-region of the ionosphere from rocket measurements during the eclipses of March 1970 and November 1966. J. Atmos. Terr. Phys. 34, 641.

MECHTLY E.A., SHIRKE J.S. 1968 : Rocket electron concentration measurements on winter days of normal and anomalous absorption. J. Geophys. Res. 73, 6243.

MEIRA L.G. (Jr) 1971 : Rocket measurements of upper atmosphere nitric oxide and their consequences to the lower ionosphere. J. Geophys. Res. 76, 202.

MILLINGTON G. 1965 : Riccati form of the wave equation. Electron. Letters 1, 184.

MITRA A.P. 1970 : HF and VHF techniques in radio wave probing of the ionosphere. J. Atmos. Terr. Phys. 32, 623.

MITRA A.P., JAIN V.C. 1963 : Interpretation of the observed solar zenith angle dependence of ionospheric absorption. J. Geophys. Res. 68, 2367.

MORONEY M.J. 1953 : Facts from figures. Penguin Books, Harmondsworth.

MULLER H.G. 1972 : Long period meteor wind oscillations. Phil. Trans. R. Soc. A271, 585.

MURGATROYD R.J. 1970 : The physics and dynamics of the stratosphere and mesosphere. Rep. Prog. Phys. 33, 817.

NARCISI R.S., BAILEY A.D. 1965 : Mass spectrometric measurements of positive ions at altitudes from 64 to 112 kilometers. J. Geophys. Res. 70, 3687.

NARCISI R.S., PHILBRICK C.R., ULWICK J.C., GARDNER M.E. 1972 : Mesospheric nitric oxide concentrations during a PCA. J. Geophys. Res. 77, 1332.

NOONAN K.K. 1969 : Investigation of the D-region. Thesis, M.Sc., University of Canterbury.

PATEL J.C., KOTADIA K.M. 1972 : Relationship between stratospheric warming and ionospheric temperature. Annls Géophys. 28, 803.

PHELPS A.V., PACK J.L. 1959 : Electron collision frequencies in nitrogen and in the lower ionosphere. Phys. Rev. Lett. 3, 340.

PHILLPOT H.R. 1969 : Antarctic stratospheric warming reviewed in the light of 1967 observations. Q. Jl R. Met. Soc. 95, 329.

PIGGOT W.R., BEYNON W.J.G., BROWN G.M., LITTLE C.G. 1957 : The measurement of ionospheric absorption. Ann. Int. Geophys. Yr. III, Part 2.

PIGGOT W.R., THRANE E.V. 1966 : The effect of irregularities in collision frequency on the amplitude of weak partial reflectons. J. Atmos. Terr. Phys. 28, 311.

POKROVSKIY G.B., TEPTIN G.M. 1970 : Features of the wind velocity spectrum at altitudes of 80-100 km. IZv., Atmospheric and Oceanic Physics (English Edition), 6, 69.

PRESTON K.F., BARR R.F. 1971 : Primary processes in the photolysis of nitrous oxide. J. Chem. Phys. 54, 3347.

QUIROZ R.S. 1974 Stratospheric warmings in the southern hemisphere deduced from satellite radiation data, 1969-73. IAMAP/IAPSO Assemblies, Melbourne, Jan. 1974.

QUIROZ R.S., GELMAN M.E. 1972 : Direct determination of the thickness of stratospheric layers from single channel satellite radiance measurements. Mon. Weather Rev. 100, 788.

REES M.H. 1963 : Auroral ionization and excitation by incident energetic electrons. Planet. Space Sci. 11, 1209.

REID G.C. 1970 : Production and loss of electrons in the quiet daytime D-region of the ionosphere. G. Geophys. Res. 75, 2551.

ROEDERER J., SHAPLEY A.H. 1973 : Overall summary of August 1972 phenomena and data. In Report U.A.G.-28. Part 1, World Data Center A for solar-terrestrial physics (Helen Coffey editor). U.S. Dept of Commerce.

ROSE G., WIDDEL H.U., AZCARRAGA A., SANCHEZ L. 1972 : Results of an experimental investigation of correlations between D-region neutral gas winds, density changes, and short-wave absorption. Radio Sci. 7, 181.

ROSSBY C.G. 1939 : Relation between variations in the intensity of the zonal circulation of the atmosphere and the displacements of the semi-permanent centers of action. J. Mar. Res. 2, 38.

ROWE J.N., FERRARO A.J., LEE H.S. 1969 : Changes in electron density and collision frequency at University Park, Pennsylvania during the stratospheric warming of 1967/68. J. Atmos. Terr. Phys. 31, 1077.

RUNDLE H.N., SULLIVAN H.M. 1972 : Upper atmospheric sodium and stratospheric warmings. Jnl Atmos. Sci. 29, 977.

RUSCH D.W., BARTH C.A. 1972 : Global satellite measurements of nitric oxide. In COSPAR symposium on D- and E-region ion chemistry (C.F. Sechrist and M.A. Geller editors), Aeronomy Report no. 48, University of Illinois, Urbana.

SCHERHAG R. 1952 : Die explosionsartigen Stratosphären-Erwärmerungen des Spätwinters. Ber. Deutsch. Wetterdienst 6, 51.

SCHERHAG R. 1969 : Stratospheric warming and polar vortex breakdown. In Solar-Terrestrial Physics : Terrestrial Aspects. (A.C. Stickland editor). Annals of the IQSY 5, M.I.T. Press.

SCHWENTEK H. 1963 : The variation of ionospheric absorption from 1956 until 1963. J. Atmos. Terr. Phys. 25, 733.

SCHWENTEK H. 1971 : Regular and irregular behaviour of the winter anomaly in ionospheric absorption. J. Atmos. Terr. Phys. 33, 1647.

SCHWENTEK H. 1973 : Shortwave fadeouts and ionospheric absorption measured at Lindau (N52.6, E8.7) in the period 15 July to 15 August 1972. In Report UAG-28 Part II, W.D.C. - A for Solar-Terrestrial Physics (Helen Coffey editor), U.S. Dept of Commerce.

SECHRIST C.F. (Jr) 1970 : Interpretation of D-region electron densities. Radio Sci. 5, 663.

SECHRIST C.F. (Jr) 1972a : Theoretical models of the D-region. J. Atmos. Terr. Phys. 34, 1565.

SECHRIST C.F. (Jr) 1972b : Interactions between the neutral atmosphere and the lower ionosphere. In Thermospheric Circulation, (Willis L. Webb editor), M.I.T. Press.

SECHRIST C.F. (Jr), MECHTLY E.A., SHIRKE J.S., THEON J.S. 1969 : Coordinated rocket measurements on the D-region winter anomaly - I. Experimental results. J. Atmos. Terr. Phys. 31, 145.

SEN H.K., WYLLER A.A. 1960 : On the generalization of the Appleton-Hartree magneto-ionic formulas. J. Geophys. Res. 65, 3931.

SHAPLEY A.H., BEYNON W.J.G. 1965 : 'Winter Anomaly' in ionospheric absorption and stratospheric warmings. Nature 206, 1242.

SHIMAZAKI T., LAIRD A.R. 1972 : Seasonal effects on distributions of minor neutral constituents in the mesosphere and lower thermosphere. Radio Sci. 7, 23.

SHIRKE J.S., RAO G.L.N. 1967 : Criteria for recognition of a winter day of high ionospheric absorption. J. Geophys. Res. 72, 2917.

SPENCER L.V. 1959 : Energy dissipation by fast electrons. National Bureau of Standards Monograph 1, Washington.

SPRENGER K., LYSENKO I.A. 1972 : The significance and interpretation of ionospheric drift measurements in the low frequency range. Phil. Trans. R. Soc. A271, 473.

STROBEL D.F. 1971 : Odd nitrogen in the mesosphere. J. Geophys. Res. 76, 8384.

STROBEL D.F. 1972a : Minor neutral constituents in the mesosphere and lower thermosphere. Radio Sci. 7, 1.

STROBEL D.F. 1972b : Nitric oxide in the D-region. J. Geophys. Res. 77, 1337.

THOMAS L. 1962 : The winter anomaly in ionospheric absorption. J. Atmos. Terr. Phys. 23, 301.

THOMAS L. 1968 : D and E-regions during days of anomalous radio wave absorption in winter. J. Atmos. Terr. Phys. 30, 1211.

THOMAS L. 1971 : The lower ionosphere. J. Atmos. Terr. Phys. 33, 147.

THORPE M.R. 1970 : Atmospheric Physics : Radio wave absorption and the mesosphere. Thesis, Ph.D., University of Canterbury.

THORPE M.R. 1971 : The phase integral correction for calculations of radio wave absorption in the ionosphere. J. Atmos. Terr. Phys. 33, 1597.

TOPPING J. 1962 : Errors of observation and their treatment. Chapman and Hall, London.

TURCO R.P., SECHRIST C.F. (Jr) 1970 : An investigation of the ionospheric D-region at sunrise. Aeronomy report no. 41, University of Illinois, Urbana.

VAMPOLA A.L. 1971 : Natural variations in the geomagnetically trapped electron population. Report TR-0059 (6260-20)-17, Aerospace Corp, Los Angeles.

VON BIEL H.A. 1971 : Determination of D-region electron densities within the scattering region. J. Geophys. Res. 76, 5365.

VON BIEL H.A., FLOOD W.A., CAMNITZ H.G. 1970 : Differential phase partial reflection technique for the determination of D-region ionization. J. Geophys. Res. 75, 4863.

WEBB W. 1966 : Structure of the stratosphere and mesosphere. Academic Press, New York & London.

WHITTEN R.C., POPPOFF I.G. 1971 : Fundamentals of Aeronomy. Wiley, New York.

WIERSMA D.J., SECHRIST C.F. (Jr) : Differential phase measurements of D-region partial reflections. Aeronomy Report no. 47, University of Illinois, Urbana.

WILLIAMS B.H., OLSEN R.O., KAYS M.D. 1972 : Stratospheric-ionospheric interaction during the passage of a planetary wave in January 1967. Radio Sci. 7, 193.

WU M., NEWELL R.E. 1972 : Correlation of D-region absorption and the 10 mb winds and temperature during IQSY. J. Atmos. Terr. Phys. 34, 1999.

ZIMMERMAN S.P., NARCISI R.S. 1970 : The winter anomaly and related transport phenomena. J. Atmos. Terr. Phys. 32, 1305.

ZIPF E.C., BORST W.L., DONAHUE T.M. 1970 : A mass spectrometer observation of NO in an auroral arc. J. Geophys. Res. 75, 6371.

ACKNOWLEDGEMENTS

I have received help from many people in the work described in this thesis. I wish to thank the following poeple in particular:

Professor A.G. McLellan for providing the opportunity and facilities to do the work.

Dr Grahame Fraser, my supervisor, who suggested this project, for many ideas, much encouragement, and a lot of practical help.

Dr J.R. Burrows of the Cosmic Rays section, Division of Physics, National Research Council, Canada, for the particle data from the ISIS-2 satellite and helpful correspondence on its application.

Mr Reid Basher, Professor W. Jones and Dr André von Biel for many discussions and ideas.

Mr R. Unwin of the Geophysical Observatory, Physics and Engineering Laboratories, D.S.I.R. and members of his staff for information about ISIS-2 and geomagnetic data.

The New Zealand Meteorological Service for atmospheric data.

The Department of Atmospheric Physics, University of Oxford, for the NIMBUS-IV data.

Mr A. Black who designed and built many of the interfaces and installed and maintained the PDP-8. Mr J. de Voil who designed and built one of the receivers and also helped with electronics problems, and Mr R. Rohleder.

The staff of the University of Canterbury Computing Centre for help with perplexing problems involving paper and magnetic tapes.

Finally I wish to thank I.C.I.(N.Z.) for the financial support provided by the I.C.I. Research Fellowship, and the New Zealand University Grants Committee for providing a Postgraduate Scholarship and the Kidson Scholarship.